NAVAL POSTGRADUATE SCHOOL
Monterey, California

THESIS

PERFORMANCE ANALYSIS OF IRTOOL AND COMPARISON TO LWKD MARINE BOUNDARY LAYER PROGRAM

by

Ioannis Christou

December 1999

Thesis Advisor: Alfred W. Cooper
Second Reader: Ron J. Pieper

Approved for public release; distribution is unlimited.

REPORT DOCUMENTATION PAGE

Form Approved OMB No. 0704-0188

1. AGENCY USE ONLY *(Leave blank)*	2. REPORT DATE	3. REPORT TYPE AND DATES COVERED
	December 1999	Master's Thesis

4. TITLE AND SUBTITLE
PERFORMANCE ANALYSIS OF IRTOOL AND COMPARISON TO LWKD MARINE BOUNDARY LAYER PROGRAM

5. FUNDING NUMBERS

6. AUTHOR (S)
Christou, Ioannis

7. PERFORMING ORGANIZATION NAME(S) AND ADDRESS(ES)
Naval Postgraduate School
Monterey, CA 93943-5000

8. PERFORMING ORGANIZATION REPORT NUMBER

9. SPONSORING / MONITORING AGENCY NAME(S) AND ADDRESS(ES)

10. SPONSORING / MONITORING AGENCY REPORT NUMBER

11. SUPPLEMENTARY NOTES
The views expressed in this thesis are those of the author and do not reflect the official policy or position of the Department of Defense or the U.S. Government.

12a. DISTRIBUTION / AVAILABILITY STATEMENT
Approved for public release; distribution is unlimited.

12b. DISTRIBUTION CODE

13. ABSTRACT *(maximum 200 words)*

This thesis evaluates the ability of the IRTOOL computer simulation program to predict mirages. Using identical input conditions taken from the MAPTIP experiment database, predicted Minimum Mirage Range (MMR) and Maximum Intervision Range (MIVR) from both the IRTOOL and IRBLEM models were extracted and compared with the measurements recorded in the database. By comparison of the algorithms it was found that discrepancies in IRTOOL mirage prediction could be ascribed to the input function for significant ocean wave height, which gave values much greater than measured or used in IRBLEM. For a significant wave height close to the measured value the IRTOOL predictions were in very close agreement with observation and with IRBLEM. IRTOOL predictions were in all cases within 2.7 km and in most cases within 1.3 km of the measurements for all ranges varying from about 7-26 km. The strong temperature gradient predicted by the model within a few meters of the water surface, uncertainties in the measured range, and the variation of 0.8 to 2 ^{0}C in Air Sea Temperature Difference are sufficient to account for the observed deviations. Differences between the model predictions and some of the problems encountered are also discussed.

14. SUBJECT TERMS	15. NUMBER OF PAGES
Refraction, Marine Boundary Layer, Atmosphere, IRTOOL, IRBLEM, Mirage, MAPTIP	190
	16. PRICE CODE

17. SECURITY CLASSIFICATION OF REPORT	18. SECURITY CLASSIFICATION OF THIS PAGE	19. SECURITY CLASSIFICATION OF ABSTRACT	20. LIMITATION OF ABSTRACT
Unclassified	Unclassified	Unclassified	UL

NSN 7540-01-280-5500

Standard Form 298 (Rev. 2-89)
Prescribed by ANSI Std. 239-18

THIS PAGE INTENTIONALLY LEFT BLANK

Approved for public release; distribution is unlimited

PERFORMANCE ANALYSIS OF IRTOOL AND COMPARISON TO LWKD MARINE BOUNDARY LAYER PROGRAM

Ioannis Christou
Lieutenant, Hellenic Navy
B.S., Hellenic Naval Academy, 1990

Submitted in partial fulfillment of the
requirements for the degree of

MASTER OF SCIENCE IN APPLIED PHYSICS

from the

NAVAL POSTGRADUATE SCHOOL
December 1999

Author: 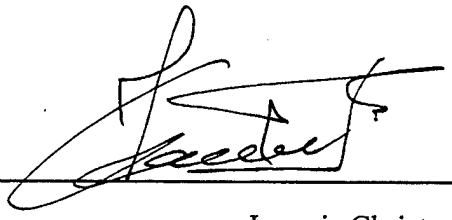

Ioannis Christou

Approved by: 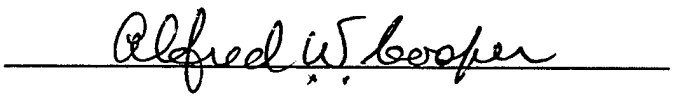

Alfred W. Cooper, Thesis Advisor

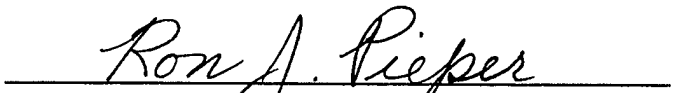

Ron J. Pieper, Second Reader

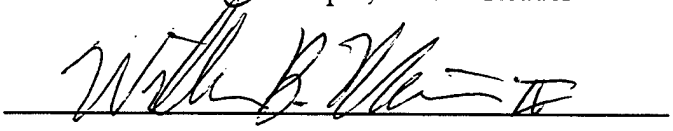

William B. Maier II, Chairman,
Department of Physics

THIS PAGE INTENTIONALLY LEFT BLANK

ABSTRACT

This thesis evaluates the ability of the IRTOOL computer simulation program to predict mirages. Using identical input conditions taken from the MAPTIP experiment database, predicted Minimum Mirage Range (MMR) and Maximum Intervision Range (MIVR) from both the IRTOOL and IRBLEM models were extracted and compared with the measurements recorded in the database. By comparison of the algorithms it was found that discrepancies in IRTOOL mirage prediction could be ascribed to the input function for significant ocean wave height, which gave values much greater than measured or used in IRBLEM. For a significant wave height close to the measured value the IRTOOL predictions were in very close agreement with observation and with IRBLEM. IRTOOL predictions were in all cases within 2.7 km and in most cases within 1.3 km of the measurements for all ranges varying from about 7-26 km. The strong temperature gradient predicted by the model within a few meters of the water surface, uncertainties in the measured range, and the variation of 0.8 to 2^{0}C in Air Sea Temperature Difference are sufficient to account for the observed deviations. Differences between the model predictions and some of the problems encountered are also discussed.

THIS PAGE INTENTIONALLY LEFT BLANK

TABLES OF CONTENTS

ACKNOWLEDGEMENT

This thesis was an excellent experience in learning about the very interesting subject of atmospheric refraction. The completion of this job was possible with the help of many people. First, I would like to thank my thesis advisors, Professors A. W. Cooper and Ron J. Pieper for their understanding, guidance, help, and contribution to my thesis work. I am thankful to the Boundary Layer Studies Group of the Meteorology Department of the Naval Postgraduate School and especially Professor Kenneth L. Davidson for the MBL program he provided and Paul Frederickson for all its useful assistance in this program. Professor Davidson was always positive in giving me an accurate answer to my questions. I would like to thank Dr. Luc Forand from DREV, for the IRBLEM code he provided and also for the provision of the data analyzed.

I want to acknowledge Steve Church from the Arete Associates for the help he provided for the IRTOOL program. Steve Church gave me important inputs to complete this job.

This project was conducted under partial support from the Naval Postgraduate School Institute for Joint Warfare Analysis and from Naval Sea Systems Command, PEO-TSC.

I want to thank my wife Niki for her loving family support, her unending encouragement and understanding which gave me the spirit to complete this thesis and

my studies in NPS successfully. My children Dimitris and Maria are as lucky to have her as I am.

Finally, I thank my wonderful parents, whose love, blessing and support give me courage and need to improve myself.

I. INTRODUCTION

A. BACKGROUND

Modern sensor and weapon systems rely on propagation of electromagnetic or electro-optic energy in an inhomogeneous atmosphere. In the coastal environment, complex spatial structures cause a great variability in the atmospheric parameters that affect the detection of low flying targets. One of the parameters among others which is responsible for the poor performance of the electro-optical systems is the gradient of refractivity caused by large vertical changes in temperature and humidity, especially near the ocean surface. Shipboard optical systems are used currently for the detection and acquisition of low flying air targets. The range performance of IRST (Infrared Search and Track) sensors is partly determined by the propagation of the atmosphere. This is why the Navy has a particular interest in determining the electro-optical properties of the lower layers of the marine atmosphere. In recent years many scientific teams from different countries have been trying to create computer based simulation, modeling, performance prediction systems and techniques, taking into account the relevant atmospheric parameters. These parameters can be obtained through sensing, numerical modeling or a combination of both, so as to assess refractive effects on detection range of low level targets including mirage and multiple image generation. In spite of the efforts that have been put forth to create computer models which give results very close to the experimental data, the detection of low flying anti-ship missiles (sea-skimmers) with high detection probability and low false alarm rates is still a challenge.

B. STUDY OBJECTIVES

The IRTOOL (Infrared tool) computer program is a simulation computation model environment joining a number of component models from various sources into a unified package that produces both a visual simulation and engineering calculations for scenarios appropriate to the Infrared Search and Track systems (IRST). It has been developed by Arete Corporation and NSWC (Naval Surface Warfare Center) under the sponsorship of the Office of Naval Research in support of the Infrared Analysis Modeling and Measurements Program (IRAMMP) to assist in the design phase of the next IRST generation. It is a DoD generated program not for sale and commercial use. A group of scientists from the Canadian Defense Research Establishment Valcartier (DREV) applied IRTOOL to data they obtained off the Netherlands coast in the MAPTIP measurements of 1993, and concluded that IRTOOL did not predict mirages in cases in which they were found experimentally. They then decided to forego the use of IRTOOL completely to concentrate on development of the local program IRBLEM (L.Forand private communication).

The IRBLEM is another computer code (a software package) for the computation of atmospheric effects on EO band systems in the marine surface layer. The ray refraction module (L(W)WKD) of IRBLEM has been evaluated in the past with the French CELAR's (Centre d'Electronique de l'Armement) PIRAM (Profils d'Indice de Refraction en Atmosphere Marine) ray refraction model using the database of the MAPTIP experiment. The results for both models were very satisfactory.

The main objective of this research is the evaluation of IRTOOL for visible/IR refraction and mirage formation in the marine boundary layer as well as the comparison of the above mentioned code with IRBLEM. For the comparison between those two models the experimental database from the MAPTIP trial, which took place in the Netherlands in 1993, by French, Canadian and German teams, was used. Using the same set of input conditions for both models we compare the predicted results with the experimental data.

A study has been made in the past year in the evaluation and comparison of the IRTOOL refraction model with the above mentioned programs IRBLEM and PIRAM [Ref. 2]. The conclusion of this effort was not very satisfactory (i.e. IRTOOL did not predict mirages in cases in which they were found experimentally). So, the second objective of this thesis is the use of as many cases (data sets) as possible, so as to cover all the possible situations and seek the modification of the IRTOOL code, if that is necessary, which may lead to greatly improved performance under mirage conditions.

THIS PAGE INTENTIONALLY LEFT BLANK

II. THEORY

A. BACKGROUND

The index of refraction n, is a dimensionless parameter given by

$$n=\frac{c}{v} \tag{1}$$

where c is the phase velocity of the electromagnetic wave (EM) in vacuum given by

$$c=\frac{1}{\sqrt{\varepsilon_o \mu_o}}=3\times 10^8 \text{ m/s} \tag{2}$$

v is the phase velocity of the EM wave in a homogeneous medium given by

$$v=\frac{1}{\sqrt{\varepsilon\mu}} \tag{3}$$

$\varepsilon_o = 8.85\times 10^{-12}$ F/m is called the permittivity of free space

$\mu_o = 1.26\times 10^{-6}$ H/m is called the permeability of free space and

ε and μ are the permittivity and permeability of the medium respectively.

Due to the fact that in general $\mu = \mu_0$ and $\varepsilon > \varepsilon_0$, the light propagates slowly through matter. The EM properties of the medium are related to the index of refraction according to Eqs. 1, 2, 3 by the equation:

$$n=\sqrt{\frac{\varepsilon\mu}{\varepsilon_o\mu_o}} \cong \sqrt{\frac{\varepsilon}{\varepsilon_0}} \tag{4}$$

Any change to propagation velocity due to the interaction with the medium results in a bending, called refraction, of the signal path (i.e., the bending of the rays). The index of refraction (n) is a function of frequency (color). This phenomenon is called dispersion and the supporting medium is called dispersive. The dependence of $n(\omega)$ on the frequency for different optical materials for the visible range is shown in Figure 1.

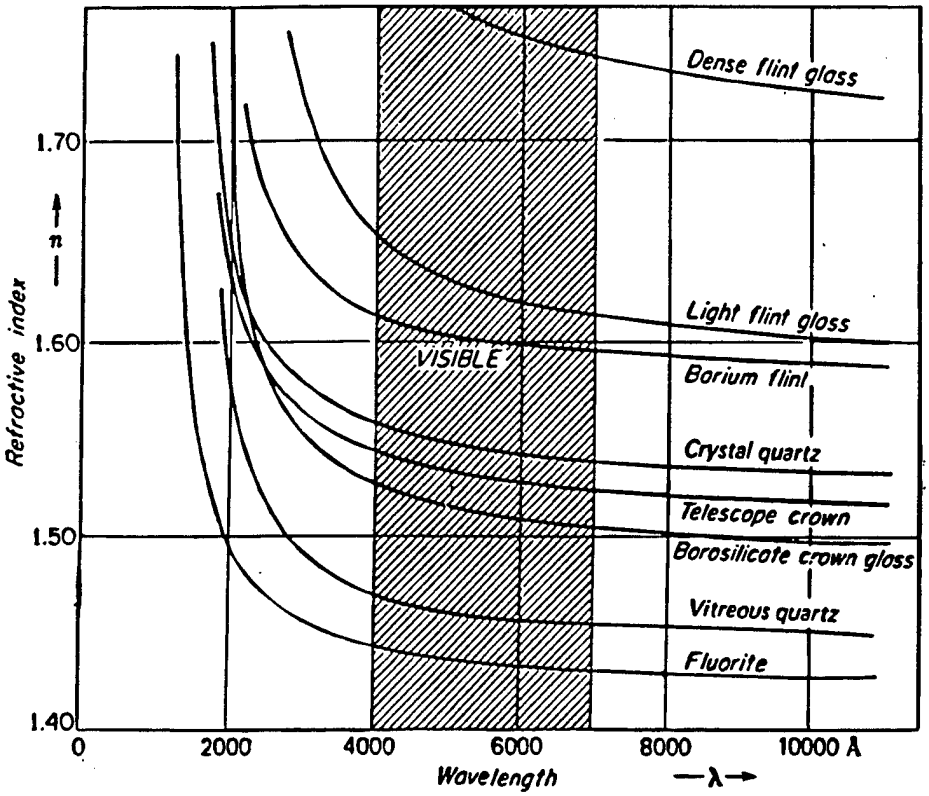

Figure 1. Dispersion curves for several different optical materials commonly used for lenses and mirrors in the visible range [Ref.1].

An important law, named after the Dutch mathematician Willebrord van Roijen Snell, states that the product of the refractive index and the sine of the angle of incidence

of a ray in one medium is equal to the product of the refractive index and the sine of the angle of refraction in a successive medium i.e., $n_1 \sin\theta_1 = n_2 \sin\theta_2$ (Figure 2). So, when a ray enters a medium of a higher refractive index it will bend toward the normal and when a ray enters a medium of lower refractive index it will deviate away from the normal (Figure 2). The denser a material is, the higher is its refractive index. Given that the phase velocity of the EM wave is $v = \frac{c}{n}$, in a denser medium the velocity of light will be lower.

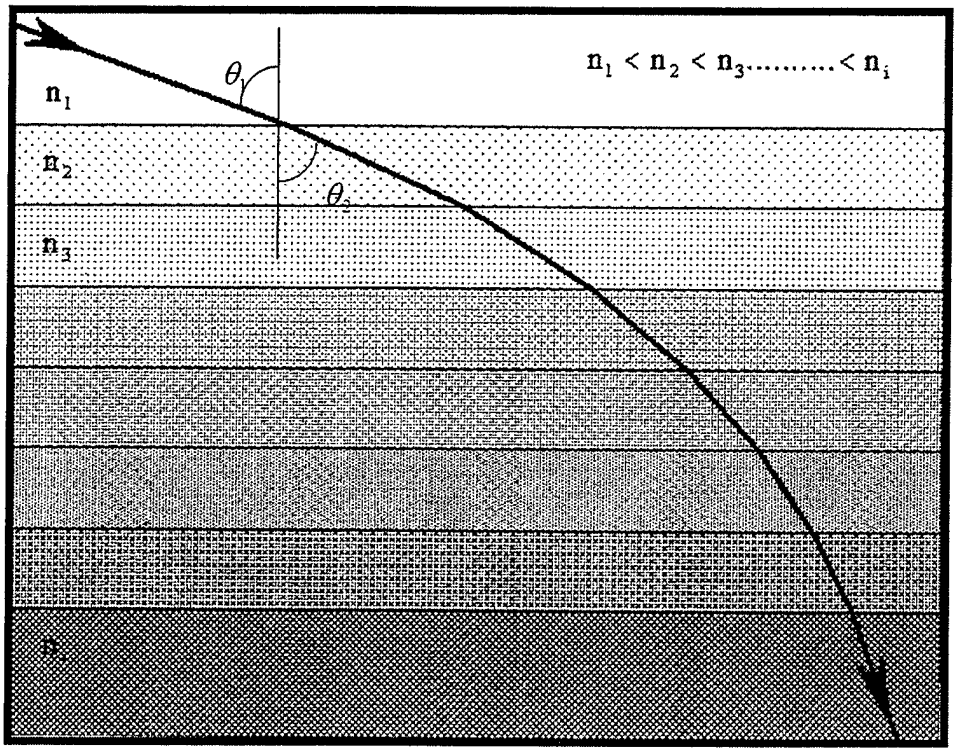

Figure 2. Refracted ray passing through different layered media of increasing refractive index [Ref. 2].

As a result we expect that light traveling through air travels more slowly as the density of the air increases. In Figure 3 the curve is the ray path of a traveling light wave and the lines perpendicular to this curve represent wave fronts. The curved path that the ray follows is due to the decrease of the air's density with height. The lower part of the wave front is lower in the atmosphere where the density is higher, so it moves more slowly than the upper part, causing the ray's bending. For an observer on earth the starlight appears to be coming from a higher elevation than the true one [Ref. 3]. This is analogous to the spoke of a spinning wheel where the outer part of the wheel is moving faster than the inner part.

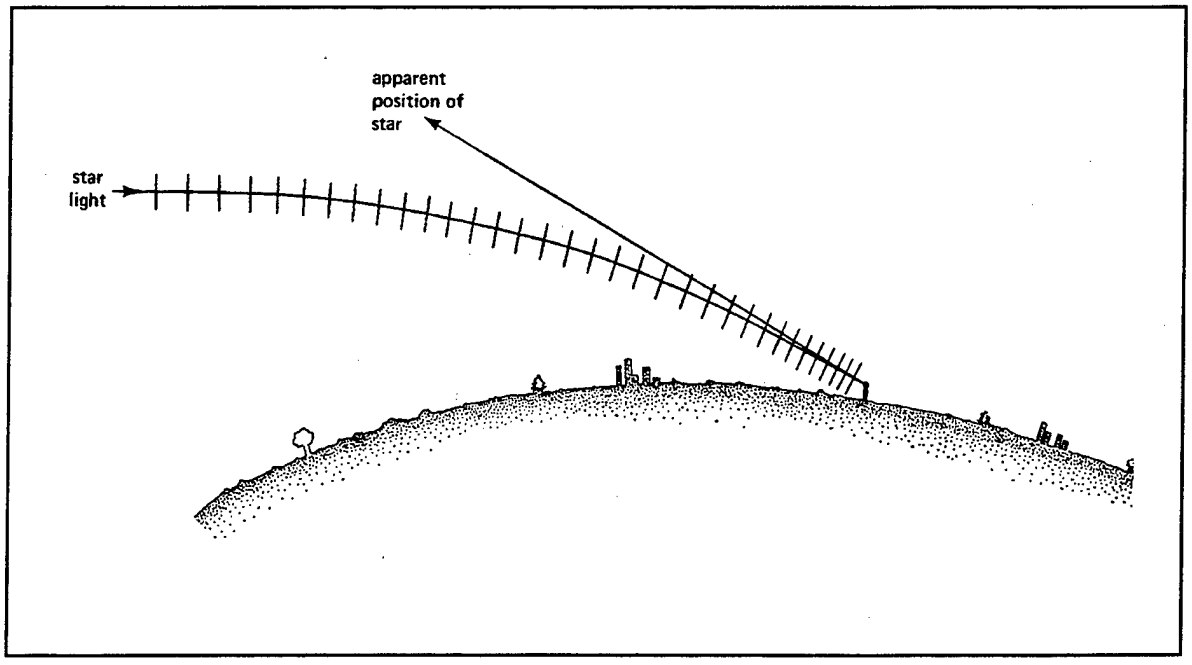

Figure 3. Starlight is bent as it passes through the atmosphere [From Ref. 3].

In order to calculate the ray bending we will use the model of Figure 4 [Ref. 4].

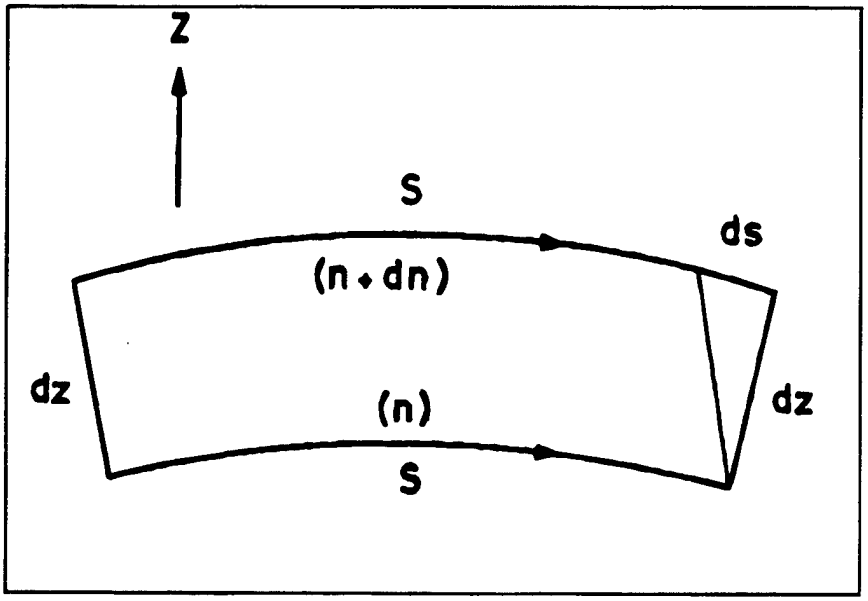

Figure 4. Beam curvature in an slightly inhomogeneous atmosphere [Ref. 4].

The adjacent ray paths separated by dz have length s and s+ds and also the refractive indices of the air along the paths are n and n+dn (dn<0). The optical path that each ray travels is stationary with respect to variations of that path (Fermat's principle). Hence,

$$\frac{\partial(ns)}{\partial z}=n\frac{\partial s}{\partial z}+s\frac{\partial n}{\partial z}=0 \tag{5}$$

But, $\frac{\partial s}{\partial z}$ is the change in the direction of the wavefront so that the direction change per unit path length (i.e. the path curvature) is:

$$\sigma=-\frac{1}{s}\frac{\partial s}{\partial z}=\frac{1}{n}\frac{\partial n}{\partial z} \quad \text{[Ref. 4]} \tag{6}$$

Because $\frac{dn}{dz}$ is negative in our case, the ray bends downward. This is usually the case in the atmosphere, so for convenience our convention will be that such a downward oriented curve has a positive radius. The value of the refractive index of air is very close to unity, and so the radius of curvature of the beam curvature is given by:

$$r = \frac{1}{\sigma} = -\frac{1}{(\frac{dn}{dz})} \tag{7}$$

Here, it is very important to note that the ray bending has a radius of curvature that depends on the gradient of the index of refraction and not on the absolute magnitude of the index of refraction itself.

B. ELECTROMAGNETIC SPECTRUM

Many times in this thesis we will refer to the EM spectrum and its wavelength bands. So, it will be very useful to introduce the EM spectrum. The EM spectrum is divided into six generic spectral regions. Four of these regions are associated with infrared imaging systems. The ultraviolet (UV) region ranges in wavelength from 0.2 to 0.4 μm. The visible region ranges in wavelength from 0.4 to 0.7 μm. The near infrared spectral region (NIR) ranges in wavelength approximately from 0.7 to 1.1 μm. The first infrared band is the short wavelength infrared band (SWIR) which approximately covers 1.1 to 2.5 μm. The second infrared band is the mid-wavelength infrared (MWIR) band and covers approximately from 2.5 to 7.0 μm. The third infrared band is the long wavelength infrared (LWIR) spectral band and it covers approximately from 7.0 to

15 μm. The fourth infrared band is the far infrared (FIR) band or very long wave infrared (VLWIR) band which covers the spectral region above 15 μm. [Ref. 5].

C. REFRACTIVE INDEX

Due to interaction that occurs between the wave electric field and the medium in which it propagates, the refractive index is different from that of the free space. We can picture the electron as attached to the end of a spring as a way to describe this interaction with a simple electron oscillator model. In that case we can show that the refractive index is a complex quantity with a real part given by:

$$n \cong 1 + \frac{Nq^2}{2m\varepsilon_0} \sum_j \frac{f_j\left(\omega_j^2 - \omega^2\right)}{\left(\omega_j^2 - \omega^2\right)^2 + \gamma_j^2\omega^2} \tag{8}$$

and the absorption coefficient (imaginary part) is given by:

$$\alpha \cong \frac{Nq^2\omega^2}{m\varepsilon_o c} \sum_j \frac{f_j\gamma_j}{\left(\omega_j^2 - \omega^2\right)^2 + \gamma_j^2\omega^2} \tag{9}$$

where N is the number of molecules per unit volume

q is the charge of the electron

m is the electron mass

ω is the frequency that drives the damped harmonic oscillator

ω_j is the natural radial radian frequency of the electrons

f_j is the number of electron with frequency ω_j (oscillator strength)

γ_j is the damping coefficient in each molecule

The real part of the refractive index represents the wave dispersion (i.e., controls the phase velocity) while the imaginary part represents wave absorption at the resonant frequency. Close to a resonance, the index of refraction drops sharply. This phenomenon is called anomalous dispersion because of this atypical behavior. The maximum absorption occurs in that region and that happens because we drive the electrons to their resonant frequency. The result is that a very large amount of energy is dissipated. Away from the resonances the index of refraction simplifies to the following form:

$$n=1+\frac{Nq^2}{2m\varepsilon_o}\sum_j \frac{f_j}{(\omega_j^2-\omega^2)} \tag{10}$$

Moreover, for transparent materials, the nearest significant resonances generally lie in the ultraviolet [Ref. 6], so that $\omega < \omega_j$. Using Taylor series we can show that in that case Eq. 10 becomes:

$$n=1+\left(\frac{Nq^2}{2m\varepsilon_o}\sum_j \frac{f_j}{\omega_j^2}\right)+\omega^2\left(\frac{Nq^2}{2m\varepsilon_o}\sum_j \frac{f_j}{\omega_j^4}\right) \tag{11}$$

With $\lambda = \frac{2\pi c}{\omega}$ we can write Eq. 11 as

$$n=1+A\,(1+\frac{B}{\lambda^2}) \tag{12}$$

with $A = \frac{Nq^2}{2m\varepsilon_o}\sum_j \frac{f_j}{\omega_j^2}$ and

$$B = \left(\frac{2\pi c}{\omega_j}\right)^2$$

This is Cauchy's equation in the two constants form. The constant A is called the coefficient of refraction and the constant B is called the coefficient of dispersion.

A more general equation, which gives the index of refraction over a large wavelength range, is the Sellmeier equation, which is also valid in the regions close to resonances. This equation for a single resonance wavelength λ_0 is given by [Ref. 1]

$$n^2 = 1 + \frac{A\lambda^2}{\lambda^2 - \lambda_0^2} \tag{13}$$

In cases of more than one resonance Eq. 13 becomes

$$n^2 = 1 + \sum_i^n \frac{A_i\lambda^2}{\lambda^2 - \lambda_i^2} \tag{14}$$

D. REFRACTIVITY

The value of the refractive index of air is very close to unity. Sometimes it is convenient to discuss refractive effects in terms of refractivity. The refractivity is proportional to the difference between n and 1 and is defined as $R=(n-1)\times 10^6$ [Ref. 1, Ref. 7]. The refractivity of the atmosphere through the visible and IR is shown in the Figure 5 [Ref. 1]. From Figure 5 we observe that in the visible range the variation with wavelength is small and in the near infrared is negligible.

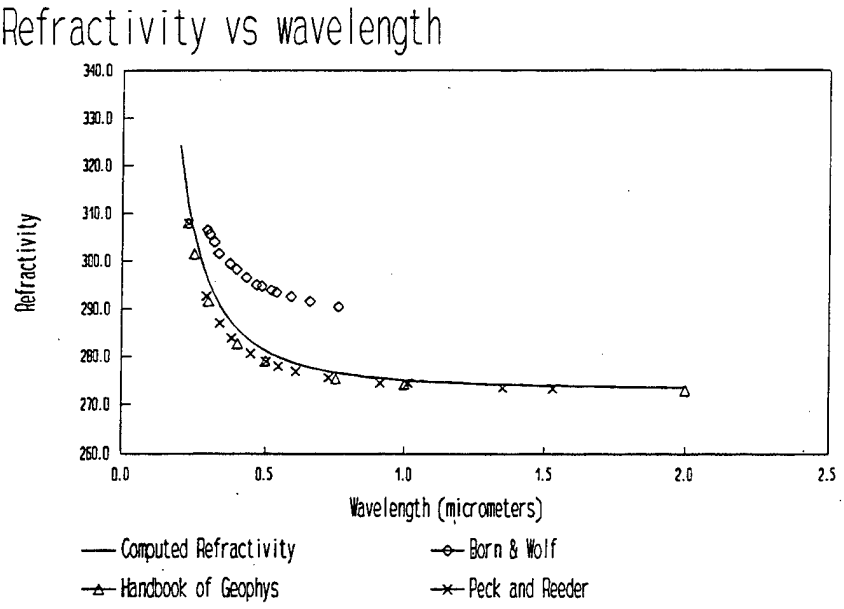

Figure 5. Atmospheric Refractivity versus wavelength. Reported measured values are compared with computation using the Edlen equation (Eq. 15) [Ref.1].

E. ATMOSPHERIC REFRACTION

Due to the electromagnetic nature of many sensors used by today's military, the EM propagation through the atmosphere is a question of extreme importance and relevance. The atmospheric refraction arises from the density variation of air which decreases almost exponentially with altitude. So, we expect that fluctuations in temperature T, humidity Q and pressure P will cause fluctuations in both the real and imaginary parts of the refractive index. Changes in the vertical gradient and to a lesser extend horizontal gradient of the index of refraction cause the atmospheric refraction. In wavelength regions remote from major absorptions the refractive index can be represented for dry air in the form [Ref. 1]:

$$n\text{-}1=\frac{77.6P}{T}\left(1+\frac{0.0075}{\lambda^2}\right)\times 10^{-6} \tag{15}$$

or in terms of the refractivity (R)

$$R=\frac{77.6P}{T}\left(1+\frac{0.0075}{\lambda^2}\right) \tag{16}$$

Where λ is the wavelength in micrometers

P is the pressure in millibars and

T is the temperature in degrees Kelvin.

In the IR and the visible, the index gradient of air is dominantly dependent on the temperature gradient in the operational windows of EO systems, where absorption is low.

F. A NON-REFRACTIVE ATMOSPHERE

In a non-refractive atmosphere (i.e., one in which the refractive index is invariant with position) electro-optical (EO) radiation follows straight line trajectories and hence the maximum detection ranges are limited by the terrestrial horizon. The range limitation due to the earth's curvature is called horizon-limited range (HLR) [Ref. 8] and for a given sensor and target height, can be obtained using

$$HLR=\sqrt{2a}\left(\sqrt{h_s}+\sqrt{h_t}\right)\times 10^{-3}\cong 3.57\left(\sqrt{h_s}+\sqrt{h_t}\right) \tag{17}$$

where HLR is expressed in kilometers

h_s is the sensor height in meters

h_t is the target height in meters and

α is the mean earth radius expressed in meters ($\alpha \cong 6370000$ m)

This value for the mean earth radius is given by [Ref. 9, Ref. 10]. Moreover in [Ref. 9] for the midlatitude winter atmosphere and custom atmosphere the radius of earth (km) that is used in the calculations of MODTRAN is α=6371 km. This is the radius of earth at the particular latitude at which the calculation is to be performed. As we will see on Data Analysis the atmospheres that will be used for the IRTOOL calculations are the midlatitude winter and custom atmosphere. So, Eq. 17 with the radius of earth as specified above will help us to evaluate the non-refractive calculations of IRTOOL.

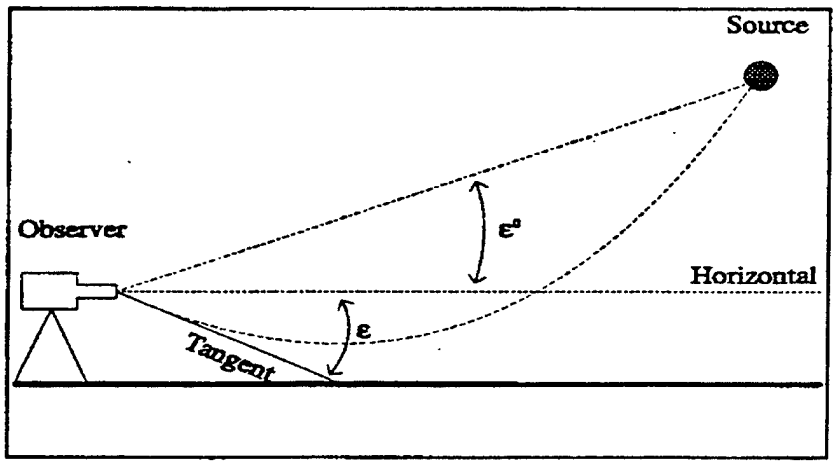

Figure 6. A non-refractive and a refractive atmosphere with the respective elevation angles ε^0 and ε. The tangent represents the observed source detection [After Ref. 14].

G. REFRACTION EFFECTS

The surface layer of the marine boundary layer influences the IR sensing of low altitude targets. Three atmospheric effects are primarily responsible for limiting sensor performance [Ref. 11]:

(a) Ray refraction

(b) Turbulent distortion

(c) Atmospheric extinction by molecules and aerosols

In this chapter we will describe only the effects of the ray refraction due to the vertical variation of the index of refraction which dominates in most cases the horizontal variations. The sign of the vertical gradient of the refractive index divides the refraction conditions into two categories. In the first one, the gradient is positive and we have subrefraction (inferior mirage) and in the second one the gradient is negative and we have superrefraction conditions (superior mirage).

Mirage, as defined by the dictionary, is an optical illusion caused by the atmospheric conditions, in which an observer sees a nonexistent body of water or an image of some object. Examples of mirages are false pools of water seen over hot desert sands or hot pavement, and at sea an inverted image of a ship seen in the sky. These phenomena are well understood and can be explained by two facts. First the light rays are bent when they pass between media of different densities and second, the boundary between two such media acts as a mirror for rays of light coming in at certain angles [Ref. 12]. Mirages can be photographed (Figure 7). For most mirage effects variations in the temperature mainly, but also in the pressure and the water vapor content of the atmosphere, cause corresponding variation in the refractive index that causes the bending of light rays as is predicted by Snell's law of refraction. The optical ray bending is determined primarily by the temperature gradient [Ref. 13]

$$\frac{dT}{dz} = \frac{T_*}{akz} \tag{18}$$

where T_* is a temperature scaling parameter, α is the ratio of the heat transfer to momentum transfer and k is the von Karman constant, approximately equal to 0.4. At low elevation, the term $\frac{1}{z}$ in Eq. 18 results in a very large temperature gradient and excessive ray bending. Before describing in more detail the subrefraction and superrefraction conditions we should have in mind that a light ray always bends toward the denser medium (colder air).

Figure 7. The desert (or hot) road mirage [From Ref. 3].

H. SUBREFRACTION (INFERIOR MIRAGE)

The kind of mirage formed over a hot surface is sometimes referred to as an inferior mirage.

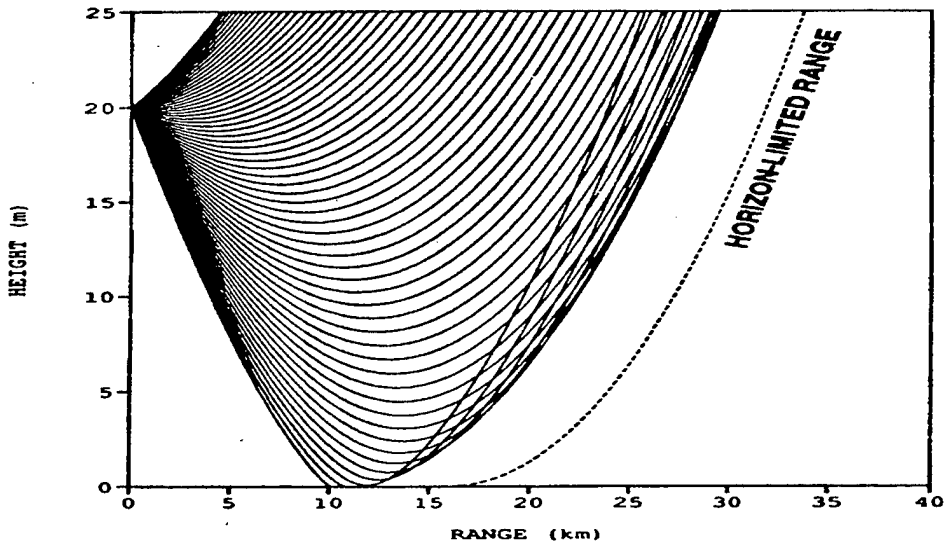

Figure 8. Ray diagram for subrefraction conditions [From Ref. 8].

The term inferior mirage refers to the fact that the upright mirage appears below its real position. This effect occurs under conditions of negative Air to Sea Temperature Difference (ASTD). From Figure 8 we can see how the light rays propagate through a subrefractive atmosphere. Rays leaving the source at angles below the horizon will be refracted upwards due to the refractive gradient leading to a crossing of ray trajectories.

The following three Figures 9, 10, 11 will help us to understand the results given from the data analysis in Chapter VII.

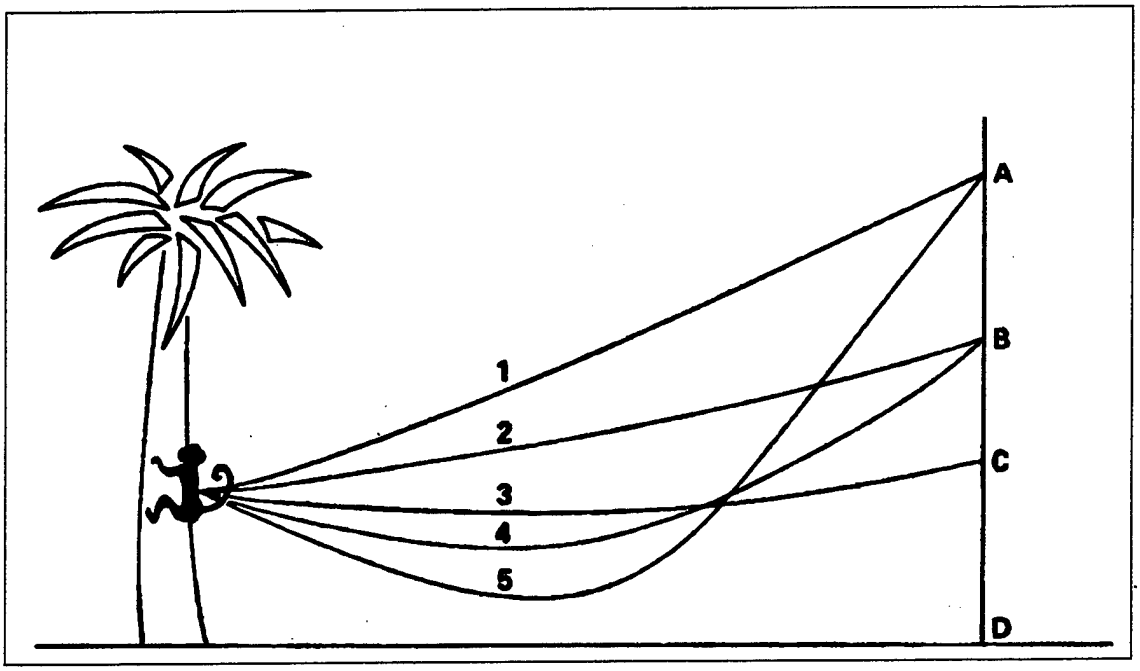

Figure 9. Ray paths under subrefractive conditions [From Ref. 3].

In the desert the sand becomes hotter than the air and heats the air layer immediately above the surface to a higher temperature than the air a few meters above. The greatest bending of the ray occurs closest to the ground because the temperature there is changing more rapidly with the height. In Figure 9 we see five rays coming from the back of the monkey part way up the tree trunk. The rays start off in different directions and hit a wall at a specific range from the tree. As we can see, rays 4 and 5, although initially directed below the other three, end up higher on the wall. If we put our eye at A we will see two views of the monkey, one direct and the other inverted. The same happens at point B only now the two images are closer than before. At point C the two images have become one, and below C we do not see any image. The point C is the lowest point at which a ray can

be received at this particular distance, as shown in Figure 10. With our eye at point C, we see the top of the tree but none of the tree trunk below the monkey.

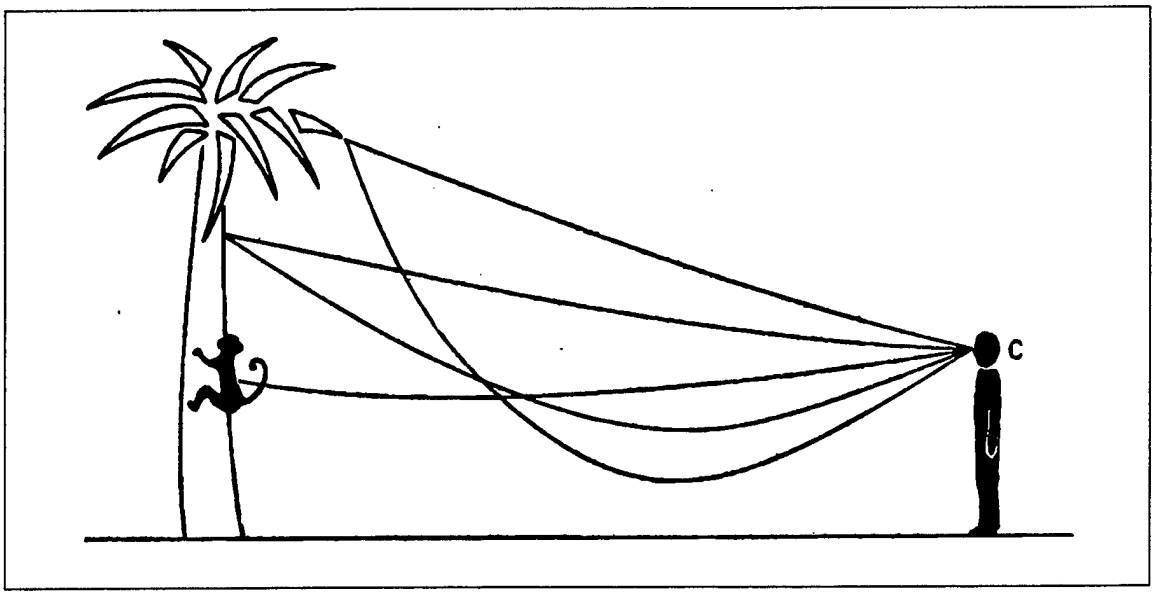

Figure 10. The origin of a vanishing line in the desert mirage [From Ref. 3].

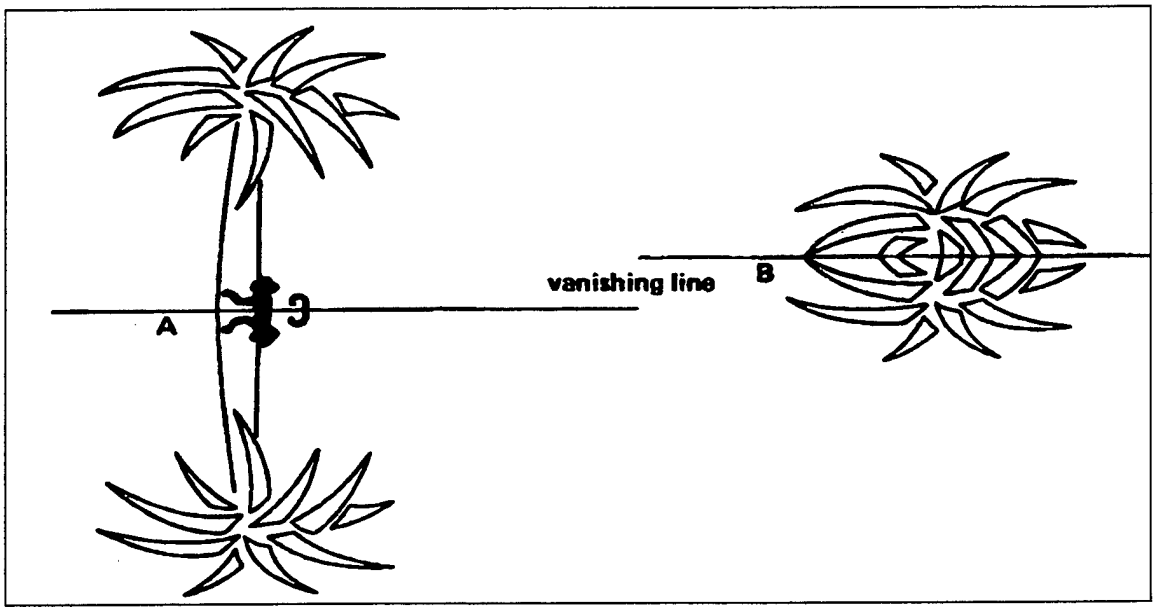

Figure 11. "The appearance of the desert mirage scene with (A) the observer positioned as shown in Figure above and (B) the observer further from the tree" [From Ref. 3].

Figure 11 (A) shows the image we see looking from point C. There is a vanishing line passing through the monkey's back. Every point on the tree below that line cannot be seen but every point above that line has two images and one of those two images is inverted. If we move further away from the tree the vanishing line will rise as shown in case B. That happens because all the rays will pass above our head. Finally, if we move even further the tree will disappear. From Figures 8, 12 we see that subrefraction conditions impose an absolute limit of detection range shorter than the terrestrial horizon (HLR).

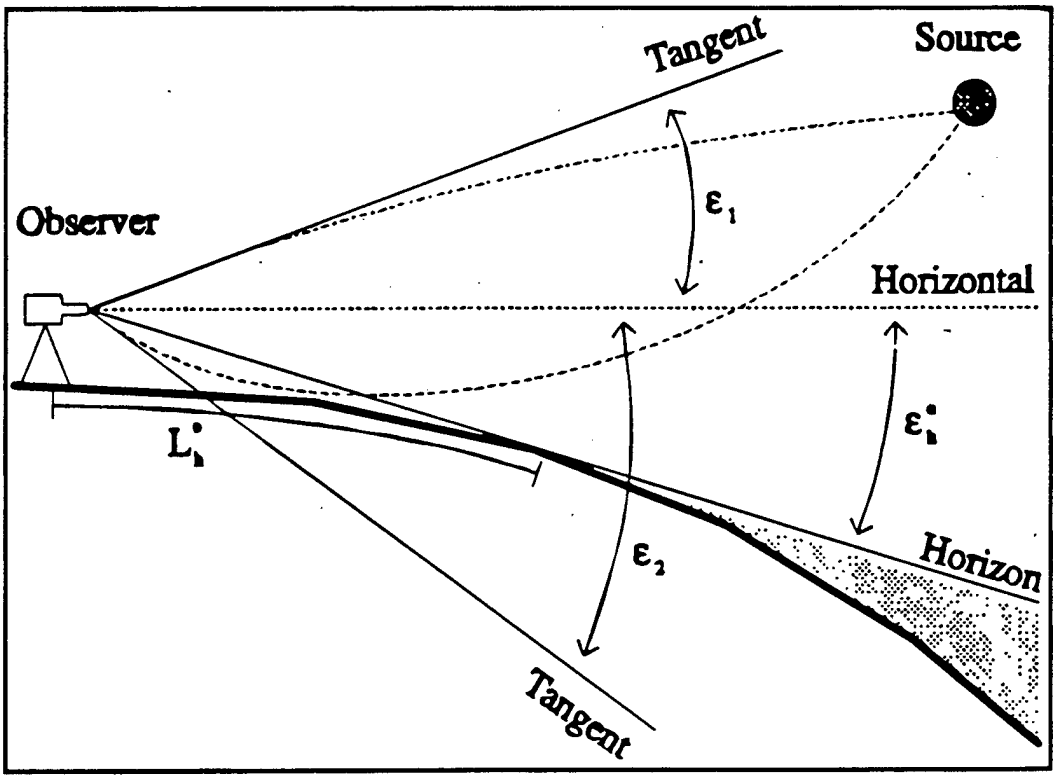

Figure 12. Under subrefractive conditions two images of the source are seen at two elevation angles. L_h^o and ε_h^o are the horizon distance and angle [From Ref. 14].

In coastal environments the appearance of subrefraction conditions is more common, especially when those conditions are driven by the sea wind. For those conditions the expression of the maximum intervision range is used to "denote the absolute detection range limit imposed by refraction for a given sensor and target height" [Ref. 8]. This range corresponds to the HLR for non-refractive conditions.

I. SUPERREFRACTION (SUPERIOR MIRAGE OR DUCTING OR LOOMING)

This effect arises when warmer air moves over a colder lake or ocean. That means that we have positive ASTD conditions causing light rays to be bent toward the earth and hence making an object appear to be raised above its true position (the object is seen above its actual position). When this condition is well developed we can see objects such as a distant ship beyond the horizon or the sun after it has set (Figure 13). For a long time this phenomenon has been called looming by sailors. The superrefractive conditions are shown in Figures 14, 15. We see that under these conditions, the downward bending of the rays can cause the detection of targets well beyond the horizon even though the target is not observable under non-refractive conditions (straight line propagation).

These conditions are not so often encountered. Depending on the season and the region of the world it is possible for them to occur near the coast, especially when warm continental air from the land is blown over cool water.

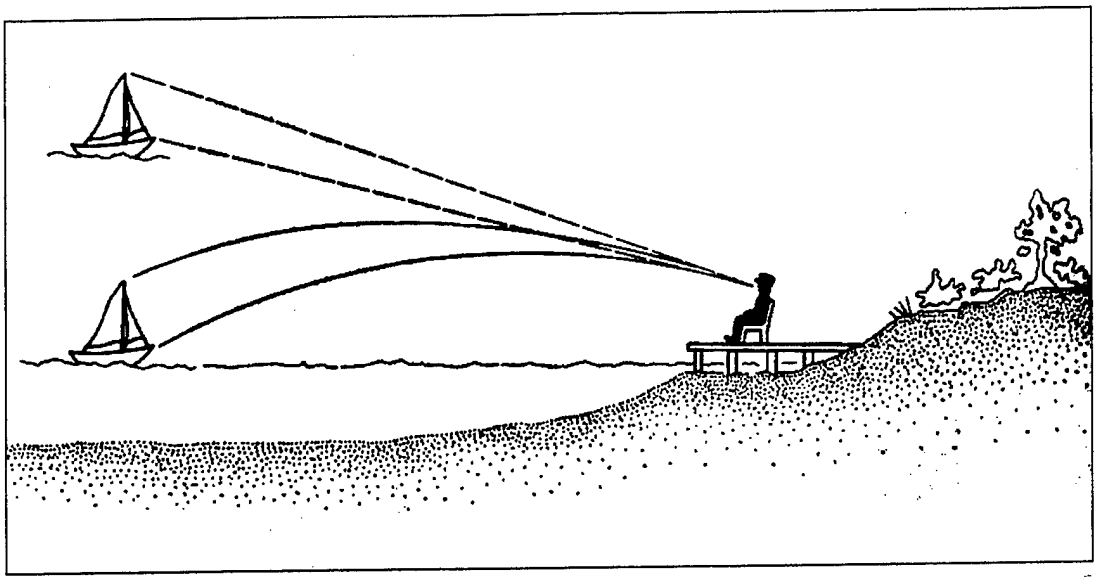

Figure 13. Rays producing a superior mirage [From Ref. 3]. The observed object is seen as an elevated, erect image. The object may be over the geometrical or "normal refraction" horizon.

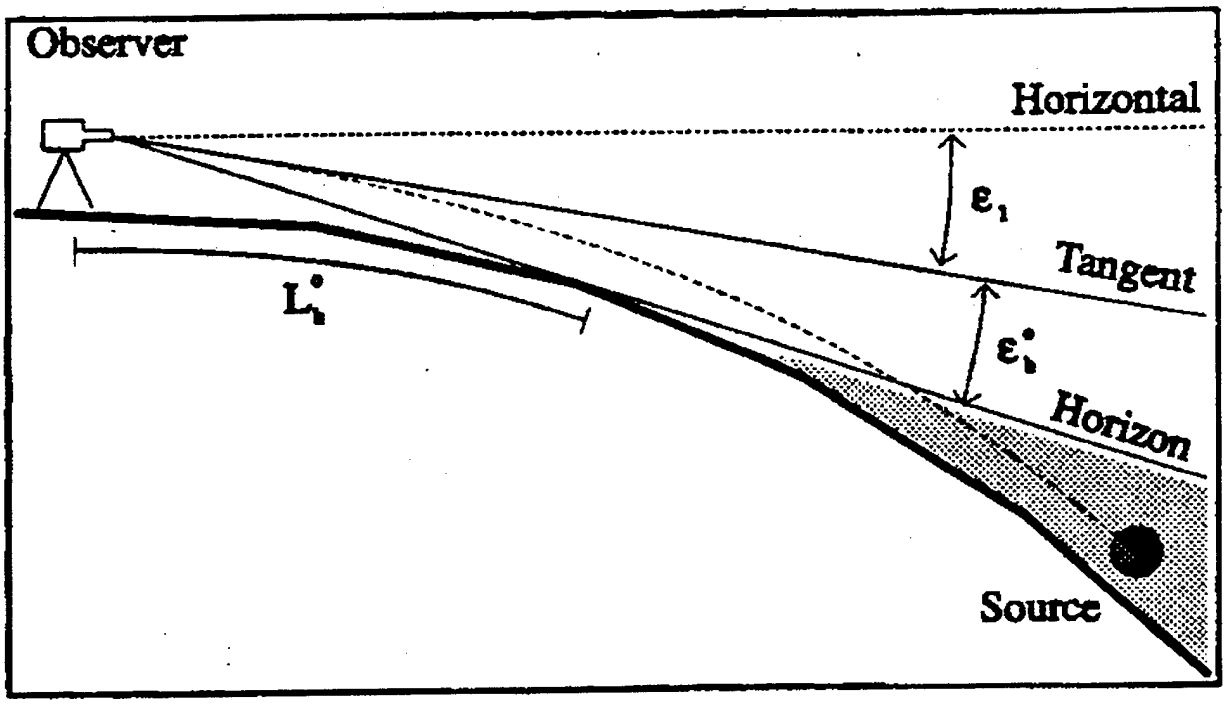

Figure 14. Under superrefractive conditions a target can be seen even when it is below the horizon. ε_1 is the elevation angle [Ref. 14].

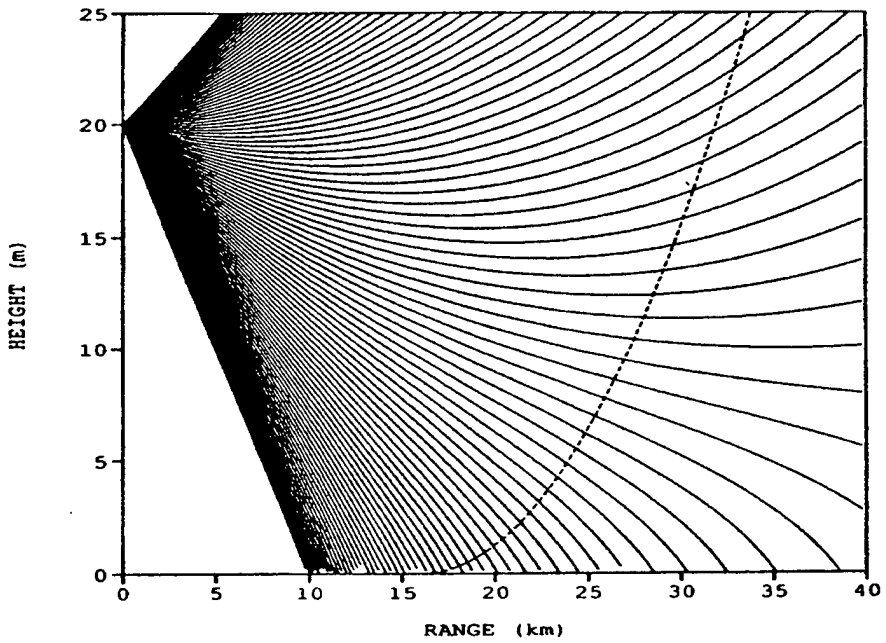

Figure 15. Ray diagram for superrefraction conditions [From Ref. 8]. As we can see the downward bending of the rays can cause the detection of targets well beyond the horizon even though the target is not observable under non-refractive conditions. The dot line crossing the ray trajectories corresponds to HLR.

THIS PAGE INTENTIONALLY LEFT BLANK

III. IRBLEM

A. GENERAL DESCRIPTION

The IRBLEM (IR Boundary Layer Effects Model) is a software package, consisting of various modules, which can be used as executable stand-alone programs. It is developed by the Defense Research Establishment, Valcartier, (DREV) Canada, and performs calculation of optical properties in a propagation volume defined by the user. Atmospheric effects such as refraction and turbulence in the marine surface layer are also considered in contrast with MODTRAN.

The surface layer theory used by IRBLEM is in general valid for the first 30 meters above the surface but with direct calls to MODTRAN calculations can be made for heights above this defined surface layer.

The IRBLEMv3.1 code was downloaded from the DREV ftp site and is a PC executable program compatible only with the MODTRAN 3v1.5. Figure 16 shows the internal modular structure of IRBLEM with the meteorological inputs situated at the top and the various outputs at the bottom. As we can see, in a surface layer domain defined by the user, vertical profiles of refractivity M(h), of aerosol extinction coefficients a(h), and of the refractive index structure parameter C_n^2 (h) are calculated in the first phase. Also, depending on whether or not MODTRAN is used, the molecular transmittance versus height is available. In the second phase, all the above mentioned profiles are used as inputs in the ray tracing program, which calculates the optical properties and atmospheric effects.

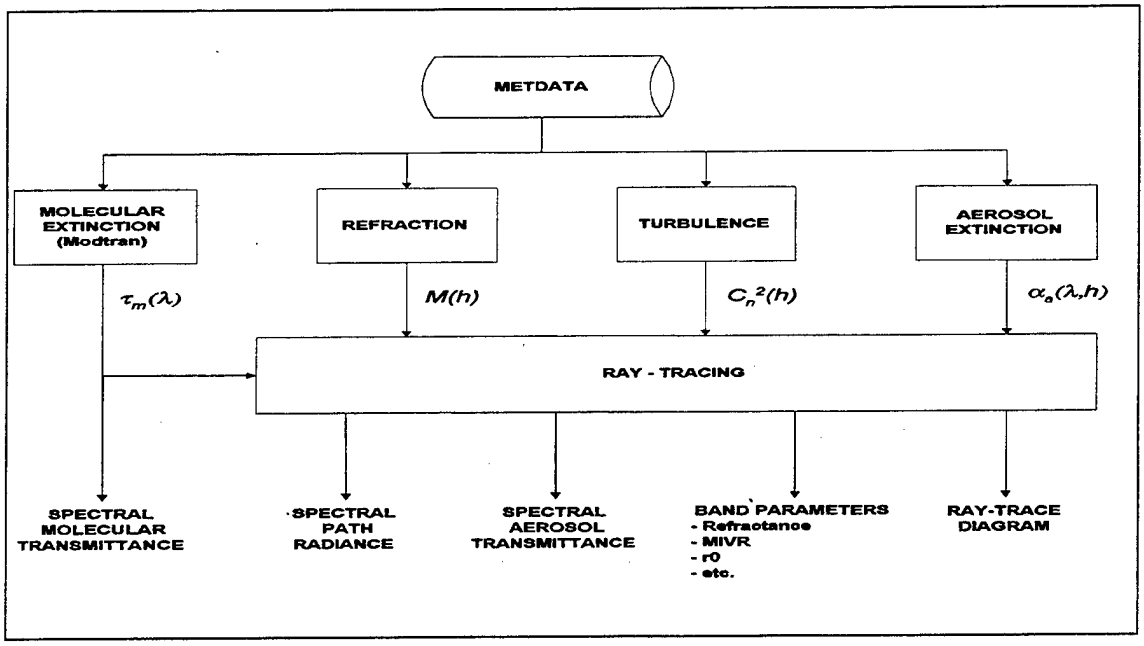

Figure 16. IRBLEM functional diagram [From Ref. 15].

B. MAIN INPUTS

The main inputs can be divided into five groups. The first group is the propagation domain, the second the meteorological conditions, the third the sensor data, the fourth the running options and the fifth one the ray tracing parameters. The active parameters that are used for each group are shown in the following Tables 1-5.

PROPAGATION DOMAIN DATA (GROUP 1)
Minimum Range and Maximum Range (km)
Maximum height (m)
Range sampling/step (km)
Height sampling/step (m)

Table 1. Propagation domain parameters in IRBLEM [After Ref.15].

METEOROLOGICAL DATA (GROUP 2)
Height of the Air Temperature sensor, Pressure sensor, and Humidity sensor in meters
Wind speed (m/sec) and height of the wind speed measurement in meters
24 hr average wind speed (m/sec)
Pressure (mbar)
Air Temperature (deg C)
Water Temperature (deg C)
Humidity (%)
Wave height ($H_{1/3}$) (m)
Visibility (Km)
Solar Radiation (W/m^2)
Air Mass parameter with values between 1-10
Precipitation type (rain, drizzle, snow, fog, no weather)
Precipitation rate (mm/h)
Fog liquid water content (g/m^3)

Table 2. Meteorological data active inputs in IRBLEM [After Ref. 15].

SENSOR DATA (GROUP 3)
Waveband (min and max wavelength) in (μm)
Sensor Height (m)

Table 3. Active sensor parameters that are used by IRBLEM [After Ref. 15].

RUN OPTIONS (GROUP 4)
Job identification number (1-999)
Spectral resolution (cm^{-1})
Aerosol computation mode (NOVAM or Kel)
Use of MODTRAN (yes or no)
Meteorological profiles mode ("wavy" or "non-wavy")

Table 4. Running options parameters in IRBLEM [After Ref. 15].

RAY-TRACING PARAMETERS (GROUP 5)
Minimum ray launching angle (deg)
Maximum ray launching angle (deg)
Maximum number of rays that will be used (integer)
Nominal ray angular separation (deg)
Nominal ray integration step (m)
Minimum ray separation angle (deg)-when approaching horizon
Range integration step for path radiance calculation (km)
Wave cut-off factor (unitless)
Total extinction surface sublayer (m)

Table 5. Ray tracing parameters in IRBLEM [After Ref. 15].

For the evaluation of the sea-particle concentration as function of the wind speed two models are available:

(1) The NOVAM relationships

(2) A new model developed by Kel Research

Also, for the computation of the refractivity profile we have two options: the "wavy" and the "non-wavy". In the first one the sea wave effect (the wave structure) is taken into account and modifies the refractivity profile produced by the non-wavy mode. The profile produced by the non-wavy mode is averaged out over a sea-wave period as a function of the wave height. According to Dion [Ref. 15] "it is deemed preferable to use the non-wavy mode until validation has been achieved."

Something that will play a crucial role to the data analysis is the FWH (Factor Wave Height). The ray cut-off height due to waves is given in IRBLEM by the following expression:

$$\text{Cut-off height} = (\text{FWH} \times H_w) + \text{minabslayer} \qquad (19)$$

That means from the water surface to the cut-off height the waves are assumed to produce a fully absorbing layer that stops all the rays. The H_w or $H_{1/3}$ is the significant wave height in meters and minabslayer is a sublayer above the surface where total extinction is assumed to exist. The significant waveheight is taken here to equal four times the rms waveheight [Ref. 11, Ref. 13]. According to [Ref. 15] for the ray-tracing parameters "These parameters are not likely to require modifications on a run-to-run basis under normal use of IRBLEM. Default values should be adequate under most circumstances." The default value for the FWH factor is given as 0.6. So, we expect that this factor will produce a significant wave height much smaller than the measured one (about 50%

smaller). In that case we expect the beginning of the mirage range to be at shorter distances.

C. MODULES AND UTILITY PROGRAMS

The main programs and utility programs that compose the IRBLEM v3.1 package are shown in Tables 6, 7 [Ref. 15]. The main programs with the asterisk(*) are the programs that are called by IRBLEM.

PROGRAM	PURPOSE
IRBLEM	Main program – Batch or Menu – based interactive mode
LWWKD*	Computation of modified refractivity profile, M(h)
WKDCN2*	Computation of C_n^2 (h), the index structure parameter profile
WKDAERX*	Computation of spectral aerosol extinction coefficient versus height, $\alpha_a(\lambda,h)$
TRANSM*	Calculation of molecular transmittance (using MODTRAN when available)
RTR*	Ray – tracing program
IRBLEMPP	IRBLEM post processor
BKGD	Give background radiance in the marine surface layer

Table 6. Main programs of IRBLEM [From Ref. 15].

UTILITY	PURPOSE
MODSET	Set path to MODTRAN (when available)
MERGPROF	Determine atmospheric profile for calculation above the surface layer
MSGCHECK	To check for warnings and error messages
EXTR	Extraction of results (scalar vs. height, spectral vs. wavelength) for display
CLEANER	Delete inputs/outputs for a given IRBLEM job ID

Table 7. Utility programs of IRBLEM [From Ref 15].

Now, lets describe in a more little details those modules that were used in this thesis.

1. LWWKD

The LWWKDv6.5 is a bulk aerodynamic model developed by DREV that produces the vertical refractivity profile and applies to RF, IR and visible wavelengths. It is based on the Monin-Obhukov similarity theory. This model uses standard meteorological measurements [Ref. 15] as inputs, namely:

Water temperature (deg C)

Air temperature (deg C)

Air humidity (%)

Wind speed (m/sec)

Pressure (mbar)

Also as input is used the wavelength and the choice of "wavy" (LWWKD) or "non-wavy" mode (LWKD). Actually, this module produces the vertical profile of modified refractivity up to 50 meters above the water. The modified refractivity is defined as [Ref. 15, Ref. 23]

$$M(h) = N(h) + 0.157h \tag{20}$$

where N = (n-1)$\times 10^6$ is the refractivity, n is the index of refraction, h is the height in meters and 0.157 is a constant in units/m. In addition to the vertical profile of modified refractivity, LWWKD produces the profiles of its first and second derivative and also the

vertical profiles of temperature, relative humidity, pressure and wind speed. The expressions for the first and second derivative of the modified refractivity are given by:

$$\frac{dM(h)}{dh} = \frac{dN(h)}{dh} + 0.15 \quad \text{(first derivative)} \tag{21}$$

$$\frac{d^2M(h)}{dh^2} = \frac{d^2N(h)}{dh^2} \quad \text{(second derivative)} \tag{22}$$

2. RTR

The RTRv6.2 is a program developed by DREV, which for a user-defined marine surface propagation layer integrates the atmospheric properties. In that calculation, ray paths calculated from the sensor (height=sensor height and range=0 km) depend on the vertical profiles. The Earth's curvature also is taken into account.

The RTR uses as inputs the outputs of all the other modules. The outputs of this program are many interesting quantities such as the MIVR, the geometrical horizon, the beginning of the mirage zone, the angular deviation i.e., the angular difference between the elevation of the initial ray and the elevation of the initial ray that hits the same coordinates under non-refractive conditions, the geometry of every ray, the refractance, aerosol transmittance, spectral path radiance and transmittance along each ray and many more.

Here, we can say that the MIVR and also the beginning of the mirage zone are meaningful quantities only under unstable conditions (subrefraction conditions-air cooler than water). In that case for a constant altitude target, a mirage appears between the

beginning of the mirage zone range and the MIVR. Under stable conditions (superrefraction conditions-air warmer than water) mirage does not occur. In that case the concept of MIVR does not apply, because the rays can reach very long ranges near the surface.

3. IRBLEMPP (IRBLEM POST-PROCESSOR)

This is a program that describes the cumulative atmospheric optical effects on imaging of a point target, which is located at coordinates given by the user (height, range).

For a given target position the IRBLEMPP calculates [Ref. 15] the apparent elevation of horizon, the elevation of the geometrical horizon, the minimum observable height (the minimum height above the water where a target can be detected at a given distance), the apparent target position, the refractance, information on the mirage image (if a mirage is present) as well as for the direct (real) image, spectral quantities such as molecular and aerosol transmittance, path radiance and many other parameters.

THIS PAGE INTENTIONALLY LEFT BLANK

IV. IRTOOL

A. GENERAL DESCRIPTION

IRTOOL is an IRST X-windows analysis tool, which was developed by Arete Associates and NSWC under the sponsorship of the Office of Naval Research in support of the Infrared Analysis Modeling and Measurements Program (IRAMMP). It is oriented towards IRST analysis [Ref. 16]. This computer program is a simulation/computational model environment, which uses a number of stand-alone executable modules in a unified package, to produce both a visual simulation and engineering calculations for scenarios appropriate to the Infrared Search and Track system.

IRTOOL includes a variety of sensor performance models, a few point source IR signature models, an atmospheric propagation model (MODTRAN and LOWTRAN) including standard atmospheric models and provision to build a local atmospheric model, a turbulence model and an atmospheric refraction model. The entire package is designed so that the users may insert local modules for their purposes. IRTOOL applies to the low altitude ocean boundary layer regime. Other features of IRTOOL other than its ability of producing simulated ocean and/or sky scenes including clouds is the injection of targets into both simulated and real scenes. This level of analysis allows visualization of the fluctuations in the observed target signal due to the obscuration by the wave crests.

For this thesis we used IRTOOL version 2.1.0 which is installed on the Sun machines in the Simulation Laboratory of the Physics Department in the Naval Postgraduate School (NPS).

B. INPUT PARAMETERS

The IRTOOL parameters are organized by subject and each subject includes one or more group of parameters. Table 8 lists the group of parameters for each subject.

The group of the input parameters is found under the Input menu. The user has three options: (1) load a previously saved set of parameters, (2) edit the present parameter values, (3) load a default set of parameter values and (4) use Advanced flow control. The fourth option is used when the user is doing several similar calculations with similar inputs. In this case, previously calculated results for the different runs can be reused and a significant amount of time can be saved. It was very useful in this thesis to use that option, especially when we had to use the same LOWTRAN file for a number of different runs. The most important consideration in using the advanced flow control is to ensure that the inputs are consistent with the results we are using.

C. MODULES

IRTOOL consists of eighteen modules which are stand alone executable programs (or groups of programs) with well-defined inputs, outputs and algorithms. The sequence in which those modules are executed is very important because some modules require as inputs some of the outputs from other modules. Module communication is accomplished with disk files. A brief description of the modules, the parameter group that is used for each of them and also their dependencies are shown in Tables 9, 10. For a specific output one or a number of modules must be executed.

Subject	Parameter Group	Comments
Sensor	Type	Contains the sensor system parameters such as the detector IFOV, detector spacing (also known as pitch or sampling), the sensor passbands, and detector efficiencies
	Polarizer	Input parameters which describe the polarizing element, if any, attached to the sensor.
	Operation	Contains the input parameters which specify where the sensor is looking, at what altitude the sensor is located, and how the sensor platform is moving.
	Scene effects	Input parameters which affect how the simulated sensor response is applied to an image.
Target	Type	Target size and emissivity.
	Trajectory	Input parameters which control the position and velocity of the target including the target speed, altitude, and ranges of interest. This menu has 5 different forms depending on how the trajectory is specified. The Pursuit/Vectored option is for targets with constant speed and altitude on collision courses with the sensor. With the Specify Range/Bearing and Range/Bearing from File options the user defines the target position relative to the sensor as a function of time. With the Specify Speed/Heading Option and Speed/Heading from File options the user provides an initial target position and defines the target velocity as a function of time. The last four options allow variable target speeds and altitudes.
	Injection	Input parameters which affect how the simulated target will be injected into an image.
Environment	Atmosphere	Input parameters which control the LOWTRAN atmosphere, solar position and how MODTRAN calculations are performed.
	Ocean	Input parameters describing physical properties of the ocean such as swell and parameters which affect how the ocean surface is modeled.
	Cloud	Input parameters specifying clear-sky or a cloud type and the associated cloud parameters

Scene Simulator	Scene Simulator	Input parameters which specify the number and size of the images to be generated by the scene simulator module.
System Performance	Performance	Input parameters which set the number of analytic system performance calculations to perform and the assumptions made about the type of processing to model.
Data Processing	IRAMMP Format Converter	Input parameters for the program which converts image data to HDF format.
	Stream Processing	Input parameters which control the input and behavior of a "stream" of modules, created in a run script.
	Preprocessor	Input parameters for controlling image processing module. Processing options include bias removal, detrend, subpatching.
	Statistical Analysis	Input parameters for the program which does statistical analysis (mean, variance, pdf,...) on images
	Spectral Analysis	Input parameters for the program which does spectral analysis (power spectral density, coherence) on images.
User	User	Parameters for user supplied modules. Several sample user modules are included with IRTool, and their input parameter sets are available to load.
Advanced Flow Control	Advanced Flow Control	Tells modules where to find inputs. Use reserved for experienced users interested in reusing previously calculated results in order to save on run time.

Table 8. Input parameters by category in IRTOOL [After Ref. 16].

The user has the capability to see what modules must be run and in what order for a specific output, by selecting between two options. Those are the Default Run Script and the Advanced Run Script under the Run option menu. These options and also for many other capabilities of IRTOOL will be referred to in the following paragraphs.

In this thesis we used some of the modules but not all of them. We will describe in a little more detail the modules that were used, the specific inputs for those modules and also their outputs.

1. Atmosphere Profiler Module

This module generates the vertical profiles of temperature, humidity, wind speed, refractive index structure parameter, pressure, mixing ratio and many other parameters. The calculation of those profiles is performed with the use of the bulk aerodynamic method and the similarity theory of Monin-Obkhov [Ref. 16]. In order to execute this module we need to enter a specific group of input parameters. Those parameters correspond to the group parameter Environment, and are shown in Table 11.

As we can see from the input parameters in Table 11, there is no input for pressure measurement. IRTOOL also assumes that all the measurements of Temperature, Humidity and Wind speed are made at the same height. This is a deficiency of the program in contrast with IRBLEM, in which for each measurement we must specify the height at which the measurement was made.

When IRTOOL performs MODTRAN calculations it does two things. First, it generates a MODTRAN input file made either from the input menus or a combination of the menus with a custom input file provided from the user. Then using this profile, it performs a sequence of MODTRAN calculations and produces the vertical profiles of the atmospheric parameters. We say vertical because is assumed that we do not have horizontal variations. Also from Table 11 we see that we have the option to select a custom atmosphere. In this case the user must provide his own LOWTRAN file with

measurements of temperature, pressure, and humidity versus height. Those measurements will transform into a LOWTRAN file that will be the basis for the generation of the vertical profiles affecting the refractivity.

Module	**Comments**
Sensor Model	Calculation of sensor transfer function and noise
Engagement	Position of target relative to sensor without ray bending
Atmosphere profiler	Profile of atmospheric boundary layer and Generation of its own LOWTRAN file
Atmosphere without radiance	Calculation of refraction (ray paths to background and target) and atmospheric distortions for the scene and for the target, if present
Atmosphere with radiance	Same as Atmosphere without radiance but also calculates path radiances and transmissivities to background and target
Target Scintillation	Detailed calculation of target scintillation due to atmospheric turbulence
Sky Radiance	Calculates a sky radiance dome as viewed from the surface of the ocean
Cloud Clutter for ESNR	Calculation of cloud PSDs at points in target trajectory
Scene Simulator	Generate images of background and Elevation profiles of the mean and variance
Target Signature	Signature image at target range and look aspect angle
Target Injector	Output scenes with injected target signature
Sensor Effects	Add effects of noise, jitter, and system transfer function to simulated images
System Performance	Analytic estimate of signal to noise ratio
IRAMW Data Format Conversion	Conversion of NATO format to HD
Preprocessor	Variety of options for orienting, subpatching, and processing HDF data
Statistical Analysis	Mean, variance, correlation and probability density estimates from HDF data
Spectral Analysis	PSD and cross spectral density estimate from HDF data

Table 9. IRTOOL module description [After Ref. 16].

Module	Parameter Group Used	Other Modules to Run
Sensor Model	Sensor Type Sensor Polarizer	None
Engagement	Sensor Operation Target Trajectory (Sensor Type and Scene Simulation used for diagnostics)	None
Atmosphere Profiler	Environment	None
Atmosphere Effects	Sensor Type Sensor Operation Environment	Atmosphere Profiler Engagement
Cloud Clutter for ESNR	Sensor Type Sensor Operation Environment Target Trajectory	Atmosphere Profiler Engagement Atmosphere Effects
Sky Radiance	Sensor Type Sensor Operation Environment	Atmosphere Profiler Atmosphere Effects
Scene Simulator	Sensor Type Sensor Operation Environment Scene Simulation	Atmosphere Profiler Atmosphere Effects Sky Radiance (if ocean is in FOV)
Target Signature	Sensor Type Atmosphere Target Type Target Trajectory	Engagement Atmosphere Profiler Atmosphere Effects
Scintillation	Sensor Type Sensor Operation Target Atmosphere	Atmosphere Profiler Atmosphere Effects Engagement
Target Injector	Sensor Type Sensor Polarizer Sensor Operation Atmosphere	Sensor Model Engagement Atmosphere Effects Scintillation Scene Simulator
Data Converter	Data Converter	None
Sensor Effects	Sensor Type Sensor Polarizer Sensor Scene Effects	Sensor Model Scene Simulator Target Injector

Table 10. Inputs used by each module by Parameter Group and Module [After Ref. 16].

PARAMETERTS	COMMENTS
LOWTRAN Atmosphere Type	The user can select one of the six available model atmospheres for the generation of the LOWTRAN file. These Atmospheres are the U.S. Standard Atmosphere, Tropical Atmosphere, Midlatitude Summer Atmosphere, Midlatitude winter Atmosphere, Subarctic Summer Atmosphere, Subarctic Winter Atmosphere and the Custom Atmosphere.
Solar Position	Options: Night or Day. If we select Day then we have to specify the Solar Azimuth and also the Solar Elevation
Constant Flux Surface Layer	Options: On or Off. If we choose On then we produce a constant flux layer with depth specified as Surface Layer Height under the Algorithm Control dialog box
Reference Height in meters	The height above the mean sea level in which measurements of temperature, relative humidity and wind speed were made. Must be between 1-30 meters.
Air Temperature at the reference height	In degrees Celsius
Relative Humidity at the reference height	In percentage (%)
Wind speed at the reference height and 24hr average wind speed	In m/sec
Wind heading	In degrees
ASTD or Water Temperature	In degrees Celsius
Algorithm Control	We specify the surface layer height refraction, the LOWTRAN spectral resolution and also we select the coastal influence parameter (ICSTL) between the values 1-10 and whether we will use refraction or straight geometry.
Ocean parameters	Swell parameters such as rms amplitude, peak frequency, heading etc.
Cloud parameters	Options: Clear Sky or Cloud type. If we select the second one we have to enter the type of the clouds, the cloud base and top altitude, the heading and speed.

Table 11. Required input parameters for the Atmosphere Profiler Module [After Ref. 16].

In this thesis we used for each data set two atmospheres: The midlatitude winter atmosphere and the custom atmosphere, because we would like to investigate how the absence of the pressure entry in input parameters affects the results. A second reason was to see if the "deficiency" of IRTOOL to use only one reference height for all the measurements can alter significantly the refractivity calculated from IRTOOL results. For those reasons we ran for the same entries the NPS Profiler (a bulk aerodynamic model to which we will refer later) and we used its predicted vertical profiles of temperature, pressure and relative humidity as inputs for the generation of the custom profile. The results are shown in the Chapter VII on Data Analysis.

2. Atmosphere Effects Module

This module calculates ray refraction, atmospheric distortions for both the target and the scene, transmissivity and path radiance. After the execution of the ray refraction calculation (description of the rays that arrive at the sensor or target), a number of outputs are available.

The Maximum Intervision Range (MIVR) (absolute limit of detection for a given target height, with respect only to ray refraction and the earth's curvature) with and without refraction (geometrical horizon), geometric results for rays to ocean, cloud and target are some of the outputs of that module. Elevation angles to target, sensor, ocean intercept and cloud intercept are calculated.

Atmospheric effects such as inferior and superior mirages are treated. Effects of atmospheric turbulence (blurring, scintillation) on the target signature based on the refractivity structure constant are also calculated. In addition atmosphere target

magnification and demagnification outputs are also produced. Moreover, if we run this module in the "with radiance" mode, additional outputs of path radiances and transmissivities from sensor-to-target and sensor-to-background are produced. For those calculations IRTOOL uses MODTRAN2 in LOWTRAN mode with a selectable frequency increment. The user has also the option to turn the refraction effects off. In this case all the calculations are based upon the straight ray geometry.

Something that is very useful to the user is the ability of IRTOOL to manage more than one passband. For each of them the module calculates the values for each target solution. This is useful for the prediction of other band-dependent quantities such as path radiance and atmospheric coherence length.

It is not possible to run the atmosphere effects module alone, because the outputs of the Atmosphere Profiler Module and the Engagement Module are required. After the execution of those two modules we must enter a specific group of input parameters. Those parameters are shown in Table 12. Parameters which are shown with an asterisk (*) must be used when we execute the Atmospheric Effects Module in the "with radiance" mode.

3. Engagement Module

The Engagement Module produces a file that describes the motion of the target relative to the sensor as a function of time. The user can specify three different types of trajectories. In the first mode the target is on a collision course with the sensor and moves with constant speed, angle of attack and at constant altitude. This mode has two user-selected options. In the first, the target direction of motion always points at the platform

position, and in the second the target moves to the predicted position of target at the time of collision. In the other two trajectory modes, the user must specify the target trajectory by providing it in an appropriate format. In the first one we have to specify the ground range and bearing from the sensor to the target as a function of time, and in the second one, the user must specify the target velocity as a function of time and an initial position.

PARAMETERS GROUR USED	**PARAMETERS**
Sensor Type	Number of Passbands (min. and max. wavelength) Aperture Diameter Sensor Sampling*
Sensor Operation	Sensor Altitude Sensor Look, Azimuth Sensor Look, Elevation
Environment	Option for refraction or straight ray geometry Solar Azimuth* Solar Elevation* LOWTRAN frequency increment* Swell rms Amplitude Cloud Base Altitude* Cloud Top Altitude*
OUTPUTS NEEDED FROM OTHER MODULES	Atmosphere Profiler Engagement (used if engagement output is available).

Table 12. Required inputs for Atmosphere Effects Module in IRTOOL.

The Engagement Module can be executed alone because it does not require the outputs from other modules. The input parameters required for the successful execution of this module are shown in the Table 13. The trajectory number of points allows us to edit the number of points calculated along the target trajectory. This number affects the execution time of the atmosphere and scintillation modules. Sometimes the user under

certain atmospheric conditions must increase this number in order to obtain reliable results. From [Ref. 2] this number must be over 100 if we want to have adequate results.

PARAMETERS GROUR USED	PARAMETERS
Sensor Operation	Sensor Altitude Sensor Look, Azimuth Sensor Look, Elevation Sensor Platform Speed Sensor Platform Heading
Target Trajectory	Trajectory Mode Target Maximum Range Target Minimum Range Target Altitude Target Speed Target Angle of Attack Initial Bearing to Target Trajectory # of points

Table 13. Required inputs for the Engagement Module in IRTOOL.

D. RUNNING OPTIONS

The Run menu allows us to select sequences of operations (each operation is performed by an entity called a module), referred to as run script. Each run script corresponds to a specific set of input parameters in memory and the selected modules. A job script contains one or more run scripts that run sequentially in the background.

Under the run menu the user can select between three commands. The Default Run Script, the Advanced Run Script and the Any Order Run Script.

In the Default Run Script, which is output oriented, the user selects an output and IRTOOL determines what calculations need to be performed. A list of modules runs with

the present set of input parameters. The advanced and any order run scripts are based on modules, where each module is responsible for doing a different set of calculations. The most common use for those run scripts is to perform data analysis or processing [Ref. 16]. In the advanced run script the user chooses what modules are run. The modules will run in the order that they appear. In the any order run script which also contains a series of modules selected by the user, the modules can be run in any order determined by the user. For the last two cases we must have in mind the dependencies between the different modules.

For this research we used mostly the default run script "Engagement (geometric), Atmosphere and Ray Refraction". In some cases we used the Advanced run script, especially when we had to use a LOWTRAN file created by the user (custom atmosphere). Table 14 shows which default run script we should use in order to get the desired output. The input parameters that we used for the default run script "Engagement (geometric), Atmosphere and Ray Refraction" are shown in the Tables 11, 12 and 13.

E. IRTOOL CONVENIENCES

IRTOOL contains user friendly interactive IDL programs for constructing inputs needed by it or for analysis of its results. These conveniences are found under the Toolbox menu. The IDL routines are used for the graphs and image display and printing, for editing the surface layer generated by the Atmosphere module, for converting measured profiles of temperature, pressure and relative humidity to a LOWTRAN file usable by IRTOOL, for adding our own interactive applications and other applications.

Desired Output	Input Parameter Groups	Default Run Script
Sensor characterization (transfer functions, blip noise, point spread function)	Sensor	Sensor
Estimate of system Performance	Sensor Sensor operation Target Trajectory Environment Scene Simulator System Performance Algorithm Control	Estimated Signal to Noise Ratio
Marine Boundary Layer profile	Environment	Atmosphere Profiler
Maximum Intervision Range, boundary profiles and horizon location	Sensor Sensor operation Environment Algorithm Control	Atmosphere and Ray Refraction (horizon location)
Location of target with refraction	Sensor Sensor operation Target Trajectory Environment Algorithm Control	Engagement (geometric), Atmosphere and Ray Refraction
Simulated images of background without sensor noise, jitter, or blur	Sensor Sensor operation Environment Scene Simulator Algorithm Control	Simulated Scene-w/o Sensor Effects
Simulated images of background with sensor noise, jitter, and blur	Sensor Sensor operation Environment Scene Simulator Sensor Effects Algorithm Control	Simulated Scene-with Sensor Effects
Images of target and simulated background without sensor noise, jitter or blur	Sensor Sensor operation Target Trajectory Environment Scene Simulator Target Injection Algorithm Control	Simulated Scene-w/o Sensor Effects, with target

Images of target and simulated background with sensor noise, jitter and blur	Sensor Sensor operation Target Trajectory Environment Scene Simulator Target Injection Sensor Effects Algorithm Control	Simulated Scene-with Sensor Effects, with target
HDF data from NATO data	IRAMMP Data Format Conversion	Data Analysis-IRAMMP Data Format Converter
Reoriented, subpatched or processed HDF data	Data Preprocessor	Data Analysis-Preprocessor
Mean, variance, correlation and probability densities from HDF data	Data Statistics	Data Analysis-Statistics
PSDs and cross spectral densities from HDF data	Data Spectral	Data Analysis-Spectral

Table 14. Inputs and Outputs for Default Run Scripts in IRTOOL [From Ref. 16].

F. OUTPUTS

IRTOOL's modules produce either line plot or image data files. The line plot files are ASCII files with the extension ".plt". They are readable and can be displayed. The image data files are in HDF format and have the file name with the extension ".img". Except those two files, IRTOOL generates error (.err extension) and log (.log) files. The error files can help the user to locate a problem that caused the module to terminate its calculations. The log files contain information about what the module did.

G. NPS PROFILER

The NPS profiler is a bulk aerodynamic Marine Boundary Layer (MBL) program which uses Monin-Obkhov similarity theory. It was created by the Meteorological

Department of the NPS and was provided by Prof. K.Davidson. The program is written in MATLAB programming language.

The meteorological parameters required by this program are air temperature, sea temperature, atmospheric pressure, wind speed, relative humidity and the heights where these measurements were made. The output is the vertical profiles of the above parameters.

We used the NPS atmosphere profiler because this code requires the measurement height for each input parameter in contrast with IRTOOL, that requires only one reference height, assuming that all measurements were taken at the same height. But as we will see from the database of the MAPTIP trial (Table 17) for some datasets this was not the case.

V. MODEL ALGORITHMS FOR REFRACTIVITY

A. INTRODUCTION

Variations of pressure, air temperature and partial pressure of the various gases in the atmosphere, with most important the water vapor due to its variation with height, cause the refraction of the EM waves. In order to model the refractivity effects in the atmosphere a method is required to determine the vertical profiles of temperature, water vapor pressure (or relative humidity) and total pressure.

B. IRBLEM

The L(W)WKD is a marine boundary layer (MBL) model which calculates the above mentioned profiles based on the similarity (scaling) theory of Monin and Obukhov [Ref. 17]. This model requires measurements of the water temperature, the air temperature, the water vapor pressure (or relative humidity), the total pressure and wind speed. The fact that the above quantities vary principally with height, allow us to express the refractive index as a function only of height, neglecting any horizontal variations.

The refractivity profile and its first derivative can be determined by the following equations assuming that the atmosphere has only two components, a dry air contribution and a water vapor contribution. From [Ref. 17, Ref. 18]

$$n(\lambda, h)=1+R(\lambda, h)\times 10^{-6} \tag{23}$$

$$R(\lambda, h)=\frac{A(\lambda)P_{\alpha}(h)}{T(h)}+\frac{B(\lambda,T)V_{p}(h)}{T(h)} \tag{24}$$

The first derivatives of the above equations are given by:

$$n'(\lambda, h)=\frac{dn(\lambda,h)}{dh}=R'(\lambda,h)\times 10^{-6} \tag{25}$$

$$R'(\lambda, h)=\frac{dR(\lambda,h)}{dh}=\frac{(AP'_{\alpha}(h)+BV'_{p}(h)-R(\lambda,h)T'(h))}{T(h)} \tag{26}$$

where n is the index of refraction

n' is the vertical gradient of the index of refraction (dimensionless)

R is the refractivity (dimensionless)

R' is the vertical gradient of the refractivity in units/meter

λ is the wavelength in micrometers

h is the height above the mean water level (MWL) in meters

P_{α} =P-V_p is the dry air atmospheric pressure (mbars)

P is the atmospheric pressure (mbars)

V_p is the water vapor pressure (mbars)

T is the air temperature (^{o}K)

A (λ) is a coefficient given by Edlen [Ref. 18] for the dry air contribution

B (λ,T) is the coefficient for the water vapor contribution

$P'_{\alpha}(h)$ is the gradient of the dry air pressure in mbars/meter

$T'(h)$ is the gradient of the temperature and

$V'_p(h)$ is the gradient of the water vapor pressure.

From [Ref. 18] the coefficients A and B can be assumed constants for the visible, near infrared, mid infrared, and far infrared. Table 15 gives the values of those coefficients for these bands.

Wavelength Band	**Range (μm)**	**A (K/mbar)**	**B (K/mbar)**
Visible	0.5-1	78.5	67.0
Near Infrared	1-3	77.7	65.0
Mid Infrared	3-5	77.5	65.0
Far Infrared	8-12	77.5	40.0
RADAR	<20 GHz	77.6	373400/T

Table 15. Values for the coefficients A, B (given by Edlen) that are used in IRBLEM for the calculation of refractivity [From Ref. 18].

With the use of the Table 15, Eq. (26) for the four wavebands can be written as:

Visible:
$$\frac{dR(\lambda,h)}{dh} = \frac{78.5}{T}\frac{dP}{dh} - \frac{78.5P}{T^2}\frac{dT}{dh} - \frac{11.5}{T}\frac{dV_p}{dh} + \frac{11.5V_p}{T^2}\frac{dT}{dh} \quad (27)$$

Near Infrared:
$$\frac{dR(\lambda,h)}{dh} = \frac{77.7}{T}\frac{dP}{dh} - \frac{77.7P}{T^2}\frac{dT}{dh} - \frac{12.2}{T}\frac{dV_p}{dh} + \frac{12.2V_p}{T^2}\frac{dT}{dh} \quad (28)$$

Mid Infrared:
$$\frac{dR(\lambda,h)}{dh} = \frac{77.5}{T}\frac{dP}{dh} - \frac{77.5P}{T^2}\frac{dT}{dh} - \frac{12.5}{T}\frac{dV_p}{dh} + \frac{12.5V_p}{T^2}\frac{dT}{dh} \quad (29)$$

Far Infrared:
$$\frac{dR(\lambda,h)}{dh} = \frac{77.5}{T}\frac{dP}{dh} - \frac{77.5P}{T^2}\frac{dT}{dh} - \frac{37.5}{T}\frac{dV_p}{dh} + \frac{37.5V_p}{T^2}\frac{dT}{dh} \quad (30)$$

C. IRTOOL

The Atmosphere Profiler Module using the bulk method and the Monin-Obukhov similarity theory produces the profiles of the index of refraction both in the surface layer and also in the region above it [Ref. 11]. Assuming again no horizontal variations, the index of refraction is given by $n = 1 + R\times10^{-6}$, where R is the refractivity and from [Ref. 11]

$$R = R_c + R_a \tag{31}$$

where R_c is the continuum value and

R_a is the contribution from anomalous dispersion by infrared resonances such as

H_2O, CO_2, O_3 etc with the more important being the contribution of water. According to the same reference "In the atmospheric H_2O transmission windows the anomalous dispersion can be neglected." Under this assumption Eq. 31 becomes

$$R \approx R_c \tag{32}$$

The continuum value of refractivity is given by [Ref. 19] as

$$R_c = R_d + R_w \tag{33}$$

where R_d is the contribution from dry air and

R_w is the contribution of water vapor.

From [Ref. 11] and [Ref. 19] the value of R_d and R_w is given by:

$$R_d = \frac{0.3789P(h)}{T(h)} R_0[1 + (5.337 - 0.0157T(h)) \times 10^{-6} P(h)] \quad (34)$$

with $$R_0 = 64.328 + \frac{29498.1}{146 - \lambda^{-2}} + \frac{255.4}{41 - \lambda^{-2}} \text{ and} \quad (35)$$

$$R_w = -1.765 \times 10^{-18}(1 - 0.0109\lambda^{-2})Q(h) \quad (36)$$

where P is the total atmospheric pressure in Torr

T is the temperature (^{0} K)

R_0 is the value of refractivity at a temperature of 15 ^{0}C and pressure of 760 Torr (1 atm)

λ is the wavelength in micrometers and

Q is the concentration of water vapor in molecules/cm^3.

For atmosphere modeling IRTOOL assumes that the slight wavelength dependence in Eqs. 35, 36 and also the small temperature and pressure dependence within the square bracket in Eq. 34 can be neglected. Under those assumptions the Eqs. 34, 35, 36 simplified further and can be written as:

$$R_d = \frac{0.3789P(h)}{T(h)} R_0 \quad (37)$$

$$R_w = -1.765 \times 10^{-18} Q(h) \quad (38)$$

$$R_0 = 272.599 \text{ (IRTOOL uses the value 272.7)} \quad (39)$$

Finally the refractivity is given by:

$$R(h)=0.3789\frac{P(h)}{T(h)}R_0-1.765\times10^{-18}Q(h)=103.326\frac{P(h)}{T(h)}-1.765\times10^{-18}Q(h) \qquad (40)$$

Using the Avogadro constant and the fact that the coefficients in Eqs. 34 through 40 have the units necessary to make the equations dimensionless we can rewrite Eq. 40 as:

$$R(h)=77.5\frac{P(h)}{T(h)}-59Q \qquad (41)$$

where P is the total pressure in mbars

T is the temperature in ^{0}K and

Q is the water vapor concentration in kg/m^3.

The ideal gas law relates the water partial pressure V_p to concentration Q by:

$$V_p=Q\frac{R_m}{FM(H_2O)}T \qquad (42)$$

where V_p is the water vapor partial pressure in Nt/m^2

$R_m=8.314\ \frac{J}{(mole)(K)}$ is the universal gas constant

$FM(H_2O)=0.018\frac{kg}{mole}$ is the formula mass of the water and

T is the temperature in degrees Kelvin.

With the use of Eq. 42 we can write Eq. 41 as:

$$R(h) = 77.5\frac{P(h)}{T(h)} - 12.7735\frac{V_p(h)}{T(h)} \tag{43}$$

where the pressures P and V_p are given in mbars and the temperature T in ^{0}K.

The first derivative of refractivity is given by:

$$\frac{dR(h)}{dh} = \frac{77.5}{T}\frac{dP}{dh} - \frac{77.5P}{T^2}\frac{dT}{dh} - \frac{12.7735}{T}\frac{dV_p}{dh} + \frac{12.7735V_p}{T^2}\frac{dT}{dh} \tag{44}$$

The vertical profiles of the parameters in Eq. 44 are calculated from the Atmosphere Profiler module of IRTOOL.

Here, we must point out that for the calculation of refractivity IRTOOL does not take into account the wavelength. That means that IRTOOL does not model dispersion (i.e., different index of refraction for different bands). So, there is no difference between the ray refraction output at visible, MWIR or LWIR. In contrast in IRBLEM the wavelength is taken into account through the coefficients A and B. The use of the passband in IRTOOL input parameters, as we showed in Chapter IV, is only for band dependent parameters as for example the coherence length (r_o).

Under the assumption that the earth may be represented by a sphere, Snell's law which describes the ray refraction in the atmosphere can be written [Ref. 20] as:

$$\frac{d}{ds}(nr\cos\beta) = 0 \tag{45}$$

where n is the refractive index at a point

r is the distance of that point from the earth's center and

β is the angle between a particular ray and the local horizon plane (Figure 17).

Using polar coordinates, the trajectory of the ray can be described with the use of the following trigonometric relation

$$\tan\beta = \frac{d\ln r}{d\vartheta} \tag{46}$$

With the use of Eqs. 45 and 46 we have that

$$\mathrm{d}\beta = \frac{d\theta}{n}(r\frac{dn}{dr} + n) \tag{47}$$

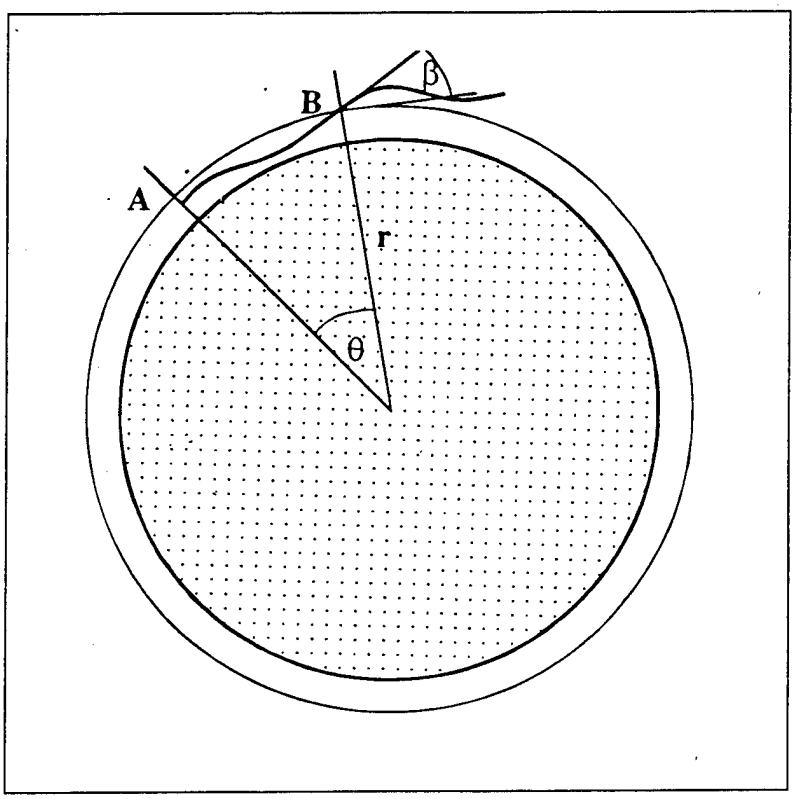

Figure 17. Ray Geometry used in the ray-tracing program of IRTOOL [After Ref. 20].

In order to calculate the ray trajectory in the form $r(\theta, \beta_0)$ where β_0 is the value of β for a specific ray when $\theta = 0$, we use the Runga-Kutta numerical integration method [Ref. 21] in Eqs. 46 and 47. After the calculation of the ray trajectory we face the problem of if and where a refracted ray actually intercepts the ocean. The ocean surface supports waves and in order to take them into account in the calculation, IRTOOL uses the significant wave height H_s or a nominal 0.2 meters whichever is greater [Ref. 11]. The significant wave height is taken to be equal to four times the rms surface elevation and is related to wind speed by an approximate relation [Ref. 11, Ref. 22]

$$H_s = 0.021u^2 \tag{48}$$

Where u is the wind speed in m/sec at 10 m height. If in addition we have a swell then Eq. 48 is modified and becomes

$$H_s = 0.021[u^2 + (swell)^2] \tag{49}$$

This is the cut-off height above the sea surface that will stop all the rays.

THIS PAGE INTENTIONALLY LEFT BLANK

VI. EXPERIMENTAL ARRANGEMENT AND PROCEDURE

A. INTRODUCTION

In 1993 and specifically from October 18 to November 3 the MAPTIP (Marine Aerosol Properties and Thermal Imager Performance) trial was held on the coast of The Netherlands. It was sponsored by RSG 8 of NATO's panel 4 and the principal goals of the trial were to study the performance of imaging systems within the marine boundary layer (MBL) and also the concentrations and properties of marine aerosols [Ref. 18]. After the trial some preliminary results were presented during the first workshop in Oslo, Norway (May 94) by most of the participating countries. The participants also agreed to create a number of working groups so as to jointly study and combine their results. Each group had a specific job to do and one of them was made responsible for analyzing and combining the results of the various refraction measurements. The coordinator of this group that was named the "Refractive Effects in the Visible and IR'' was chosen to be Dr. Forand from DREV (Canada) [Ref. 14].

B. EXPERIMENTAL TECHNIQUES

During the MAPTIP trial there were used two different experimental methods. In the first, a number of observation devices, namely visible and IR cameras, were placed at known heights at a beach station and a spatial array of radiation sources was placed at different known heights above the MWL on a platform located at a specific distance from the beach station. This arrangement was used for the comparison of the observed angles

between the various sources with both the geometric angles between the sources and those predicted by the models that are to be compared. In this way, keeping the range constant, the refractive effects of varying the height of the observers or the sources (Height Scan) could be studied.

In the second method, the same beach station was used while the radiation sources were placed on a moving platform such as a ship. In this way, the elevations of the observers and the sources were kept constant, while the range between the station and the ship was continuously varied (Range Scan). This method was used for the recording of two parameters. The first is the Maximum Intervisibility Range (MIVR) which is the range at which a source at a particular height disappears below the horizon, and the second is the Minimum Mirage Range (MMR) which is the minimum range at which a mirage (if there is one) of a particular source begins to be observed.

C. THE EXPERIMENTAL SETUP

Figure 18 shows the geographical location of the beach station at Katwijk from which the observed data were taken (WPB), the location of the Meetpost Noordwijk (MPN) platform (WPN), the various waypoints (labeled from A to G) and the tracks (marked by the solid lines) followed by the Hr. Ms. Tydeman. Figure 19 shows the beach station at Katwijk and the positions of the different cameras that were used during the experiment. The cameras were placed at different heights above mean water level and their types and characteristics are summarized in Table 16. The stationary platform (Figure 20) was fixed at a specific distance (10.4 km) from the beach station and eight

500W halogen lamps were mounted to the platform structure at heights from 3.57 m to 19.84 m above the mean water level. The lamps (targets) were also spaced horizontally so as to minimize any possible overlap of the recorded images and secondary images. Finally, for the second technique the Hr. Ms. Tydeman was used as a moving platform and the layout of the sources is shown in Figure 21. Six 500W halogen lamps were mounted at various heights from 3.34 m to 20.7 m above the water level at the stern of the ship. The ship was asked to steer in a straight course away from the shoreline while a series of visible/IR cameras located on the beach station were used to record the refraction effects.

D. THE MAPTIP REFRACTION DATASET

Thirty events were observed during the MAPTIP experiment. Thirteen of those, labeled from A to M, referred to Hr. Ms. Tydeman (ship tracking events) and the remaining seventeen referred to the stationary MPN platform (MPN observation events). The large dataset consists of video recordings obtained with the cameras we mentioned above. The data starting with the letter "T" referred to the ship and those which start with the letter "P" referred to the platform.

The weather conditions were also obtained using a weighted average from measurements taken by different participants in the trial. Due to the large dataset it was decided that only a portion of the events would be studied in great detail. This subset consists of six sets of data. Each set of data consists of a ship tracking event and two MPN observation events taken before and after the ship event. The weather conditions

and especially the water temperature, air temperature, relative humidity, air pressure, wind speed and direction, water level with respect to MWL (tide height), $H_{1/3}$ wave height, solar radiation, rain rate and the heights of the sensors at which those conditions were measured are given in Table 17. From this table, we observe that the ASDT (Air to Surface Difference Temperature) is negative. That means that the MBL (Maritime Boundary Layer) is unstable and sub-refractive and so various mirage phenomena are expected to occur. Finally Table 18 shows the cameras that were used for each of the events and their heights above the mean water level.

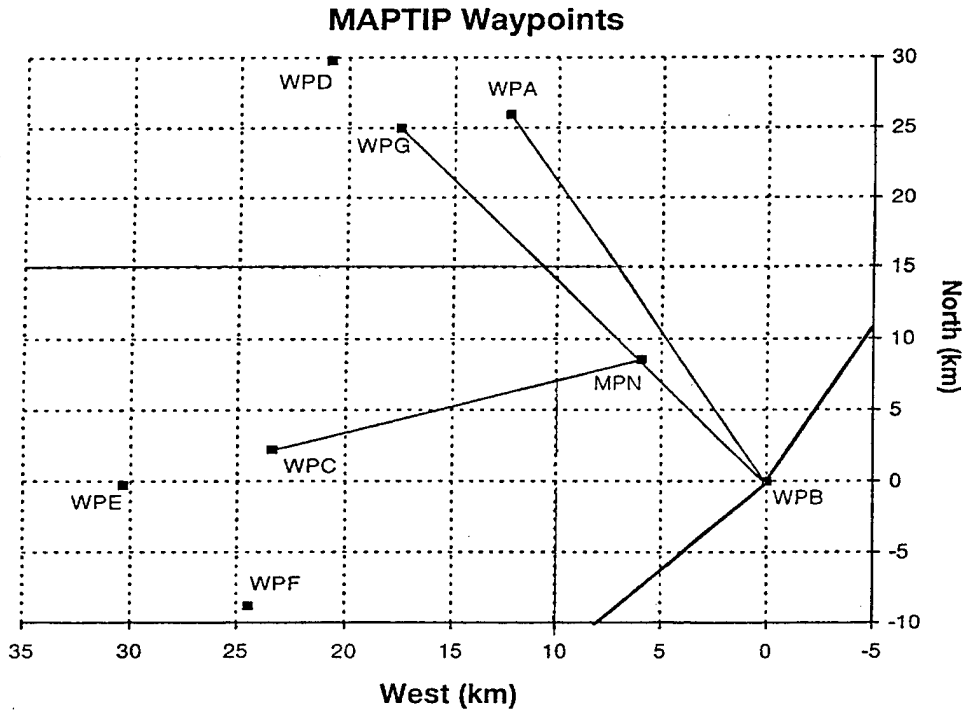

Figure 18. Map of the geographic location of the MPN and the various waypoints with respect to the Beach House at Katwijk and the tracks followed by the Hr. Ms. Tydeman [From Ref. 17].

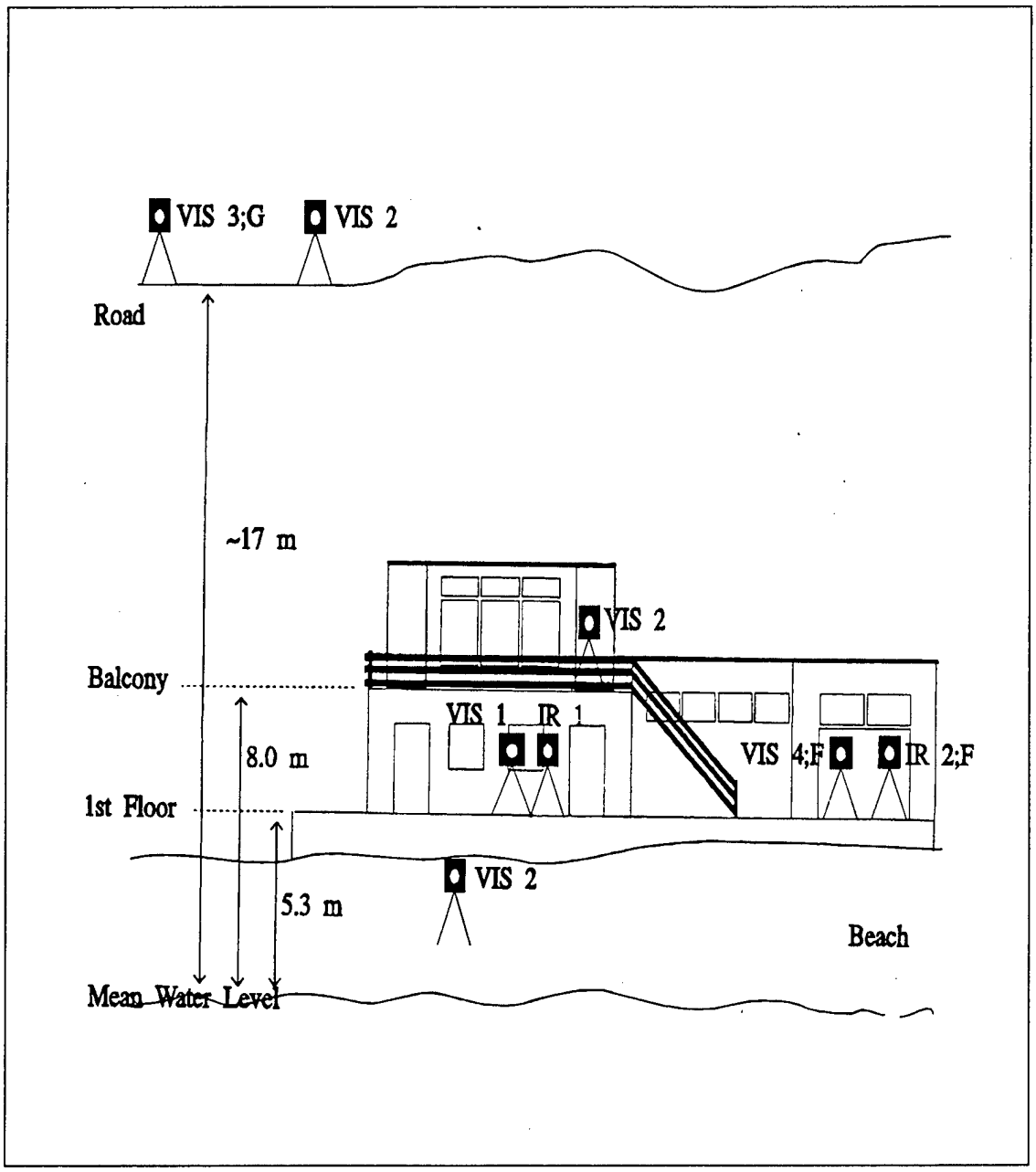

Figure 19. Schematic diagram of the beach station showing the location of the various cameras during the MAPTIP trial [From Ref. 17].

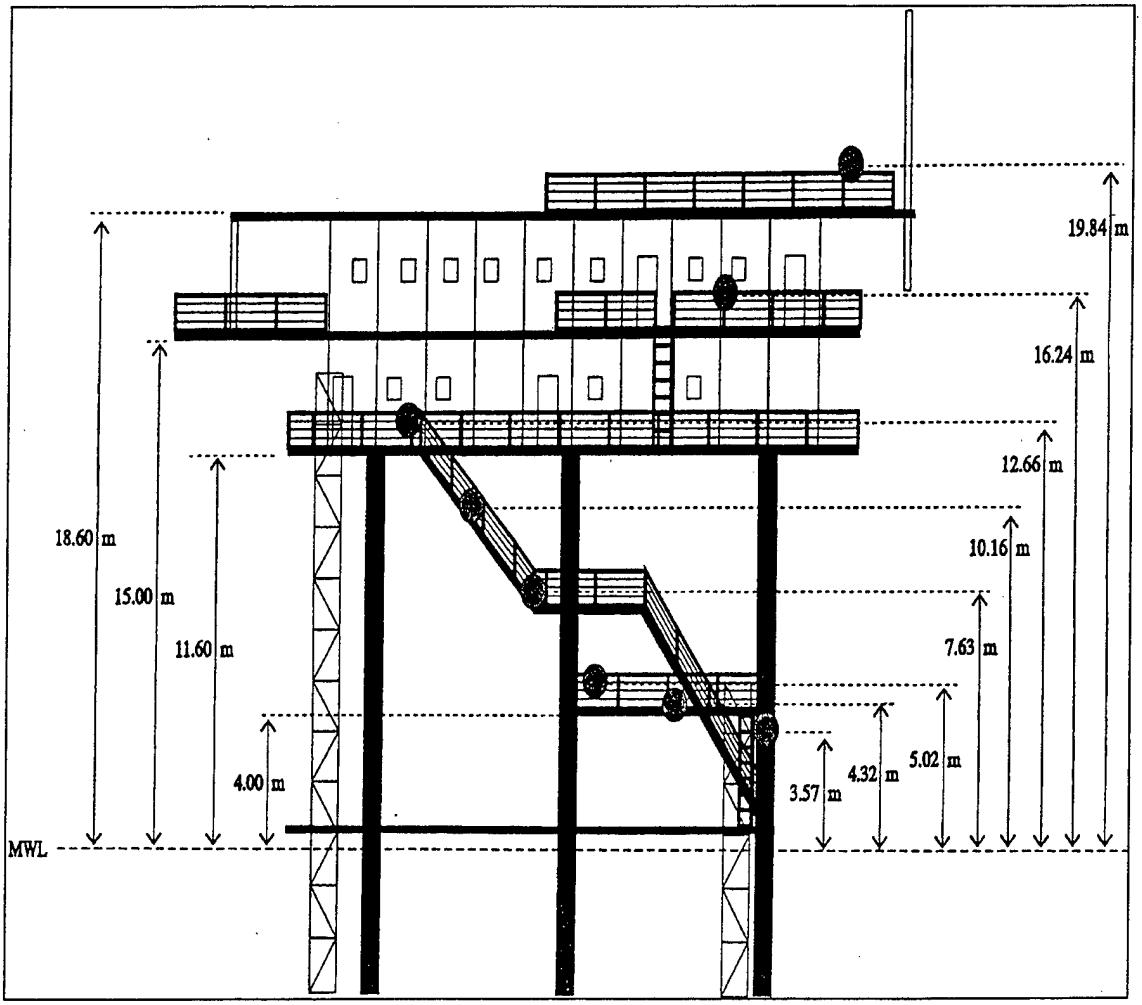

Figure 20. Schematic diagram of the MPN platform showing the placement of the eight 500 Watt halogen lamps [From Ref. 17].

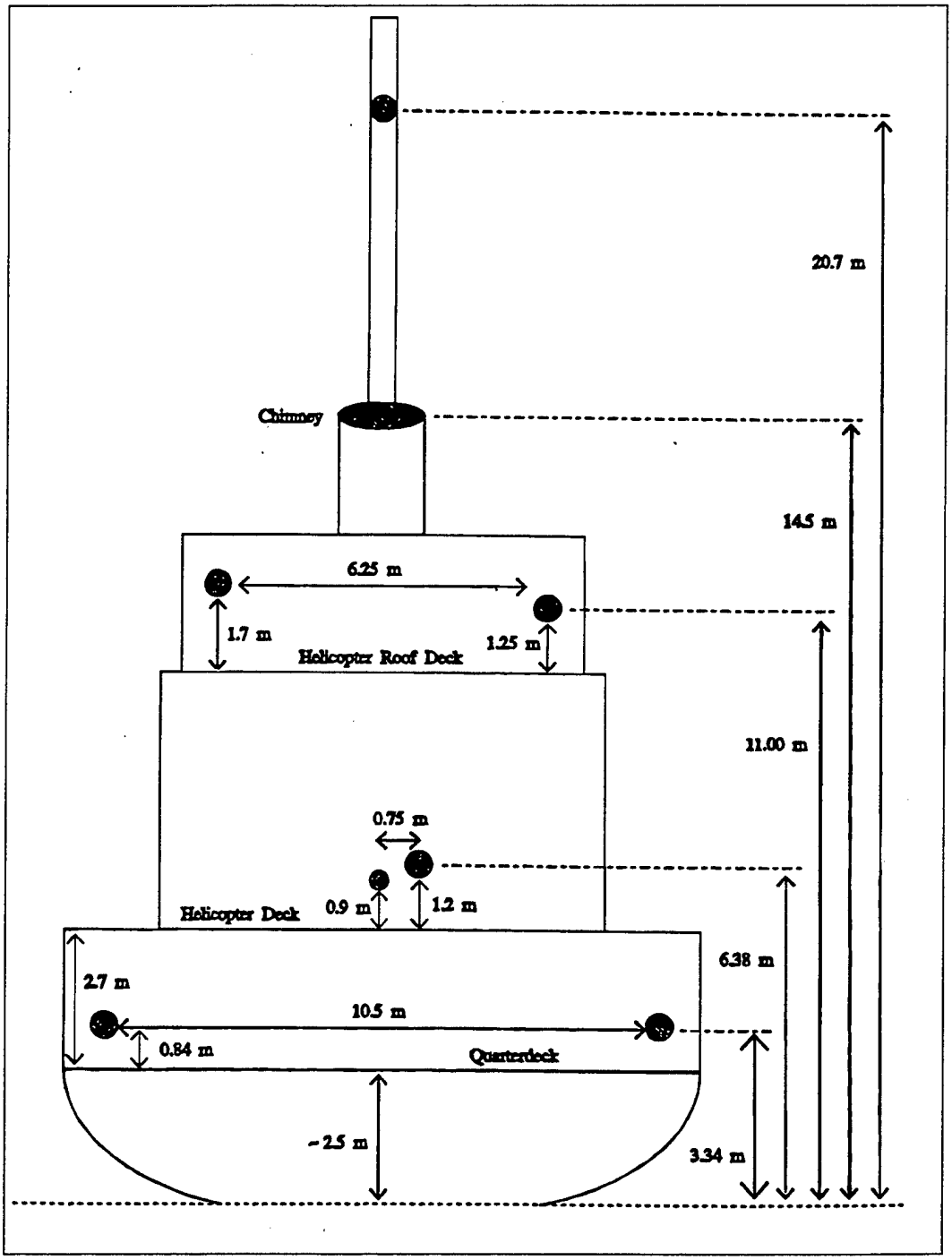

Figure 21. The Hr. Ms. Tydeman with the placement of the six halogen lamps, the exhaust stack and the stern light 0.9 m above the helicopter deck [From Ref. 17].

Camera	Country	Type	Wavelength (μm)	Resolution (μrad/pixel)
V1	Canada	Sony CCD	>0.85	6.23 ± 2%
V2	Canada	Sony CCD	>0.715	9.15 ± 2%
IR1	Canada	Mitsubishi	3-5	9.91 ± 2%
V3; G	Germany	CCD	Visible	11.94 ± 2%
V4; F	France	Sony CCD	Visible	161 ± 5%
IR2; F	France	Castor	8-12	139 ± 5%
IR3; F	France	Mitsubishi	3-5	468 ± 5%

Table 16. Types and characteristics of the visible and infrared cameras that were used during the MAPTIP trial [After Ref. 17].

	SET 1			SET 2			SET 3		
Parameters	**P-F2**	**T-B***	**P-F3**	**P-I3**	**T-D***	**P-I4**	**P-J2**	**T-E**	**P-J5**
Date (dd-mm-yy)	20-10-93	20-10-93	20-10-93	22-10-93	22-10-93	22-10-93	22-10-93	22-10-93	22-10-93
Start (hh:mm)	7:29	7:25	8:12	14:46	14:45	15:33	20:22	20:45	21:59
Stop (hh:mm)	7:34	8:25	8:19	14:51	15:40	15:36	20:24	21:55	22:01
Water Temp. (C)	12.7	12.5	13.1	12	12.4	12.3	12	12.4	12.1
Ht. of Sensor 1 (m)	12	12	12	3.4	3.4	3.4	3.4	3.4	3.4
Air Temp. (C)	8.3	8.4	8.6	9.2	9.1	8.9	7.4	7.4	7
Rel. Humidity (%)	65	65	64	69	72	73	79	76	73
Air Pressure (mbar)	1026	1026	1026	1026	1025	1026	1028	1027	1027
Ht. of Sensor 2 (m)	22.6	22.6	22.6	3.4	3.4	3.4	3.4	3.4	3.4
Wind Speed (m/s)	4.5	5	6.2	10	9.8	10	9	9.1	9.5
Wind Direction (deg)	287	280	210	60	50	45	62	60	60
Water Level (m)	0.44	0.33	0.13	-1.02	-1.02	-1.02	0.5	0.32	0.13
Wave Height (m)	0.18	0.17	0.16	0.98	0.98	1	0.94	0.91	0.86
Solar Radiat. (W/m2)	80	70	70	42	30	15	0	0	0
Rain Rate (mm/10min)	0	0	0	0	0	0	0	0	0
ASTD (C)	-4.4	-4.1	-4.5	-2.8	-3.3	-3.4	-4.6	-5	-5.1
	SET 4			**SET 5**			**SET 6**		
Parameters	**P-M1**	**T-F**	**P-M2**	**P-M9**	**T-G**	**P-M10**	**P-P2**	**T-K**	**P-P3**
Date (dd-mm-yy)	25-10-93	25-10-93	25-10-93	25-10-93	25-10-93	25-10-93	28-10-93	28-10-93	28-10-93
Start (hh:mm)	3:17	3:35	4:50	14:53	15:40	16:34	8:08	8:35	9:18
Stop (hh:mm)	3:18	4:40	4:53	14:55	16:25	16:37	8:10	9:35	9:24
Water Temp. (C)	11.6	11.6	11.6	11.6	11.5	11.5	11.6	11.7	11.7
Ht. of Sensor 1(m)	3.4	3.4	3.4	3.4	3.4	3.4	3.4	3.4	3.4
Air Temp. (C)	10.8	11	11	10.2	10.3	10	8.9	9.2	9
Rel. Humidity (%)	72	73	74	76	77	77	80	80	78
Air Pressure (mbar)	1028	1030	1029.5	1031	1031	1031	1027	1027	1027
Ht. of Sensor 2 (m)	3.4	3.4	3.4	3.4	3.4	3.4	3.4	3.4	3.4
Wind Speed (m/s)	8	7.3	7.5	7	8.2	7	4.8	4.1	4.1
Wind Direction (deg)	30	25	30	40	30	35	70	82	80
Water Level (m)	-0.47	-0.51	-0.53	-0.67	-0.78	-0.78	-0.75	-0.79	-0.79
Wave Height (m)	0.9	0.92	0.97	0.91	0.93	0.92	0.51	0.51	0.51
Solar Radiat. (W/m2)	0	0	0	20	5	0	50	75	90
Rain Rate (mm/10min)	0	0	0	0	0	0	0	0	0
ASTD (C)	-0.8	-0.6	-0.6	-1.4	-1.2	-1.5	-2.7	-2.5	-2.7
Note: * -WPC course									

Table 17. The dataset (events and their associated meteorological conditions) that was used for the purposes of analysis [From Ref. 17].

Events	Visible 1 Camera (Canada)	Visible 2 Camera (Canada)	IR1 (3-5) Camera (Canada)	Visible 3 Camera (Germany)	Visible 4 Camera (France)	IR2 (8-12) Camera (France)	IR3 (3-5) Camera (France)
P2010F2	7.04 m						
P2010F3	7.04 m						
T2010B		6.44 m	6.89 m				
P2210I3	7.04 m			20 m			
P2210I4	7.04 m						
T2210D		6.39 m	7.04 m				
P2210J2	7.04 m	8.91 m		20 m			
P2210J5	7.04 m	8.91 m					
T2210E	7.04 m						
P2510M1	7.04 m	3.85 m	7.04 m				
P2510M2	7.04 m	3.85 m	7.04 m				
T2510F	7.04 M	8.83 m	7.04 m	20 m	6.63 m	6.79 m	6.71 m
P2510M9	7.04 m	3.85 m	7.04 m				
P2510M10	7.04 m	3.85 m	7.04 m				
T2510G	7.04 m	3.85 m	7.04 m		6.63 m	6.79 m	6.71 m
P2810P2	7.04 m	3.85 m					
P2810P3		3.85 m	7.04 m				
T2810K	7.04 m	3.85 m	7.04 m	20 m	6.63 m	6.79 m	6.71 m

Table 18. The cameras that were used for each of the events during the MAPTIP trial and their heights above the mean water level [After Ref. 18].

VII. DATA ANALYSIS

A. INTRODUCTION

A comparison of IRBLEM with the French model PIRAM, using the same database shown in Table 17, was described in 1997. The results were very satisfactory for both but better for IRBLEM [Ref. 17].

In 1998, an effort was made to compare IROOL, IRBLEM and PIRAM under the same set of input conditions [Ref. 2]. The ship tracking events of the MAPTIP experiment were used and the analysis showed that IRTOOL produces MMRs at greater ranges than both the observed ones and those predicted from the other two models. As is known, for a target at a constant altitude under subrefractive conditions a mirage appears only when this target is in a specific range zone limited by the MMR and MIVR. When the MMR moves towards greater ranges the range zone gets narrower. As a result, some of the targets that were in the range zone before, may be now out of it and mirages will not be predicted for them. So, we expect that IRTOOL may not predict mirage for some targets for which mirages were found experimentally. As mentioned in Chapter I, Forand at DREV applied IRTOOL to data obtained off the Netherlands coast in the MAPTIP measurements in 1993 and concluded that IRTOOL did not predict mirage in cases in which they were found experimentally (L. Forand, private communication). According to the discussion above, this opinion is in agreement with the results that were obtained during the analysis in [Ref. 2].

B. DATA ANALYSIS

In this chapter we will compare the IRTOOL and IRBLEM models and also we will examine again the capability of IRTOOL for producing mirage effects, using the database shown in Table 17.

The appearance of the mirage effects depends on refractivity. For that reason we will examine the profile of refractivity as it is produced from the two models. Also we will examine the profiles of temperature, humidity and pressure because refractivity depends on those profiles. We will discuss any differences in the results and we will make suggestions for IRTOOL such as to improve its results and to get the best fit agreement with the experimental data.

In order to be consistent with the previous two analyses we will use the IRBLEM program as it was used in [Ref. 18] and instead of extrapolating the results from that reference as was done in [Ref. 2] we will run the IRBLEM code. According to [Ref. 18] IRBLEM and PIRAM were employed using a wave height equal to 1.3 times the measured $H_{1/3}$ wave height (the "significant wave height") and also equal to 1.0 times the measured $H_{1/3}$. Moreover, in the analysis both modes of the refraction module of IRBLEM were used, the "wavy" (L(W)WKD) and the "non-wavy" mode (LWKD). The conclusion was that the combination of a wave height equal to 1.3 times the measured wave height with the non-wavy mode produces results closer to the observed data [Ref. 17]. So, in our analysis we will use those conditions. After the completion of the data analysis it will possible to compare all the models (IRTOOL, IRBLEM, and PIRAM) using the results from this thesis and the results from [Ref. 18]. The results of our analysis

are presented here referenced by the "Event index", referring to the measurements of the MAPTIP experiment.

Before we proceed, it is very important to note that the wave height in Table 17 is the measured $H_{1/3}$ wave height and not the rms wave height [Ref. 18]. For that analysis all the heights we will refer to are above the water level (i.e., the height of the tide is taken into account). The height of the tide is also shown in the Table 17 (water level). Events starting with the letter P refer to the stationary platform and those with the letter T refer to the moving platform (ship).

1. P2010F2

The conditions under which this event took place are shown in Table 17. The camera used was the visible (V1) camera positioned at height h_s = 6.6 m above the water level. The comparison of the computations for this event is shown in Figure 22, where the solid line with the circles represents a non-refractive atmosphere, the squares represents the observed data, the rhombus represents the prediction from the IRBLEM code and the triangles the data predicted from the IRTOOL code. As we can see, IRBLEM predicts mirages for the same targets as the experimental data, while IRTOOL does not predict the mirage for the target at 7.19 m and also does not detect the target at 3.13 m. We can also observe that any target below $\approx$ 3 m will not be detected from IRBLEM. This height increases to $\approx$3.5 m for IRTOOL. For a non-refractive atmosphere any target below $\approx$0.5 m should be below the horizon. Finally, the shape of the curves that both models produce

deviates from the observations in the region of their cusps. It is also clear from Figure 22 that the results predicted from IRBLEM are much better than from IRTOOL.

As we have already mentioned in Chapter IV, IRTOOL does not use the measurement of pressure as an input parameter even though the pressure is used in the calculation of refractivity (Eqs. 43, 44). The same model also assumes that all the measurements of temperature, humidity, pressure and wind speed are made at the same height. From Table 17 the air temperature and humidity were measured at 12 m while the anemometer was placed at a height of 22.6 m. For those two reasons we used the atmosphere profiler of IRTOOL to create a custom profile. This profile was created using the NPS profiler in IRTOOL, in which the pressure is an input and also requires the measurement height for each parameter. In Figures 23A, 23B, 23C we see the profiles of humidity, temperature and pressure generated from the atmosphere profiler module of IRTOOL using the midlatitude winter atmosphere (symbol "x") and the custom atmosphere (symbol "o"). The generation of this custom atmosphere was made as follows:

First, we run the NPS profiler with the same input parameters to create the profiles of temperature, relative humidity, pressure and wind speed. These profiles are then used in conjunction with the Atmosphere Shaper under the Toolbox menu of IRTOOL to produce the custom atmosphere. In Figures 23A, 23B, 23C are also shown the profiles as they were calculated from the LWKD refraction model of IRBLEM (solid line). In Figure 23A (humidity profile) we see no difference between the profiles except that at the surface the relative humidity calculated from IRBLEM is 108% which is a non-physical result. On

the other hand in IRTOOL the relative humidity cannot exceed 100%. In Figure 23B (temperature profile) the profiles of the midlatitude winter atmosphere and custom atmosphere are identical but there is a slight difference from the profile predicted from IRBLEM, especially in the first few meters above the water surface. Here we must note that IRTOOL calculates the right temperature of the sea surface (12.7^0 C) in contrast with IRBLEM, which gives a temperature of 11.58^0 C. In Figure 23C (pressure profile) we observe that the profile of pressure predicted from IRBLEM and that which is predicted from IRTOOL using the custom atmosphere are exactly the same, unlike the IRTOOL with the midlatitude winter atmosphere, which predicts different values for the pressure. There is a difference of 9.5 mbar or 7.12 Torrs. In spite of this both models give the same pressure gradient. That means the error in using the midlatitude winter atmosphere instead of the custom atmosphere for the calculation of refractivity will be less than 0.93% in accordance with Eq. 43 and Figure 23C. From Figure 23D we observe also a small difference in the wind speed profiles between our models. Here we must notice that the wind speed at the water surface calculated from IRBLEM is 0.72 m/sec. On the other hand IRTOOL always assumes that the wind speed at the sea surface is 0 m /sec. This is another difference between the two models.

As we have already mentioned, the refraction (ray bending) depends on the gradient of refractivity and not on the absolute magnitude of the refractivity itself. That means that we are interested in the final result, which is the profile of refractivity or its gradient. In Figure 23E is shown the profile of refractivity. We see that for the same

height, the custom atmosphere and the midlatitude winter atmosphere lead to different values for the refractivity but from Figure 23F the gradient of refractivity for those two atmospheres is the same. That means the error in pressure is neglible in the calculation of refractivity and also the restriction to use only one reference height does not affect at all the final result which is the gradient of refractivity, at least for that event. From the same Figure 23F, we see a slight difference in the first few meters between IRTOOL and IRBLEM. We observe that the first derivative of refractivity for IRTOOL is greater than that of IRBLEM. That means, the path curvature of the rays in IRTOOL for the first few meters is stronger or the radius of curvature of the ray is smaller (Eqs. 6, 7). So, the refraction effects in IRTOOL are stronger for the first few meters. So, we expect that the MMR (Minimum Mirage Range) of IRTOOL moves toward shorter ranges. Also, this strength of refraction is the reason that IRTOOL does not predict an image of the target at 3.13 m. This can be understood by looking in Figure 9. But if the MMR in IRTOOL moves to shorter ranges than IRBLEM then we should expect a mirage at least for the target at 7.19 m. The reason that this does not happen must lie in the cut-off height. We recall from Chapter V that another significant factor that affects the propagation of the low level rays is the significant wave height or cut-off height. An increased wave height would move the predicted MMR to longer ranges. The significant wave height that was calculated and used for the ray tracing program in IRTOOL was H_s=0.51 m. On the other hand in the ray tracing program of IRBLEM the height of H_s=0.17 m was used according to the Eq. 19 with $H_w = 1.3 \times H_{1/3}$ and minabslayer=0.03 m. The difference between the

cut-off heights that were used in the ray tracing programs is responsible for the failure of IRTOOL to predict the mirage for the target at 7.19 m. In order to make sure that this is true, we edit the FWH of IRBLEM so as to produce the cut-off height of IRTOOL. For that reason we used the value of FWH=2.05. The reason that we edit the cut-off height of IRBLEM instead of IRTOOL is that in IRBLEM if we change the FWH we do not change the calculated profiles. On the other hand the only way to change the cut-off height in IRTOOL is to use a wind speed different than the measured one. But doing this will change the profiles and so we will not be able to compare those models under the same set of input conditions. Previously, we said that the restriction of IRTOOL to use only one reference height does not affect at all the calculation of the refractivity gradient. This was true at least for that event. On the other hand, the use of only one reference height will affect the calculation of the cut-off height which is a crucial factor for the ray-tracing. That happens because the wind speed at 10 m height is used for the calculation of the cut-off height in IRTOOL. In this event we used as a reference height the height of 12 m because most of the measurements were made at this height. But the anemometer was at the height of 22.6 m. That means the cut-off height that was calculated was not correct. If we had used as reference height the height of 22.6 m then the extrapolated wind at 10 m would be lower, and as a result the cut-off height would be smaller because in the calculation of the significant height the wind speed was used in quadrature. The results with the edit cut-off height of IRBLEM are shown in Figure 24. Now, IRBLEM does not predict the mirage for the target at 7.19 m, but the target at 3.13 m is still detectable.

Figure 25 shows the measured ASTD from the Hr. Ms. Tydeman for the period from 06:45 to 08:25 GMT. The event that we analyzed took place from 07:29 to 07:34 GMT and the ASTD that was used was ASTD = -4.4 ^{0}C. According to Figure 25 there is a variation in ASTD of approximately 2 ^{0} C from 10-20 km. That means the results can be further improved if we take into consideration this figure. Using a lower magnitude of ASTD the strength of the refraction for both models will be reduced, and the results will be moved closer to the observed data. Figure 26 shows the results for an ASTD = -3.9 ^{0} C, and using the same cut-off height for both models. The target at 3.13 m is not detected from IRTOOL, but this time IRBLEM does not predict the mirage of the target at 4.58 m. Decreasing the refraction even more by using an ASTD = -3.7 ^{0} C (Figure 27) we observe that IRTOOL now detects the target at 3.13 m. The results are moving even closer to the observations but for the target at 4.58 m IRBLEM does not predict the mirage. With an ASTD = -3.4 ^{0} C (Figure 28) there is very good agreement between the predicted and the observed data, and both models give approximately the same solutions. It is important to note that the change in ASTD affects IRTOOL more than IRBLEM as we can see from Figures 24, 26, 27 and 28.

2. P2010F3

The conditions under which this event took place are shown in Table 17. The camera used was the visible (V1) positioned at height h_s = 6.91 m above the water level.

From Table 17 we see that the air temperature and humidity were measured at 12 m while the anemometer was placed at a height of 22.6 m. For the reference height in

IRTOOL we used 12 m. This will produce an error less than 3% in the value of the wind speed at the height of the 22.6 m, and so we do not expect the results to change significantly. But in order to minimize any error we generated the wind speed profile from the NPS profiler. The wind speed that was calculated at 12 m was 6.03 m/sec, and that was the value of the wind speed that we used in the input parameters of IRTOOL. The value of the wind speed at 12 m as it was predicted from the NPS profiler is in agreement with that of IRBLEM.

As we can see in Figure 29, IRBLEM gives mirages for the same targets as the experimental data, when IRTOOL does not predict the mirages for the targets at 7.5 m and 4.89 m. Also, it does not detect the target at 3.44 m. We can also observe that any target below $\approx$ 3 m will not be detected from IRBLEM. This height increases to $\approx$3.5 m for IRTOOL. For a non-refractive atmosphere any target below $\approx$1 m should be below the horizon. Finally, the shape of the curves that both models produce does not follow the data in the region of their cusps. From the same figure it is also clear that the results predicted from IRBLEM are much better than from IRTOOL.

In Figures 30A, 30B, 30C, 30D, 30E, 30F we see the profiles of humidity, temperature, pressure, wind speed, refractivity and gradient of refractivity as they were generated from the atmosphere profiler module of IRTOOL using the midlatitude winter atmosphere (symbol "x") and the custom atmosphere (symbol "o") and also those that were generated from the refraction module of IRBLEM (solid line). From the Figures 30A and 30B we observe that at 0 m the value of the humidity is again greater than 100% and the temperature $1\,^{0}$C less than the measured one. In IRTOOL for the same height the

relative humidity is 100% and the water temperature 13.1 ^{0}C which is in agreement with the value given in Table 17. From Figure 30D we observe a small difference in the wind speed profiles and also that the wind speed at the water surface calculated from IRBLEM is 0.53 m/sec. From Figure 30F we observe that again the two atmospheres that we used in IRTOOL give exactly the same results for the gradient of refractivity (ray bending). The error in pressure using the midlatitude winter atmosphere (Figure 30C) is about 0.9% and so it is not going to affect the profile of the gradient of refractivity. Also, we observe a slight difference in the first few meters between IRTOOL and IRBLEM. The first derivative of refractivity in IRTOOL is greater than that in IRBLEM. This means that the path curvature of the rays in IRTOOL for the first few meters is stronger or in another words the radius of curvature of the ray is smaller. So, we expect that the MMR (Minimum Mirage Range) of IRTOOL moves toward shorter ranges. This strength of refraction is the reason that IRTOOL does not predict the target at 3.44 m. But if the MMR in IRTOOL moves to shorter ranges than IRBLEM then we should expect a mirage at least for the targets at 4.89 m and 7.5 m. So, we edited the cut-off height in IRBLEM (FWH=4.18) for the same reasons that we mentioned in the event P2010F2. The significant wave height that was calculated and used from IRTOOL was H_s=0.90 m and for IRBLEM was H_s=0.155 m (actually the same as the measured wave height). Even though we used a lower value for the wind speed in the input parameters of IRTOOL, the calculated significant wave height is still much greater than the measured one (error

82%). The results with the edit cut-off height of IRBLEM are shown in Figure 31. Here only IRBLEM predicts an image for the target at 3.44 m, which is still detectable.

Figure 25 shows the measured ASTD from the Hr. Ms. Tydeman for the period from 06:45 to 08:25 GMT. The event that we analyze took place from 08:12 to 08:19 GMT and the ASTD that was used was ASTD = -4.5 ^{0}C. According to Figure 25 there is a variation in ASTD approximately 2 ^{0}C from 10-20 km. That means the results can be further improved if we take into consideration this figure. Using a lower magnitude of ASTD the strength of the refraction for both models will be reduced, moving the results closer to the observed data. In this case we expect that for a specific ASTD the IRTOOL will detect the target at 3.44 m, but we are not sure if it will continue to predict the mirage of the target at 4.19 m (unless if we run the IRTOOL code for each ASTD). On the other hand the sure thing is that IRBLEM will continue not to predict the mirage of any target, except maybe the target at 3.44 m.

3. P2810P2

The conditions under which this event took place are shown in Table 17. The camera used was the visible (V2) positioned at height h_s = 4.6 m above the water level.

From Table 17 we see that all the meteorological measurements were made at the same height of 3.4 m. That means we do not have to use the NPS profiler to get the value of the wind speed at 3.4 m. As we can see in Figure 32, IRBLEM gives mirages for the same targets as the experimental data while IRTOOL does not predict the mirage for the target at 5.77 m. We can also observe that any target below $\approx$ 3.8 m will not be detected

by IRBLEM. This height increases to $\approx$4 m for IRTOOL. For a non-refractive atmosphere any target below $\approx$1 m should be below the horizon. Finally, the shape of the curves that both models produce does not follow the data in the region of their cusps. From the same figure it is also clear, that the IRBLEM prediction results are much better than IRTOOL.

In Figures 33A, 33B, 33C, 33D, 33E, 33F we see the profiles of humidity, temperature, pressure, wind speed, refractivity and gradient of refractivity as they were generated from the atmosphere profiler module of IRTOOL using the midlatitude winter atmosphere (symbol "x") and the custom atmosphere (symbol "o") and also those that were generated from the refraction module of IRBLEM (solid line). From the Figures 33A and 33B we observe that at 0 m the value of the humidity is again greater than 100% and the temperature 0.7^{0}C less than the measured one. In IRTOOL for the same height the relative humidity is 100% and the water temperature 11.6^{0}C which is in agreement with the value given in Table 17. From Figure 33 D we observe a small difference in the wind speed profiles and also that the wind speed at the sea surface calculated from IRBLEM is 0.7 m/sec. From Figure 33C we observe that the error in the second term of Eq. 44 using the midlatitude winter atmosphere instead the custom atmosphere for the calculation of the pressure profile will not be greater than 0.90%. This is shown in Figure 33F. We observe that again the two atmospheres that were used in IRTOOL give the same results for the gradient of refractivity (ray bending). Also, we observe a slight difference in the first few meters between IRTOOL and IRBLEM. The first derivative of

refractivity in IRTOOL is bigger than that in IRBLEM. That means that the path curvature of the rays in IRTOOL for the first few meters is stronger or in another words the radius of curvature of the ray is smaller. So, we expect that the MMR (Minimum Mirage Range) of IRTOOL moves toward shorter ranges. This strength of refraction is the reason (for IRTOOL) that the target at 4.32 m is at the limit of detection. But if the MMR in IRTOOL moves to shorter ranges than IRBLEM, then we should expect a mirage at least for the target at 5.77 m. So, we edit the cut-off height in IRBLEM (FWH=0.95) for the same reasons that we mentioned in event P2010F2. The significant wave height that was calculated and used from IRTOOL was H_s=0.66 m (bigger than the measured wave height) and for IRBLEM was H_s=0.43 m (smaller than the measured wave height). The results with the edit cut-off height of IRBLEM are shown in Figure 34. Here IRBLEM does not predict the mirages for the targets at 5.12 m and 5.77 m.

Figure 35 shows the measured ASTD from the Hr. Ms. Tydeman for the period from 08:15 to 09:40 GMT. The event that we analyzed took place from 08:08 to 08:10 GMT which is very close to the period in which the measurement of ASTD were made by the ship. As we can see from Figure 35 both the air temperature and water temperature increase linearly with the range. The maximum variation that was observed for ASTD was about $0.3\,^{0}$ C and so, uncertainties due to any horizontal inhomogeneities can largely be neglected. Using also the fact that the calculated cut-off height in IRTOOL (0.66 m) is very close to the measured significant wave height (0.51 m), this is a representative event

in which it is shown that IRTOOL calculates a stronger refractive atmosphere than IRBLEM.

4. T2010B

The conditions under which this event took place are shown in Table 17. The camera used was the visible (V2) camera positioned at height $h_s = 6.11$ m and the infrared (IR1) camera positioned at height $h_s = 6.56$ m above the water level.

In Figure 36 the solid line with the black circles represents the MIVR for a non-refractive atmosphere as calculated from IRBLEM, the solid line with the white circles represents the MIVR for a non-refractive atmosphere as calculated from IRTOOL, the solid line with the squares represents the observed MIVR, the solid line with the rhombus represents the predicted MIVR from IRBLEM and the solid line with the triangles the MIVR predicted from the IRTOOL code. The Maximum Intervision Range (MIVR) constitutes for a given target height an absolute limit of detection range, which is less than the geometrical optical sight range [Ref 14]. In Figure 38, the solid line with the squares represents the observed MMR, the solid line with the rhombus represents the predicted MMR from IRBLEM and the solid line with the triangles the MMR predicted from the IRTOOL code. All the curves that were used in Figures 36, 38 to connect the various points are second order polynomial fits. The Minimum Mirage Range (MMR) is the range that represents the beginning of the mirage zone and is determined by the ray with the lowest initial elevation which does not hit the water surface. As we can see from Figure 36 (MIVR) for the visible V2 camera there is a difference (about 850 m) in the

prediction of the MIVR of a non-refractive atmosphere between the IRTOOL and IRBLEM. This range corresponds to the maximum detection range for a given target height and it is affected only by the earth's curvature and the wave height. Equation 17 that gives the HLR does not take into account the wave height. In order for the wave height to be a factor in the determination of the maximum detection range Eq. 17 must be modified as follows:

$$\mathrm{HLR} = \sqrt{2(a+H_w)} \times \left(\sqrt{(h_s - H_w)} + \sqrt{(h_t - H_w)}\right) \times 10^{-3} \cong$$

$$\sqrt{2a} \times \left(\sqrt{(h_s - H_w)} + \sqrt{(h_t - H_w)}\right) \times 10^{-3} \cong$$

$$3.57 \times \left(\sqrt{(h_s - H_w)} + \sqrt{(h_t - H_w)}\right) \qquad (50)$$

where HLR is expressed in kilometers

h_s is the sensor height in meters

h_t is the target height in meters

a is the earth radius expressed in meters ($a \approx 6370000$ m) and

H_w is the wave height in meters.

Using as H_w in Eq. 50 the significant wave height that was produced by IRTOOL we obtain the same results as those calculated from IRTOOL for the MIVR of a non-refractive atmosphere (for the given target heights). On the other hand, the results calculated from IRBLEM for the MIVR in a non-refractive atmosphere are not in agreement with Eq. 50 but with Eq. 17. That means IRBLEM does not take into account the wave height (significant wave height) in the calculation for the prediction of the

geometrical optical sight range. We also verified this by the fact that when we edited the factor wave height (FWH) using a much bigger value than the nominal the results for the geometrical optical sight range did not change at all.

From Figure 36 we observe that the MIVRs predicted from IRTOOL under refractive conditions are about 2.7 to 2.76 km shorter than the measured values, while for IRBLEM they are 2.16 to 2.38 km shorter.

In Figures 37A, 37B, 37C, 37D, 37E, 37F we see the profiles of humidity, temperature, pressure, wind speed, refractivity and gradient of refractivity as they were generated from the atmosphere profiler module of IRTOOL using the midlatitude winter atmosphere (symbol "x") and the custom atmosphere (symbol "o") and also those that were generated from the refraction module of IRBLEM (solid line). From Table 17 we see that the air temperature and humidity were measured at 12 m while the anemometer was placed at a height of 22.6 m. For the reference height in IRTOOL we used 12 m. This will produce an error less than 2% for the correct value of the wind speed at the height of 22.6 m, and so we do not expect the results to change significantly. But in order to minimize any error we generated the wind speed profile from the NPS profiler. The value of the wind speed as it was extracted at 12 m was used in the input parameters of IRTOOL. From the Figures 37A and 37B we observe that at 0 m the value of the humidity is again greater than 100% and the temperature 1^{0}C less than the measured value. In IRTOOL for the same height the relative humidity is 100% and the water temperature 12.5^{0}C which is in agreement with the value given in Table 17. From Figure

37D we see a slight difference in the wind speed profiles and also we observe that the wind speed at the sea surface calculated from IRBLEM is 0.69 m/sec. From Figure 37C we observe an error in the values of pressure using the midlatitude winter atmosphere. This error is not bigger than 0.9% and so it will not change the first derivative of refractivity. This is shown in Figure 37F in which the two atmospheres that were used in IRTOOL give the same results for the gradient of refractivity (ray bending). Also, we observe a difference in the first few meters between IRTOOL and IRBLEM. The first derivative of refractivity in IRTOOL is bigger than in IRBLEM. That means, the path of the rays in IRTOOL for the first few meters is more curved, or in other words the radius of curvature of the ray is smaller. So, we expect that the MIVR calculated by IRTOOL will move toward shorter ranges. This is the reason for the differences between the results.

From Figure 38 we observe that IRTOOL calculates a MMR for the given target heights which is about 1.44 to 2.5 km longer than the observed one, while IRTOOL calculates a MMR about 0.4 to 0.6 km shorter. The significant wave height that was used is a very important (crucial) factor for the determination of the MMR. We expect that an increased significant wave height would move the predicted MMRs to longer ranges for both models and also would lower the maximum predicted height for a mirage. The significant wave height calculated from IRTOOL was 0.61 m while for IRBLEM it was 0.1626 m. So, in order to compare both models for the same cut-off wave height we edited the Factor Wave Height (FWH) in IRBLEM. The reason that we edited the height in IRBLEM instead in IRTOOL has been explained in the analysis of the event P2010F2.

The MMR calculated from IRBLEM which is now about 1.8-3.2 km longer than the recorded one is shown in Figure 38 (solid line with the symbol "+"). The change in the wave height did not change the results for the MIVR in IRBLEM. This is because the MIVR is not affected as much as the MMR from the change of the significant wave height unless we use a very big wave height.

Figure 25 shows the measured ASTD from the Hr. Ms. Tydeman during that event. The ASTD that we used was $-4.1\,^{0}$C but according to Figure 25 there is a variation in ASTD of approximately $2\,^{0}$C from 10-20 km. That means the results can be further improved if we take into consideration this figure. Using a smaller magnitude of ASTD the strength of the refraction for both models will be reduced, resulting in curves that will move to greater ranges i.e., toward the measured data (under the assumption that both models use the same significant wave height of 0.1626 m).

Figures 39, 41 show the results of the model comparison for the data observed by the IR1 (3-5 μm) infrared camera positioned at height h_s = 6.56 m above the water level. As we can see from Figure 39 (MIVR) the IRTOOL model results for the MIVR are 2.3 to 2.5 km shorter and the IRBLEM results are 1.6 to 2.1 km shorter than the observed ones. Also the non-refraction range that is predicted from IRBLEM is 0.7-1.0 km longer than the one predicted from IRTOOL. That happens because IRBLEM did not take into account the wave height for the prediction of the geometrical optical sight range as we have already mentioned in the analysis of this event with the visible (V2) camera. The non-refraction range predicted from IRTOOL is shorter than the real one (if we could

have measured it) because the significant wave height that was used in Eq. 50 (0.61 m) is bigger than the real measured one (0.17 m). All the profiles calculated from IRTOOL are in agreement with the profiles that were calculated for the same event with the V2 camera because IRTOOL does not model dispersion. For IRBLEM the profiles of temperature, humidity, pressure and wind speed remain the same while the profiles of refractivity (Figure 40A) and its gradient (Figure 40B) differ slightly from before, due to the different coefficients A, B that are used for the mid-infrared in the equation of refractivity. So, we expect about the same results as before. From Figure 41 we observe that the IRTOOL model results for the MMR are 1.65 to 2.17 km longer and the IRBLEM results are 0.4 to 0.8 km shorter than the observed ones. The significant wave height that was used for the prediction of those results is 0.61 m for IRTOOL and 0.1626 m for IRBLEM. When we edited the FWH of IRBLEM to produce the same wave height as IRTOOL the MMR calculated from IRBLEM was 1.94 to 2.7 km toward greater ranges than the observed values. The results are shown in Figure 42 (solid line with the symbol "+"). Also, this change in the wave height did not alter the results for the MIVR produced from IRBLEM at all for the reason that we explained earlier.

Figure 25 shows the measured ASTD from the Hr. Ms. Tydeman during that event. The ASTD that we used was $-4.1\,^{0}C$ but according to Figure 25 there is a variation in ASTD of approximately $2\,^{0}C$ from 10-20 km. That means the results can be further improved if we take into consideration this figure. Using a smaller magnitude of ASTD the strength of the refraction for both models will be reduced, resulting in curves that will

move to greater ranges i.e., toward the measured data (under the assumption that both models use the same significant wave height of 0.16 m). Taking into account the fact that the equation used for the refractivity in IRTOOL and the equation used in IRBLEM for the mid-infrared are almost identical and also the fact that the pressure and humidity profiles are in good agreement we can say that the difference in the results occurs due to the difference in the temperature profiles between the two models for the first few meters.

The use of the custom atmosphere profile in IRTOOL instead of the mid-latitude winter atmosphere does not change the results at all as we saw for all the events that we examined until now. For that reason, for the analysis of the following events the mid-latitude winter atmosphere will be used.

5. P2210J2

The conditions under which this event took place are shown in Table 17. The camera used was the visible (V2) positioned at height h_s = 8.421 m above the water level.

From Table 17 we see that all the measurements were made at the same height of 3.4 m. As we can see from the observed data in Figure 42, a mirage was observed for the targets at 3.82 and 4.52 m but not for the target at 3.07 m. Both models IRBLEM and IRTOOL do not detect the target at 3.07 m, and also they do not predict mirage for the targets at 3.82 m and 4.52 m. For a non-refractive atmosphere any target below $\approx$2 m should be below the horizon. The results that both models give are in good agreement with each other but not with the observed data.

In Figures 43A, 43B, 43C, 43D, 43E and 43F we see the profiles of humidity, temperature, pressure, wind speed, refractivity and gradient of refractivity as they were generated from the atmosphere profiler module of IRTOOL using the midlatitude winter atmosphere (dash line) and those that were generated from the refraction module (LWKD) of IRBLEM (solid line). From the Figures 43A and 43B we observe that at 0 m the value of the humidity is again greater than 100% and the temperature 1.4^{0}C less than the measured one. In IRTOOL for the same height the relative humidity is 100% and the water temperature 12^{0}C which is in agreement with the value given in Table 17. From Figure 43D we observe very good agreement in the wind speed profiles and also that the wind speed at the water surface calculated from IRBLEM is now 0.01 m/sec. From Figure 43C the error in the pressure profile using the midlatitude winter atmosphere is not greater than 0.97%, and so we do not expect any change in the results. Because neither model predicts a mirage for any target we expect that the results will not change significantly when we edit the cut-off height in IRBLEM. The significant wave height that was calculated and used from IRTOOL was H_s=2.29 m (much bigger than the real measured wave height) and for IRBLEM was H_s=0.76 m (smaller than the real measured wave height). The results with the edit cut-off height of IRBLEM are shown in Figure 44 and as we see they do not change significantly (the changes can not be observed on the scale we use).

Figure 45 shows the measured ASTD from the Hr. Ms. Tydeman for the period from 20:00 to 22:10 GMT. The event that we analyzed took place from 20:22 to 20:24

GMT which is close to the period in which the measurements of ASTD were made by the ship. As we can see from Figure 45 there is a variation in ASTD of about 0.8^{0} C and so this horizontal inhomogeneity could have an effect on the agreement between the models and the data.

6. P2510M1

The conditions under which this event took place are shown in Table 17. The camera used was the visible (V1) positioned at height h_s = 7.51 m above the water level and also the visible (V2) camera positioned at height h_s = 4.32 m above the water level.

From Table 17 we see that the all the meteorological measurements were made at the same height of 3.4 m. As we can see from the recorded data in Figure 46, no mirage was observed for the given target heights and both models IRBLEM and IRTOOL do not predict any mirage for any target height for this set of conditions. For a non-refractive atmosphere any target below $\approx$2 m should be below the horizon. The results that both models give are in good agreement among themselves and also with the experimental data. In Figures 47A, 47B, 47C, 47D, 47E and 47F we see the profiles of humidity, temperature, pressure, wind speed, refractivity and gradient of refractivity as generated from the atmosphere profiler module of IRTOOL using the midlatitude winter atmosphere (dash line) and those that were generated from the refraction module (LWKD) of IRBLEM (solid line). From the Figures 47A and 47B we observe that at 0 m the value of the humidity is now about 100% (100.92%) and the temperature 11.3^{0}C which is almost in agreement with the measured value. In IRTOOL for the same height

the relative humidity is 100% and the water temperature 11.6 ^{0}C in agreement with the value given in Table 17. From Figure 47D we observe very good agreement in the wind speed profiles and also that the wind speed at the water surface calculated from IRBLEM is now 0.01 m/sec. Looking in the Figure 47C the error in the pressure profile using the midlatitude winter atmosphere is not greater than 0.97%, and so we do not expect any change in the results. In Figure 47E we observe that the gradient of refractivity is almost identical between the two models and also the temperature profiles (Figure 47B), with a slight difference at heights above 5 m. Because neither model predicts a mirage for any target we expect that the results are not going to change significantly when we edit the cut-off height in IRBLEM. The significant wave height that was calculated and used from IRTOOL was H_s=1.75 m (much bigger than the real measured wave height) and for IRBLEM was H_s=0.73 m (smaller than the real measured wave height). The results with the edit cut-off height of IRBLEM (not shown) are the same as in Figure 46.

Figure 48 shows the measured ASTD from the Hr. Ms. Tydeman for the period from 03:10 to 05:25 GMT. The event that we analyzed took place from 03:17 to 03:18 GMT. As we can see from Figure 48 there is a variation in ASTD of about 0.8 ^{0} C, and so this horizontal inhomogeneity could have an effect on the agreement between the models and the data.

With the visible (V2) camera the results are the same as with the visible (V1) camera. From Table 17 we see that all the measurements were made at the same height of 3.4 m. As we can see in Figure 49 no mirage was observed for the given target heights

and neither model IRBLEM or IRTOOL predicts any mirage for any target height for this set of conditions. For a non-refractive atmosphere any target below ≈3.5 m should be below the horizon. The results that the two models give are in good agreement between themselves and also with the experimental data. The profiles of humidity, temperature, pressure, wind speed, refractivity and gradient of refractivity for IRTOOL and IRBLEM are the same as the previous ones (47A-47F), because IRTOOL does not model dispersion and because we are still in the visible, so the coefficients A, B of IRBLEM do not change. The significant wave heights that were used from both models are the same as previously and the results when we edit the cut-off height in IRBLEM will not change.

7. P2810P3

The conditions under which this event took place are shown in Table 17. The camera used was the visible (V2) positioned at height h_s = 4.64 m above the water level.

From Table 17 we see that the all the measurements were made at the same height of 3.4 m. As we can see from Figure 50, neither model IRBLEM or IRTOOL predicts the mirage for the target at 5.81 m but the rest of the results are in very good agreement between themselves and with the recorded data. For a non-refractive atmosphere any target below ≈1 m should be below the horizon. This height increases to about ≈4 m for IRBLEM and a little more for IRTOOL (4.2 m). This is a very representative event because the cut-off height calculated from IRTOOL was 0.49 m, almost the same as the real measured significant wave height (0.51 m). Also, the cut-off height that was used from IRBLEM was 0.43 m. That means, for this event both models were compared under the same (almost) cut-off height, very close to the real one, and so the results that we get

are representative of their ability to predict the values of the real data. Even if we edit the cut-off height in IRBLEM, so as to agree with the cut-off height of IRTOOL, the results in IRBLEM will not change (any change will not be observable on the range scale that we use) because of the small difference in the cut-off heights between the models.

In Figures 51A, 51B, 51C, 51D, 51E and 51F we see the profiles of humidity, temperature, pressure, wind speed, refractivity and gradient of refractivity as generated from the atmosphere profiler module of IRTOOL using the midlatitude winter atmosphere (dash line) and those that were generated from the refraction module (LWKD) of IRBLEM (solid line). From Figures 51A and 51B we observe that at 0 m the value of the humidity is 104.8% which is not a physical result, and the temperature 0.8^{0}C less than the measured value, in spite of the fact that we used the measured value in the inputs to IRBLEM. In IRTOOL for the same height the relative humidity is 100% and the water temperature 11.7^{0}C in agreement with the value given in Table 17 and the value that we used in the IRTOOL inputs. From Figure 51D we observe very good agreement in the wind speed profiles and also the wind speed at the water surface calculated from IRBLEM is 0.72 m/sec. Looking in Figure 51C the error in the pressure profile using the midlatitude winter atmosphere is not greater than 0.91%, and so we do not expect any change in the results. In Figure 51F we observe that the gradients of refractivity for the two models are in very good agreement. For that reason both models predict almost the same results.

Figure 35 shows the measured ASTD from the Hr. Ms. Tydeman for the period from 08:15 to 09:40 GMT. The event that we analyzed took place from 09:18 to 09:24 GMT. As we can see from Figure 35 both the air temperature and water temperature increase linearly with the range. The maximum variation that we measured for ASTD was about $0.3\,^{0}$ C, and so uncertainties due to any horizontal inhomogeneities can largely be neglected. As a result this is also a very good event for the comparison between the two models.

8. T2810K

The conditions under which this event took place are shown in Table 17. The cameras used were the visible (V1) camera and the infrared (IR1) camera both positioned at height h_s = 7.83 m above the water level.

In Figure 52 the black solid line with the black circles represents the MIVR for a non-refractive atmosphere as calculated from IRBLEM, the black solid line with the white circles represents the MIVR for a non-refractive atmosphere as calculated from IRTOOL, the black solid line with the squares represents the observed MIVR, the black solid line with the rhombus represents the predicted MIVR from IRBLEM and the black solid line with the triangles the MIVR predicted from the IRTOOL code. In Figure 54, the squares represent the observed MMR, the rhombus represents the MMR predicted from IRBLEM and the triangles the MMR predicted from the IRTOOL code. All the curves that were used in Figure 52 to connect the various points are second order polynomial fits. As we can see from Figure 52 (MIVR) for the visible V1 camera there is a difference

(about 700 m) in the prediction of the MIVR in a non-refractive atmosphere between the IRTOOL and IRBLEM. Using as H_w in Eq. 50 the significant wave height that was produced by IRTOOL we obtain the same results as those calculated from IRTOOL for the MIVR of a non-refractive atmosphere (for the given target heights). On the other hand, the results calculated from IRBLEM for the MIVR in a non-refractive atmosphere are not in agreement with Eq. 50 but with Eq. 17. That means IRBLEM does not take into account the wave height (significant wave height) in the calculation for the prediction of the geometrical optical sight range.

From Figure 52 we observe that the MIVR predicted from IRTOOL under refractive conditions is about 1.26 to 1.69 km shorter than the measured one, while for IRBLEM it is 0.91 to 1.53 km shorter than measured.

In Figures 53A, 53B, 53C, 53D, 53E, 53F we see the profiles of humidity, temperature, pressure, wind speed, refractivity and gradient of refractivity as they were generated from the atmosphere profiler module of IRTOOL using the midlatitude winter atmosphere (dash line) and also those that were generated from the refraction module of IRBLEM (solid line). From the Figures 53A and 53B we observe that at 0 m the value of the humidity is again greater than 100% and the temperature 0.7^{0}C less than the measured one. In IRTOOL for the same height the relative humidity is 100% and the water temperature 11.7^{0}C which is in agreement with the value given in Table 17. From Figure 53D we see a slight difference in the wind speed profiles and also we observe that the wind speed at the sea surface calculated from IRBLEB is 0.72 m/sec. From Figure

53C we observe an error in the values of pressure using the midlatitude winter atmosphere. This error is not bigger than 0.9% and so it will not change the first derivative of refractivity. In Figure 53F we observe that the gradients of refractivity are in very good agreement between the two models, although there is a slight difference for the first few meters between the two models. The first derivative of refractivity in IRTOOL is bigger than in IRBLEM. That means, the path curvature of the rays in IRTOOL for the first few meters is greater or in other words the radius of curvature of the ray is smaller. So, we expect that the MIVR calculated from IRTOOL will move toward shorter ranges. This is the reason for the difference between the results.

From Figure 54 we observe that IRTOOL calculates a MMR for the given target heights which is about 38 to 204 m longer than the observed one, while IRBLEM calculates a MMR about 19 to 161m longer than observed. The significant wave height that was used is a very important factor for the determination of the MMR. We expect that an increased significant wave height would move the predicted MMRs to longer ranges for both models and also would lower the maximum predicted height for a mirage. The significant wave height calculated from IRTOOL was 0.49 m while for IRBLEM it was 0.42 m.

This is an extremely good case because both models use about the same cut-off height which is also very close to the measured one (0.51 m). And in this case we got very good results for both models. In order to see how the results in IRBLEM will change when we change its cut-off height we edited the Factor Wave Height (FWH) so as to produce the same cut-off height as IRTOOL. The MMR calculated now from

IRBLEM, which is about 0.23-0.5 km longer than the recorded one, is shown in Figure 54 (symbol "*"). The change in the wave height did not change the results for the MIVR in IRBLEM. This is because the MIVR is not affected as much as the MMR from the change of the significant wave height unless a very big wave height is used.

Figure 35 shows the measured ASTD from the Hr. Ms. Tydeman during that event. The ASTD that we used was -2.5^{0}C. As we can see from Figure 36 both the air temperature and water temperature increase linearly with the range. The maximum variation that we measured for ASTD was about 0.3^{0} C, and so uncertainties due to any horizontal inhomogeneities can largely be neglected. As a result this is a very good event for the comparison between the two models.

For the IR1 camera IRTOOL predicts exactly the same results as with the visible (V1) camera because both cameras were placed at the same height and because IRTOOL does not model dispersion. The results for IRBLEM we expect to be a little different because the coefficients A, B that are used for the calculation of refractivity are band dependent. All the profiles for IRTOOL remain the same as before while for IRBLEM only the profiles of the refractivity and its first gradient change (Figures 56A and 56B). Figures 55, 57 show the results of the model comparison for the MMR and MIVR. As we can see in Figure 55 (MIVR) the IRBLEM results are 0.63 to 1.44 km shorter than the observed values while for IRTOOL are 0.98-1.58 km shorter. From Figure 57 we observe that the IRTOOL and IRBLEM model results for the MMR are in very good agreement with the observed ones. In order to see how the results in IRBLEM will change when we

change its cut-off height we edited the Factor Wave Height (FWH) so as to produce the same cut-off height as IRTOOL. The MMR calculated now from IRBLEM, which is about 0.21-0.4 km longer than the recorded one, is shown in Figure 57 (symbol "✶"). The change in the wave height did not change the results for the MIVR in IRBLEM.

Figure 35 shows the measured ASTD from the Hr. Ms. Tydeman during that event. The ASTD that we used was -2.5^{0}C. As we can see from Figure 35 both the air temperature and water temperature increase linearly with the range. The maximum variation that we measured for ASTD was about 0.3^{0} C, and so uncertainties due to any horizontal inhomogeneity can largely be neglected. As a result this is a very good event for the comparison between the two models.

9. T2510F

The conditions under which this event took place are shown in Table 17. The cameras used were the visible (V1), the visible (V2), the visible (V3), the visible (V4), the infrared (IR1) and the infrared (IR2) camera. For all the plots, the black solid line with the black circles represents the MIVR for a non-refractive atmosphere as calculated from IRBLEM, the black solid line with the white circles represents the MIVR for a non-refractive atmosphere as calculated from IRTOOL, the squares represent the observed MIVR or MMR, the rhombus represents the MIVR or MMR predicted from IRBLEM and the triangles the MIVR or MMR predicted from the IRTOOL code.

The visible (V1) camera was positioned at $h_s = 7.55$ m above the water level. As we can see from Figure 58 there is a difference (about 2 km) in the prediction of the

MIVR in a non-refractive atmosphere between the IRTOOL and IRBLEM. Using as H_w in Eq. 50 the significant wave height that was produced by IRTOOL (1.46 m) we obtain the same results as those calculated from IRTOOL for the MIVR of a non-refractive atmosphere (for the given target heights). On the other hand, the results calculated from IRBLEM for the MIVR in a non-refractive atmosphere are not in agreement with Eq. 50 but with Eq. 17. That means IRBLEM does not take into account the wave height (significant wave height) in the calculation for the prediction of the geometrical optical sight range. From the same figure we observe that the MIVR predicted from IRTOOL under refractive conditions is about 0.85 to 1.65 km shorter than the measured value, while for IRBLEM it is 700 to 950 m shorter. It is interesting to note that even though we have subrefractive conditions (ASTD = -0.6^0C) the MIVR is at greater ranges than the geometrical horizon. The ray curvature depends upon the index of refraction gradient, which depends upon the gradients in density. For neutral stability conditions (ASTD about 0), the air density is still decreasing with height and the ray is curved around the earth slightly compared to a straight ray. It apparently takes a more negative ASTD than -0.6^0C (depending also on wind speed) to undo this effect.

From the profile of the air density (not shown) we observe that the gradient of the air density became negative at the height of about 2 m. That means the air density starts to decrease at that height. Taking into account that the significant wave height produced by IRTOOL was 1.46 m and also the fact that the sensor was placed at 7.55 m above the water level we have a height region in which the air density decreases with height. So, the

rays bend downward and we detect at ranges beyond the horizon. This can also be seen from the gradient of refractivity (Figure 59F) in which the gradient starts to become negative at the height of 2 m.

In Figures 59A, 59B, 59C, 59D, 59E, 59F we see the profiles of humidity, temperature, pressure, wind speed, refractivity and gradient of refractivity as generated from the atmosphere profiler module of IRTOOL using the midlatitude winter atmosphere (dash line) and also those that were generated from the refraction module of IRBLEM (solid line). From Figures 59A and 59B we observe that at 0 m the value of the humidity is 102% which is a non-physical result, and the temperature 0.24^{0}C less than the measured value. In IRTOOL for the same height the relative humidity is 100% (sea surface 100% saturated) and the water temperature 11.6^{0}C which is in agreement with the value given in Table 17. From Figure 59D we see a slight difference in the wind speed profiles above 5 m. From Figure 59C we observe an error in the values of pressure using the midlatitude winter atmosphere. This error is not bigger than 1.2% and so it will not alter significantly the first derivative of refractivity. In Figure 59F we observe that the gradients of refractivity are in very good agreement between the two models, although there is a slight difference for the first few meters between the two models. The first derivative of refractivity in IRTOOL is bigger than in IRBLEM. That means, the path curvature of the rays in IRTOOL for the first few meters is greater, or in other words the radius of curvature of the ray is smaller. So, we expect that the MIVR calculated with

IRTOOL will move toward shorter ranges. The results that are shown in Figure 58 are in very good agreement between both models and the measured data.

In Figure 60 we observe that MMRs were observed for targets from 11 m to 21 m above the water level but not at 3.34 m, 6.08m and 6.38 m above the water level. IRTOOL does not predict a mirage for the given target heights while IRBLEM predicts the existence of weak secondary images, or image stretching, for all the targets above 6 m. The relative strengths for the formation of secondary images can be seen by comparing the range difference, at any elevation, between the predicted MIVR and MMR.

The significant wave height that was used is a very important factor for the determination of the MMR. We expect that an increased significant wave height would move the predicted MMRs to longer ranges for both models and also would lower the maximum predicted height for a mirage. The significant wave height calculated from IRTOOL was 1.46 m while for IRBLEM it was 0.74 m. In order to see how the results in IRBLEM will change when we change its cut-off height we edited the Factor Wave Height (FWH) so as to produce the same cut-off height as IRTOOL. Now IRBLEM does not predict mirages for the given target heights. The change in the wave height changed slightly the results for the MIVR in IRBLEM. Now the MIVRs move towards shorter ranges (Figure 58, symbol "*").

The visible (V2) camera was positioned at h_s = 9.34 m above the water level. As we can see from Figure 61 the MIVR predicted from IRTOOL under refractive conditions is about 1 to 1.4 km shorter than the measured value, while for IRBLEM it is 0.7 to 1 km

shorter. The profiles of humidity, temperature, pressure, wind speed, refractivity and gradient of refractivity for both models are identical to those that were generated for the same event with the visible (V1) camera (59A-59F). In Figure 62 we observe that MMRs were measured only for the target at 20.7 m above the water level. IRTOOL does not predict a mirage for the given target heights while IRBLEM predicts the existence of weak secondary images for all targets above 6 m. The mirage range for the target at 20.7 m is about 750 m shorter than the measured value. The significant wave height that was used is a very important factor for the determination of the MMR. We expect that an increased significant wave height would move the predicted MMRs to longer ranges for both models and also would lower the maximum predicted height for a mirage. The significant wave height calculated from IRTOOL was 1.46 m while for IRBLEM it was 0.74 m. In order to see how the results in IRBLEM will change when we change its cut-off height we edited the Factor Wave Height (FWH) so as to produce the same cut-off height as IRTOOL. Now, neither IRBLEM nor IRTOOL predicts a mirage for the given target heights. The change in the wave height changed slightly the results for the MIVR in IRBLEM (Figure 61, symbol "*").

The visible (V3) camera was positioned at $h_s = 20.51$ m above the water level. As we can see from Figure 63 the MIVR predicted from IRTOOL under refractive conditions is about 2.3 to 2.9 km longer than measured, while for IRBLEM it is 2.88 to 3 km longer. The profiles of humidity, temperature, pressure, wind speed, refractivity and gradient of refractivity for both models are the same as those that were generated for the same event

with the visible (V1) camera (59A-59F). Figure 64 shows that IRTOOL does not predict the existence of any mirages and also that no MMR was observed for the given target heights, while IRBLEM predicts the existence of weak secondary images for all targets above 11 m. The significant wave height that was used is a very important factor for the determination of the MMR. The significant wave height calculated from IRTOOL was 1.46 m while for IRBLEM it was 0.74 m. In order to see how the results in IRBLEM will change when we change its cut-off height we edited the Factor Wave Height (FWH) so as to produce the same cut-off height as IRTOOL. Now IRBLEM does not predict a mirage for the given target heights. The change in the wave height changed slightly the results for the MIVR in IRBLEM (Figure 63, symbol "*").

The visible (V4) camera was positioned at h_s = 7.14 m above the water level. As we can see from Figure 65 the MIVR predicted from IRTOOL under refractive conditions is about 0.5 to 1.4 km shorter than the measured one, while for IRBLEM it is 0.4 to 0.65 km shorter. The profiles of humidity, temperature, pressure, wind speed, refractivity and gradient of refractivity for both models are the same as those that were generated for the same event with the visible (V1) camera (59A-59F). Figure 66 shows that only a single MMR data point was observed, due to the target at height 20.7 m, and also that neither model predicted the existence of any secondary images. When we edited the cut-off height in IRBLEM so as to be the same as in IRTOOL the results related to MMR did not change as we expected, but the MIVRs were moved a little (Figure 65, symbol "*").

The infrared (IR1) camera was positioned at h_s = 7.55 m above the water level. As we can see from Figure 67 the MIVR predicted from IRTOOL under refractive conditions is about 0.7 to 1.5 km shorter than the measured one, while for IRBLEM it is 0.5 to 0.8 km shorter. All the profiles for IRTOOL remain the same as before while for IRBLEM only the profiles of the refractivity and its first gradient changed (Figures 68A and 68B) due to the band dependent coefficients A, B that are used for the calculation of refractivity. As we can see from Figure 68B the curves of the gradient of refractivity for the two models are in better agreement compared with the visible cameras. That happened because in the mid-infrared the equations that are used in the two models for the calculation of refractivity are approximately the same. Figure 69 shows that IRTOOL does not predict the existence of any mirages for the given target heights and also that only one MMR data point was observed, due to the target at 20.7 m. IRBLEM predicts the existence of weak secondary images for all targets above 6 m. The significant wave height that was used is a very important factor for the determination of the MMR. The significant wave height calculated from IRTOOL was 1.46 m while for IRBLEM it was 0.74 m. When we edited the cut-off height in IRBLEM so as to be the same as IRTOOL, IRBLEM did not predict the existence of any secondary image but now the MIVRs were changed a little (Figure 67, symbol "*").

The infrared (IR2) camera was positioned at h_s = 7.3 m above the water level. As we can see from Figure 70 only one MIVR data point was observed for the target at 14.5 m above the water level (ship's stack) and for that point the IRTOOL predicted a MIVR

which is about 70 m longer while IRBLEM predicted a MIVR 800 m shorter. All the profiles for IRTOOL remain the same as before while for IRBLEM only the profiles of the refractivity and its first gradient changed (Figures 71A and 71B) due to the band dependent coefficients A, B that are used for the calculation of refractivity. As we can see from Figure 71B the gradient of refractivity in IRBLEM in this case is bigger than in IRTOOL. That means the ray bending is greater in IRBLEM, which results the MIVRs and MMRS to move in shorter ranges. Figure 72 shows that no MMR was measured for the ship's stack and also that the IRTOOL did not predict the existence of any mirages for any target heights, while IRBLEM predicted the existence of weak secondary images for all the targets above about 4 m from the water level. When we edited the cut-off height in IRBLEM so as to be the same as IRTOOL, IRBLEM did not predict the existence of any secondary image, but the MIVR for the target at 14.5 m was changed slightly (Figure 70, symbol "*").

Figure 48 shows the measured ASTD from the Hr. Ms. Tydeman for the period from 03:10 to 05:25 GMT. The air temperature was quite steady near 11.2^{0} C during the track while the sea temperature was steady near 11.6^{0} C for the first 32 km before jumping up to 12.4^{0} C. As no lights were visible beyond 32 km the slight horizontal variation in ASTD (0.4^{0} C) is not expected to have a significant effect on the agreement between the models and the data.

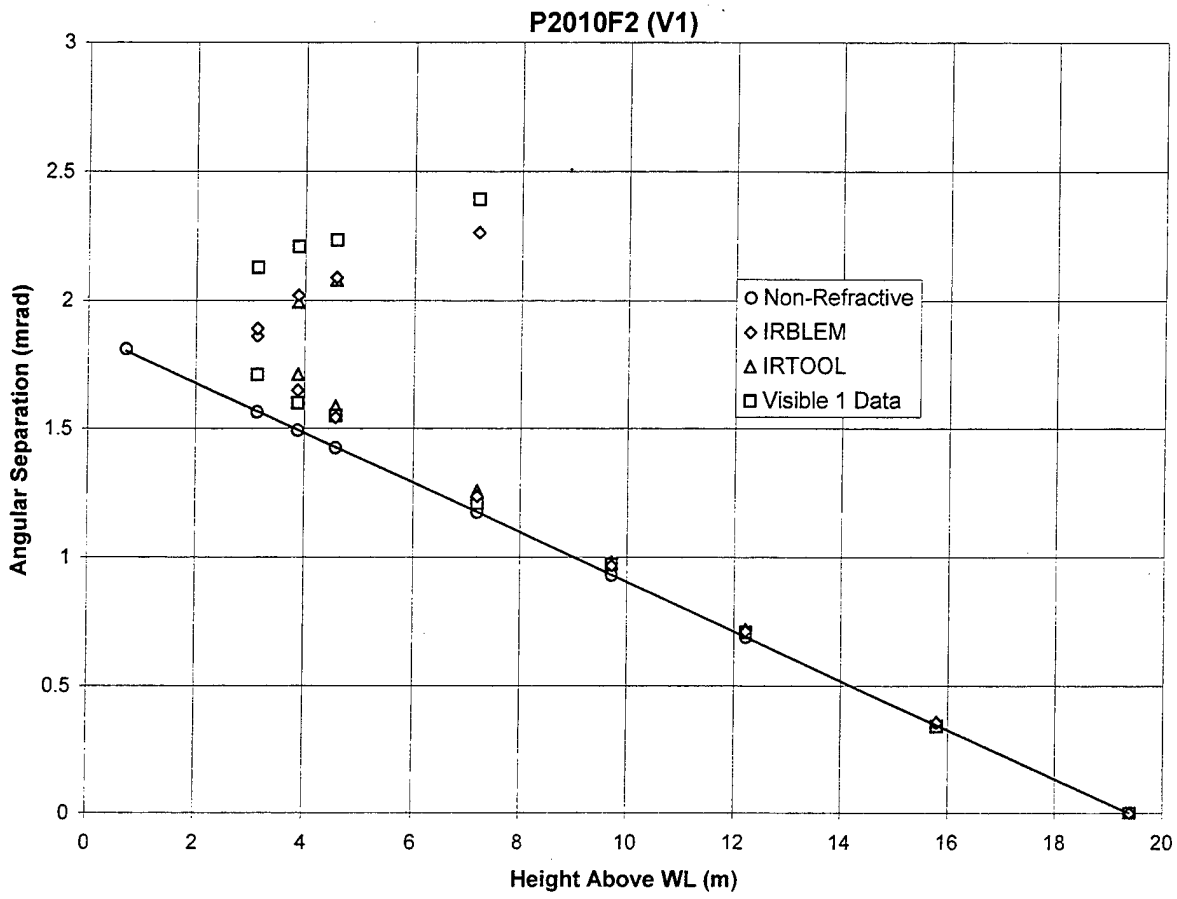

Figure 22. Comparison of IRTOOL and IRBLEM model calculations for the P2010F2 event measured by the visible V1 camera. The Angular Separation is the elevation angle of each image relative to the higher target source. Each image in the upper branch is a mirage.

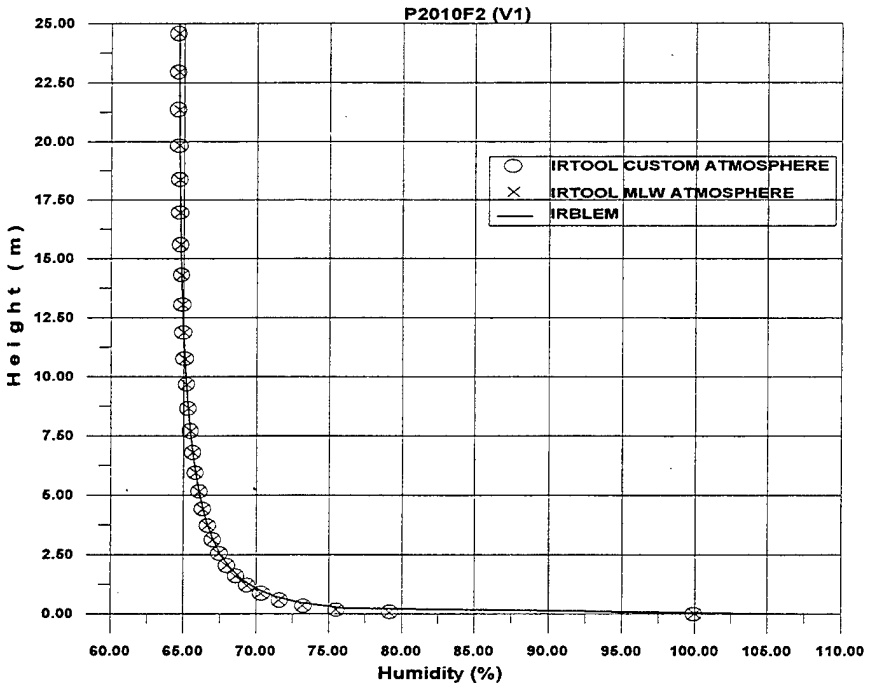

Figure 23A. Humidity profiles as predicted from IRTOOL (using the Mid-Latitude Winter and Custom atmosphere) and IRBLEM model.

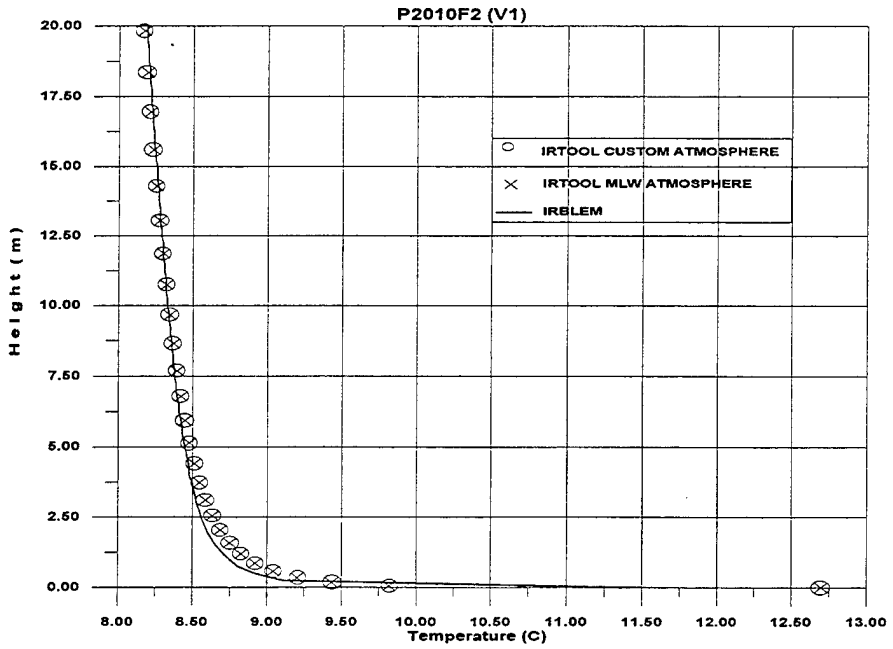

Figure 23B. Temperature profiles as predicted from IRTOOL (using the Mid-Latitude Winter and Custom atmosphere) and IRBLEM model.

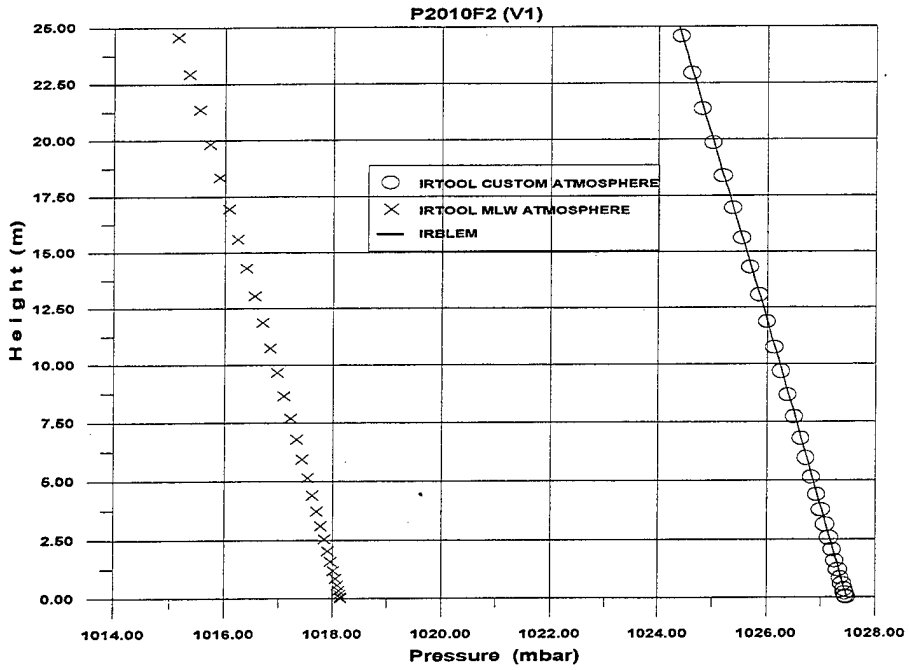

Figure 23C. Pressure profiles as predicted from IRTOOL (using the Mid-Latitude Winter and Custom atmosphere) and IRBLEM model.

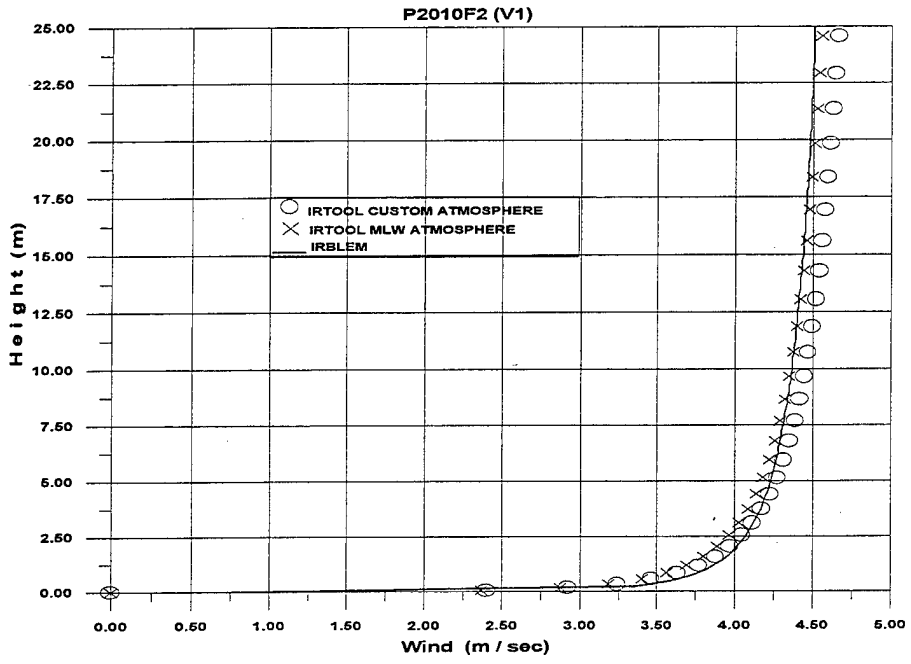

Figure 23D. Wind speed profiles as predicted from IRTOOL (using the Mid-Latitude Winter and Custom atmosphere) and IRBLEM model.

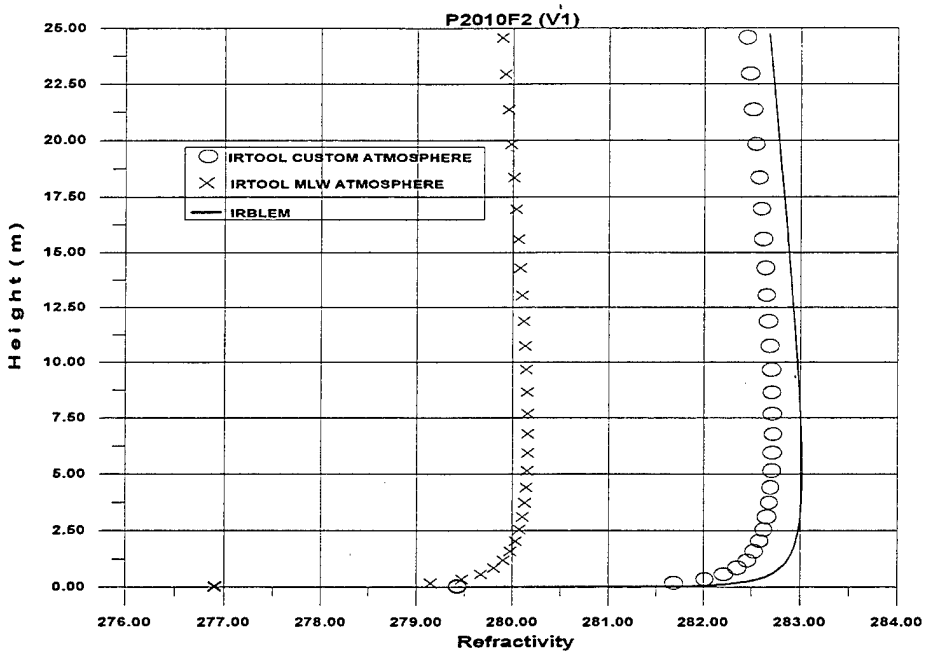

Figure 23E. Refractivity profiles as predicted from IRTOOL (using the Custom atmosphere) and IRBLEM model.

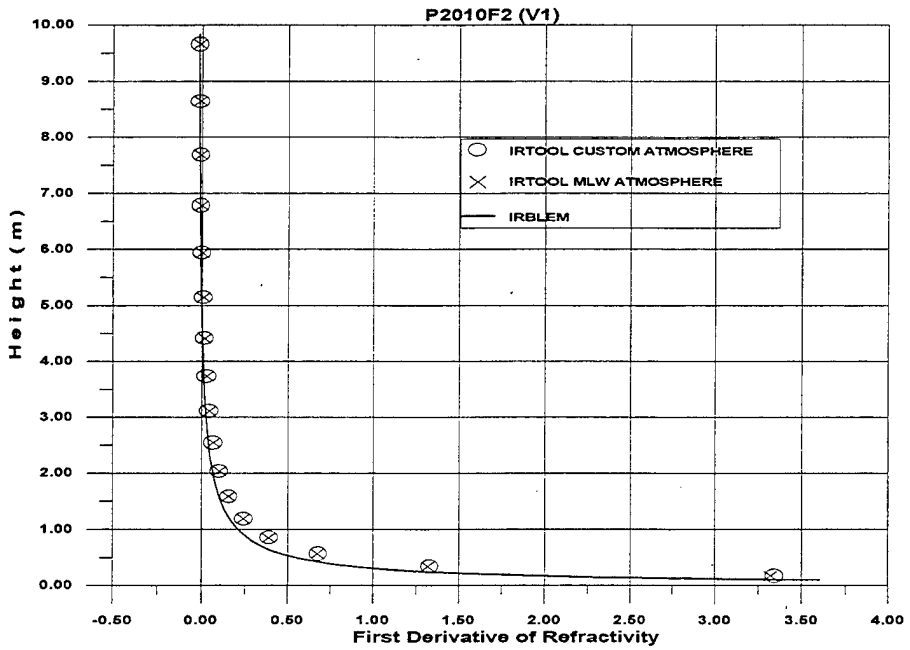

Figure 23F. Gradient of the Refractivity profile as predicted from IRTOOL (using the Mid-Latitude Winter and Custom atmosphere) and IRBLEM model.

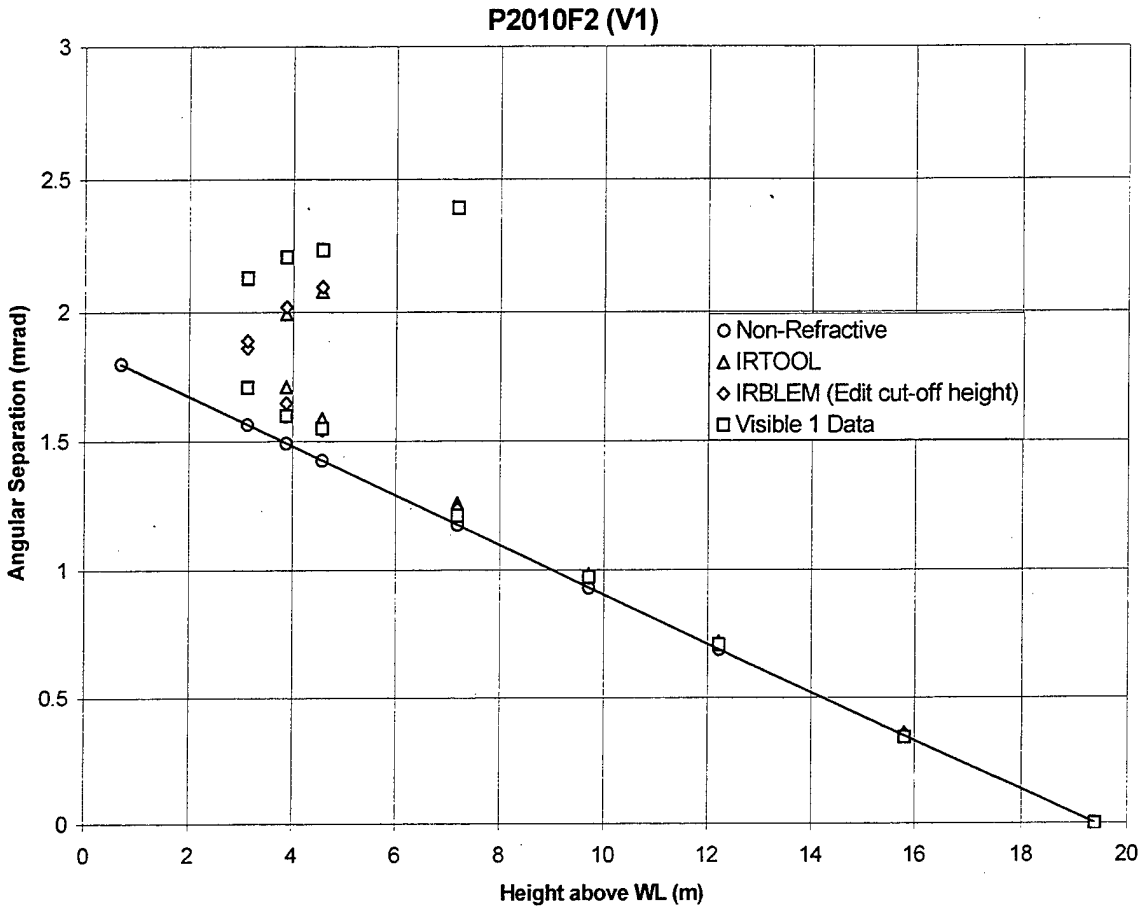

Figure 24. Comparison of IRTOOL and IRBLEM model calculations after editing the cut-off height of IRBLEM, for the P2010F2 event measured by the visible V1 camera.

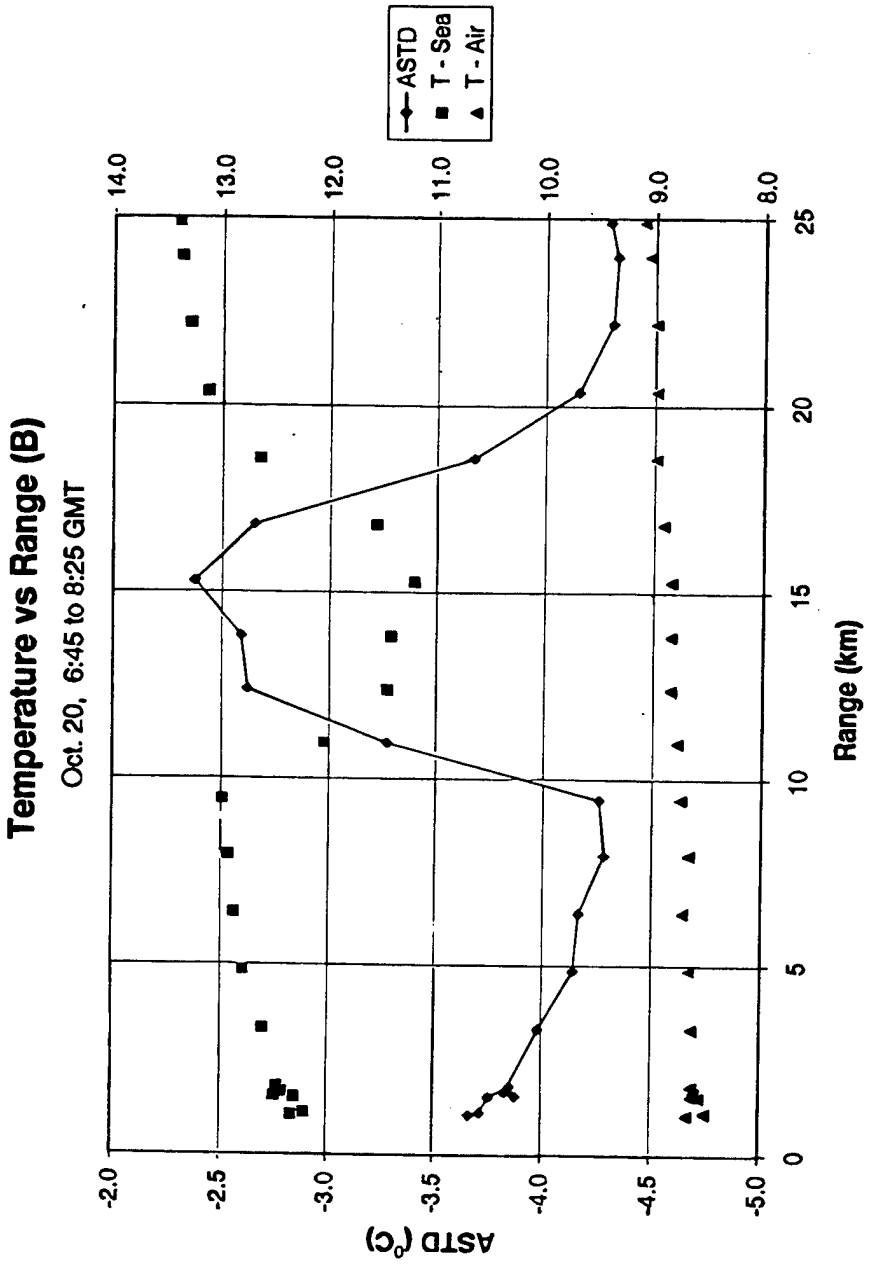

Figure 25. Variation of the sea temperature along the ship's course during ship tracking event B.

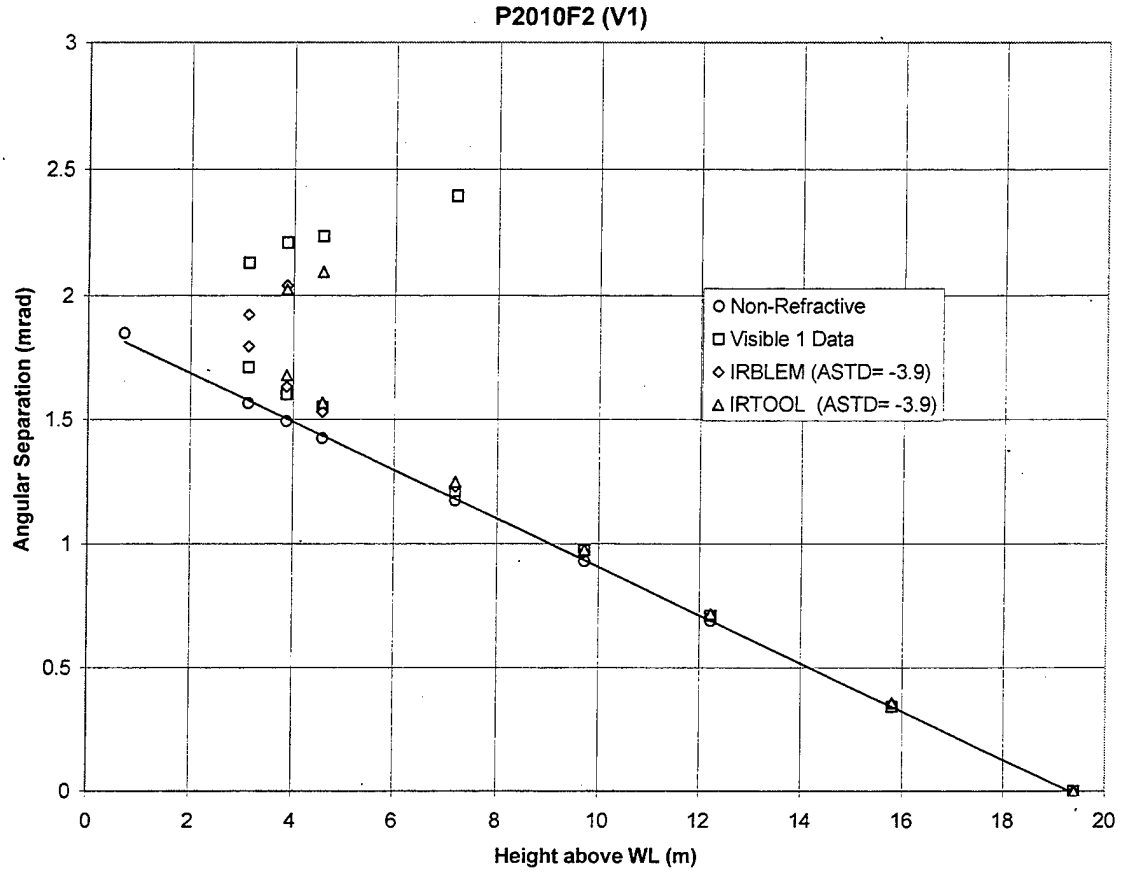

Figure 26. Comparison of IRTOOL and IRBLEM model calculations for the P2010F2 event measured by the visible V1 camera for ASTD = -3.9 ^{0}C.

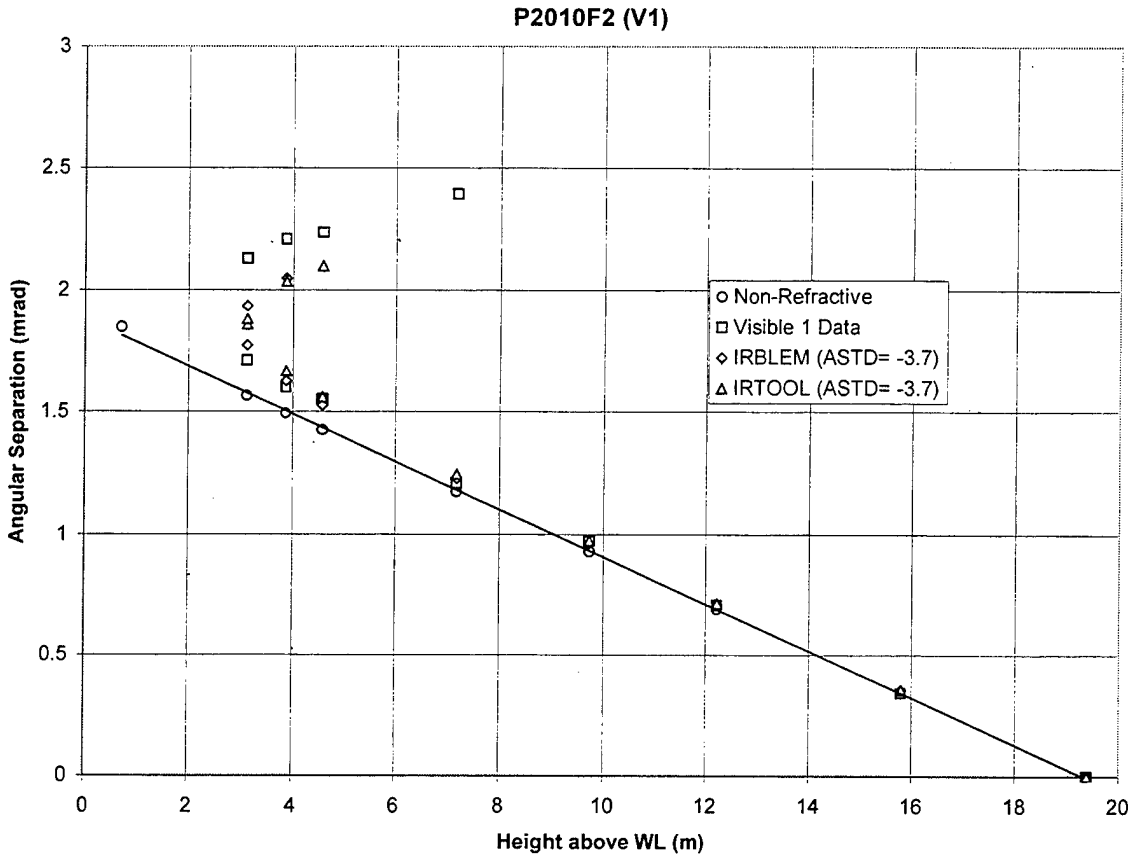

Figure 27. Comparison of IRTOOL and IRBLEM model calculations for the P2010F2 event measured by the visible V1 camera for ASTD = -3.7 ^{0}C.

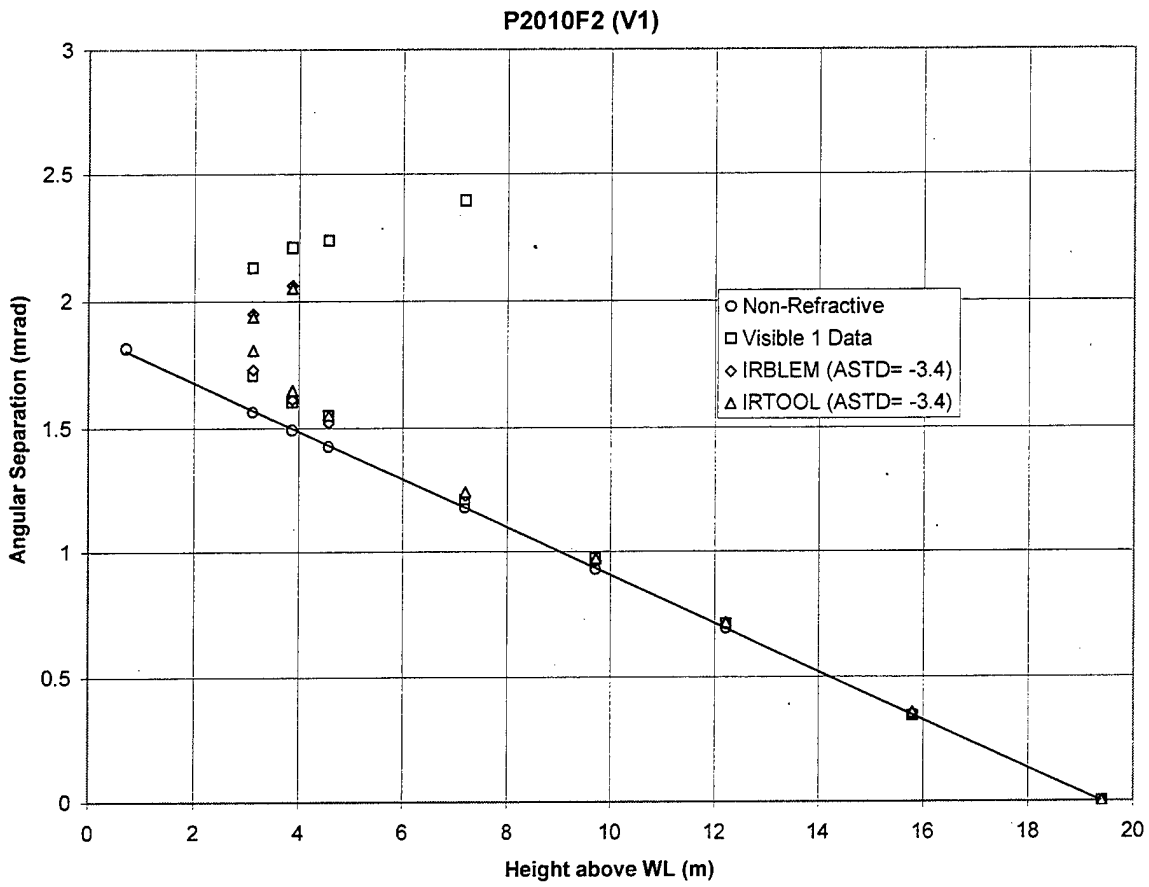

Figure 28. Comparison of IRTOOL and IRBLEM model calculations for the P2010F2 event measured by the visible V1 camera for ASTD = -3.4 ^{0}C.

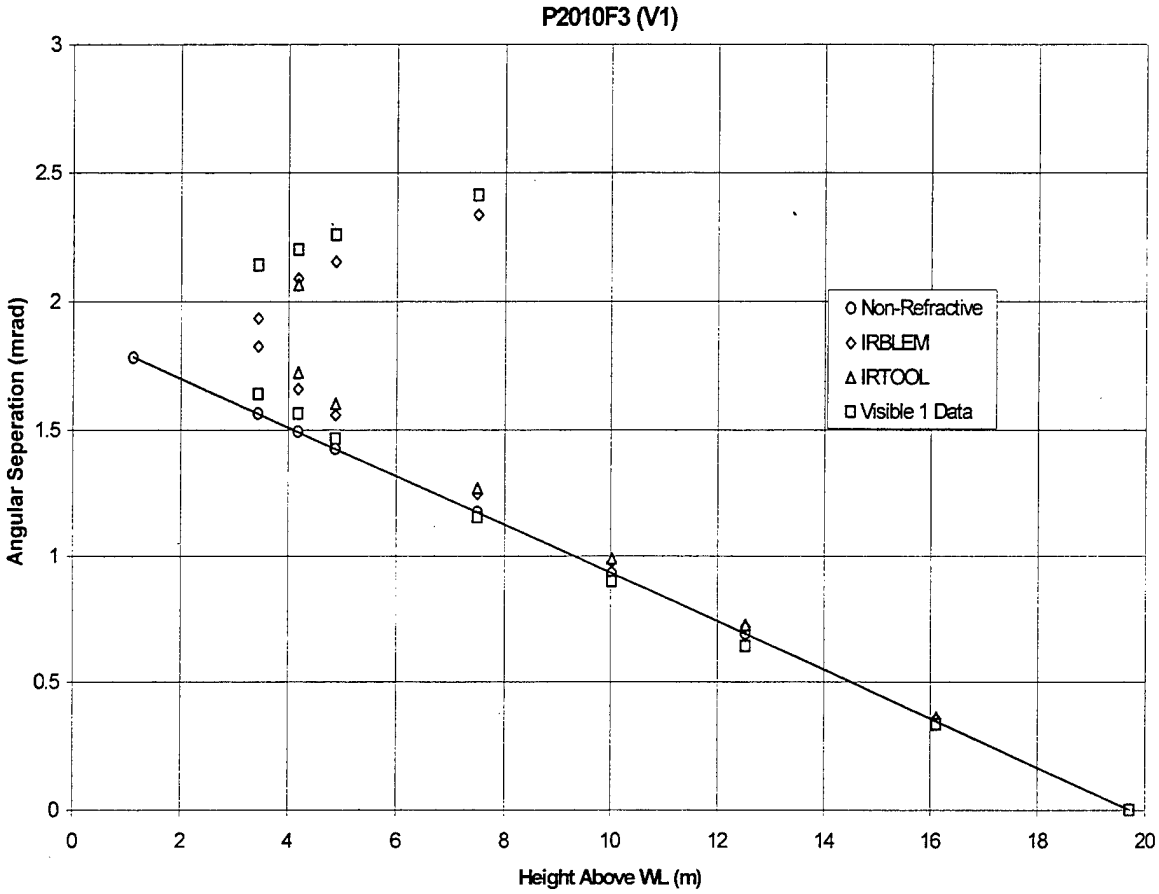

Figure 29. Comparison of IRTOOL and IRBLEM model calculations for the P2010F3 event measured by the visible V1 camera.

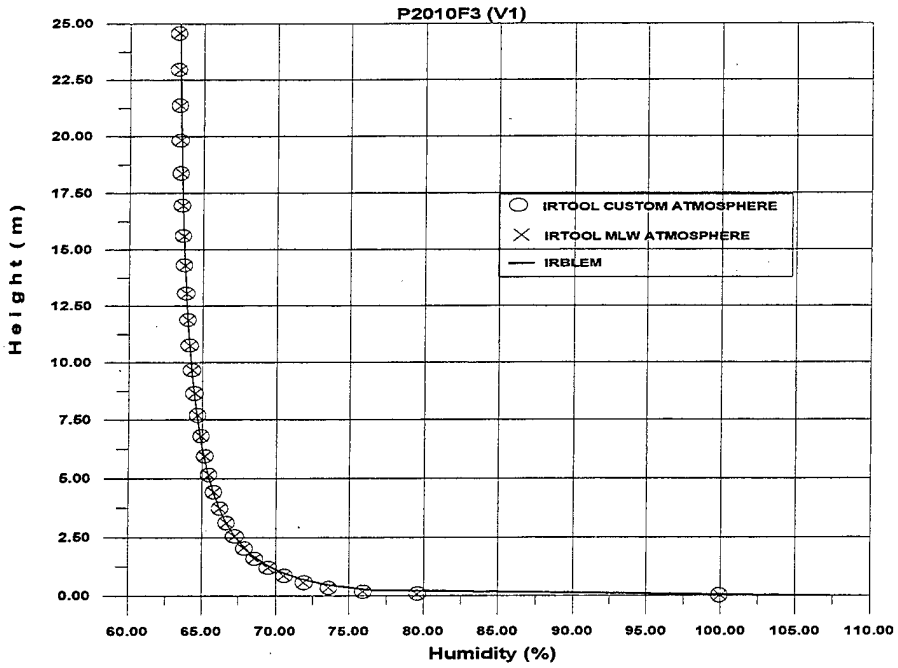

Figure 30A. Humidity profiles as predicted from IRTOOL (using the Mid-Latitude Winter and Custom atmosphere) and IRBLEM model.

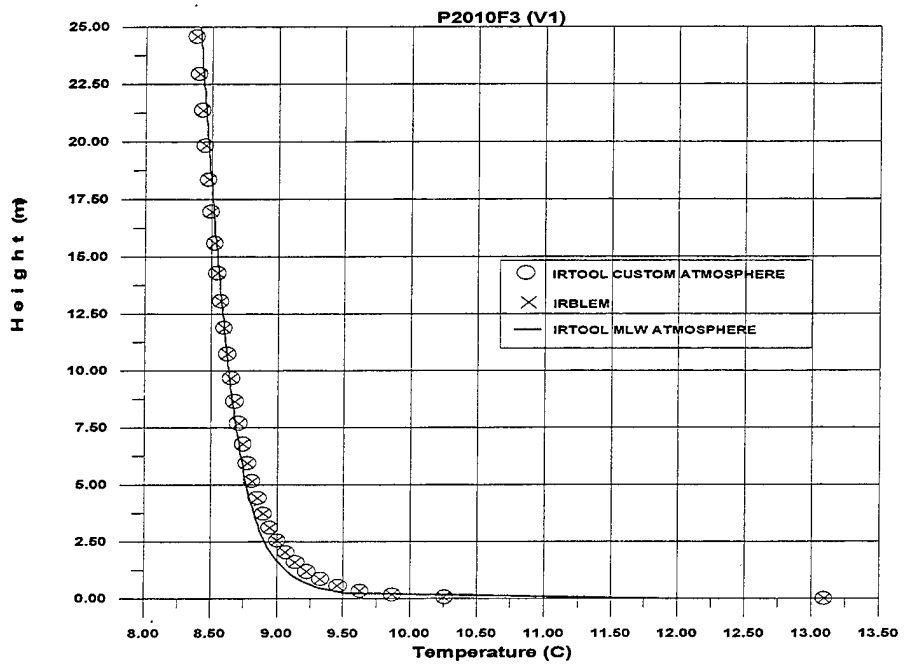

Figure 30B. Temperature profiles as predicted from IRTOOL (using the Mid-Latitude Winter and Custom atmosphere) and IRBLEM model.

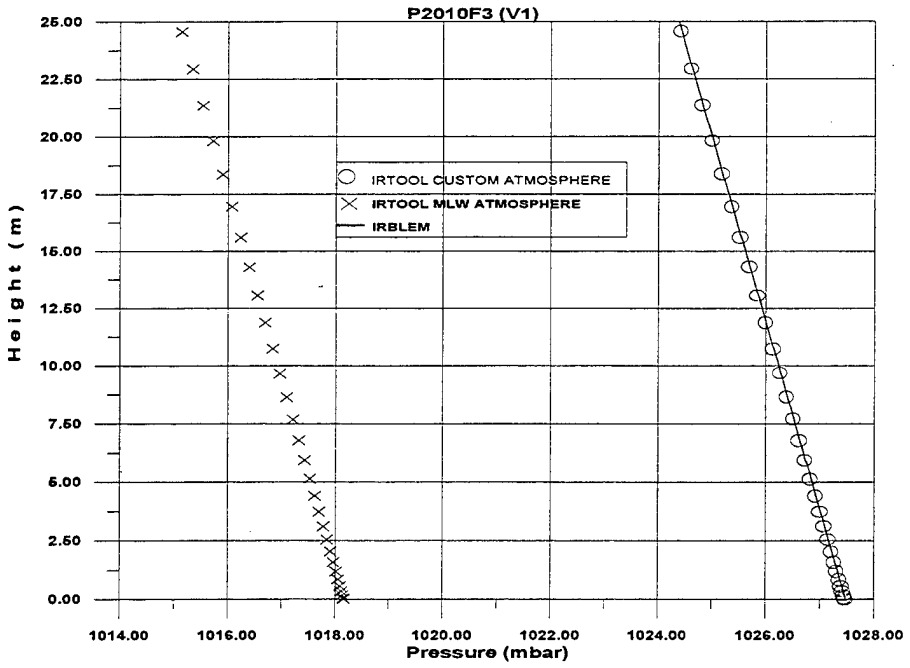

Figure 30C. Pressure profiles as predicted from IRTOOL (using the Mid-Latitude Winter and Custom atmosphere) and IRBLEM model.

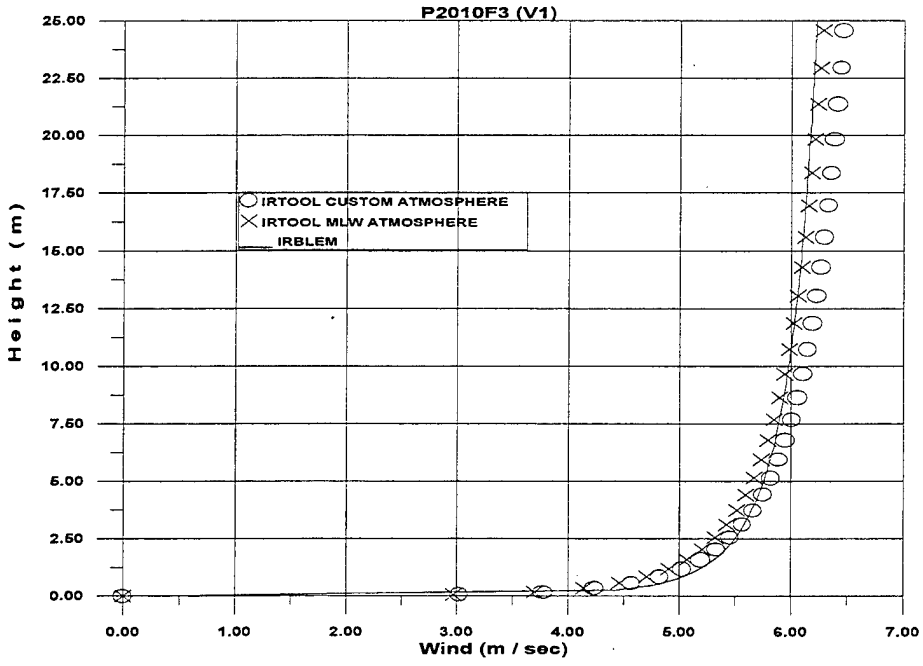

Figure 30D. Wind speed profiles as predicted from IRTOOL (using the Mid-Latitude winter and Custom atmosphere) and IRBLEM model.

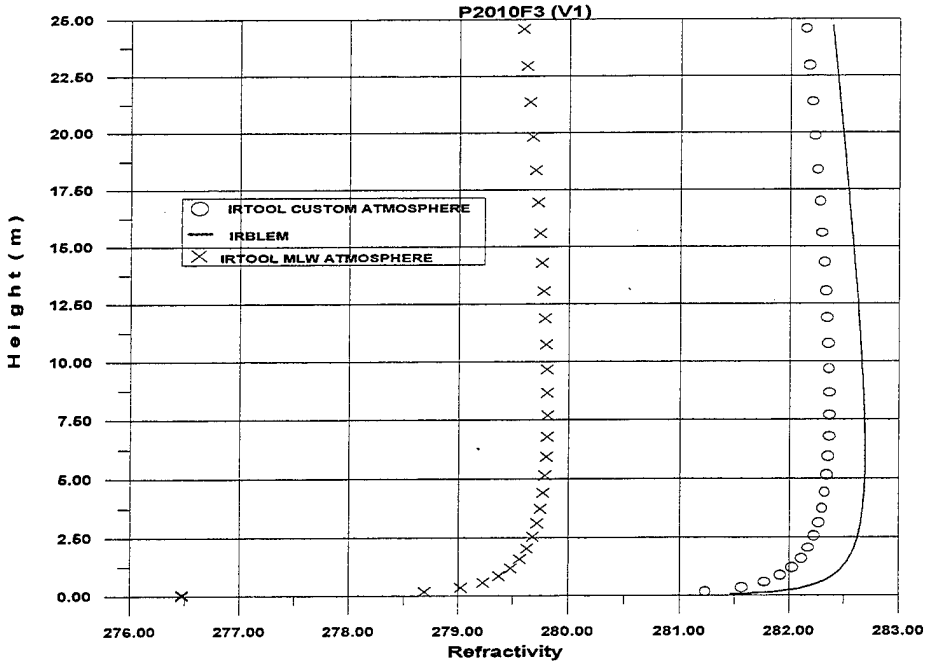

Figure 30E. Refractivity profiles as predicted from IRTOOL (using the Mid-Latitude Winter and Custom atmosphere) and IRBLEM model.

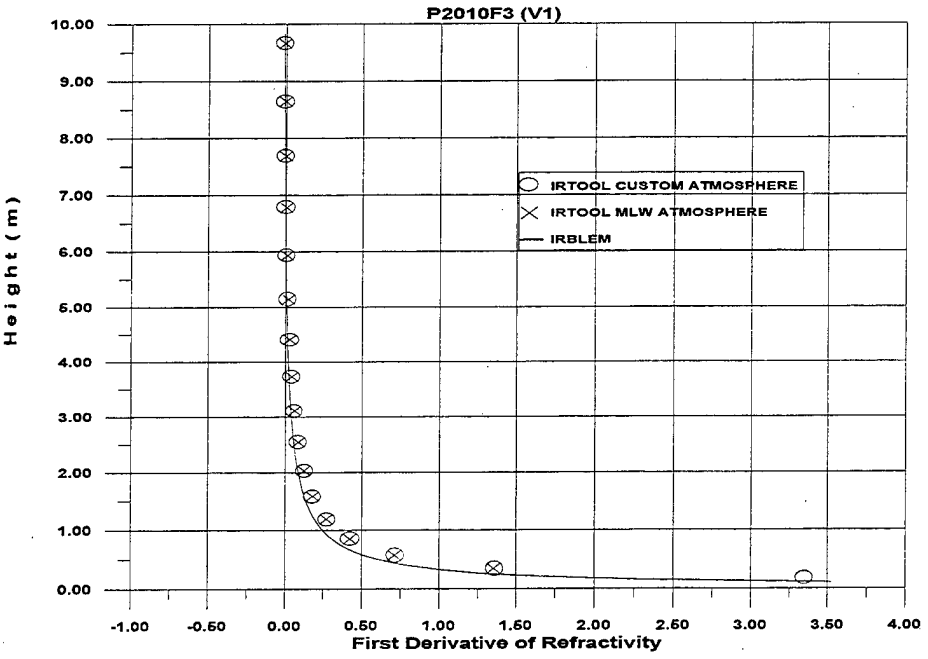

Figure 30F. Gradient of the Refractivity profile as predicted from IRTOOL (using the Mid-Latitude Winter and Custom atmosphere) and IRBLEM model.

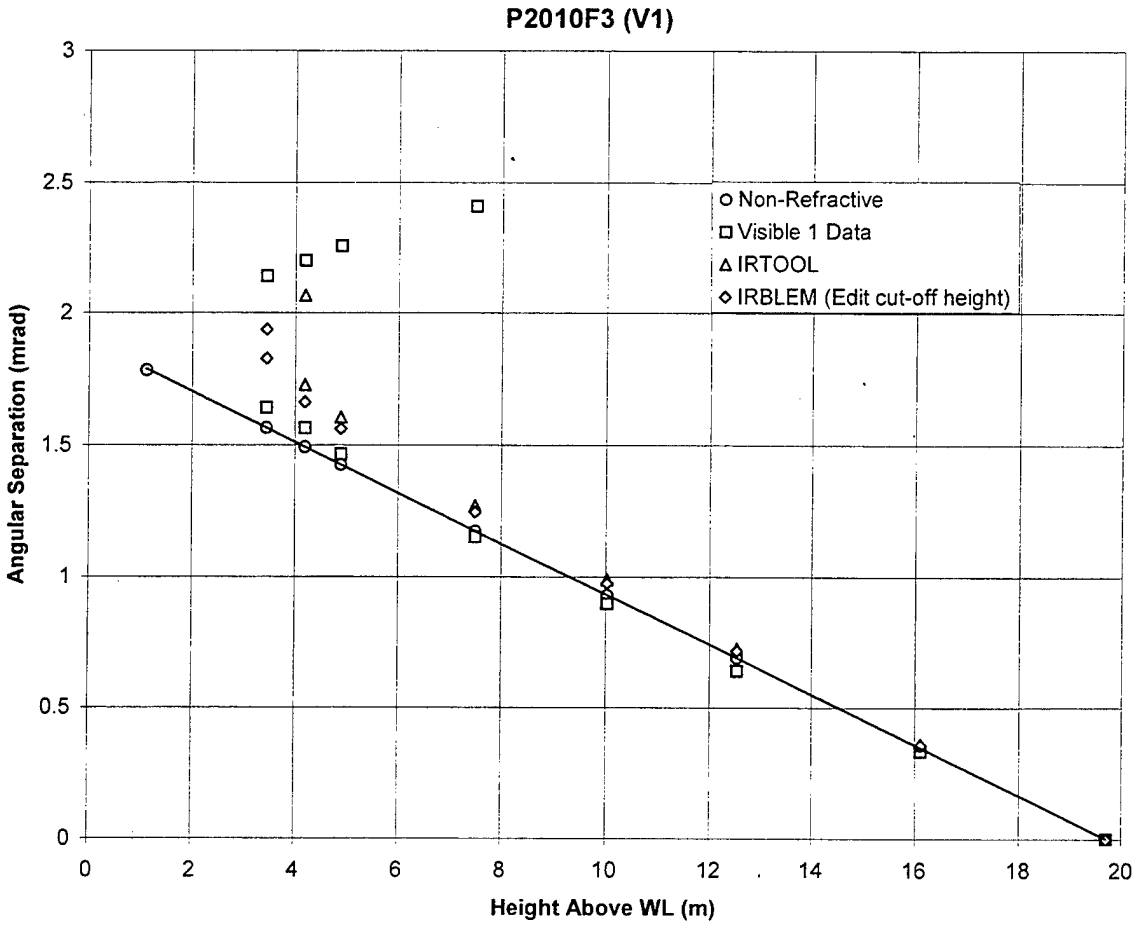

Figure 31. Comparison of IRTOOL and IRBLEM model calculations after editing the cut-off height of IRBLEM, for the P2010F3 event measured by the visible V1 camera.

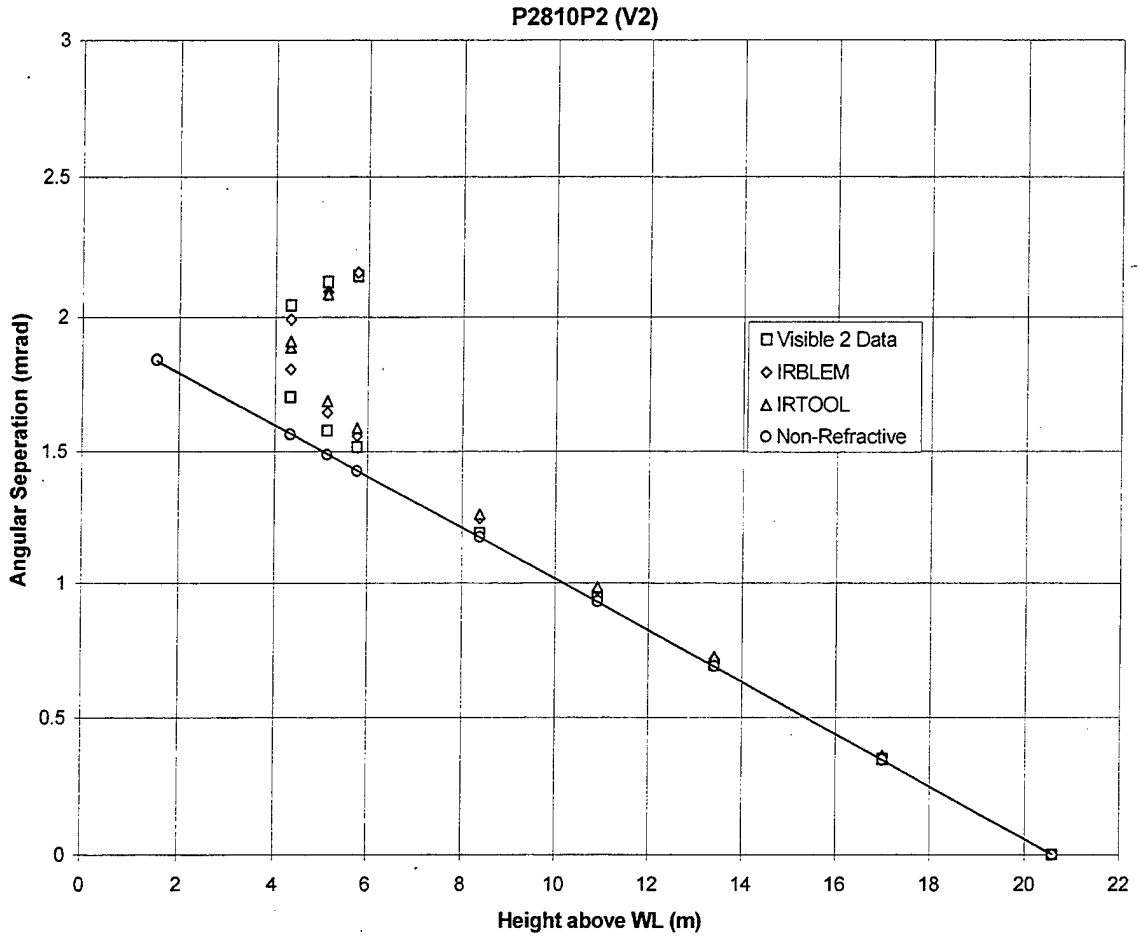

Figure 32. Comparison of IRTOOL and IRBLEM model calculations for the P2810P2 event measured by the visible V2 camera.

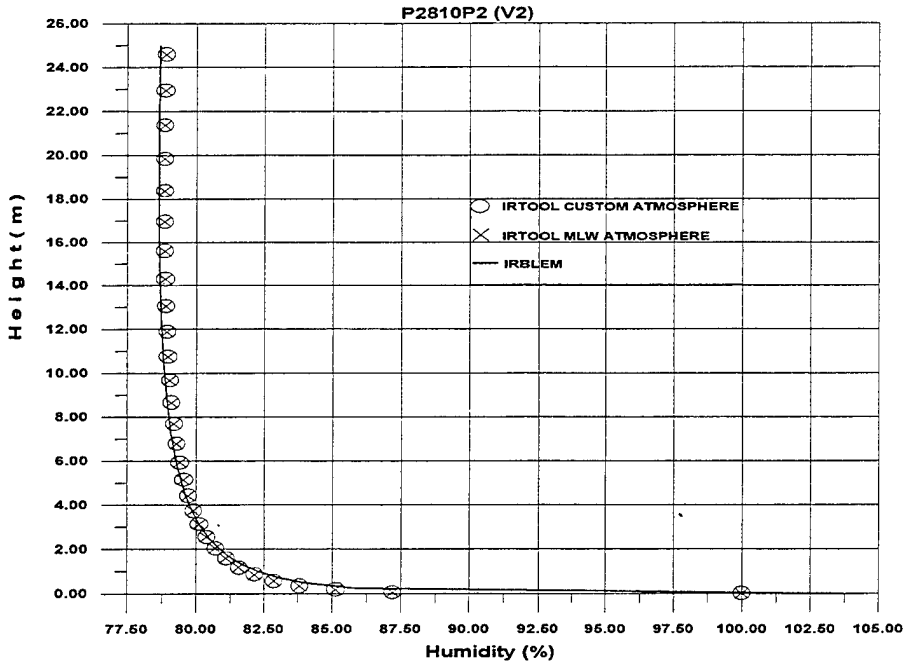

Figure 33A. Humidity profiles as predicted from IRTOOL (using the Mid-Latitude Winter and Custom atmosphere) and IRBLEM model.

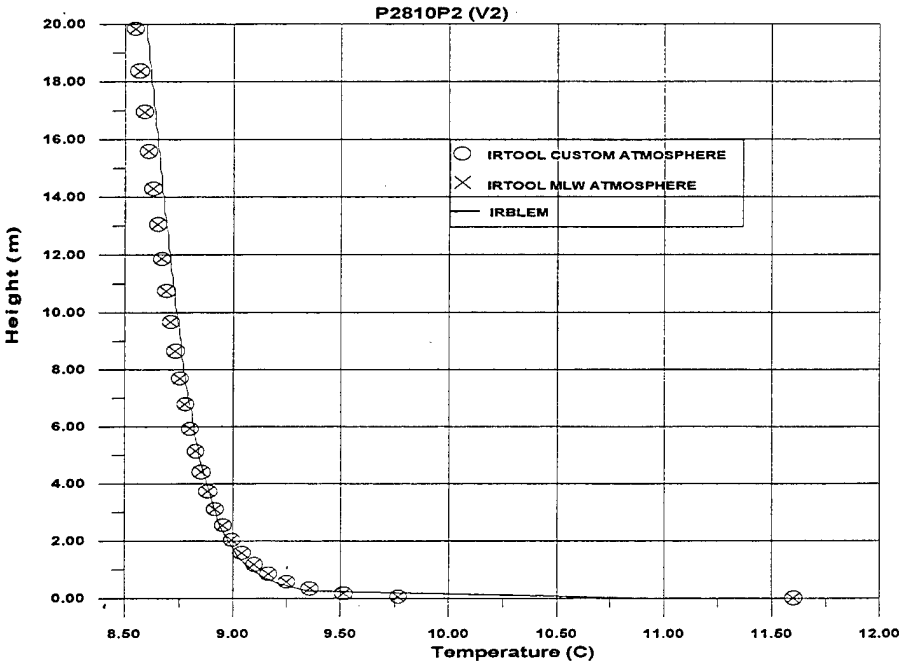

Figure 33B. Temperature profiles as predicted from IRTOOL (using the Mid-Latitude Winter and Custom atmosphere) and IRBLEM model.

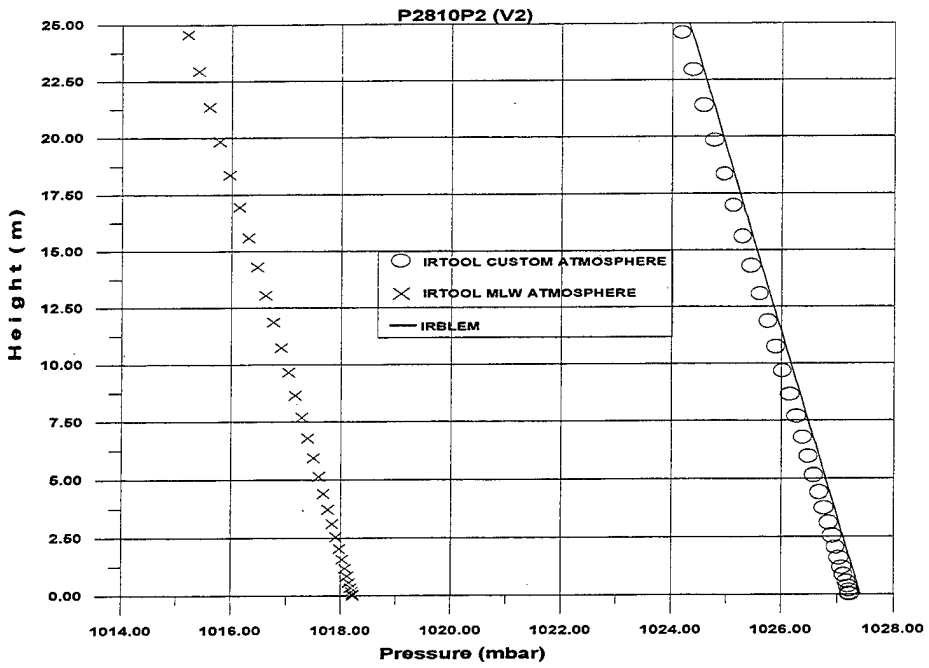

Figure 33C. Pressure profiles as predicted from IRTOOL (using the Mid-Latitude Winter and Custom atmosphere) and IRBLEM model.

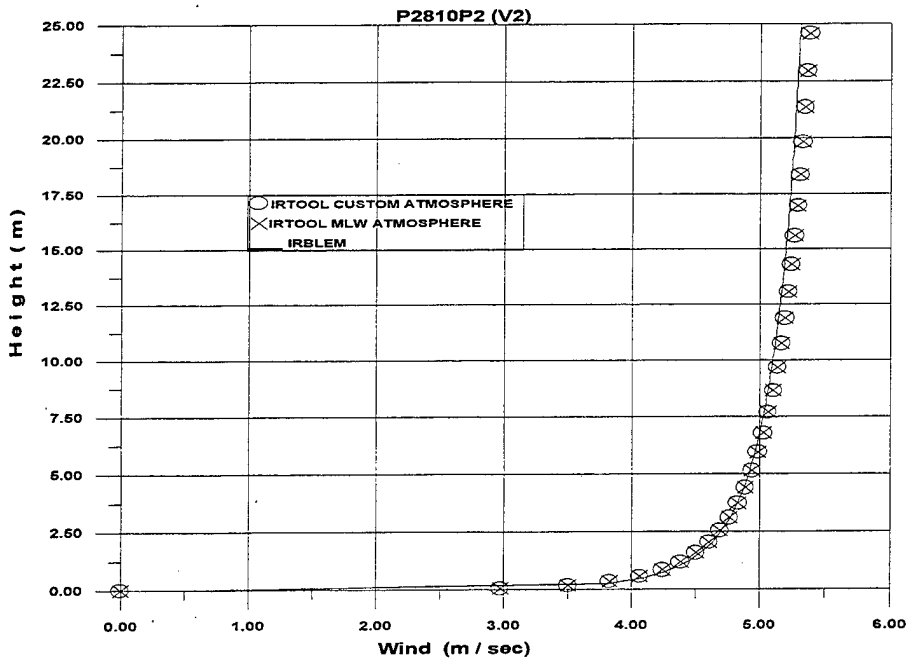

Figure 33D. Wind speed profiles as predicted from IRTOOL (using the Mid-Latitude Winter and Custom atmosphere) and IRBLEM model.

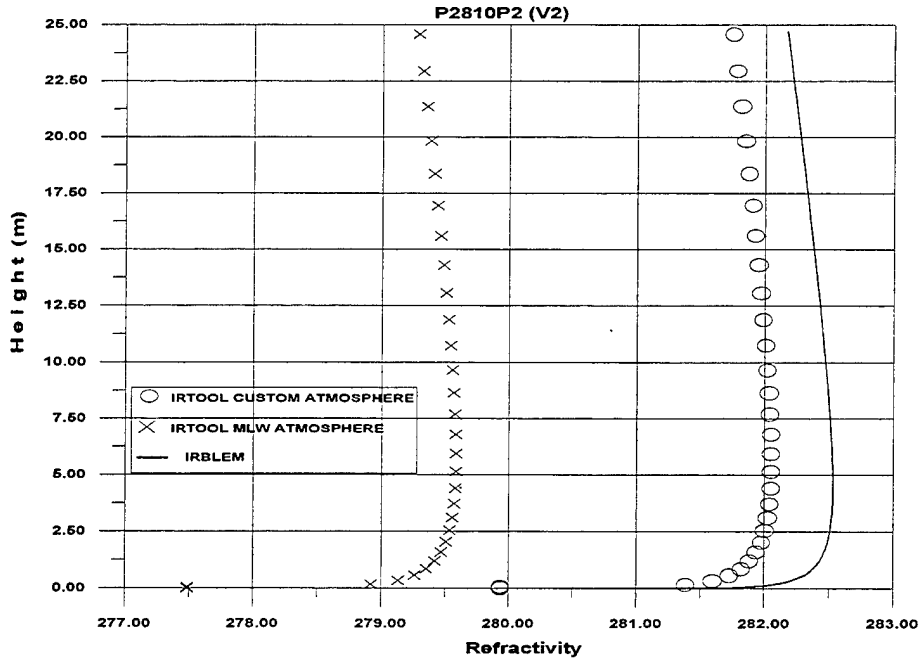

Figure 33E. Refractivity profiles as predicted from IRTOOL (using the Custom atmosphere) and IRBLEM model.

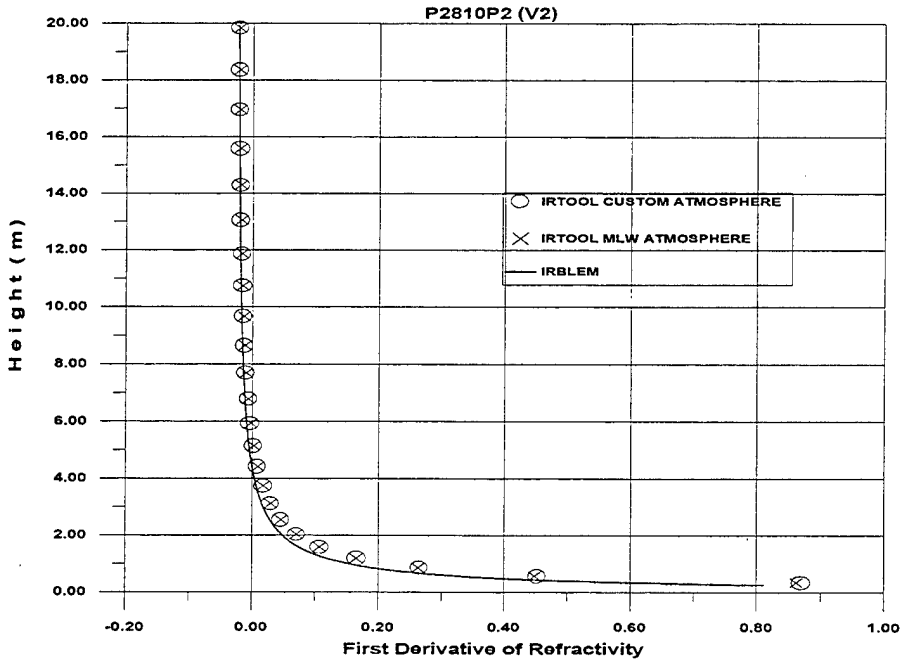

Figure 33F. Gradient of the Refractivity profile as predicted from IRTOOL (using the Mid-Latitude Winter and Custom atmosphere) and IRBLEM model.

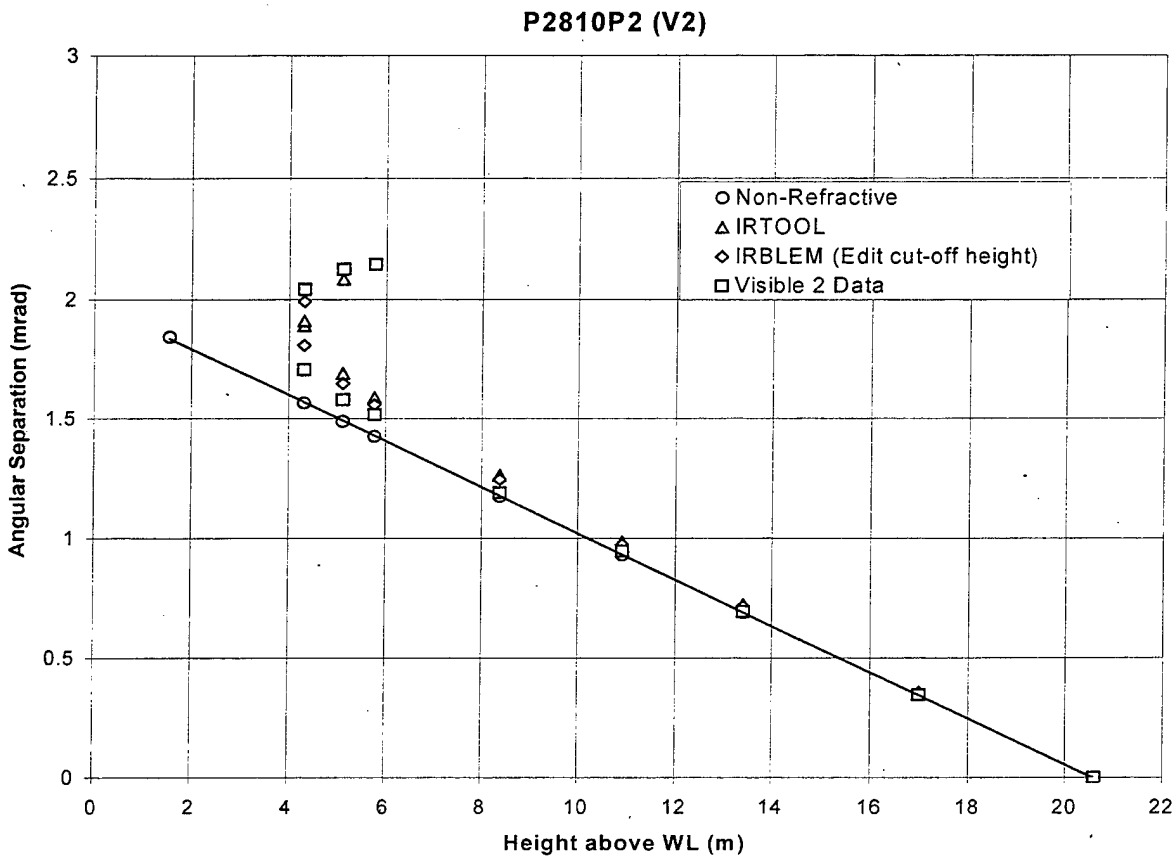

Figure 34. Comparison of IRTOOL and IRBLEM model calculations after editing the cut-off height of IRBLEM, for the P2810P2 event measured by the visible V2 camera.

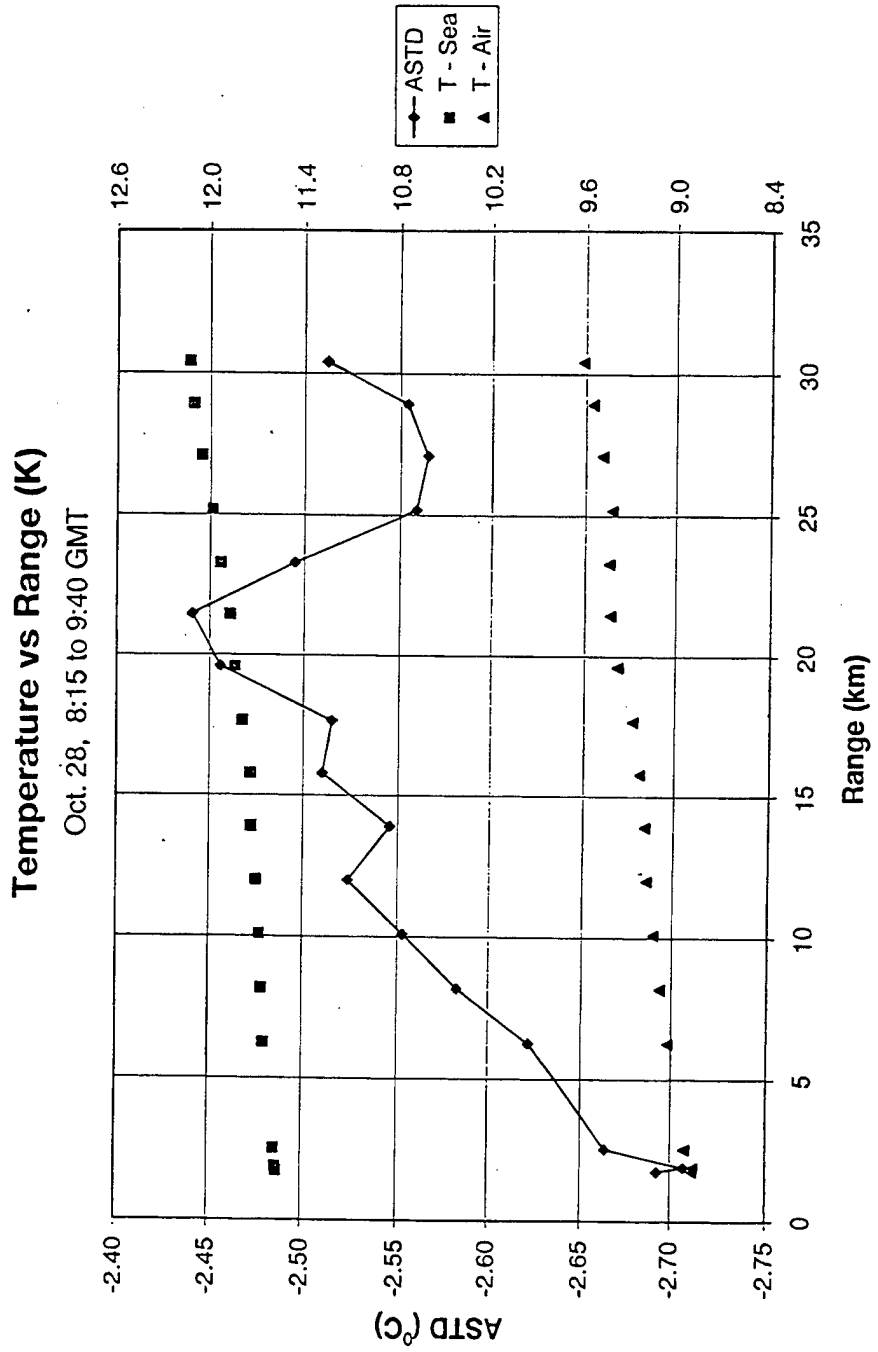

Figure 35. Variation of the sea and air temperature along the ship's course during ship tracking event K.

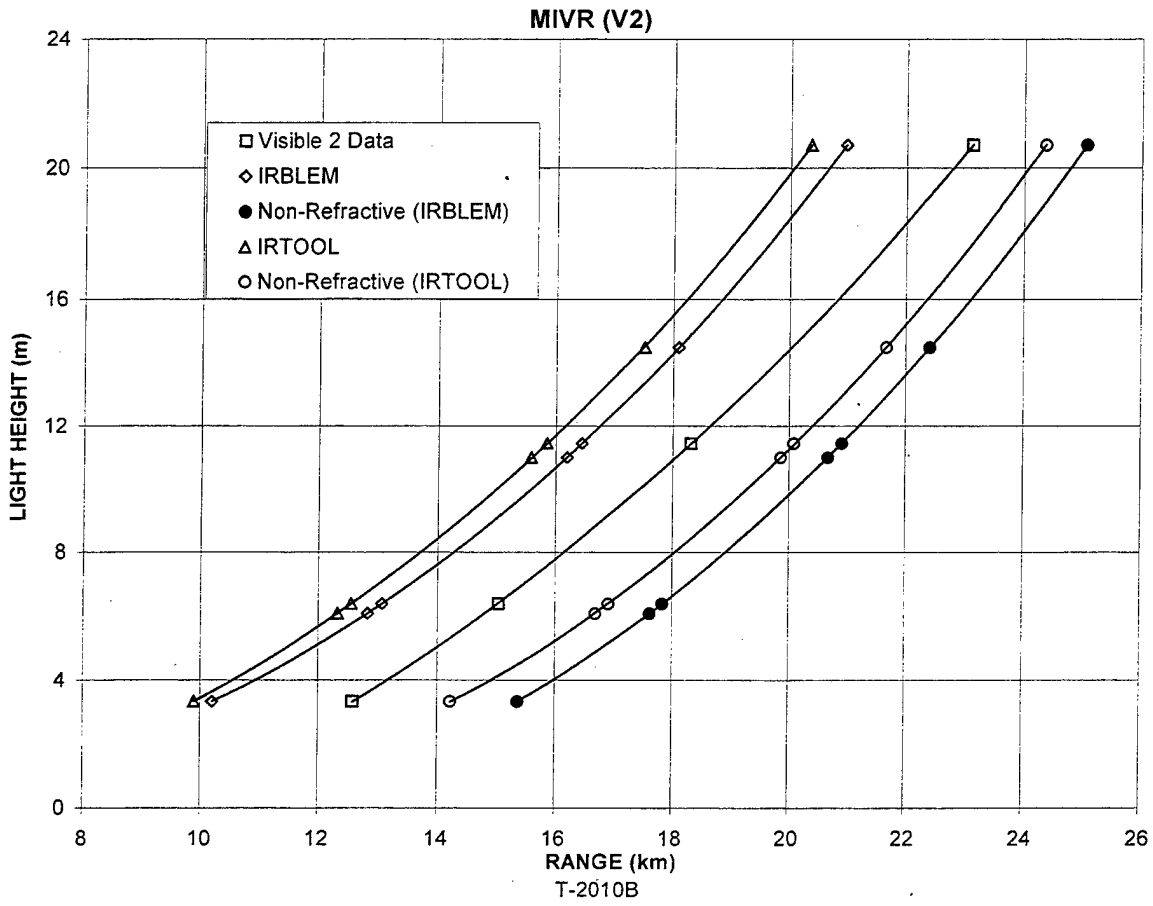

Figure 36. Comparison of the LWKD and IRTOOL model MIVRs with the ship-tracking data measured by the visible (V2) camera.

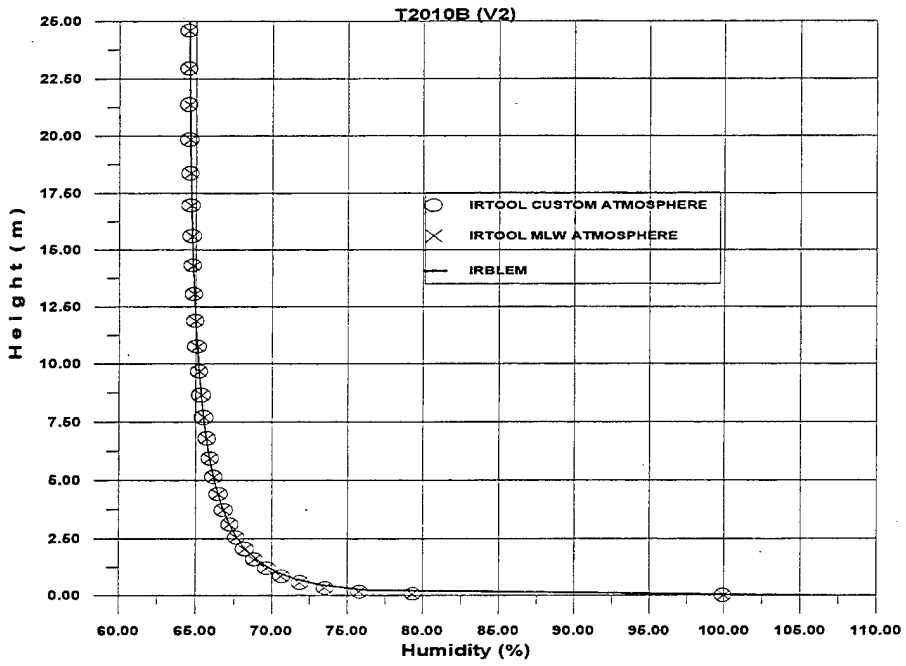

Figure 37A. Humidity profiles as predicted from IRTOOL (using the Mid-Latitude Winter and Custom atmosphere) and IRBLEM model.

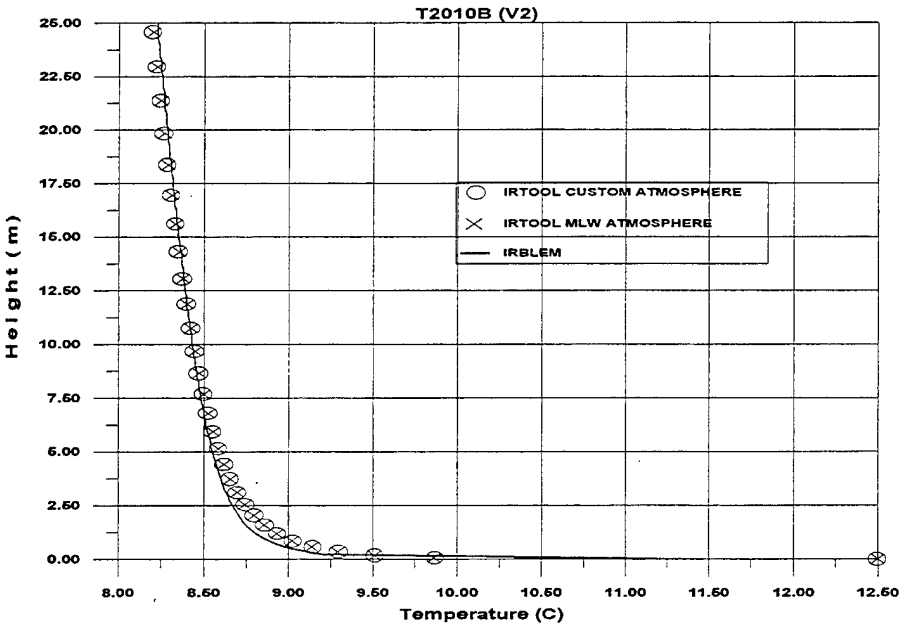

Figure 37B. Temperature profiles as predicted from IRTOOL (using the Mid-Latitude Winter and Custom atmosphere) and IRBLEM model.

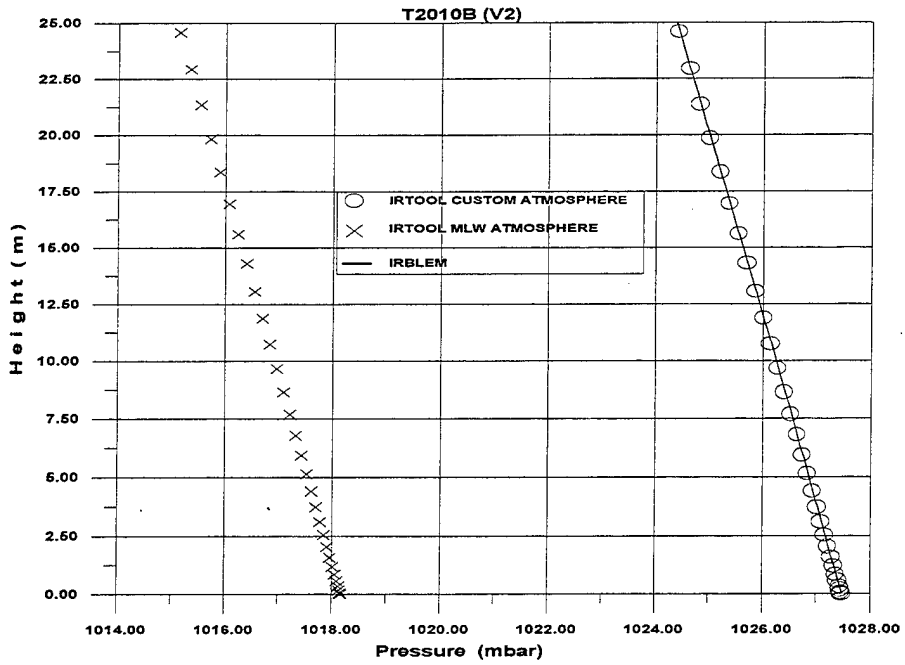

Figure 37C. Pressure profiles as predicted from IRTOOL (using the Mid-Latitude Winter and Custom atmosphere) and IRBLEM model.

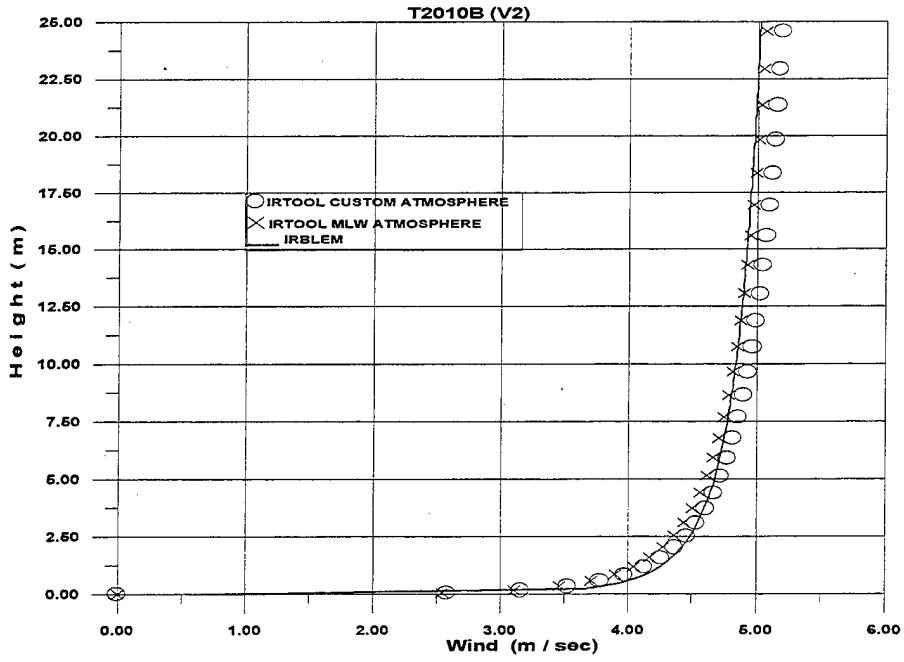

Figure 37D. Wind speed profiles as predicted from IRTOOL (using the Mid-Latitude Winter and Custom atmosphere) and IRBLEM model.

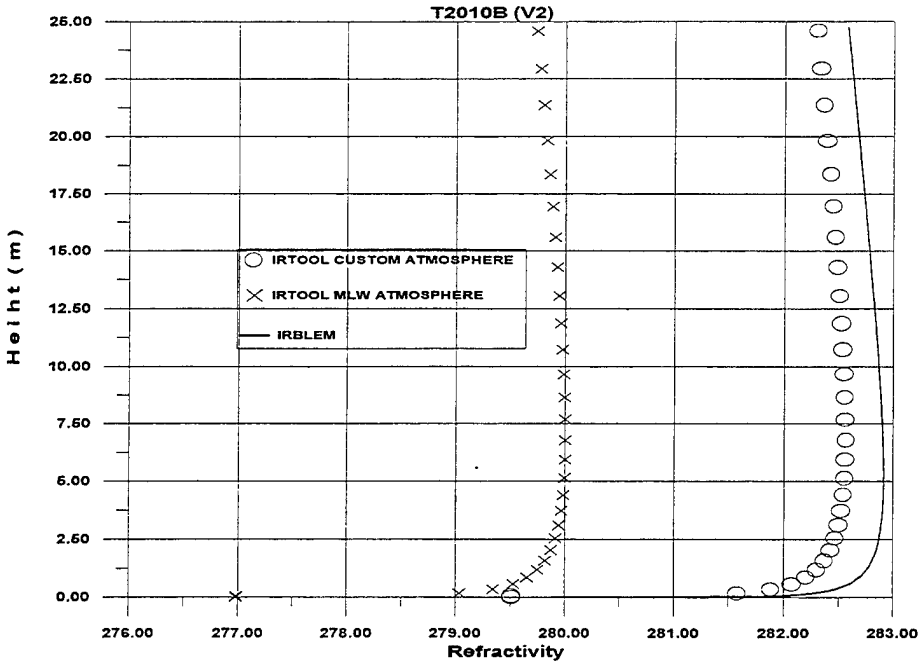

Figure 37E. Refractivity profiles as predicted from IRTOOL (using the Custom atmosphere) and IRBLEM model.

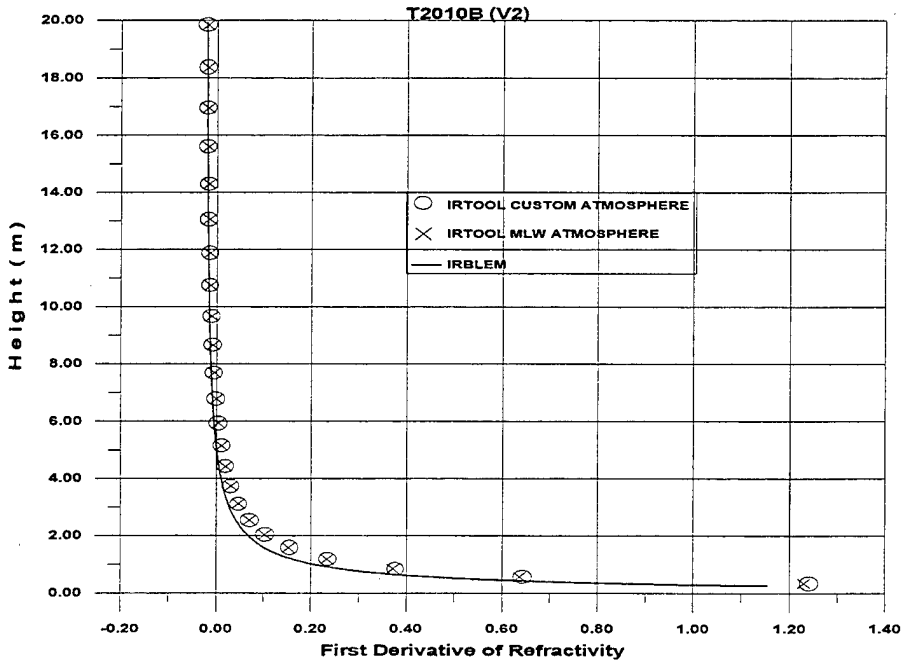

Figure 37F. Gradient of the Refractivity profile as predicted from IRTOOL (using the Mid-Latitude Winter and Custom atmosphere) and IRBLEM model.

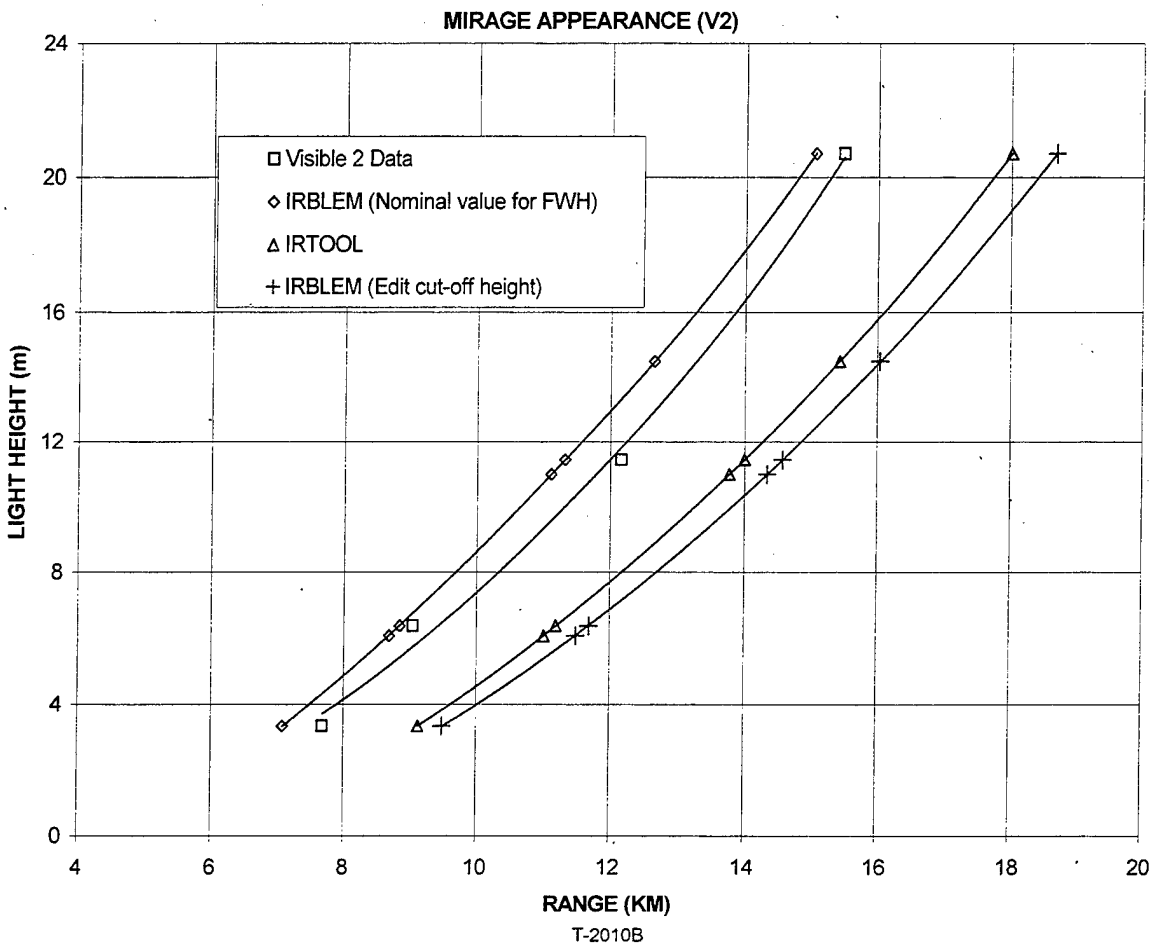

Figure 38. Comparison of the LWKD and IRTOOL model MMRs with the ship-tracking data measured by the visible (V2) camera.

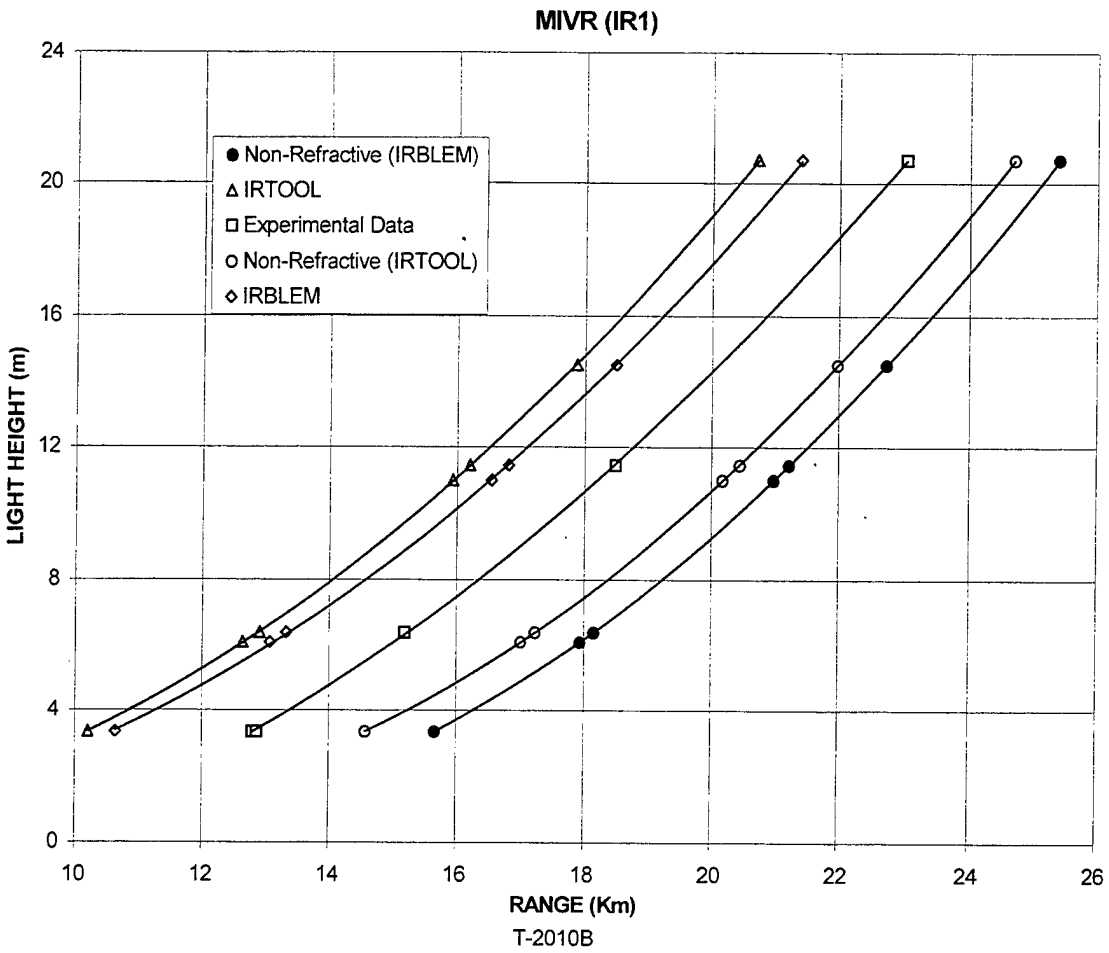

Figure 39. Comparison of the LWKD and IRTOOL model MIVRs with the ship-tracking data measured by the infrared (IR1) camera.

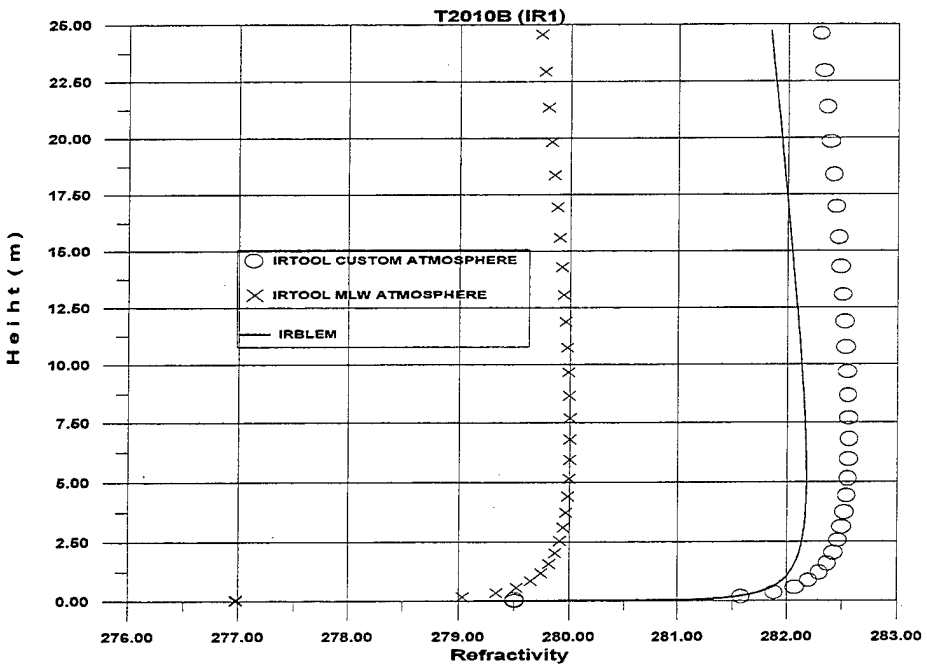

Figure 40A. Refractivity profiles as predicted from IRTOOL (using the Mid-Latitude Winter and Custom atmosphere) and IRBLEM model.

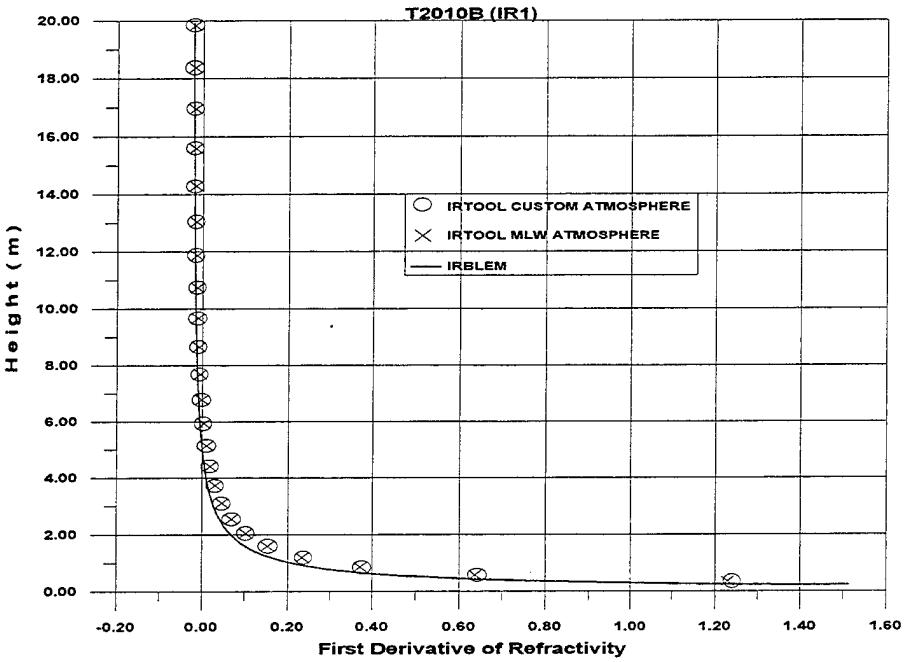

Figure 40B. Gradient of the Refractivity profile as predicted from IRTOOL (using the Mid-Latitude Winter and Custom atmosphere) and IRBLEM model.

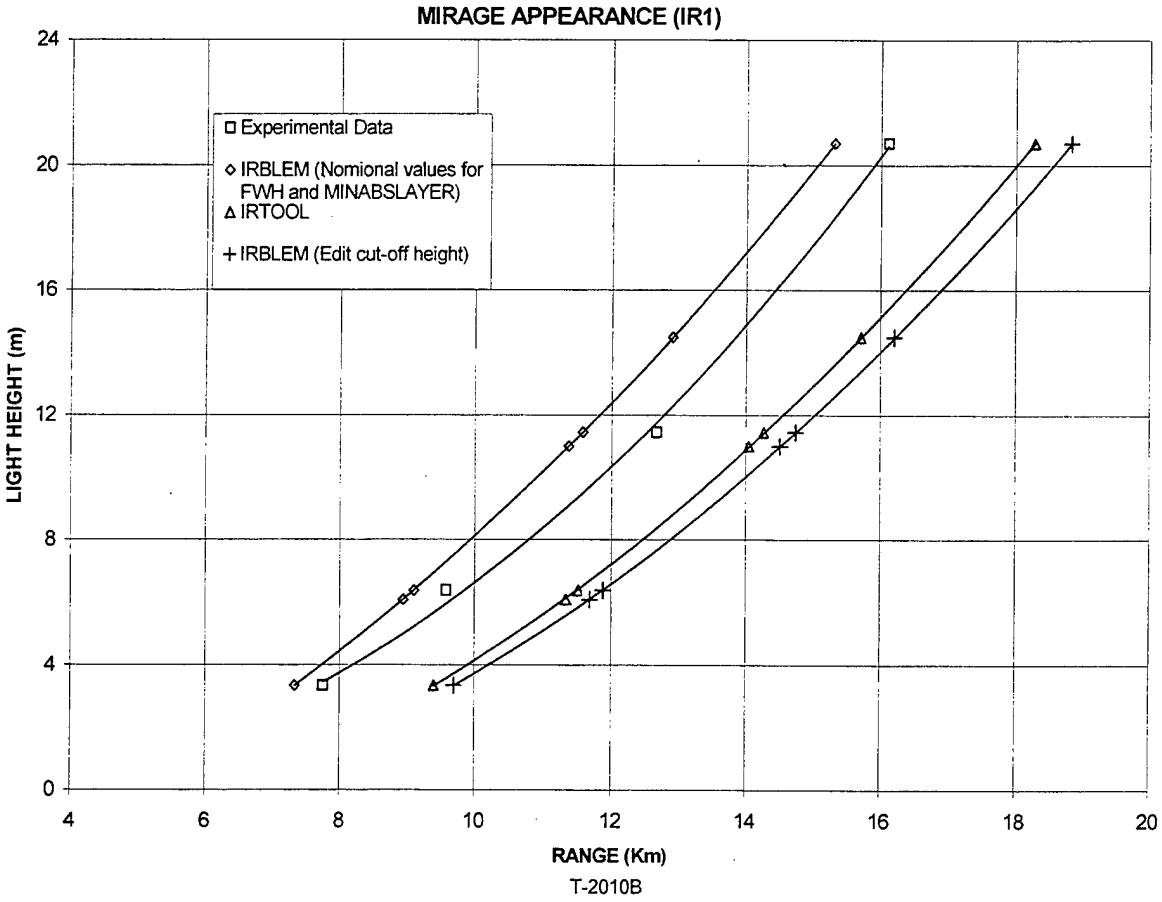

Figure 41. Comparison of the LWKD and IRTOOL model MMRs with the ship-tracking data measured by the infrared (IR1) camera.

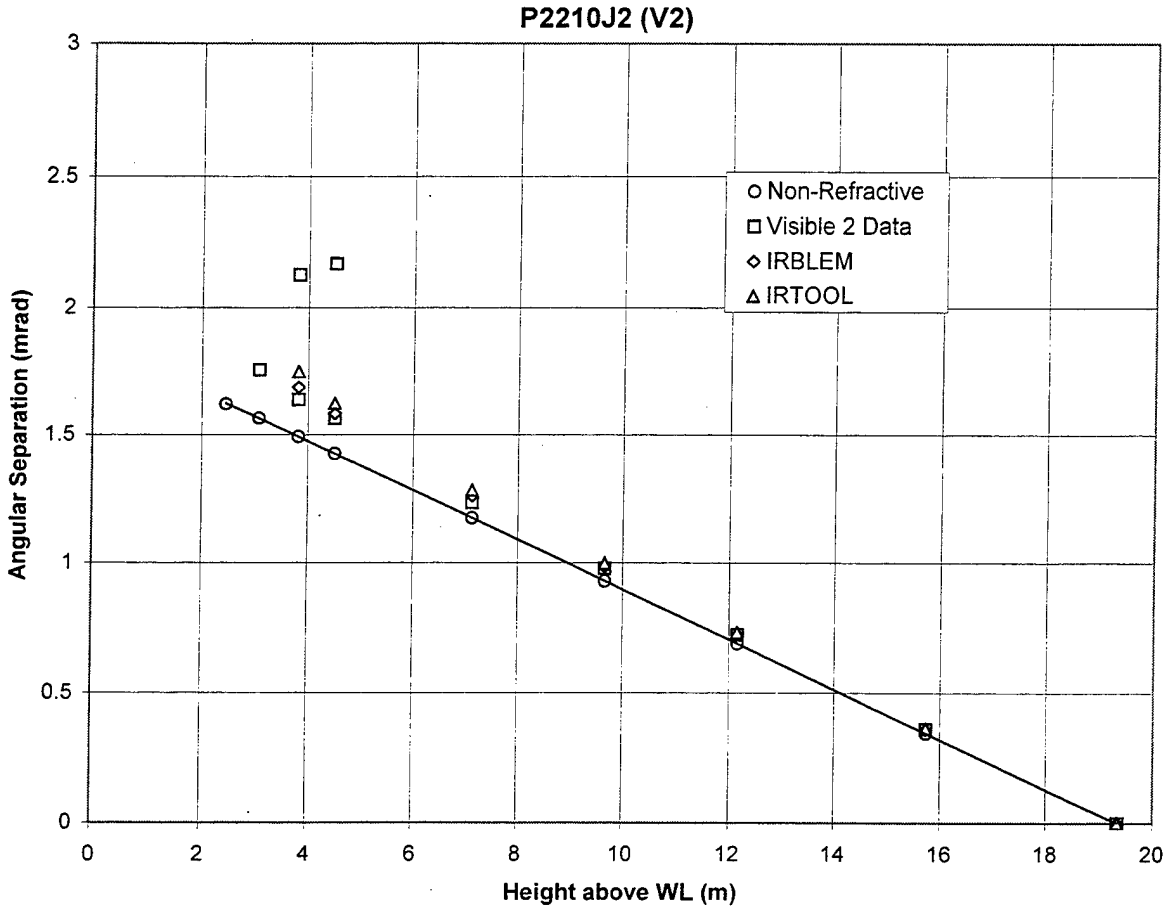

Figure 42. Comparison of IRTOOL and IRBLEM model calculations of IRBLEM, for the P2210J2 event measured by the visible V2 camera.

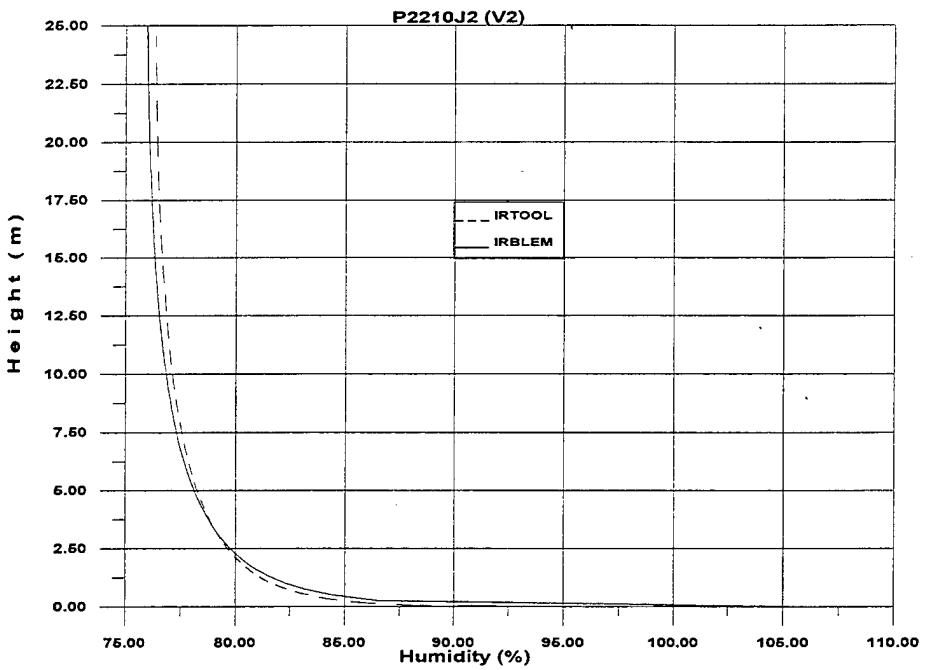

Figure 43A. Humidity profiles as predicted from IRTOOL (using the Mid-Latitude Winter atmosphere) and IRBLEM model.

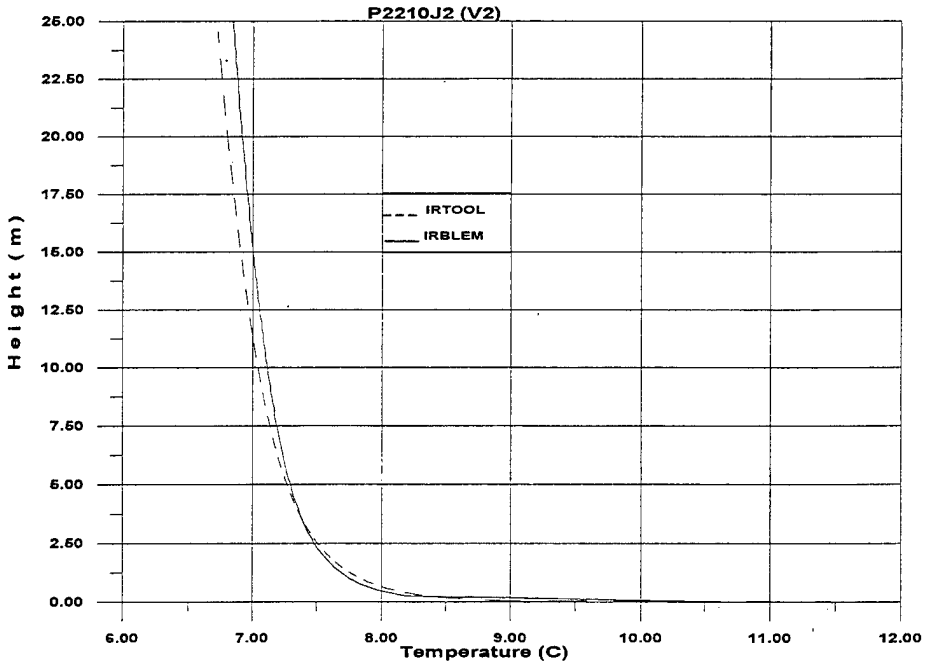

Figure 43B. Temperature profiles as predicted from IRTOOL (using the Mid-Latitude Winter atmosphere) and IRBLEM model.

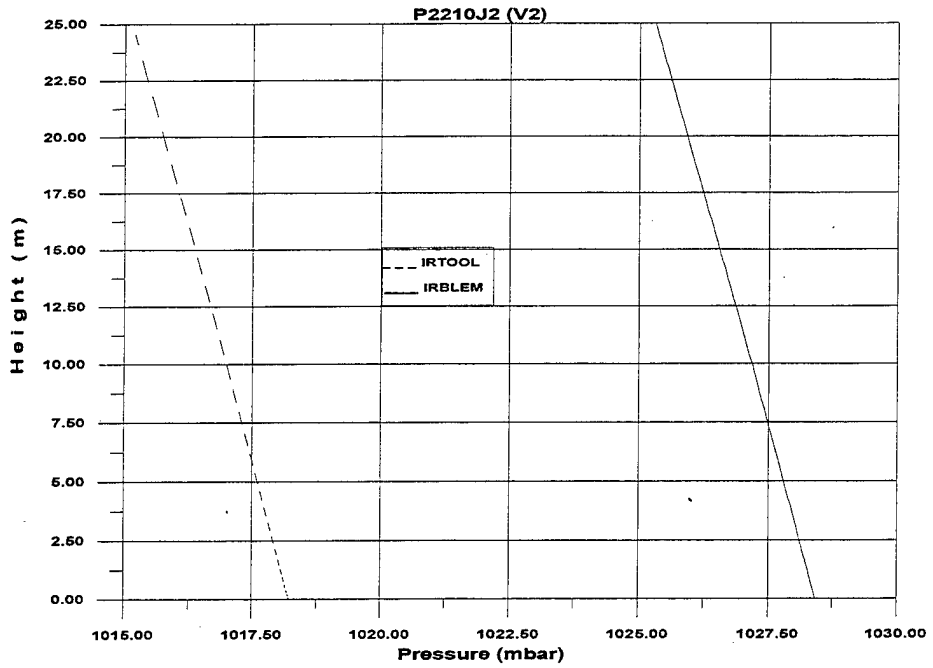

Figure 43C. Pressure profiles as predicted from IRTOOL (using the Mid-Latitude Winter atmosphere) and IRBLEM model.

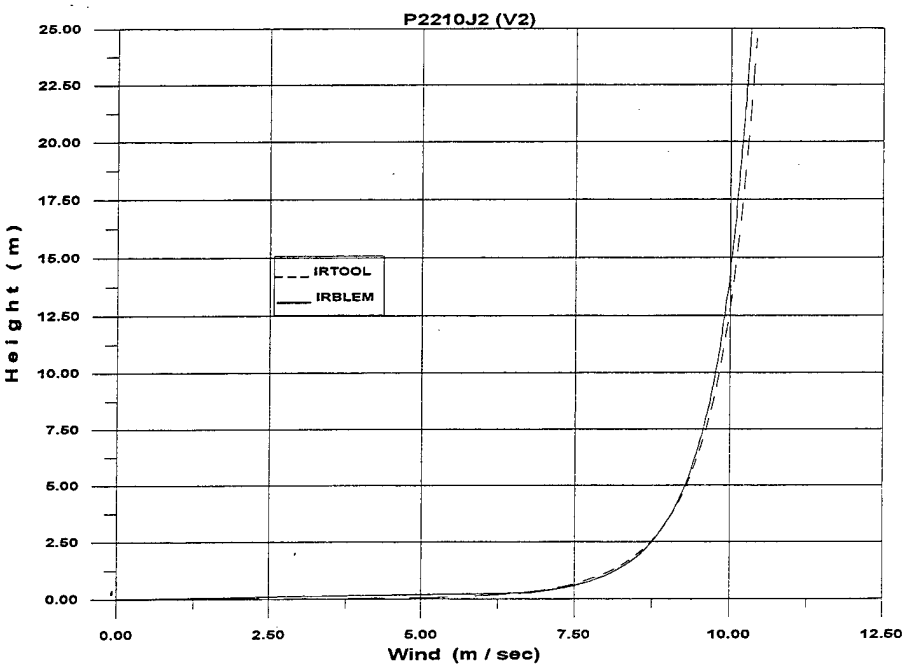

Figure 43D. Wind speed profiles as predicted from IRTOOL (using the Mid-Latitude Winter atmosphere) and IRBLEM model.

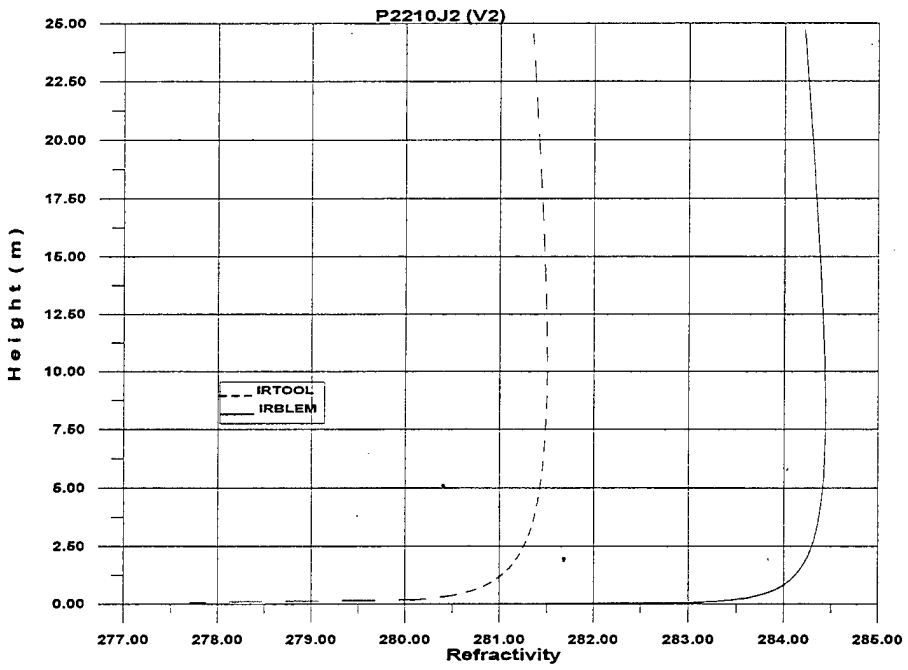

Figure 43E. Refractivity profiles as predicted from IRTOOL (using the Mid-Latitude Winter atmosphere) and IRBLEM model.

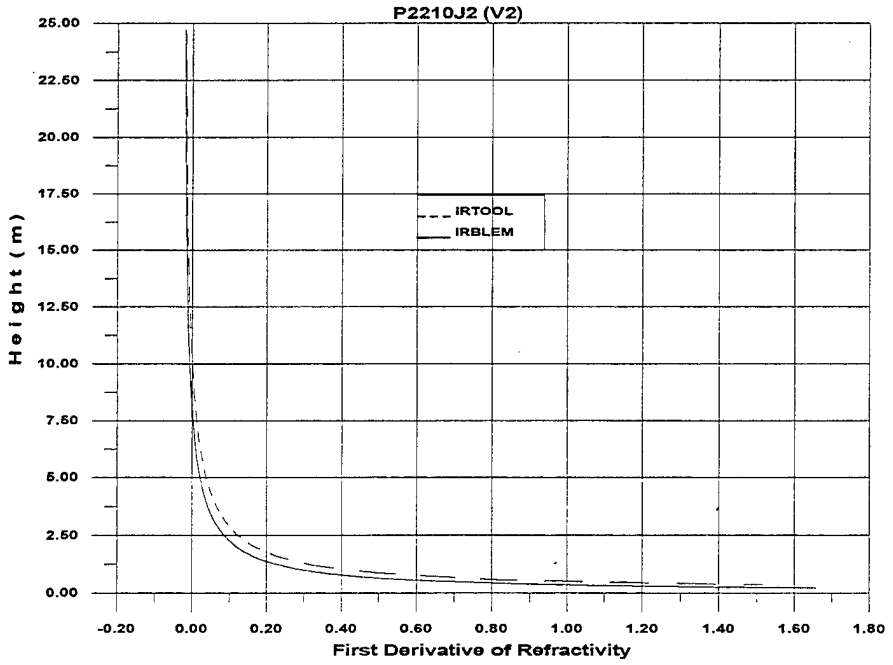

Figure 43F. Gradient of the Refractivity profile as predicted from IRTOOL (using the Mid-Latitude Winter atmosphere) and IRBLEM model.

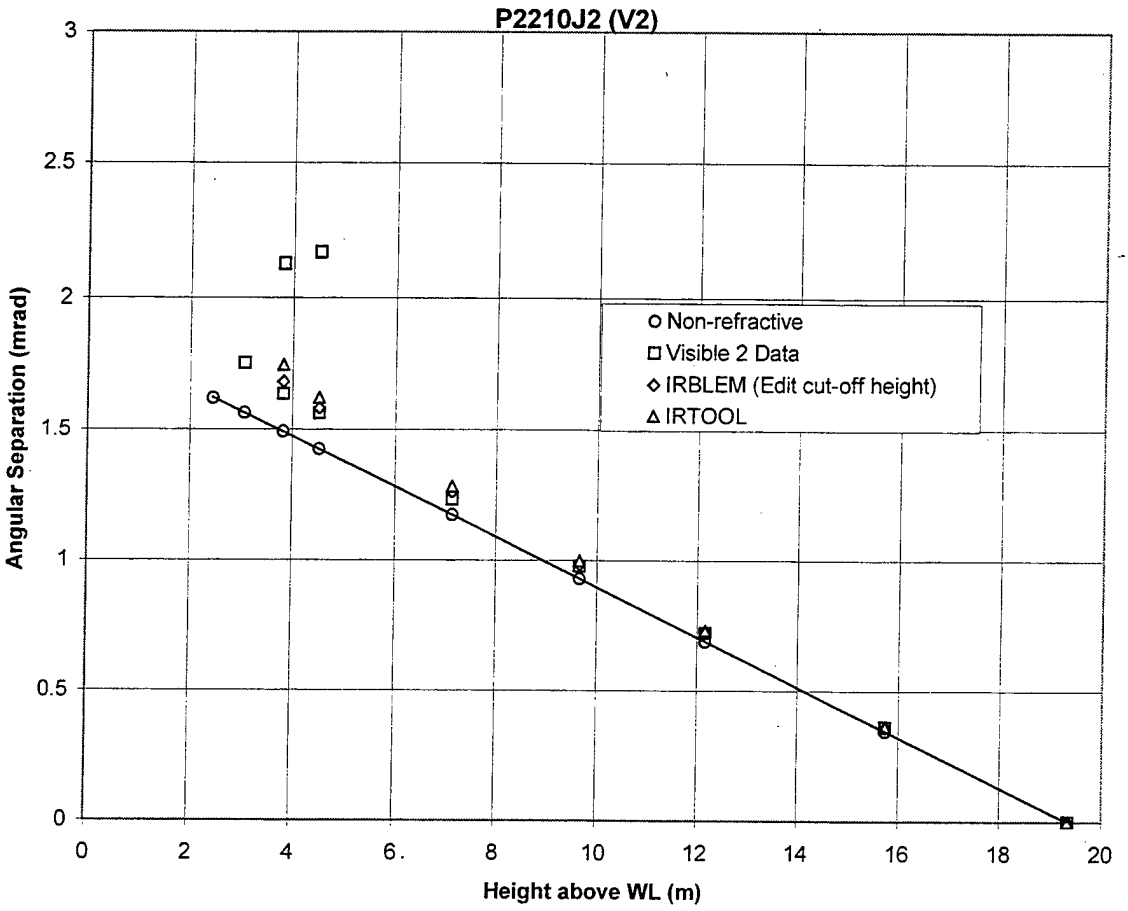

Figure 44. Comparison of IRTOOL and IRBLEM model calculations after editing the cut-off height of IRBLEM for the P2210J2 event measured by the visible V2 camera.

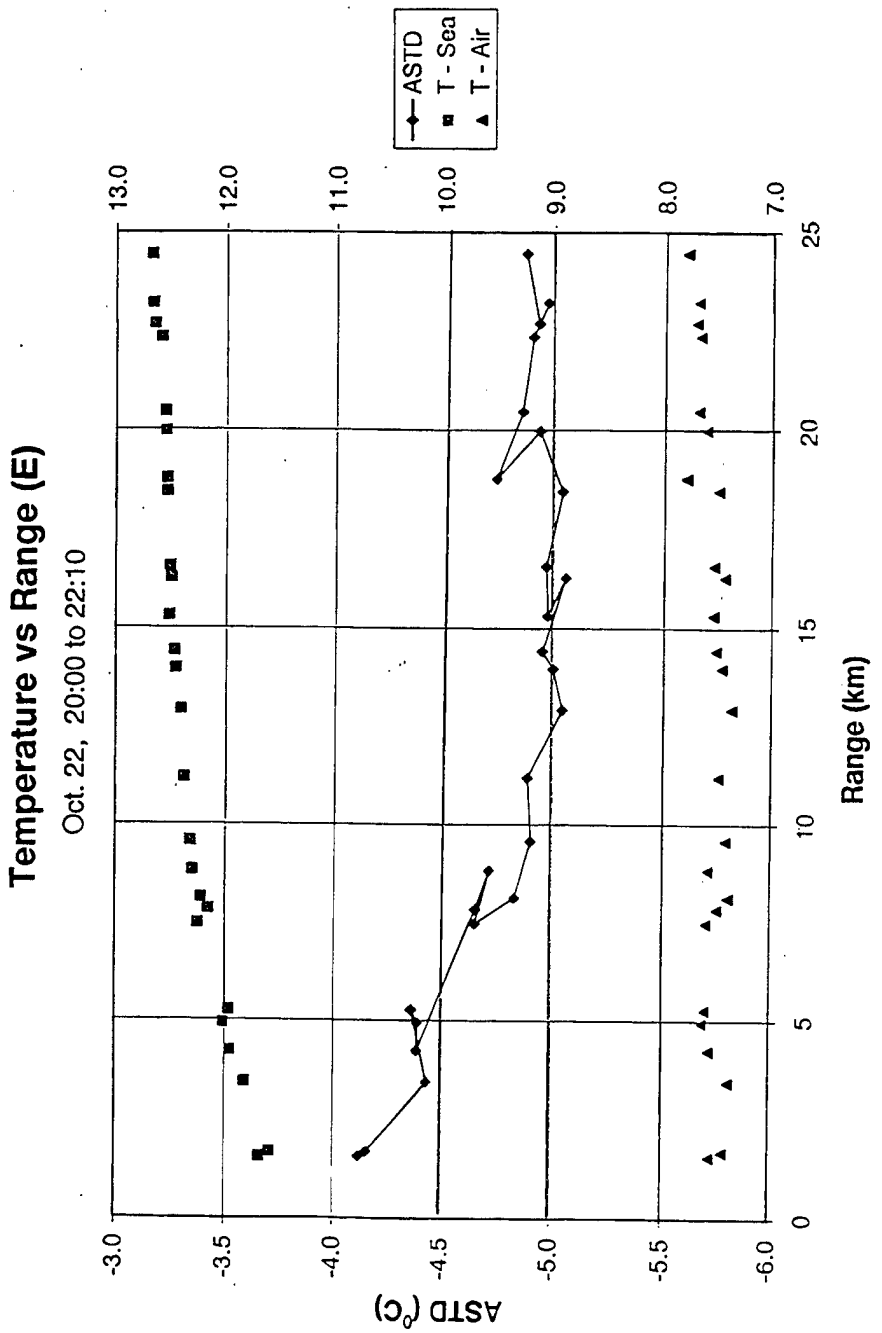

Figure 45. Variation of the sea and air temperature along the ship's course during ship tracking event E.

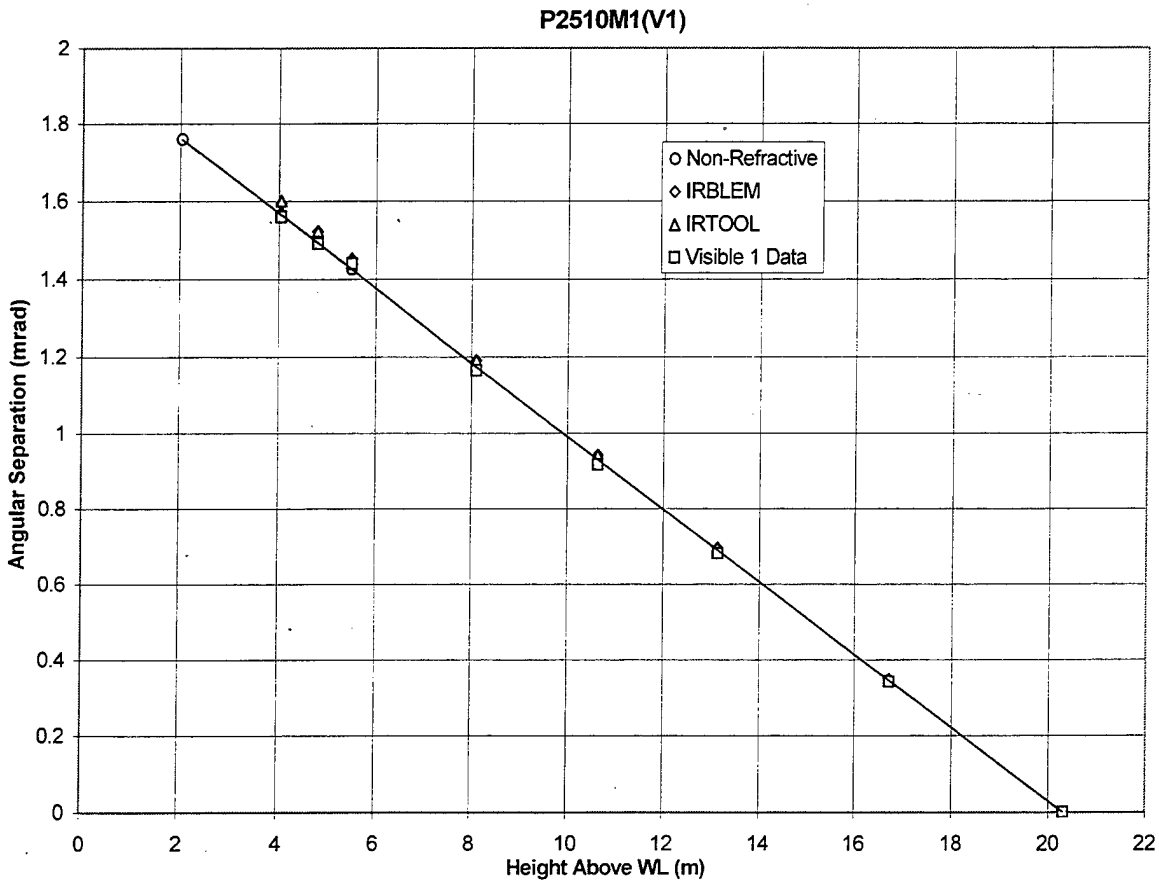

Figure 46. Comparison of IRTOOL and IRBLEM model calculations for the P2510M1 event measured by the visible V1 camera.

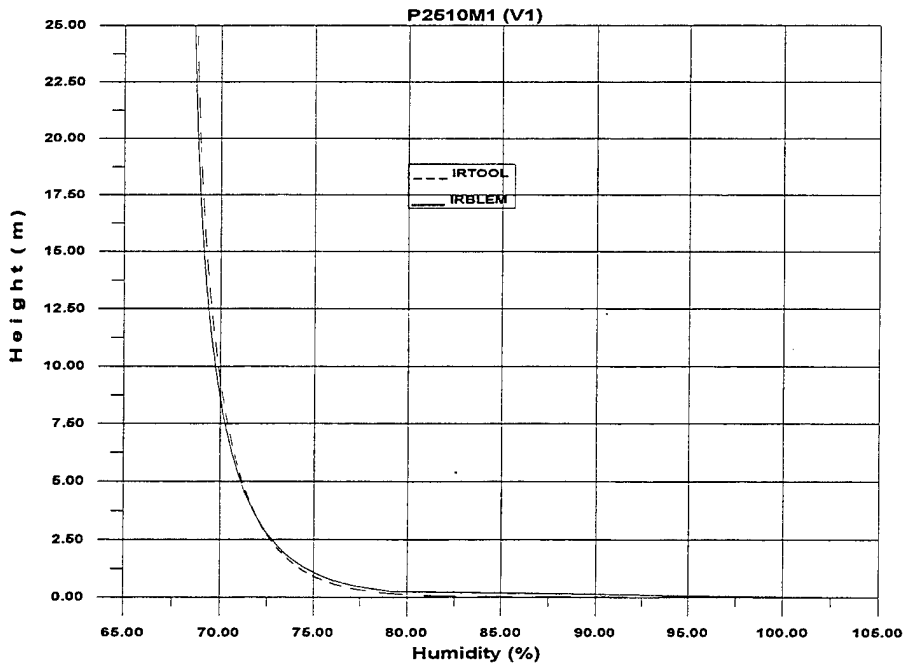

Figure 47A. Humidity profiles as predicted from IRTOOL (using the Mid-Latitude Winter atmosphere) and IRBLEM model.

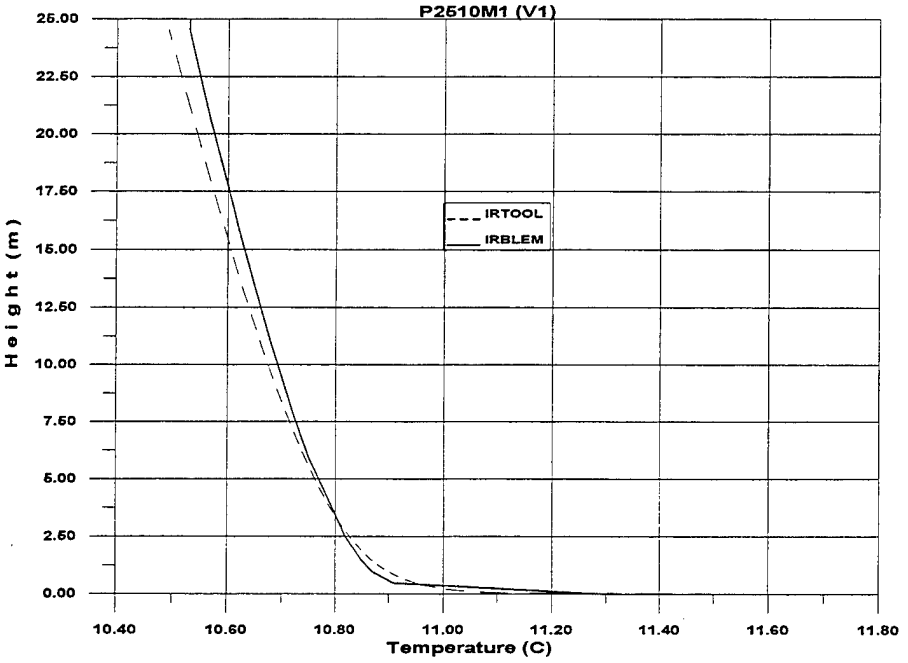

Figure 47B. Temperature profiles as predicted from IRTOOL (using the Mid-Latitude Winter atmosphere) and IRBLEM model.

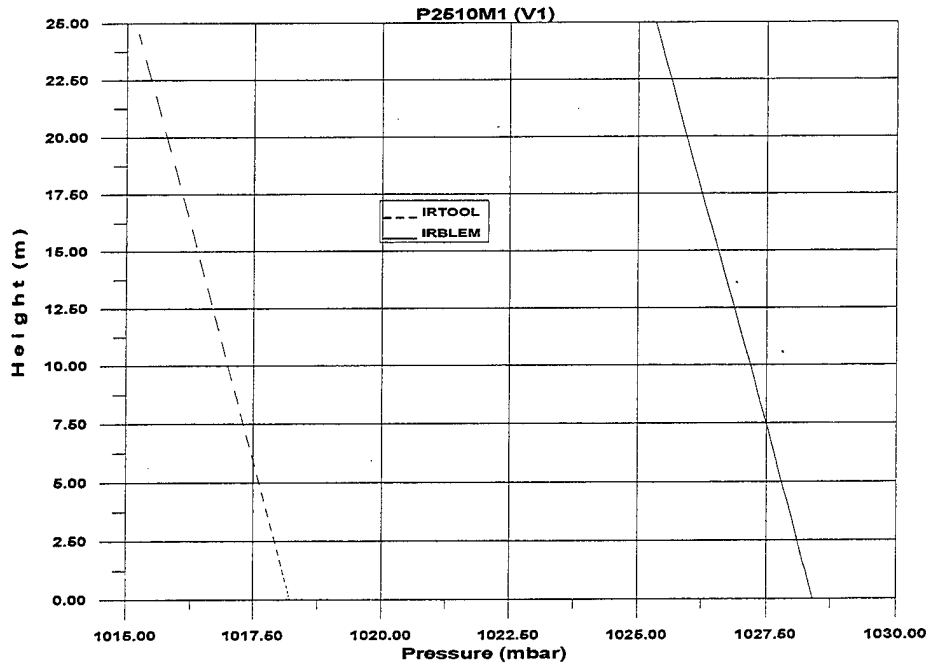

Figure 47C. Pressure profiles as predicted from IRTOOL (using the Mid-Latitude Winter atmosphere) and IRBLEM model.

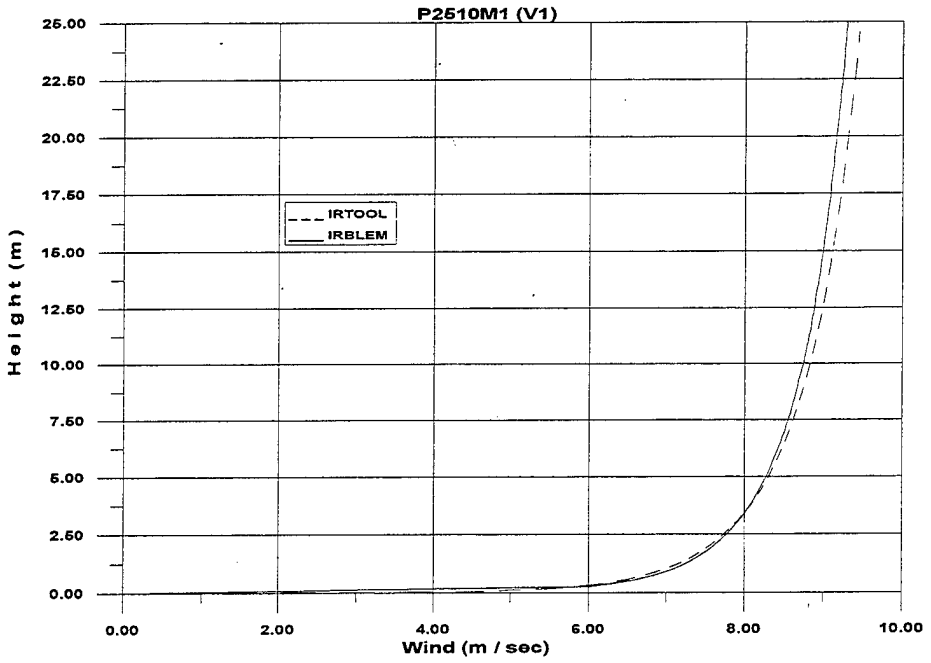

Figure 47D. Wind speed profiles as predicted from IRTOOL (using the Mid-Latitude Winter atmosphere) and IRBLEM model.

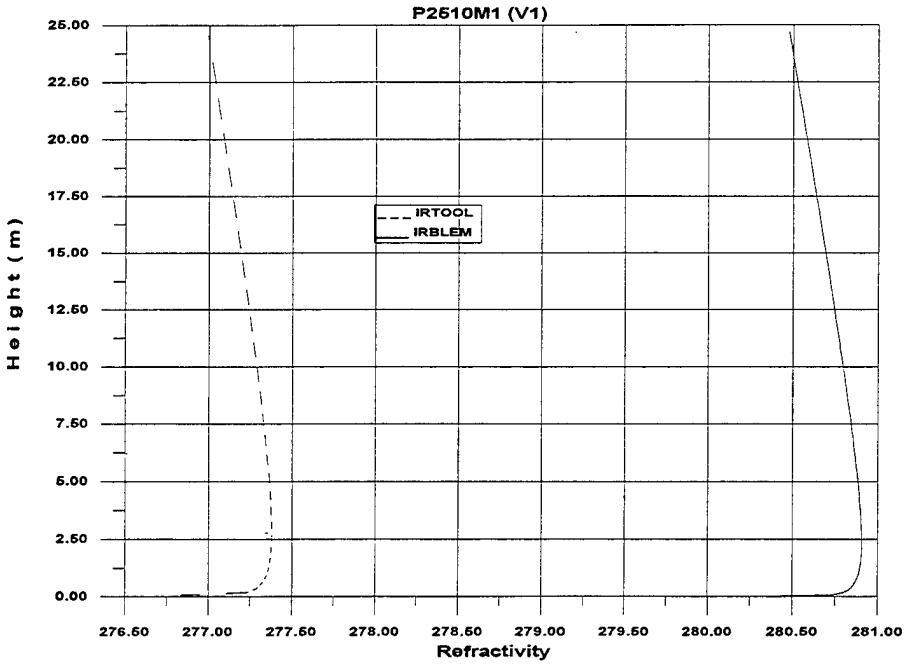

Figure 47E. Refractivity profiles as predicted from IRTOOL (using the Mid-Latitude Winter atmosphere) and IRBLEM model.

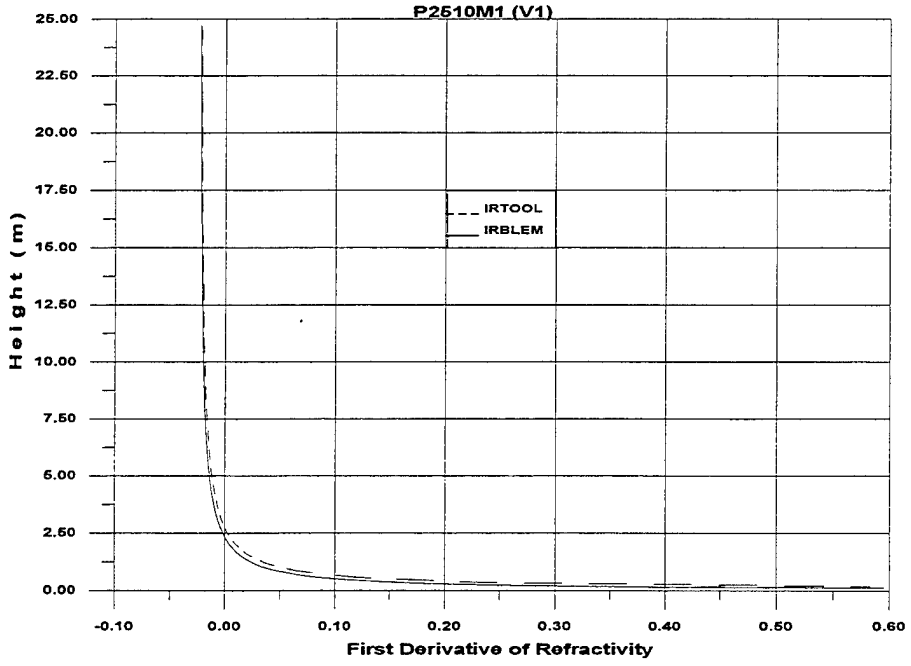

Figure 47F. Gradient of the Refractivity profile as predicted from IRTOOL (using the Mid-Latitude Winter atmosphere) and IRBLEM model.

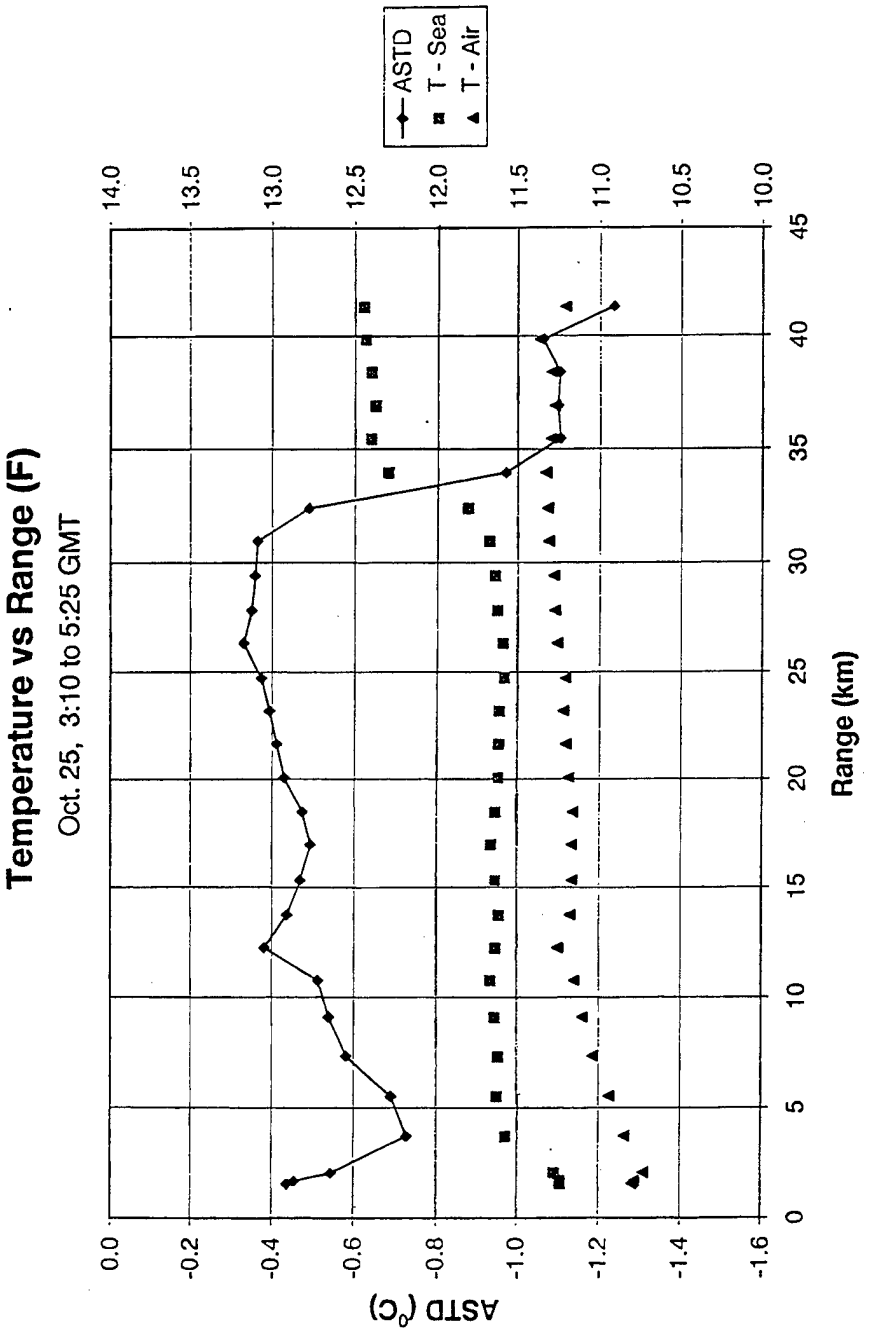

Figure 48. Variation of the sea and air temperature along the ship's course during ship tracking event F.

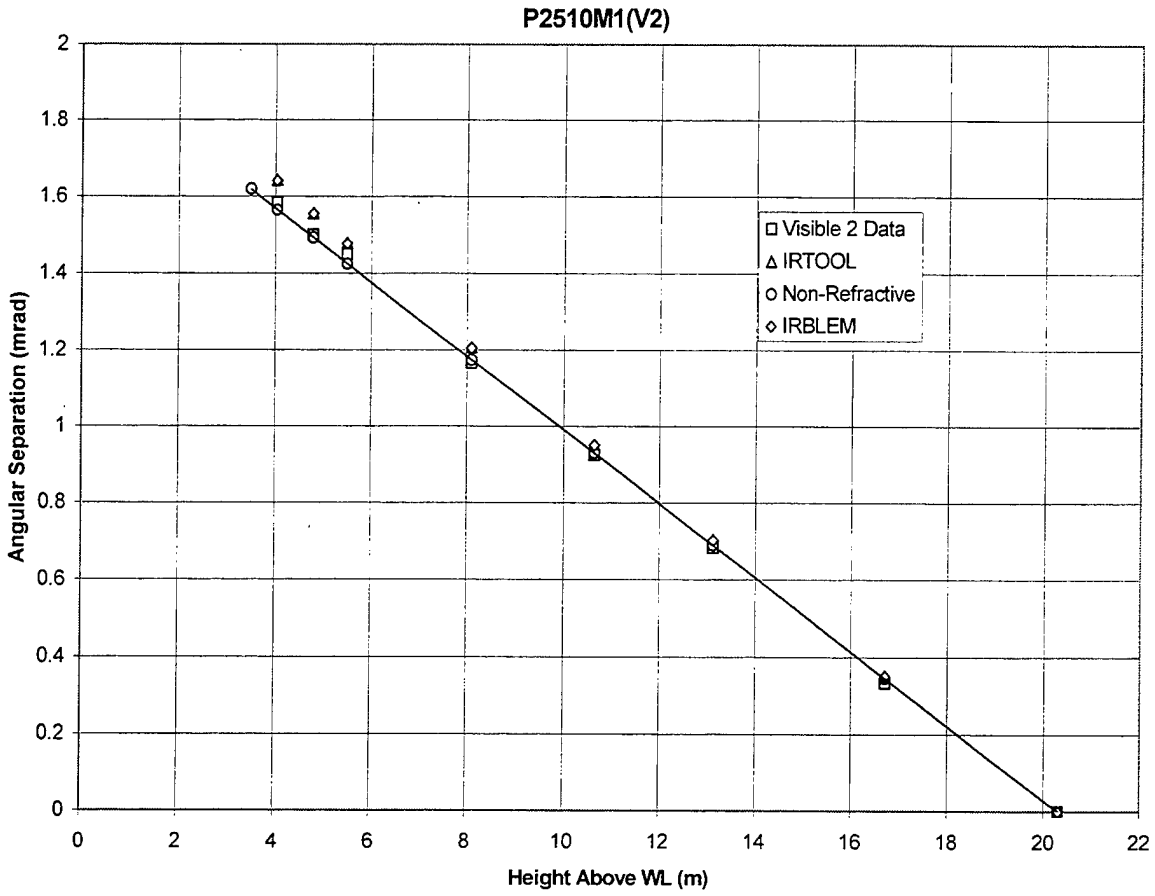

Figure 49. Comparison of IRTOOL and IRBLEM model calculations for the P2510M1 event measured by the visible V2 camera.

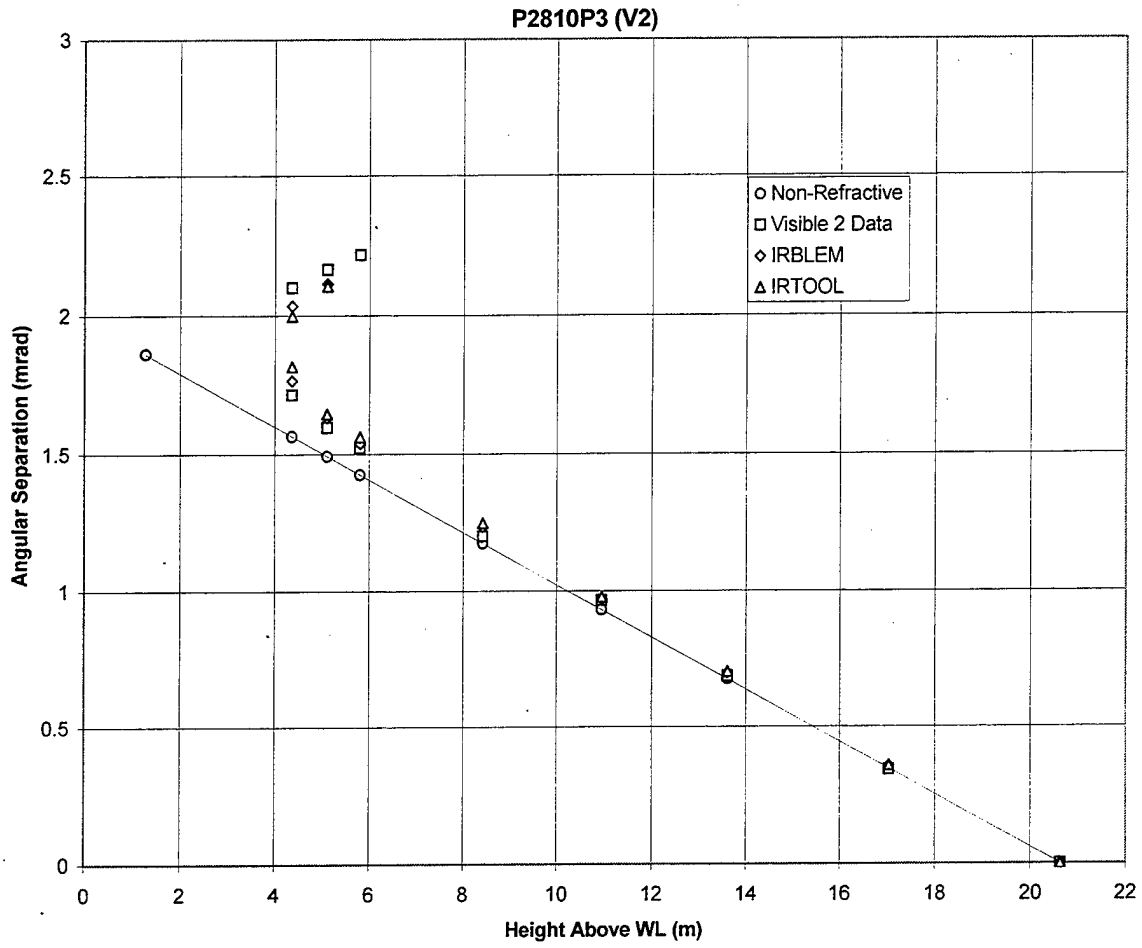

Figure 50. Comparison of IRTOOL and IRBLEM model calculations for the P2810P3 event measured by the visible V2 camera.

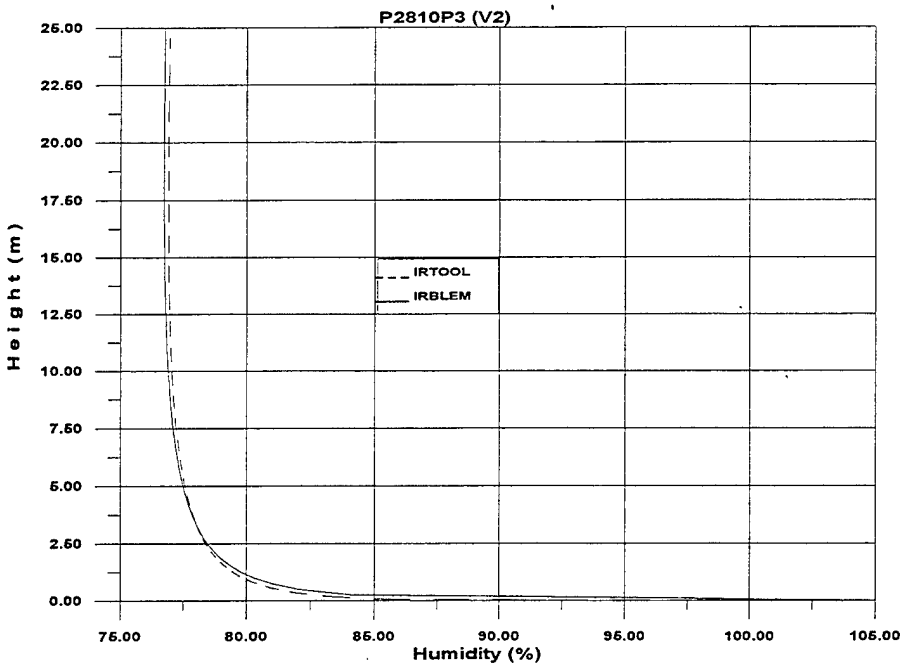

Figure 51A. Humidity profiles as predicted from IRTOOL (using the Mid-Latitude Winter atmosphere) and IRBLEM model.

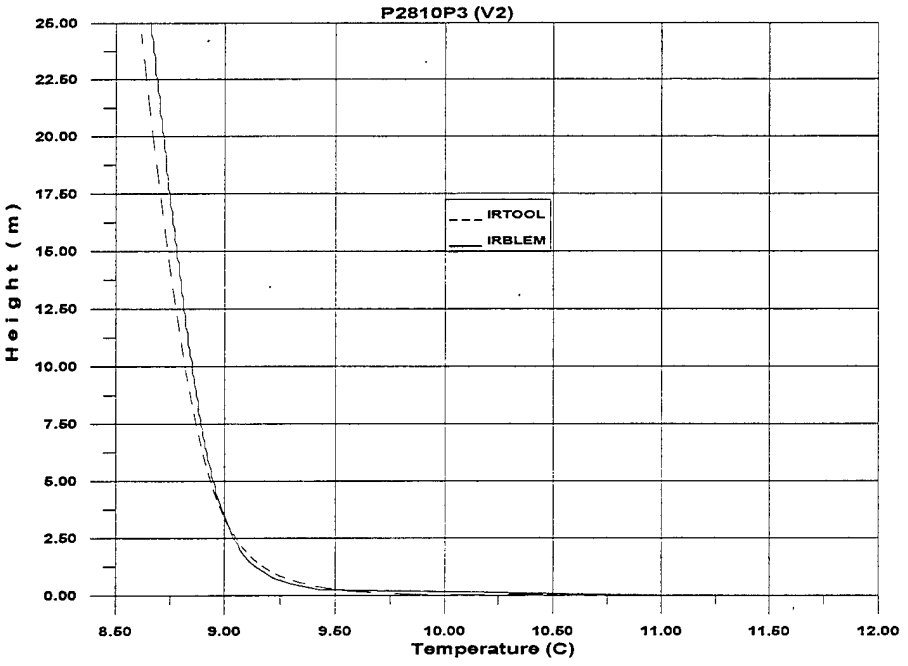

Figure 51B. Temperature profiles as predicted from IRTOOL (using the Mid-Latitude Winter atmosphere) and IRBLEM model.

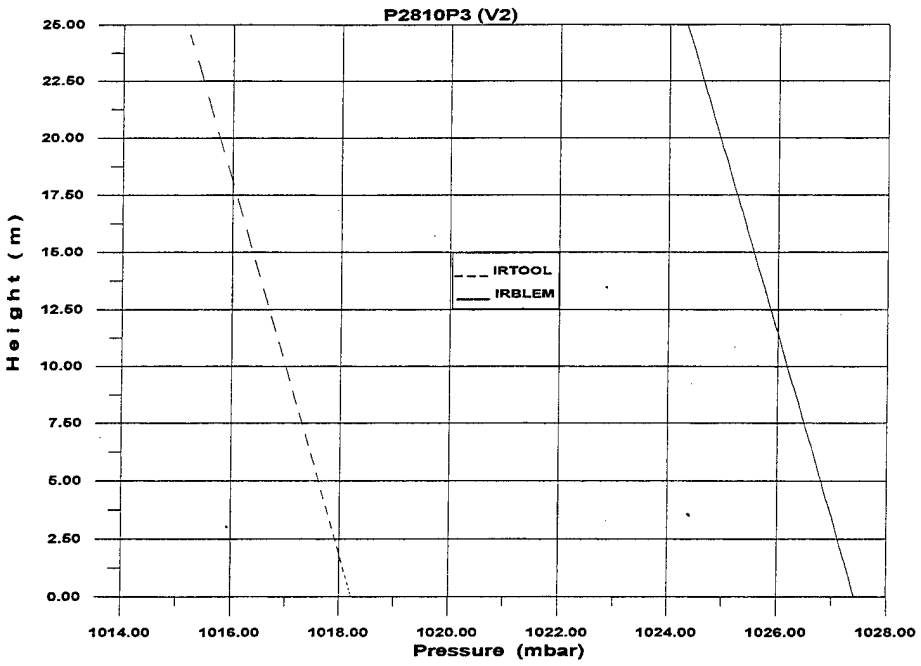

Figure 51C. Pressure profiles as predicted from IRTOOL (using the Mid-Latitude Winter atmosphere) and IRBLEM model.

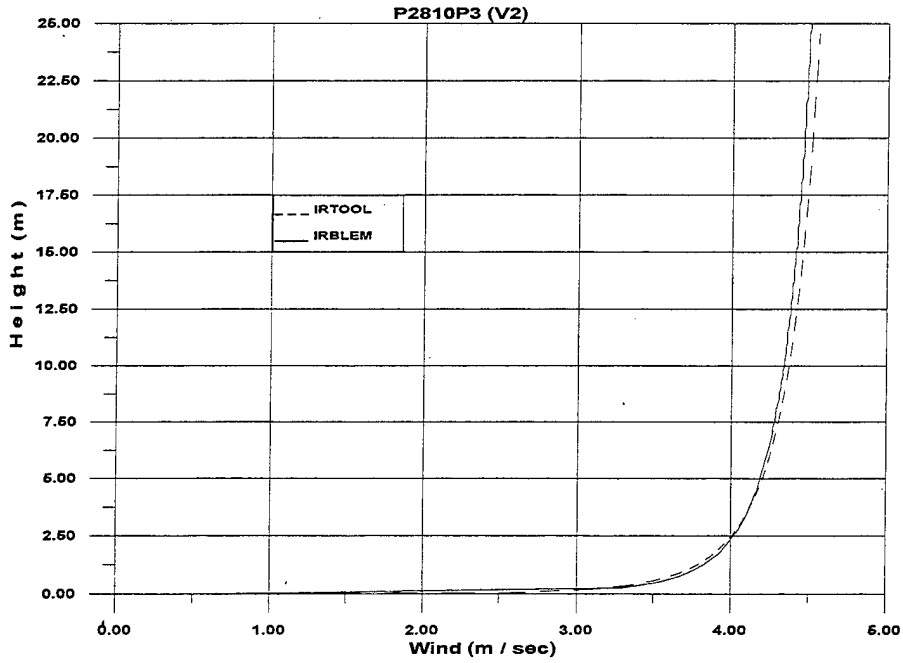

Figure 51D. Wind speed profiles as predicted from IRTOOL (using the Mid-Latitude Winter atmosphere) and IRBLEM model.

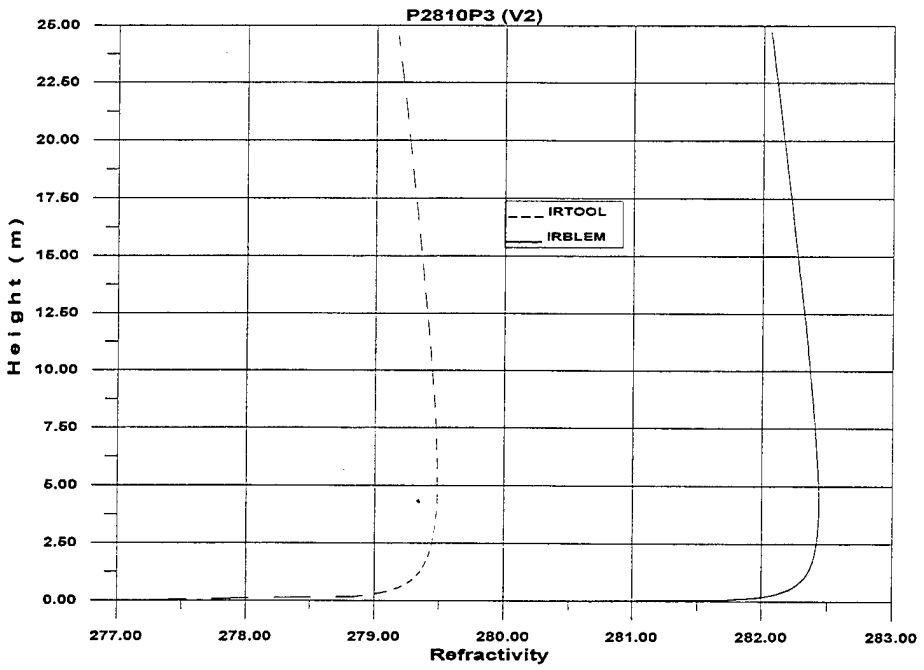

Figure 51E. Refractivity profiles as predicted from IRTOOL (using the Mid-Latitude Winter atmosphere) and IRBLEM model.

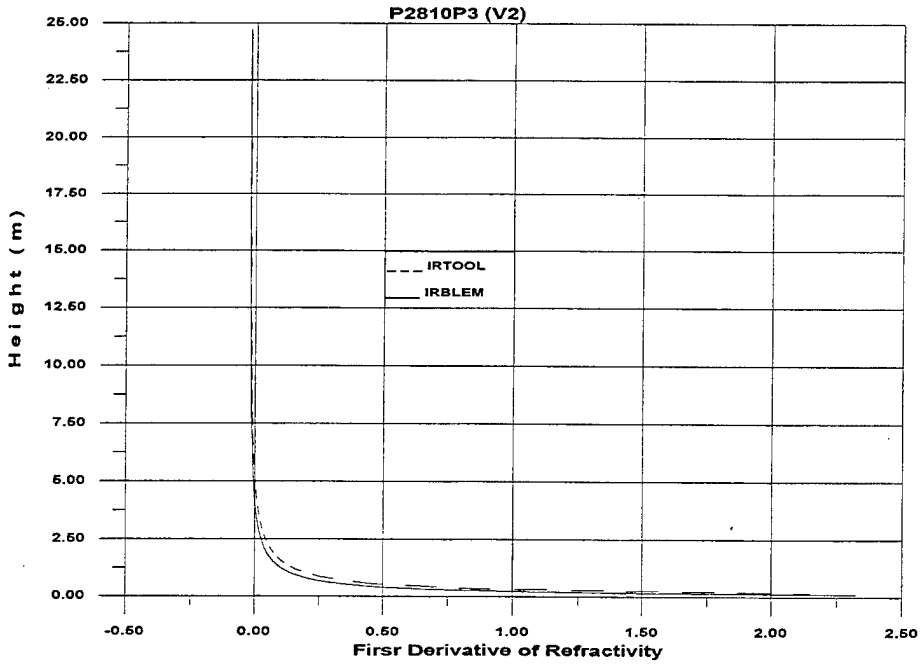

Figure 51F. Gradient of the Refractivity profile as predicted from IRTOOL (using the Mid-Latitude Winter atmosphere) and IRBLEM model.

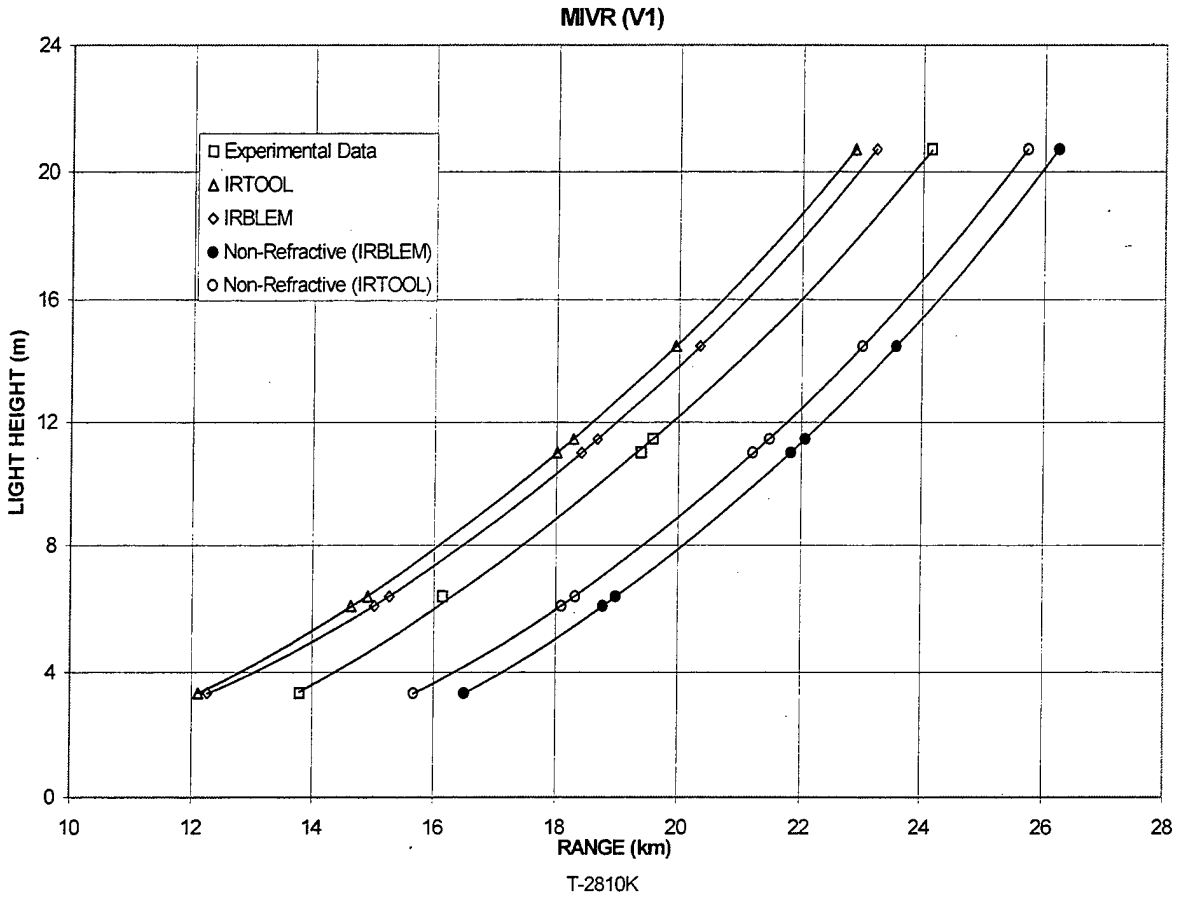

Figure 52. Comparison of the IRBLEM and IRTOOL model MIVRs with the ship-tracking data measured by the infrared (V1) camera.

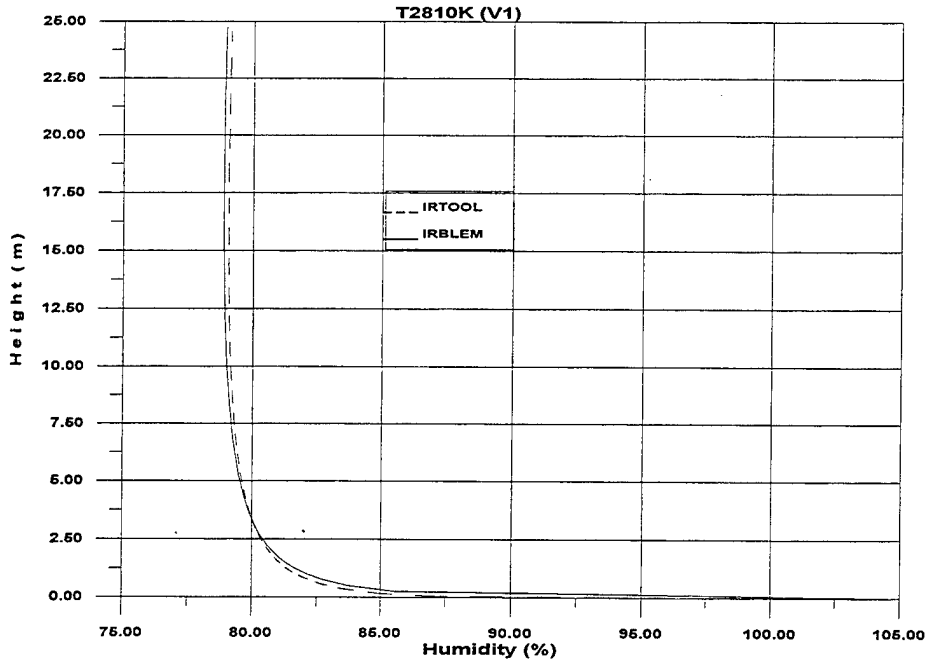

Figure 53A. Humidity profiles as predicted from IRTOOL (using the Mid-Latitude Winter atmosphere) and IRBLEM model.

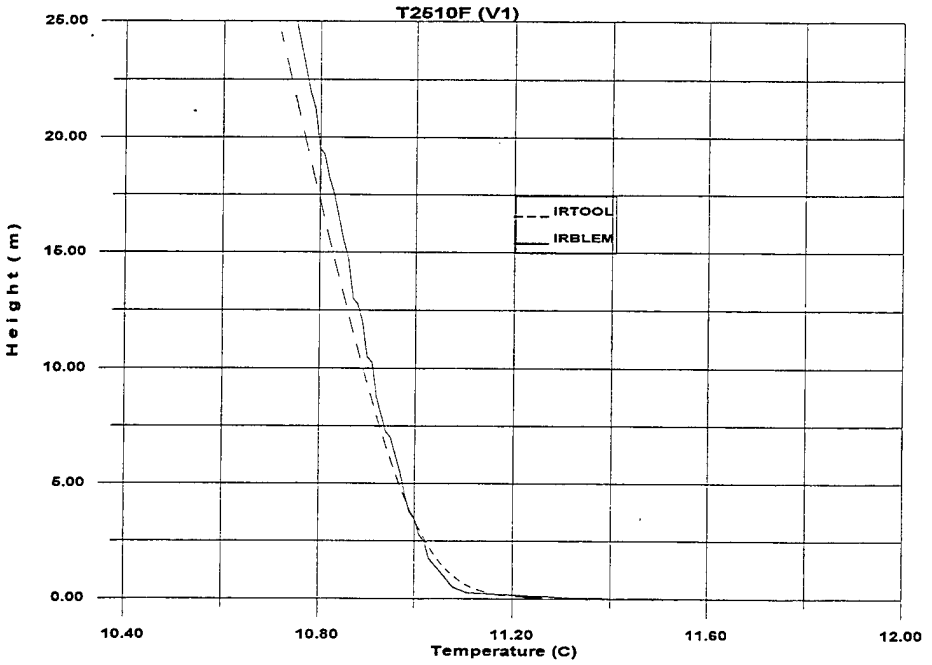

Figure 53B. Temperature profiles as predicted from IRTOOL (using the Mid-Latitude Winter atmosphere) and IRBLEM model.

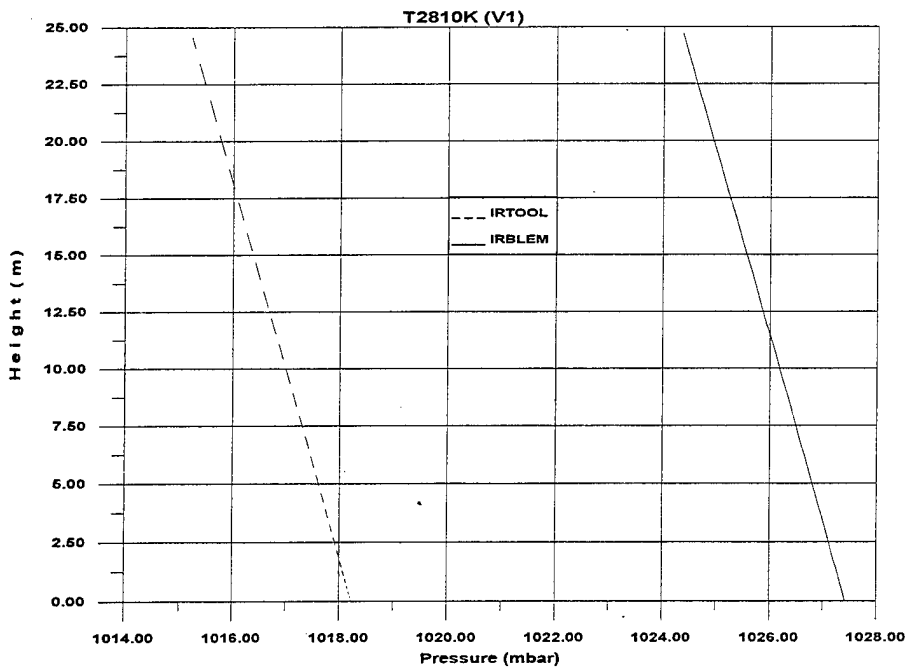

Figure 53C. Pressure profiles as predicted from IRTOOL (using the Mid-Latitude Winter atmosphere) and IRBLEM model.

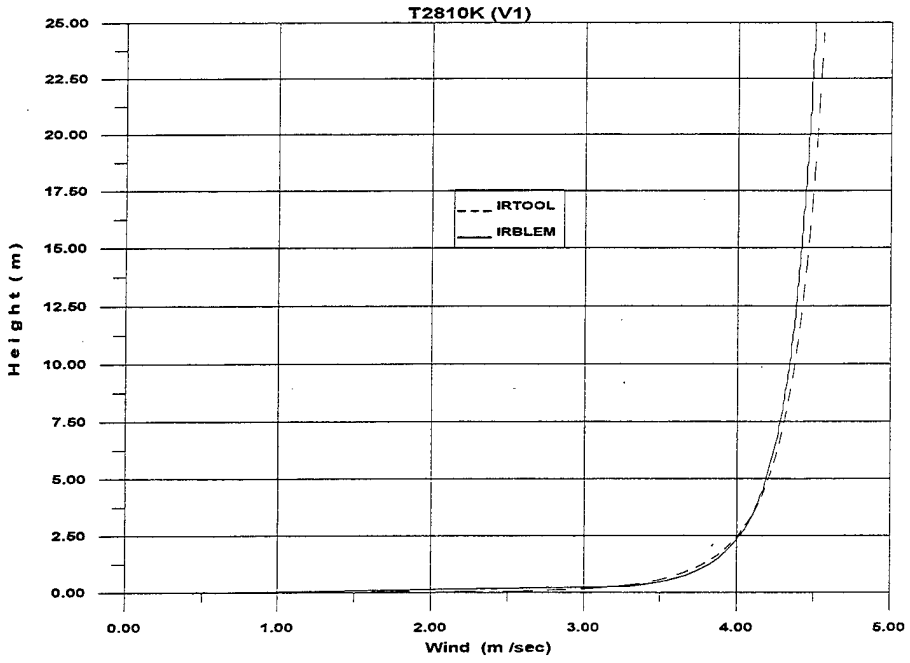

Figure 53D. Wind speed profiles as predicted from IRTOOL (using the Mid-Latitude Winter atmosphere) and IRBLEM model.

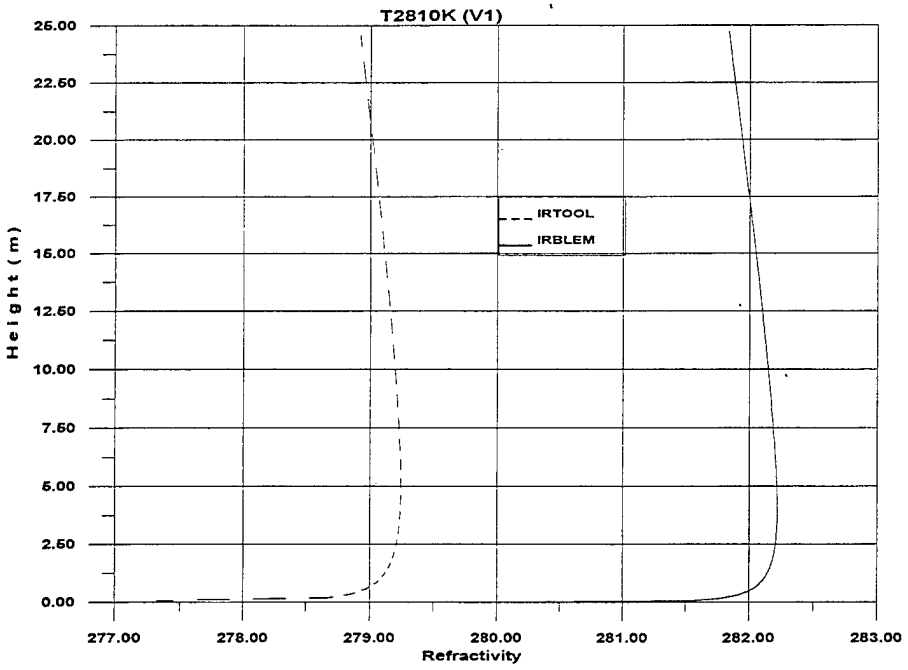

Figure 53E. Refractivity profiles as predicted from IRTOOL (using the Mid-Latitude Winter atmosphere) and IRBLEM model.

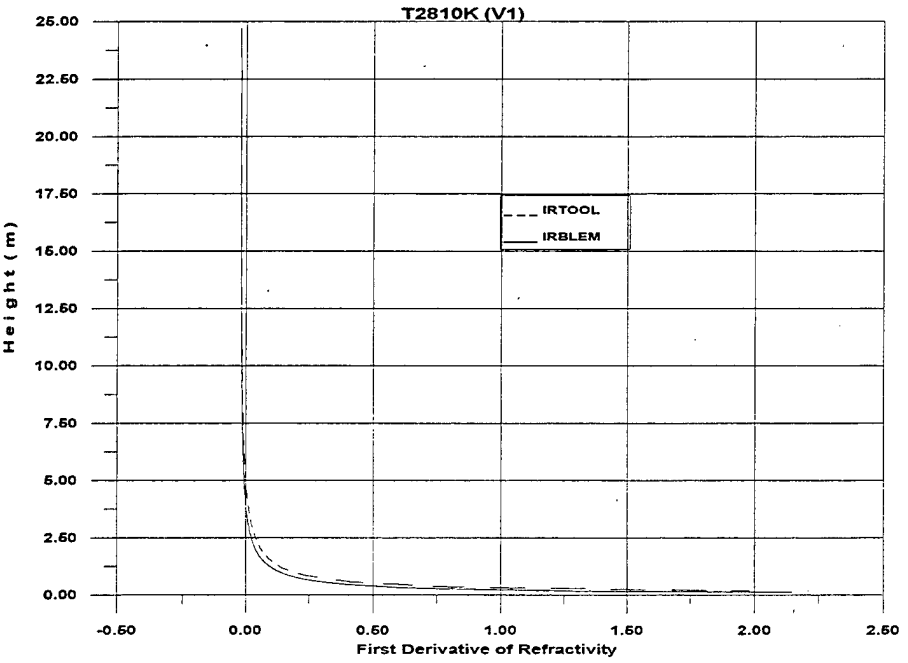

Figure 53F. Gradient of the Refractivity profile as predicted from IRTOOL (using the Mid-Latitude Winter atmosphere) and IRBLEM model.

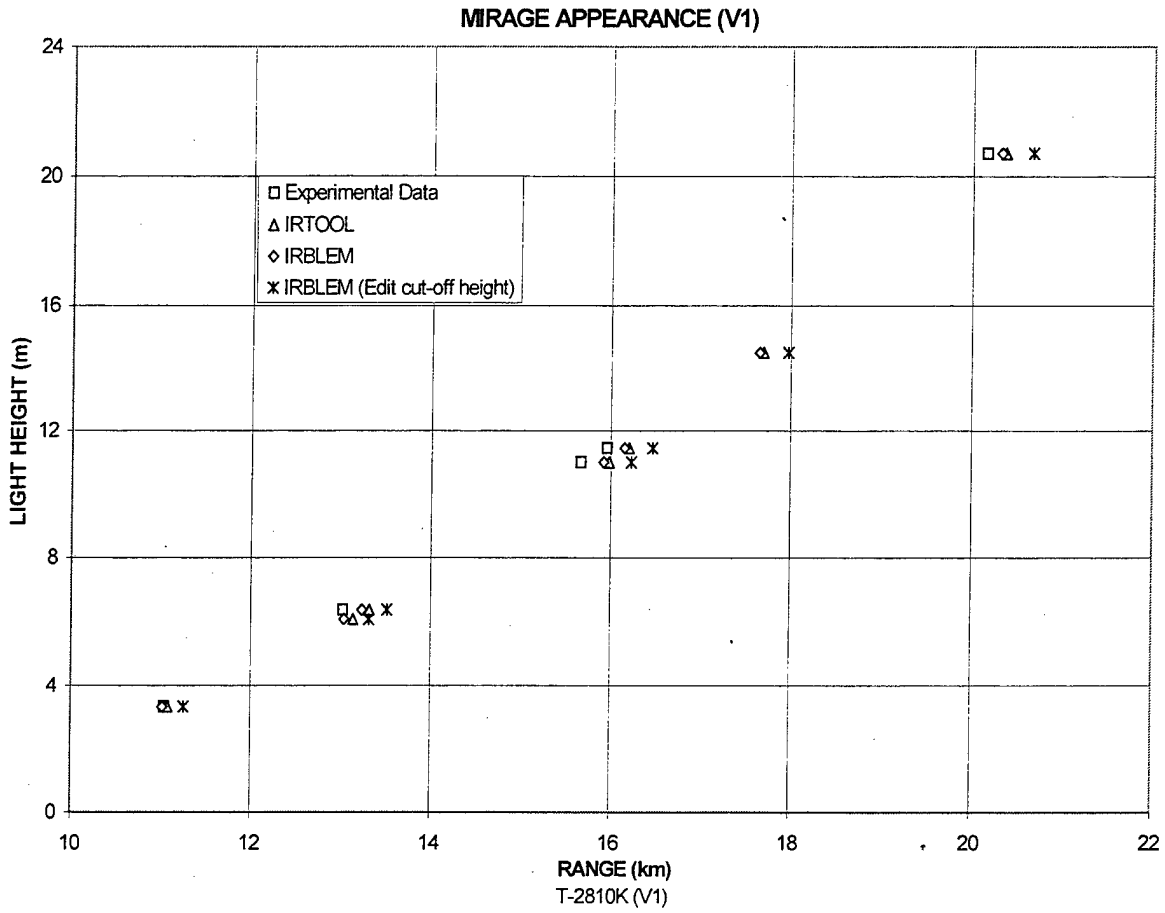

Figure 54. Comparison of the IRBLEM and IRTOOL model MMRs with the ship-tracking data measured by the infrared (V1) camera.

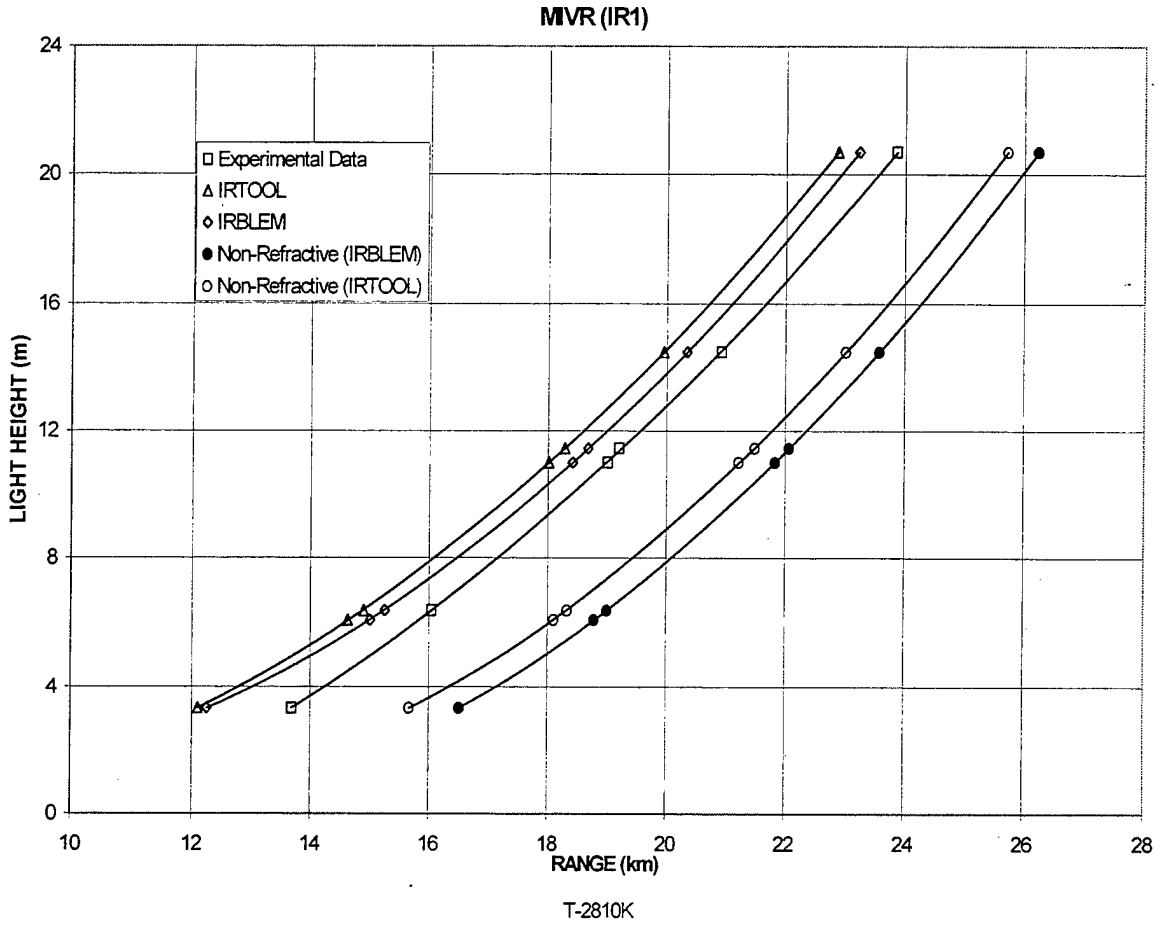

Figure 55. Comparison of the IRBLEM and IRTOOL model MIVRs with the ship-tracking data measured by the infrared (IR1) camera.

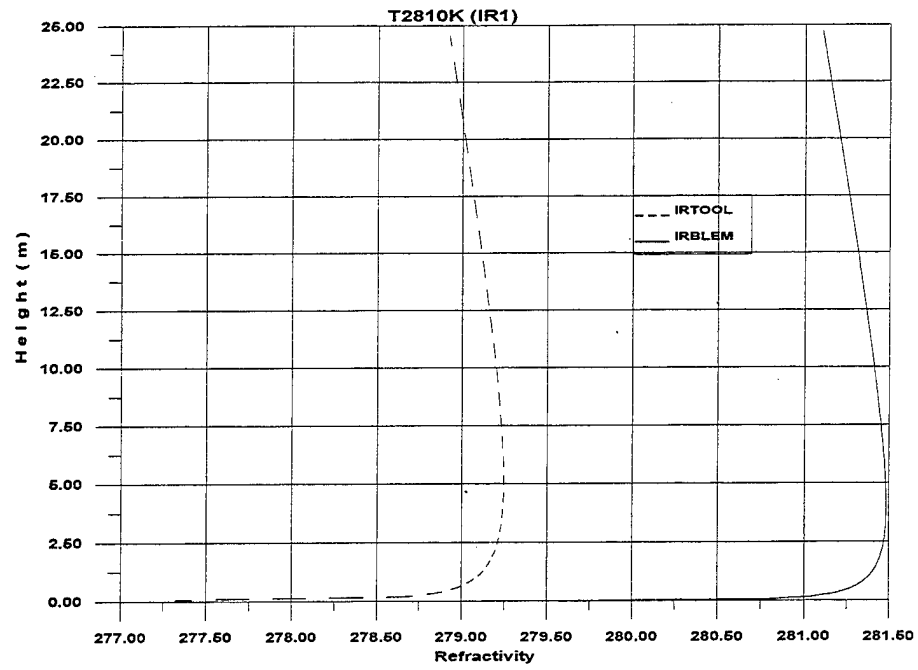

Figure 56A. Refractivity profiles as predicted from IRTOOL (using the Mid-Latitude Winter atmosphere) and IRBLEM model.

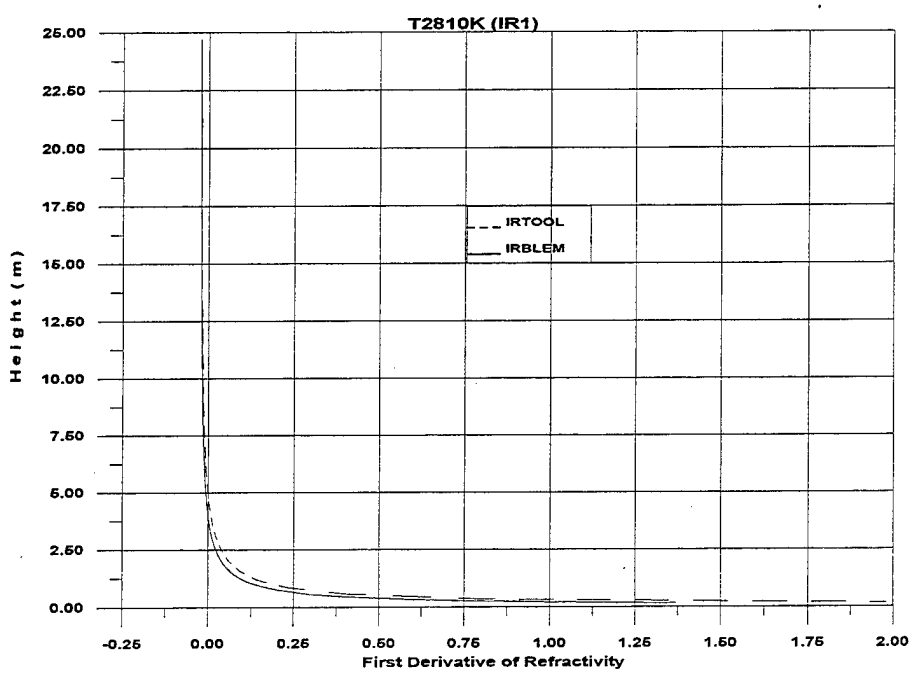

Figure 56B. Gradient of the Refractivity profile as predicted from IRTOOL (using the Mid-Latitude Winter atmosphere) and IRBLEM model.

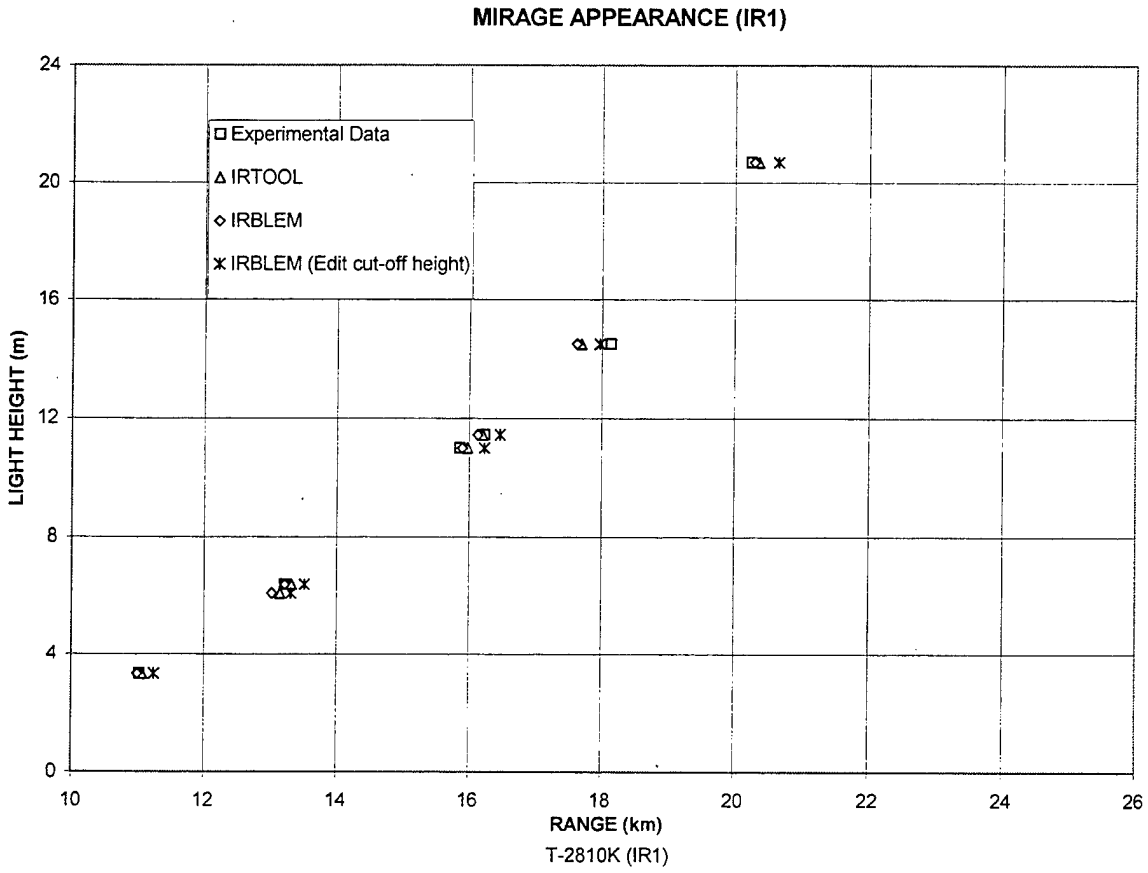

Figure 57. Comparison of the IRBLEM and IRTOOL model MMRs with the ship-tracking data measured by the infrared (IR1) camera.

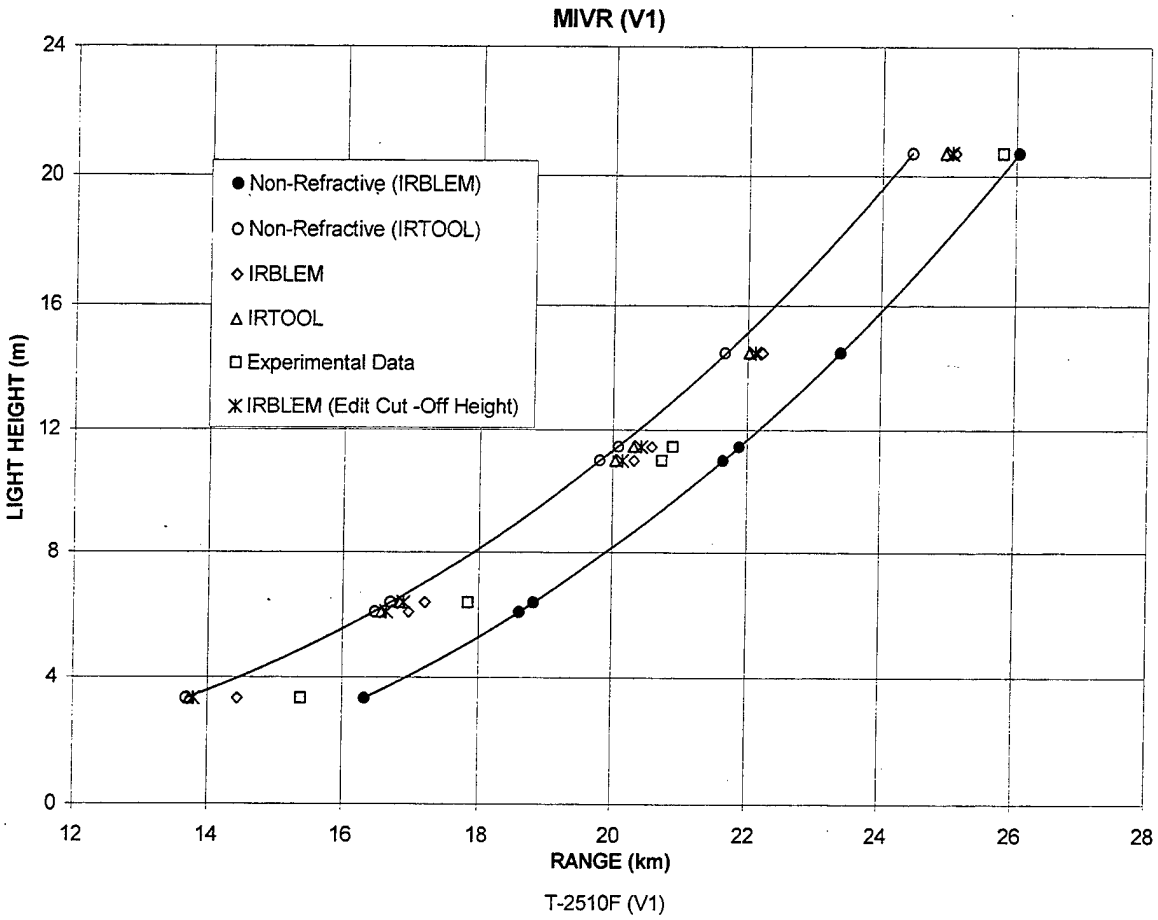

Figure 58. Comparison of the IRBLEM and IRTOOL model MIVRs with the ship-tracking data measured by the visible (V1) camera.

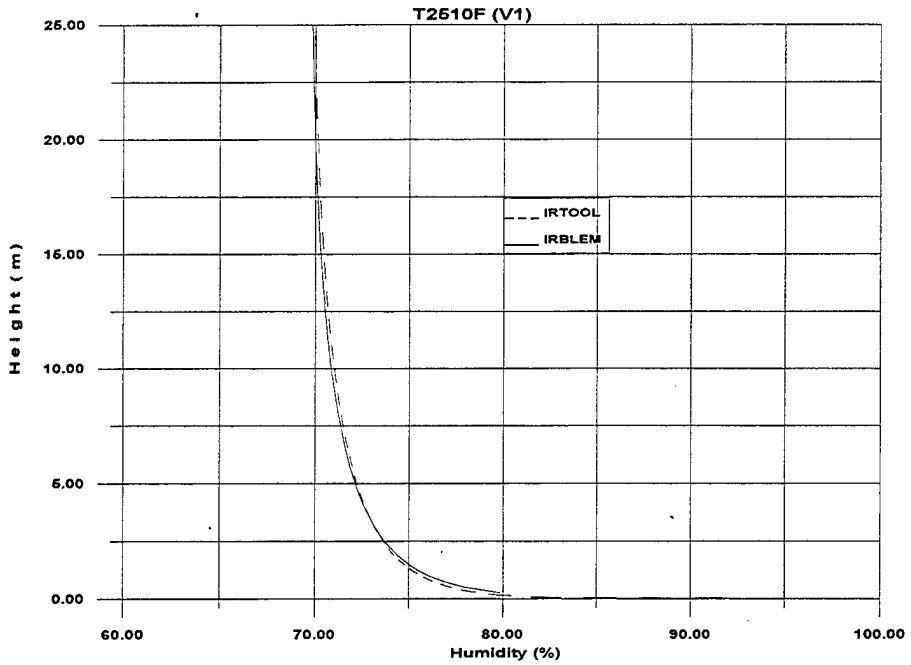

Figure 59A. Pressure profiles as predicted from IRTOOL (using the Mid-Latitude Winter atmosphere) and IRBLEM model.

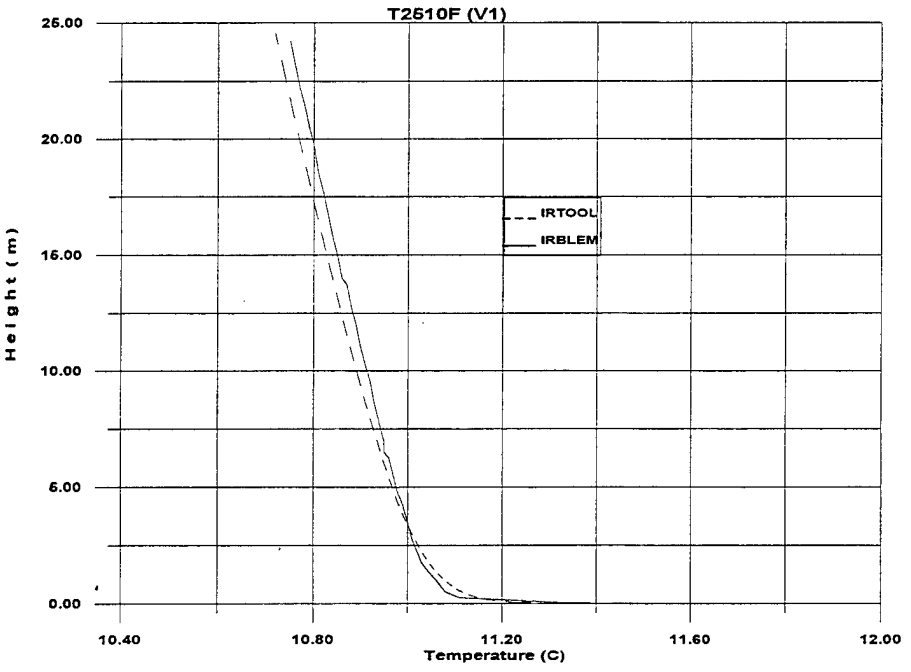

Figure 59B. Temperature profiles as predicted from IRTOOL (using the Mid-Latitude Winter atmosphere) and IRBLEM model.

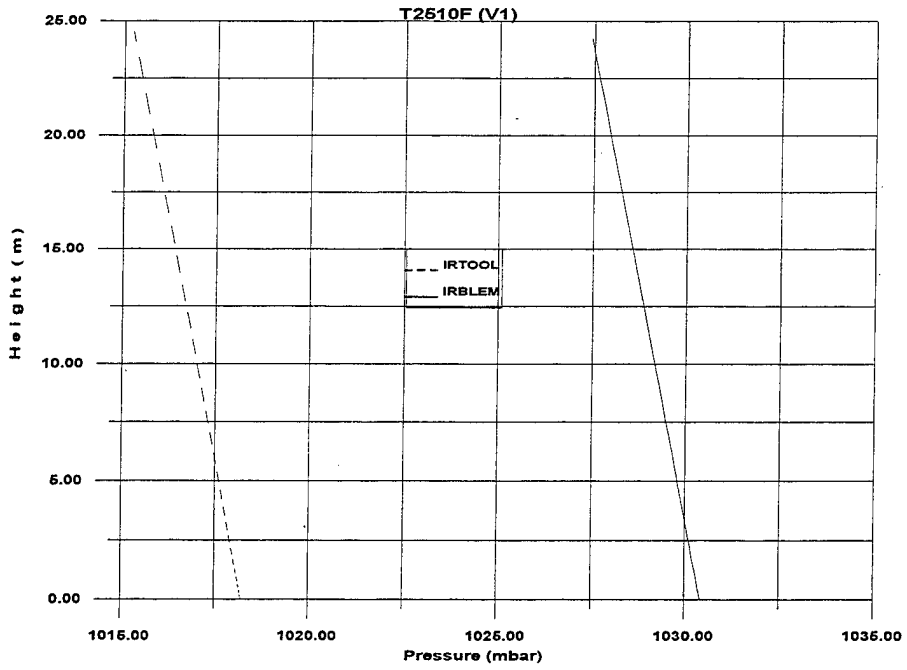

Figure 59C. Pressure profiles as predicted from IRTOOL (using the Mid-Latitude Winter atmosphere) and IRBLEM model.

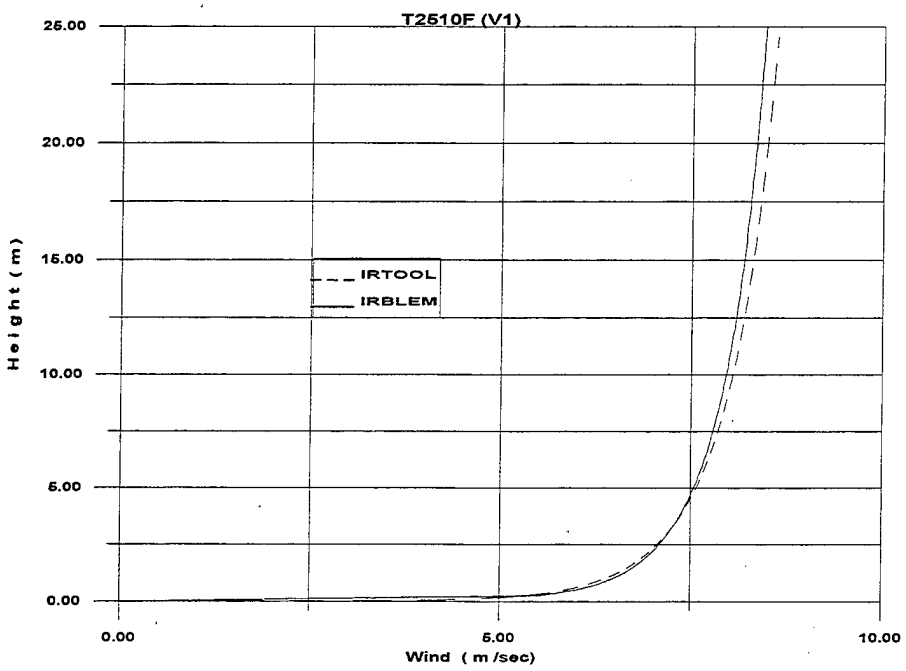

Figure 59D. Wind speed profiles as predicted from IRTOOL (using the Mid-Latitude Winter atmosphere) and IRBLEM model.

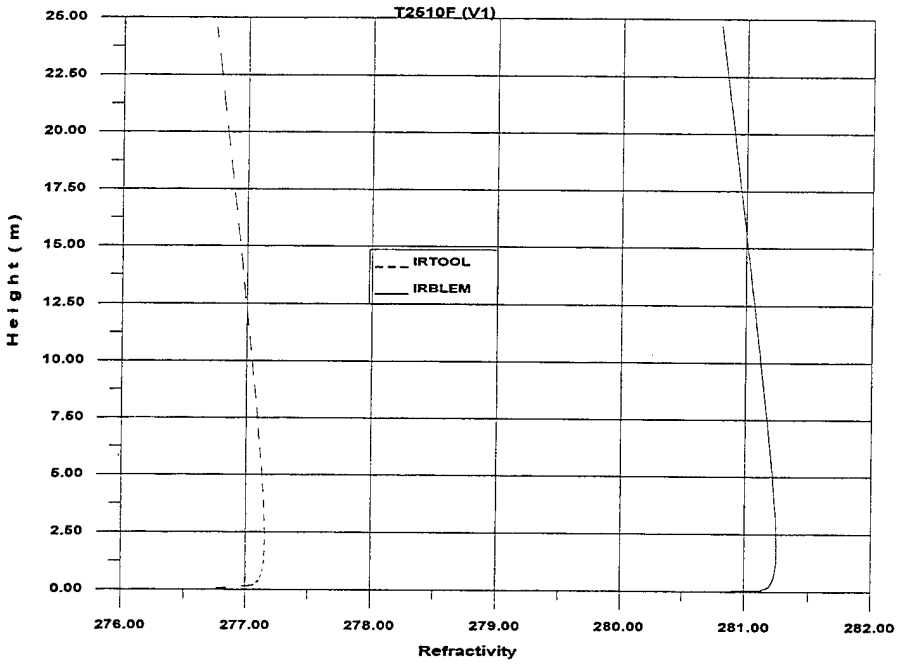

Figure 59E. Refractivity profiles as predicted from IRTOOL (using the Mid-Latitude Winter atmosphere) and IRBLEM model.

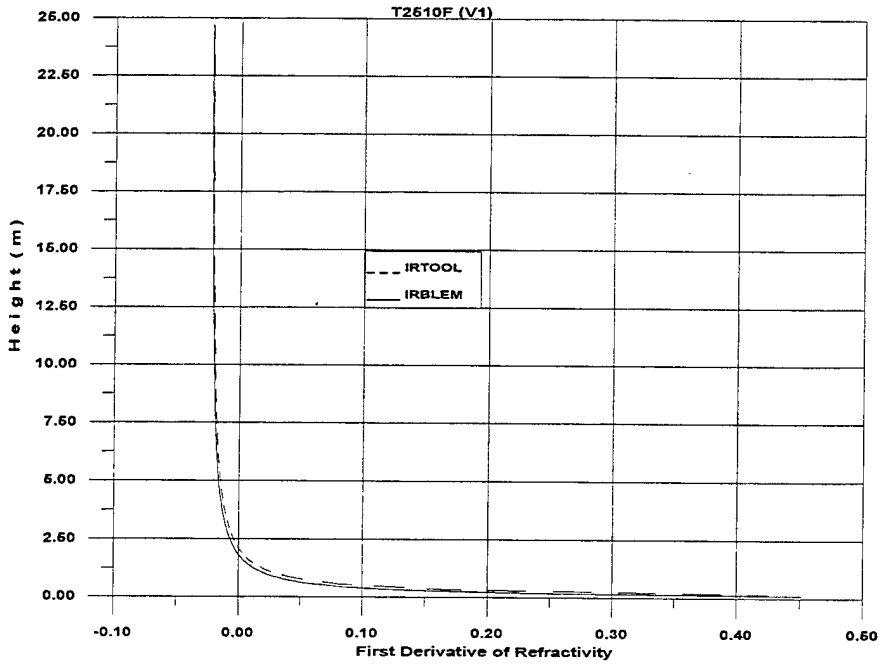

Figure 59F. Gradient of the Refractivity profile as predicted from IRTOOL (using the Mid-Latitude Winter atmosphere) and IRBLEM model.

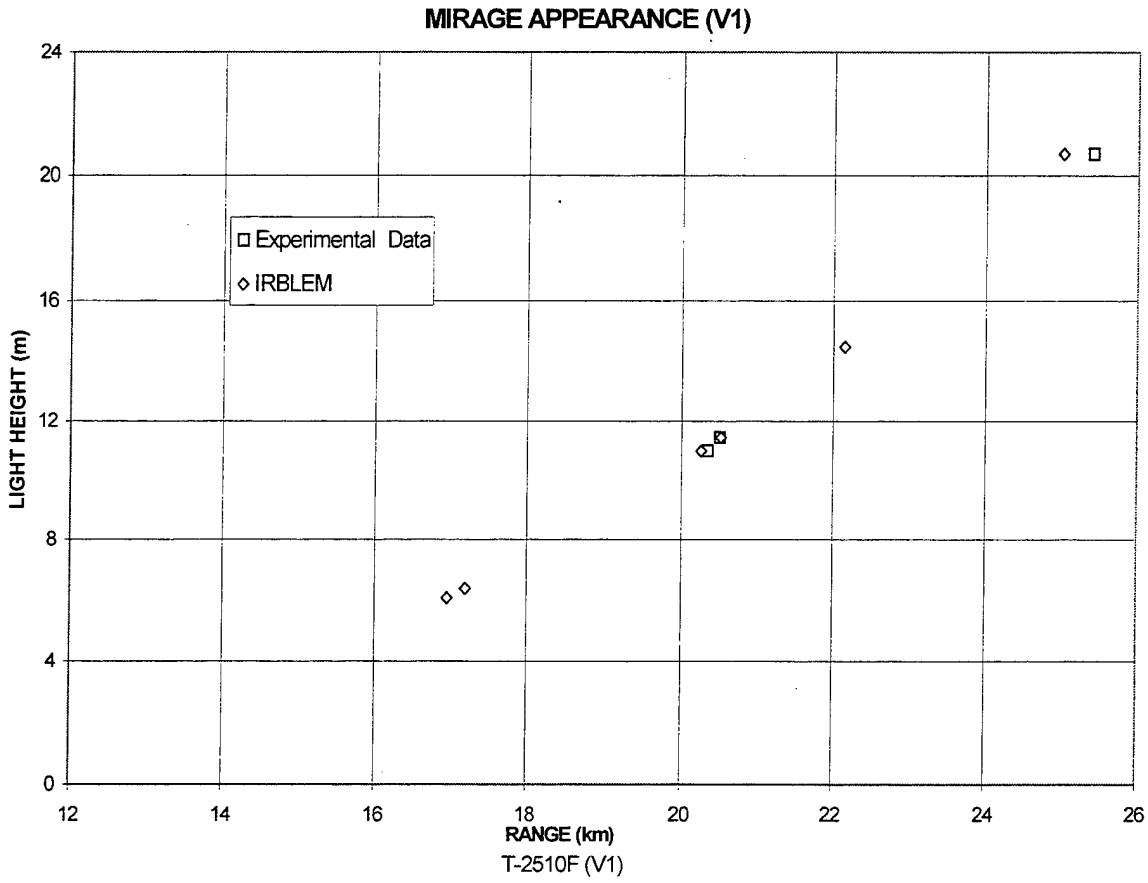

Figure 60. Comparison of the IRBLEM and IRTOOL model MMRs with the ship-tracking data measured by the visible (V1) camera.

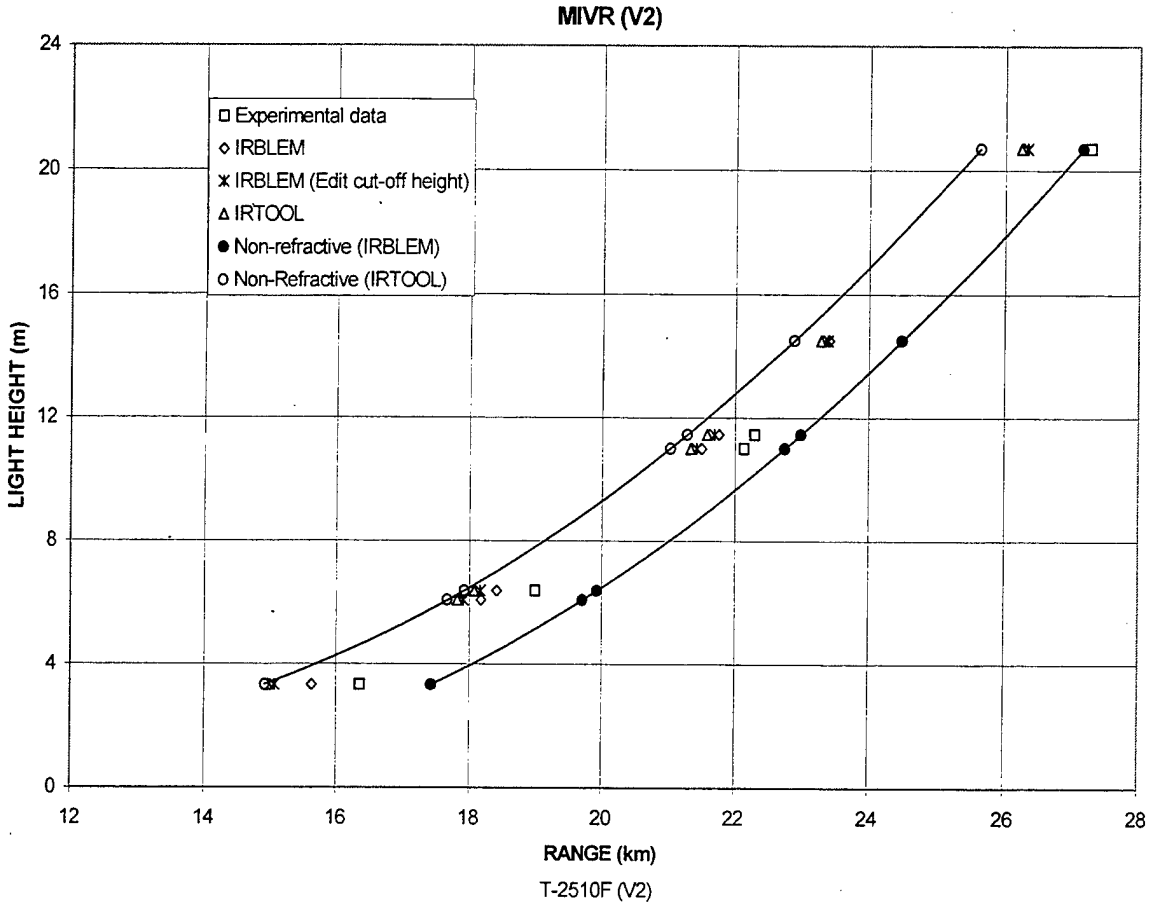

Figure 61. Comparison of the IRBLEM and IRTOOL model MIVRs with the ship-tracking data measured by the visible (V2) camera.

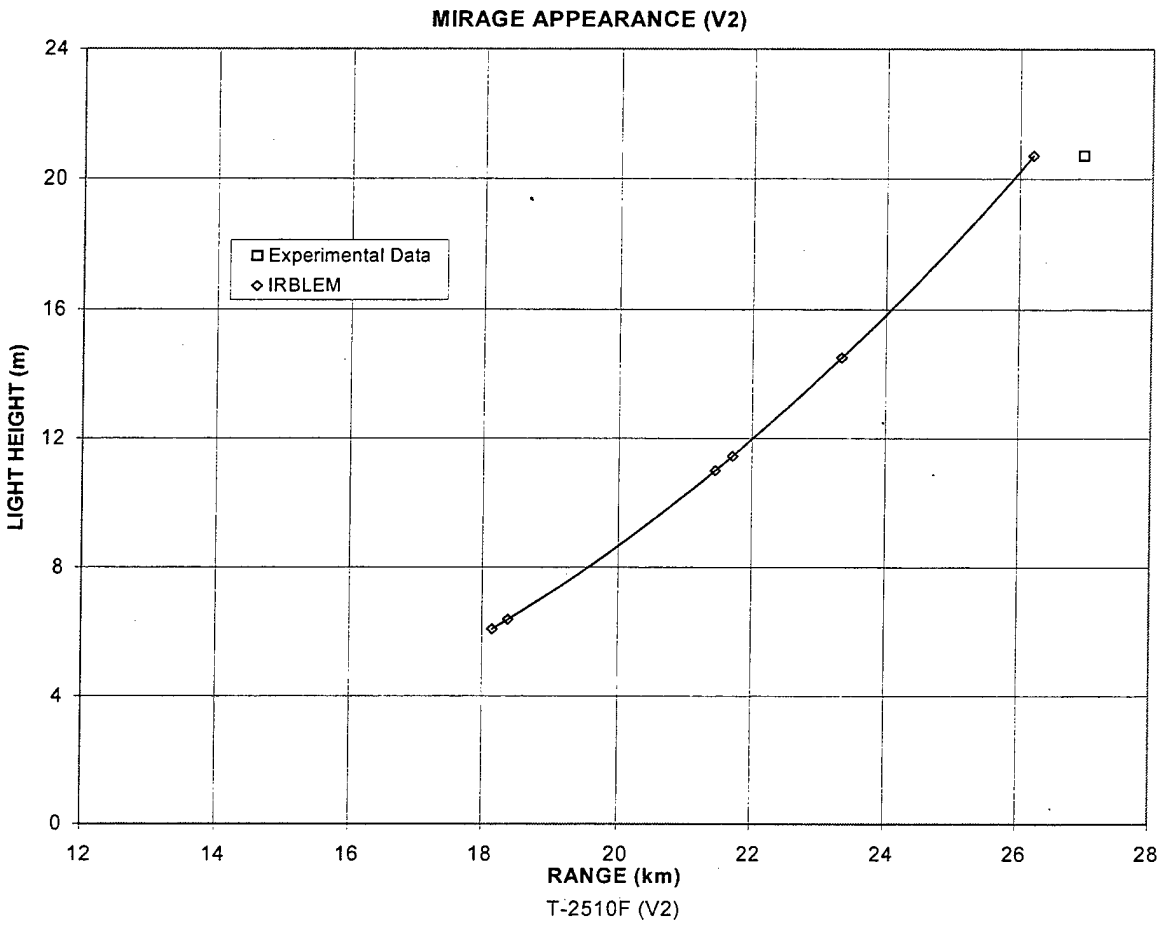

Figure 62. Comparison of the IRBLEM and IRTOOL model MMRs with the ship-tracking data measured by the visible (V2) camera.

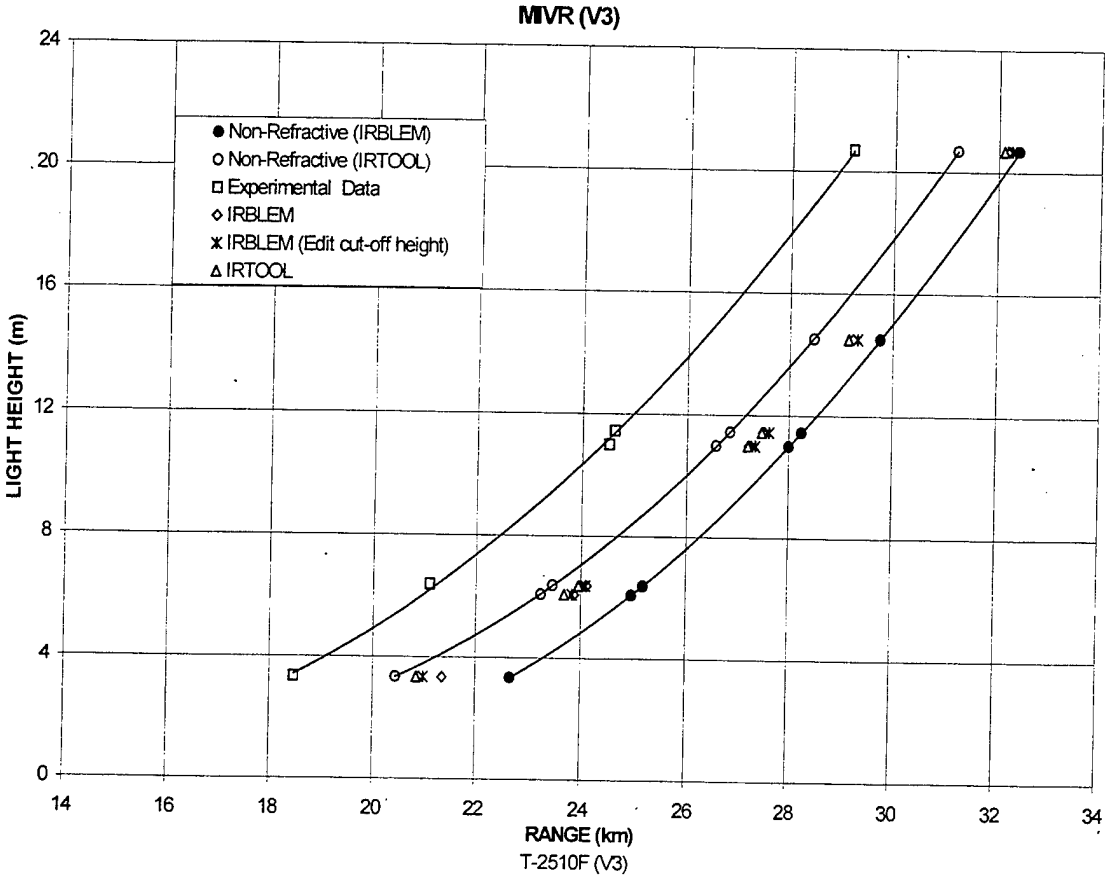

Figure 63. Comparison of the IRBLEM and IRTOOL model MIVRs with the ship-tracking data measured by the visible (V3) camera.

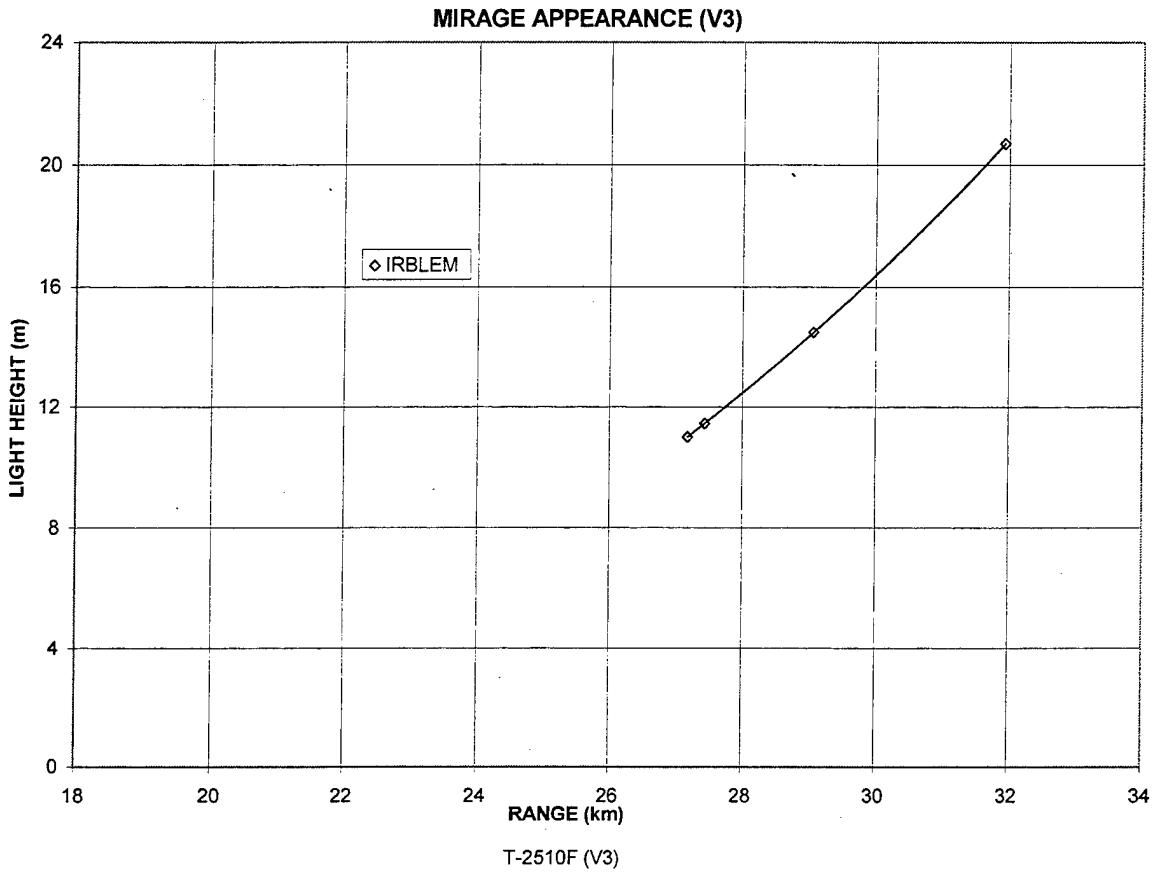

Figure 64. Comparison of the IRBLEM and IRTOOL model MMRs with the ship-tracking data measured by the visible (V3) camera.

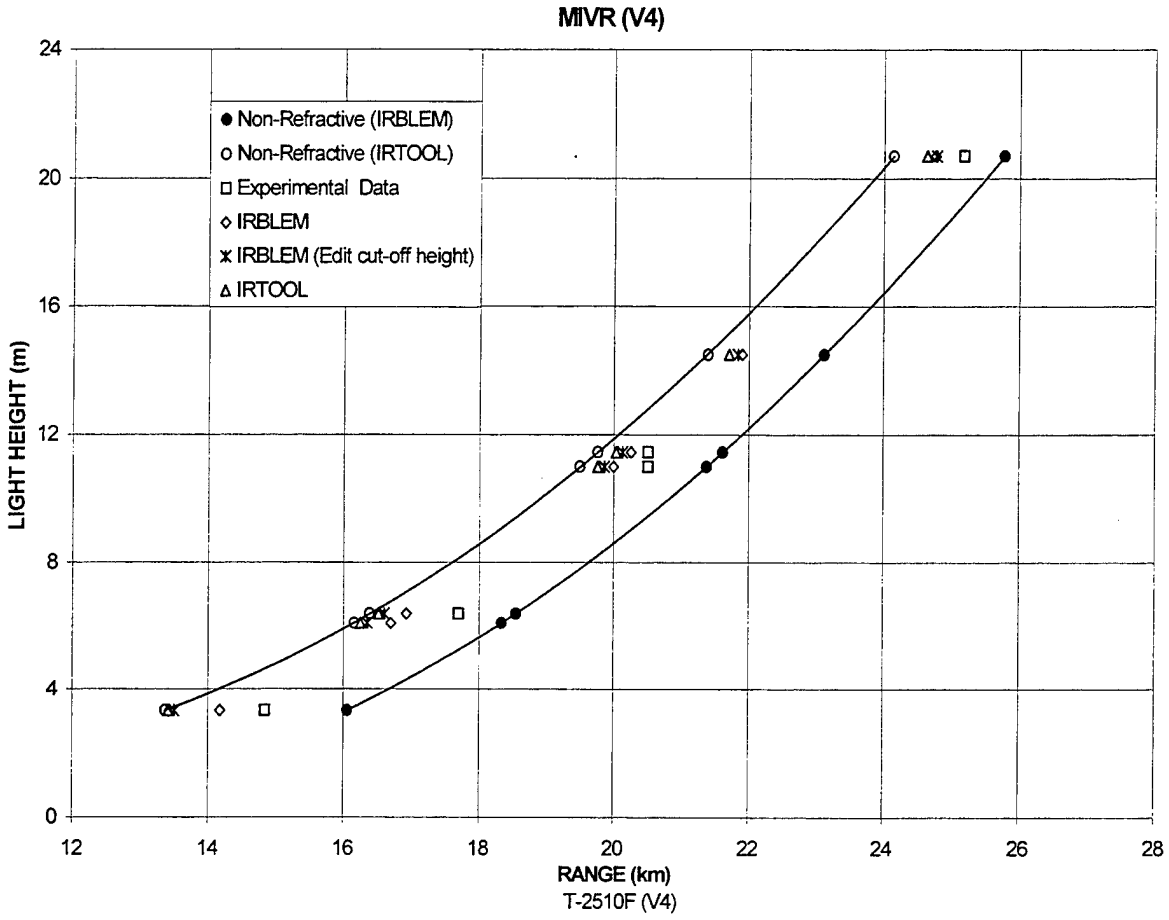

Figure 65. Comparison of the IRBLEM and IRTOOL model MIVRs with the ship-tracking data measured by the visible (V4) camera.

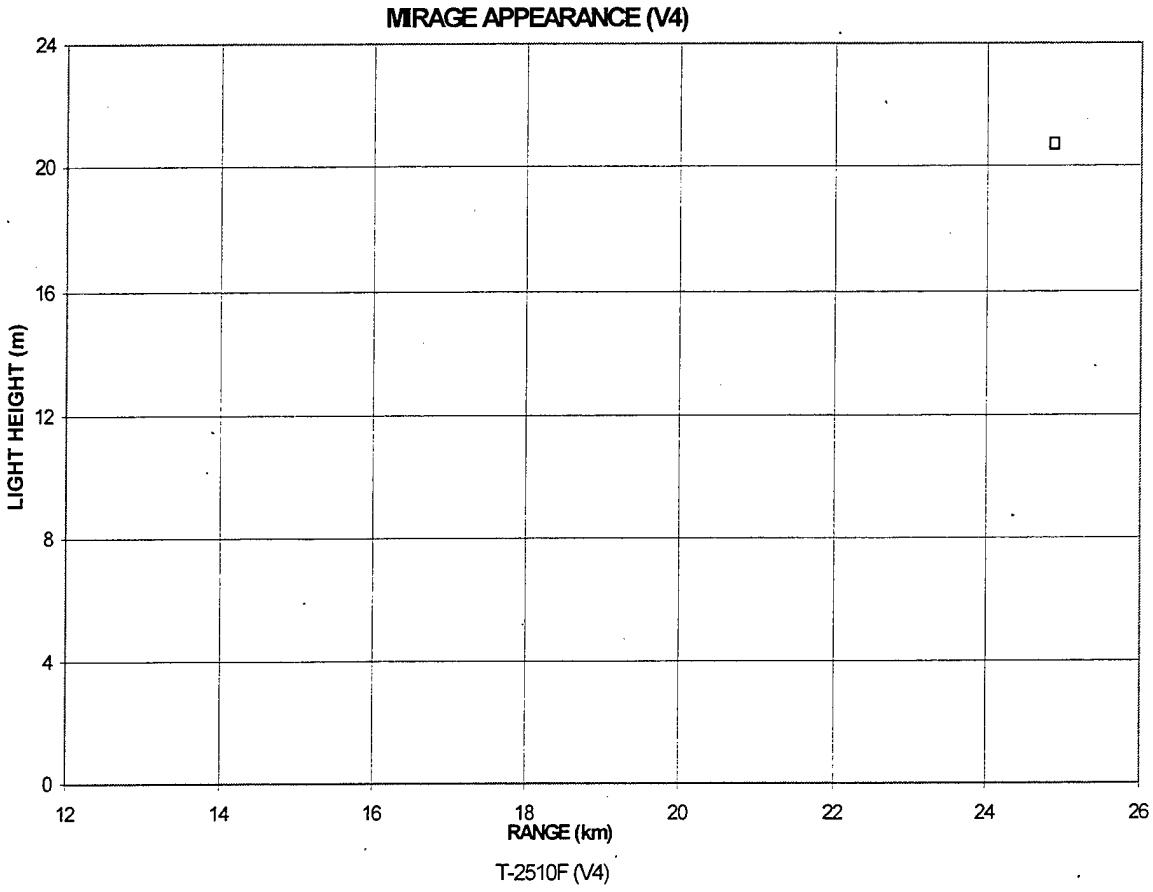

Figure 66. Comparison of the IRBLEM and IRTOOL model MMRs with the ship-tracking data measured by the visible (V4) camera. Neither IRBLEM nor IRTOOL shows a mirage for this case even though we had one observed mirage for the target at 20.7 m.

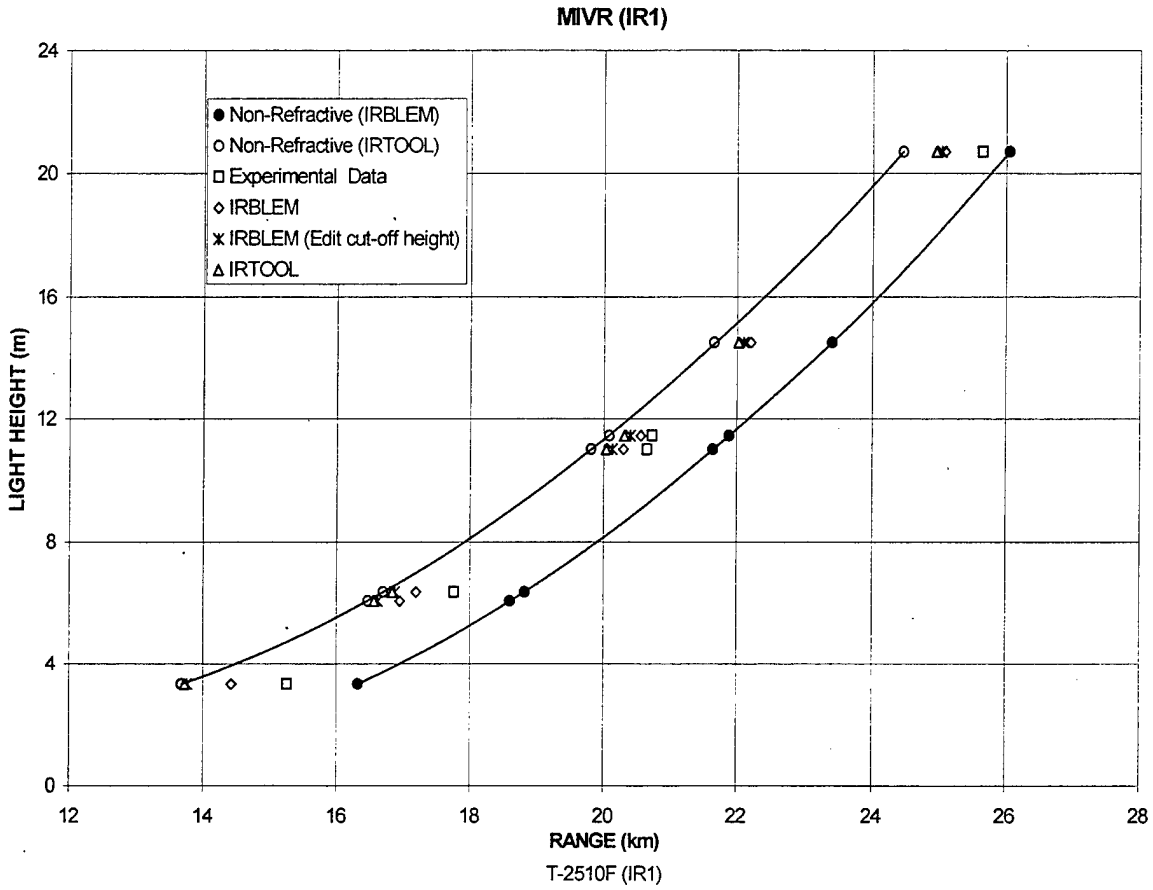

Figure 67. Comparison of the IRBLEM and IRTOOL model MIVRs with the ship-tracking data measured by the infrared (IR1) camera.

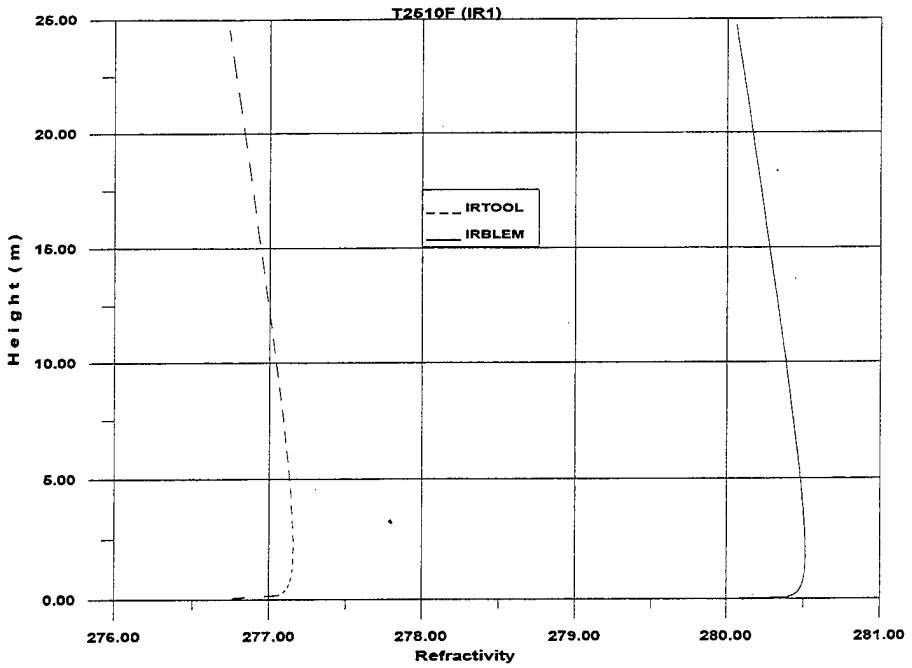

Figure 68A. Refractivity profiles as predicted from IRTOOL (using the Mid-Latitude Winter atmosphere) and IRBLEM model.

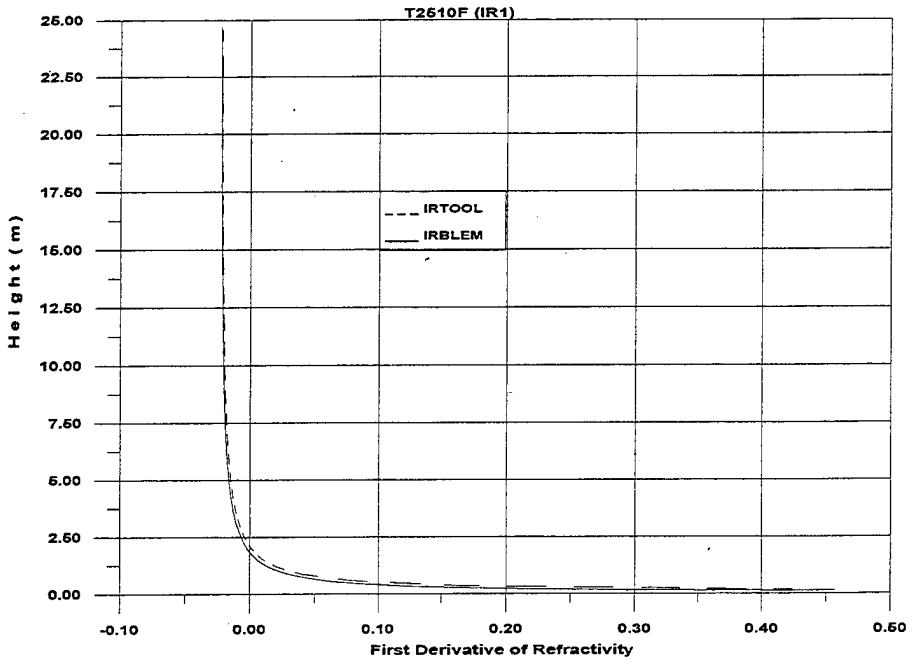

Figure 68B. Gradient of the Refractivity profile as predicted from IRTOOL (using the Mid-Latitude Winter atmosphere) and IRBLEM model.

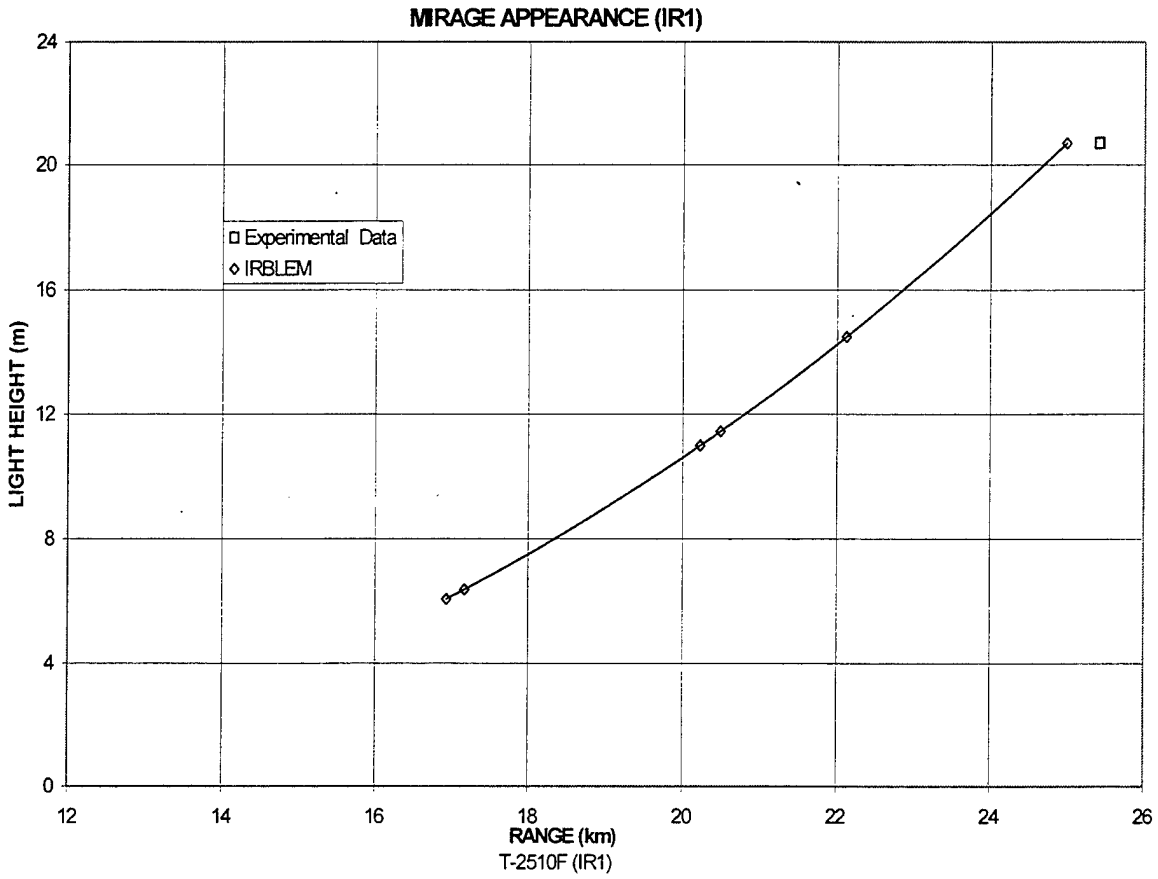

Figure 69. Comparison of the IRBLEM and IRTOOL model MMRs with the ship-tracking data measured by the infrared (IR1) camera.

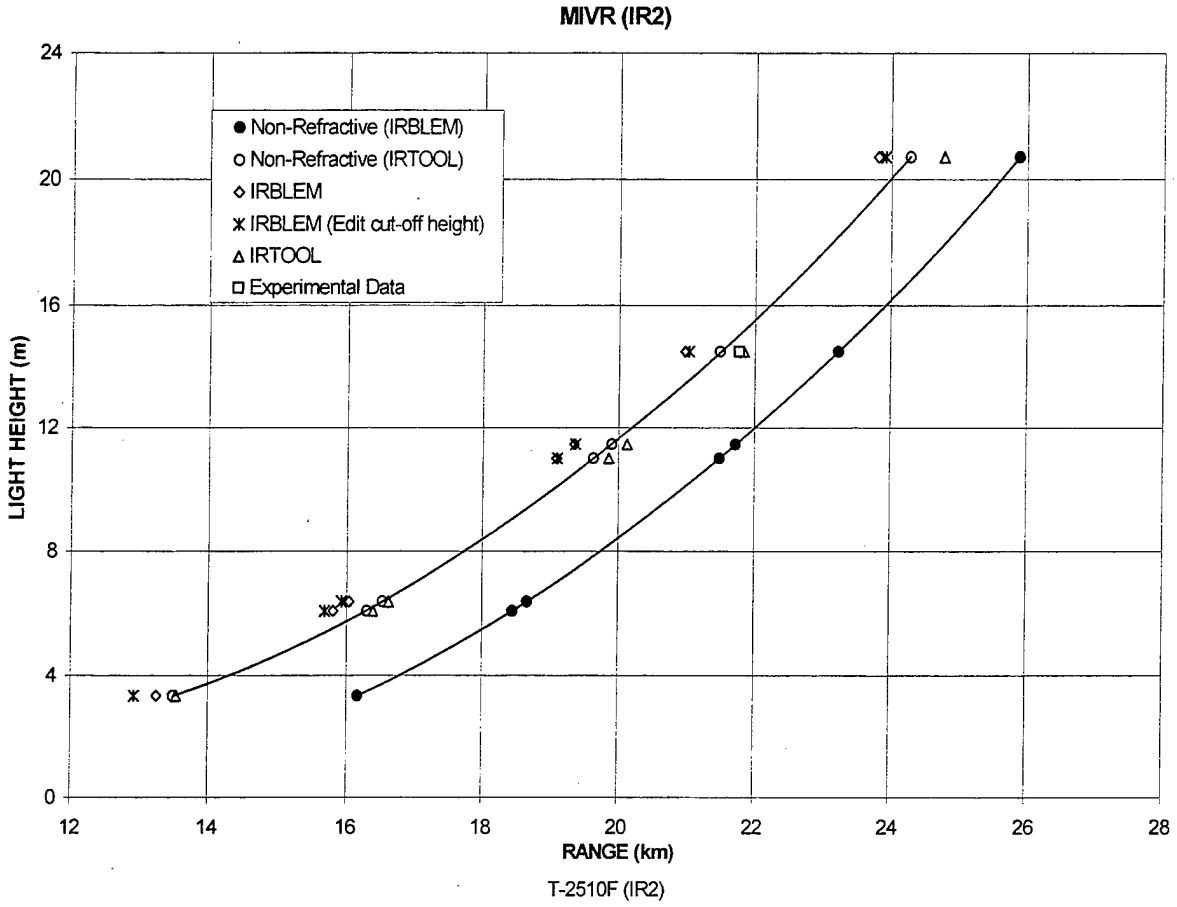

Figure 70. Comparison of the IRBLEM and IRTOOL model MIVRs with the ship-tracking data measured by the infrared (IR2) camera.

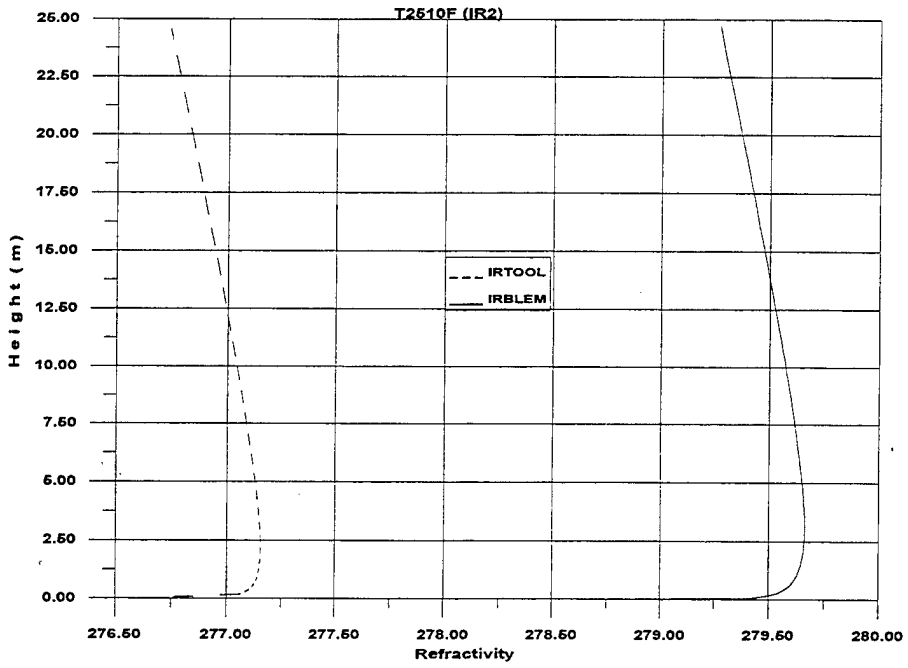

Figure 71A. Refractivity profiles as predicted from IRTOOL (using the Mid-Latitude Winter atmosphere) and IRBLEM model.

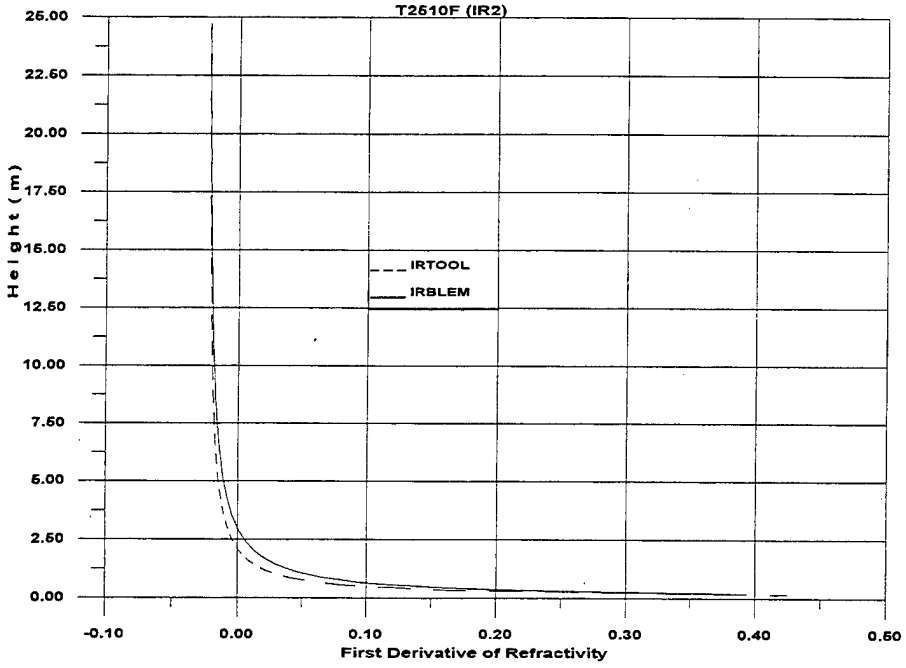

Figure 71B. Gradient of the Refractivity profiles as predicted from IRTOOL (using the Mid-Latitude Winter atmosphere) and IRBLEM model.

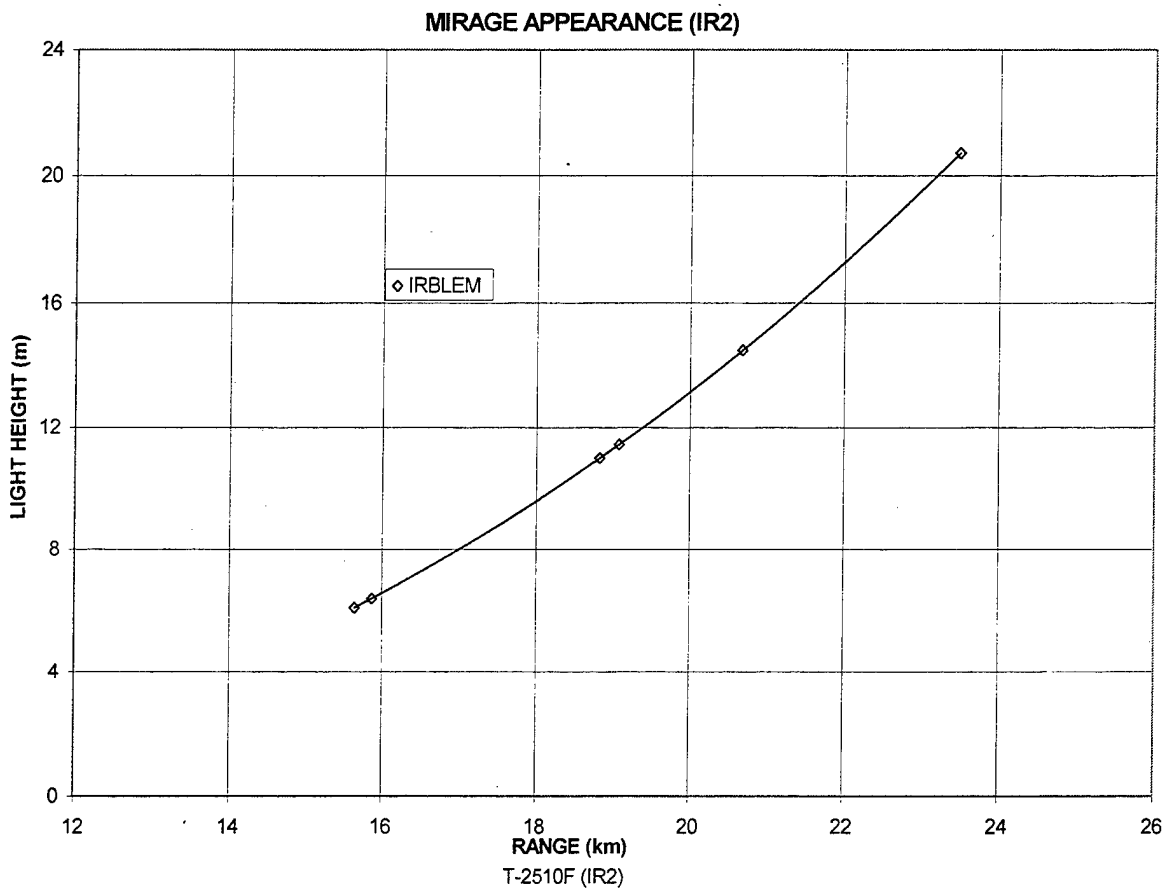

Figure 72. Comparison of the IRBLEM and IRTOOL model MMRs with the ship-tracking data measured by the infrared (IR2) camera. IRTOOL shows no mirage for this case and none was observed.

VIII. CONCLUSIONS

In this thesis we compared the refractivity data obtained during the MAPTIP trial at Katwijk Netherlands in 1993 with the predictions made by the non-refractive atmospheric (geometric) model and the refraction models of IRTOOL and IRBLEM. Due to the large amount of data only a portion of these data with the concurrent meteorological conditions were chosen here, so as to cover an appreciable range of ASTDs and wind velocities sampled at various times of the day. The events chosen were often observed by cameras from more than one participating nation.

The extended research showed that IRTOOL could predict mirages in cases in which they were found experimentally if the code cut-off height is decreased significantly. As noted, the wave height is an important factor that controls the Maximum Mirage Height (MXMH) or the beginning of the mirage zone. When the wave height increases, the MXMH decreases, or the beginning of the mirage zone moves to longer ranges and vice versa. In the ray-tracing program in IRBLEM the cut-off height is controlled by the Factor Wave Height (FWH) which is an input parameter. The value of this factor can be very useful for the purposes of research so as to seek the ideal cut-off height, meaning that using different FWH the more appropriate cut-off height which will correspond to the real one can be estimated. The nominal value of FWH (0.6) that is used in this thesis results in a cut-off height $0.78H_{1/3}$, and seems to be very accurate. In cases where the cut-off height used by IRTOOL and IRBLEM was almost the same (events P2810P3 and T2810), the results given by the two models were almost identical and in

very good agreement with the observed data. In all other cases where the cut-off height used by IRTOOL was much greater than both the one used by IRBLEM and the measured value, IRTOOL seemed to give poor predictions for the mirages. The equation that IRTOOL uses to calculate the cut-off height seems to be inaccurate. The results given by IRTOOL would be improved significantly if this equation were modified or even better if the measurement of the wave height was an input in the IRTOOL input parameters as is done in IRBLEM. A deficiency of IRTOOL is that in some cases the measurement of the wind speed is taken at a different height from the other meteorological measurements, while the program assumes that all the measurements were taken at the same height. This results in an error in the wind speed profile and consequently in the cut-off height, the calculation of which is based on the wind speed at 10 m height.

One difference between the two models is that the pressure is not an input parameter in IRTOOL, while it is in IRBLEM. As was shown, the error in using the midlatitude winter atmosphere with its default pressure profile is no greater than 0.93% and so its contribution to the gradient of refractivity is neglible.

Another difference between the two models is that IRTOOL does not model dispersion in the calculation of refractivity as it only uses one equation for all the wavebands. IRBLEM, on the other hand, uses four different equations dependent on the wavelength. From these four equations only the equation that is used for the far infrared deviates significantly from the other three (the equations for the visible, near and mid infrared) and from the equation used by IRTOOL. As was expected for the visible, near and mid infrared, both models predicted about the same results (for the same cut-off

height), which were in very good agreement with the observed data. Moreover, in the far infrared the results predicted by IRTOOL were much better than those predicted by IRBLEM.

The general impression given by the analysis is that the refractivity profile, which is primarily dependent upon the temperature profile, produced by IRTOOL causes more ray bending than that produced by the LWKD model of IRBLEM. Therefore IRTOOL becomes more effective in the prediction of mirages.

From the results of the comparison with the MPN observation data, both models give a good fit to the experimental data under the assumption that both use the same cut-off height which controls the MXMH. Because of the quality of the fit to the MPN data, we expect the fit of these models to the ship-tracking events to be reasonably good. In the visible, near and mid infrared the MIVR prediction from IRTOOL was always within 2.7 km from the measured data. The highest deviation in the results occurred when the variation in the ASTD measured by the ship was significant (in the order of 2^{0}C). In cases where this uncertainty was small (about 0.3^{0}C) the MIVR prediction from IRTOOL was within 1.3 km from the measured data. For the same wavebands the MIVR prediction from IRBLEM was always within 2.4 km from the measured data, when the uncertainty in ASTD measured from the ship was big enough, while in cases where this horizontal inhomogeneity was small the MIVR predictions were within 1 km from the measured data. In the far infrared IRTOOL MIVR predictions were much better than IRBLEM. In order to compare the MMR results we make the assumption that both models use the

same cut-off height, namely that used by IRBLEM, which was always closer to the measured $H_{1/3}$ wave height. In this case the MMR results for both models are in good agreement among themselves and with the experimental data. The IRBLEM results are always within 0.8 km from the experimental data while those for IRTOOL are always within 1.2 km and more often than not well within 0.5 km of the measured data. These discrepancies are quite reasonable as the uncertainty in the measured range was about 200 m. The ship was often bouncing up and down in the waves by several meters so that for a source at a height of 10 m a variation in height of 1 m could lead to variation in the predicted MIVR of about 500 m.

Some of the differences between the predictions obtained from the different models and the experimental data are due to the gradient profiles used by the models and particularly the temperature profile near the water surface. The temperature profile could be modified so as to better describe the region close to the water surface. In particular a weaker temperature gradient for the first few meters would allow the curves to move towards the measured data. Another reason that we have already mentioned was the horizontal ASTD's inhomogeneity measured from the Hr. Ms. Tydeman. Generally, we can say that variations in ASTD affect IRTOOL more than IRBLEM. Even though the results from IRBLEM are slightly better than IRTOOL, we must note that in most of the cases the humidity calculated from IRBLEM at the sea surface was greater than 100% which is a non-physical result. Also, the water temperature used by IRBLEM does not correspond to the measured value even though the measured value is an input in the IRBLEM parameters.

The comparison of the geometric models of the ship-tracking events between IRBLEM and IRTOOL showed that in all cases IRBLEM calculates a geometrical range greater than IRTOOL. We showed that this happens because IRBLEM does not take into account the wave height for the calculation of the geometrical optical sight range.

Finally, it is reasonable to conjecture whether the differences in the results produced from the ray tracing programs of IRTOOL and IRBLEM are dependent only upon the refractivity profiles. Another factor that might produce significant discrepancies between the predictions of the two models is the difference in the ray tracing algorithms. To remove such doubts, several refractivity profiles produced by the two models for a number of cases should be used as an input to a common ray-tracing program and their corresponding outputs should be compared. This could probably be the objective of a future research. However, in this thesis we showed that in cases such as the events P2810P3 and T2810K, where the profiles of the gradient of refractivity were very similar and also the cut-off height that was used from each model was almost the same, the results predicted from the two models were in extremely good agreement. So, it is safe to say that the differences in the results produced by the two models appear to be solely due to the differences between the profiles generated from IRTOOL and IRBLEM.

THIS PAGE INTENTIONALLY LEFT BLANK

LIST OF REFERENCES

1. A. W. Cooper and E. C. Crittenden, Lecture notes from PH 4253, *Electro-optic Sensors and Systems,* Naval Postgraduate School, Monterey, California, September 1998.

2. Georgopoulos, Antonios, "Performance analysis of IRTOOL ray refraction program and comparison to LWKD and PIRAM marine boundary layer programs," M.S. Thesis, Naval Postgraduate School, Monterey, California, 1998.

3. R.Greenler, *Rainbows, halos and glories,* Cambridge University Press, 1980.

4. D. C. Williams and H. Kahmen, "Two Wavelength Angular Refraction Measurement" in *Geodetic Refraction: Effects of Electromagnetic Wave Propagation Through the Atmosphere*, Springer-Verlag Berlin, Heidelberg, New York, Tokyo, 1984.

5. G. C. Holst, "Electro-Optical Imaging System Performance", SPIE optical Engineering Press 1995.

6. D. J. Griffiths, " Introduction to Electrodynamics", Prentice- Hall, 2 nd edition, 1989.

7. P. Walker, "Propagation modeling and experiments: Aerosol influences on marine atmospheric surface layer optics," Naval Postgraduate School, Monterey, in *Propagation and Imaging through the Atmosphere II, SPIE Proceedings,* pp.102-107, vol. 3433, 1998.

8. D. Dion, "Refraction Effects on EO System Detection Ranges in Coastal Environments" in *Propagation Assessment in Coastal Environments,* AGARD Conference Proceedings 567, 1995.

9. Berk, A., Bernstein, L.S. and Robertson, D.C., "MODTRAN: A Moderate Resolution Model for LOWTRAN7," U.S. Air Force Geophysics Lab., Hanscom AFB, Massachusetts, 1989.

10. "The Astronomical Almanac for the Year 1993," Nautical Almanac Office United States Naval Observatory.

11. "IRTOOL Atmosphere Modeling," Arete Report ARW-96-303-002-TR, October 1996.

12. Hecht, *Optics,* Addison-Wesley Publishing Company, 3rd Edition, 1998.

13. M. Mermelstein, E. Takken, R. Priest, E.Stone, and T.Thorpe, "Target Detection and Wave Obscuration at the Ocean Horizon," Naval Research Laboratory, Washington, D.C, 1997.

14. L. Forand, D. Dion, and J. Beaulieu, "Marine aerosol properties and thermal imager performance (MAPTIP): Canada's Measurements of Refraction Effects," in *Propagation Assessment in Coastal Environments,* AGARD Conference Proceedings 567, 1995.

15. Denis Dion, "IR Boundary Layer Effects Model (IRBLEM)," Version 3.1, DREV (Canada), 22nd October 1998.

16. IRTOOL Reference Manual Version 2.0.0, Arete Associates (P.O. Box 6024 Sherman Oaks, California 91413), November 1995.

17. L. Forand, "Marine aerosol properties and thermal imager performance (MAPTIP): refractive effects in the visible and IR," Defense Research Establishment Valcartier, Canada, in *Image Propagation through the Atmosphere, SPIE Proceedings,* vol. 2828, 1996.

18. L. Forand, D. Dion, Y. Hurtaud and K. Stein, "MAPTIP Workgroup report: Refractive effects in the visible and the Infrared," Defense Research Establishment Valcartier, Canada, June 1997.

19. Hill, R. J., S. F. Clifford and R. S. Lawrence, "Refractive-index and absorption fluctuations in the infrared caused by temperature, humidity, and pressure fluctuations," in *Journal of Optical Society of America,* vol. 70, no. 10, pp. 1192-1205, October 1980.

20. W. G. Rees, C. M. Roach and C. H. F. Glover, "Inversion of Atmospheric Refraction data," in *Journal of Optical Society of America A,* vol. 8, no. 2, pp. 330-338, 1991.

21. W. H. Press, B. P. Flannery, S. A. Teukolsky, and W. T. Vetterling, *Numerical Recipes*, Chapter 15, p. 558, Cambridge University Press, 1986.

22. Kinsman, U., W*ind Waves, their Generation and Propagation on the Ocean Surface,* Prentice-Hall, New Jersey, 1965.

23. K. L. Davidson, Lecture notes from MR 4416, Atmospheric Factors in Electromagnetic and Optical Propagation, 1999.

24. M. I. Skolnik, "Propagation of Radar Waves" in *Introduction to Radar Systems,* McGraw- Hill, Company, 1962.

25. IRTOOL Tutorial and Examples Version 1.4, Arete Associates (P.O. Box 6024 Sherman Oaks, California 91413), February 1995.

26. IRTOOL Reference Manual Version 1.4, Arete Associates (P.O. Box 6024 Sherman Oaks, California 91413), February 1995.

27. J. Luc Forand, "Horizontal non-homogeneous effects in the marine boundary," Defense Research Establishment Valcartier, Canada, in *Propagation and Imaging through the Atmosphere, SPIE Proceedings,* pp. 180-191, vol. 3125, 1997.

28. J. L. Forand, D. Dion, M. Duffy, S. Gathman, K. Littfin, A. de Jong, G. de Leeuw, and K. Davidson, "An Extensive Analysis of Low-Level IR Transmission Measurements taken over a 15 km Path during EOPACE with IRBLEM," in *Propagation and Imaging through the Atmosphere II, SPIE Proceedings,* pp. 90-101, vol. 3433, 1998.

THIS PAGE INTENTIONALLY LEFT BLANK

INITIAL DISTRIBUTION LIST

No. Copies

1. Defense Technical Information Center.....2
   8725 John J. Kingman Rd., STE 0944
   Ft. Belvoir, VA 22060-6218

2. Dudley Knox Library.....2
   Naval Postgraduate School
   411 Dyer Rd.,
   Monterey, CA 93943-5101

3. Chairman, Code PH.....1
   Department of Physics
   Naval Postgraduate School
   Monterey, CA 93943-5121

4. Professor Alfred. W. Cooper, Code PH/Cr.....2
   Department of Physics
   Naval Postgraduate School
   Monterey, CA 93943-5121

5. Professor Ron J. Pieper, Code EC/Pr.....1
   Department of Electrical and Computer Engineering
   Naval Postgraduate School
   Monterey, CA 93943-5121

6. Engineering & Technology.....1
   Curricular Office (Code 34)
   Naval Postgraduate School
   Monterey, CA 93943

7. COMMANDING OFFICER.....1
   SPAWARSYSCEN SAN DIEGO
   ATTN: Dr. D. R. Jensen, D883
   49170 Propagation Path,
   San Diego, 92152-7385

8. NAVAL SEA SYSTEMS COMMAND.....1
PEO Expeditionary Warfare,
ATTN: Mr. J.E. Misanin,
2531 Jefferson Davis Highway
National Center 2-Room 12E52
Arlington, VA 22242-5170

9. Embassy of Greece.....1
Naval Attaché
2228 Massachusetts Avenue, N.W.
Washington, DC 20008

10. Ioannis Christou.....3
Gr. Labraki 321
Keratsini 18757
Athens
GREECE

11. Arete Associates.....1
ATTN: Steve Church
P.O. Box 6024
Sherman Oaks, CA 91413

12. Defense Research Establishment Valcartier.....1
Electro-optics and Surveillance Division
ATTN: Luc Forand
2459 Pie XI Blvd., North
Val-Belair, Quebec, G3J 1X5
CANADA